THE USE OF MULTIPLE CHANNELS IN GRADED INDEX FIBRE TO INCREASE BANDWIDTH CAPACITY IN OPTICAL FIBRE COMMUNICATIONS

by

Siriaksorn Jakborvornphan

A Dissertation Submitted to the

School of Engineering and Design

in Partial Fulfillment of the Requirements

for the Degree of

Doctor of Philosophy

UNIVERSITY OF SUSSEX

July, 2017

Declaration

I hereby declare that this thesis has not been and will not be, submitted in whole or in part to another University for the award of any other degree.

Signature: .....

Acknowledgement

First and foremost I would like to sincerely express all my gratitude and appreciation to my first supervisor, Dr. Rupert Young, for his expert guidance and the most valuable support throughout my academic pursuits at the University of Sussex. Back in January 2015, I first discussed with Dr. Rupert Young about the overall goals of this research project to apply for a fully funded Chancellor's International Research Scholarship (CIRS), and if it would not have been for him, surely I would have not been accepted for the award and completed this dissertation today. Thank you for your encouragement and the full support from the CIRS during the completion of my degree.

Then, I would like to equally thank to my second supervisor, Dr. Phil Birch, who has supported me with strong supervision throughout the duration of my research. Without his help and support at strategic times, I would have not had a delightful experience at the research laboratory.

I am thankful to Vincent Brulis for his suggestions in the simulation and useful discussions on the simulation results.

Finally, I would also like to say special thanks to my beloved family and Padipat Pleumworasawat (my boyfriend) for their endless support and encouragement.

UNIVERSITY OF SUSSEX

Siriaksorn Jakborvornphan

DOCTOR OF PHILOSOPHY

The use of multiple channels in graded index fibre to increase bandwidth capacity in optical fibre communications

ABSTRACT

Nowadays we are living in a well-developed technological world, supporting new services and networks with vast amounts of data streams that are being pushed through fibre optic communications systems. Thus the use of optical fibres as a transmission medium is being progressively increased for deployment in ever-wider fields. A significant increasing demand of global social information in modern communication is leading to an exponentially increasing demand for high transmission carrying capacity via fibre optical network systems. This drives towards a higher information carrying capacity than the standard systems can handle. To meet the higher bandwidth requirements with a higher capacity per cross sectional area of the fibre for future communications, maximising the density of the channels is seen as an effective solution, accomplished by simultaneously propagating the individual channels within the same fibre. A new multiplexing technique, spatial division multiplexing (SDM) based on a multi-core fibre (MCF) and a multi-mode fibre (MMF), has proved it is possible to overcome the current limitation of the carrying capacity.

Our greatest concern in this research is to overcome the limited transmission capacity of current existing optical fibre systems and to progressively increase the bandwidth capacity with a simple and cost effective approach. This can be accomplished by transmitting a multiplicity of channels down a single graded-index fibre (GI-MMF) with a large core diameter. This would allow a significant increase communication bandwidths for a range of short haul communications. The proposed method exploits the phenomenon of self-imaging in the GI fibre due to the interference between the excited modes which leads to the reproduction of the original beam profile periodically along the distance of propagation. This allows the maintainance of crosstalk levels between the plurality of communication channels lower than -25 dB, and also ensures a reduction of optical losses in the perturbed-tolerance fibre for short-reach networks. We observe that crosstalk levels of nearly -30 dB can be achieved for eight spatially independent transmission channels in a GI fibre of 200 μm diameter with a well separated angle of a 45° spacing distance between adjacent channels, and with an optimum distance of 60 μm from the centre of the structure.

In addition, the key studies in this work have emphasised the theoretical studies in the perspective of the fractional Fourier transform (FRT), a generalisation of the Fourier transform, and the formation of reproductions of the incident arbitrary beam profiles, defined in term of Gaussian beams with an equivalent beam diameter of 10 μm at their corresponding self-imaging distance. It was found that the launched beams simultaneously propagate and re-arranging themselves periodically at the self-imaging planes along the length of the simulated commercially available fibres and the proposed large core GI-MMF, structured with 200/400 μm (core/cladding) diameters with a numerical aperture of 0.132. The results of self-imaging length intervals were in a good agreement with the analytical predication in both of a single channel transmission and a high-density transmission.

Fibre bending and harsh environmental variations are of particular importance to most optical links since they affect the transmission capabilities of the fibre system. We have demonstrated the behaviour of light propagation in both a perfectly straight graded index fibre and as the fibre undergoes perturbations due to bending and temperature changes. A low propagation loss of 0.75 dB/5° bend was found for a single channel transmission, whilst the less sensitive to bending effects of approximately 6.27 dB/5° bend were realised from four spatial channels in our proposed large core-small NA GI-MMF with the curvature radius of 400 mm. More interestingly, bending does introduce a critical issue for the realisation of the re-imaging of the spatial channels at the self-imaging planes.

On the other hand, the self-imaging effect of the graded index multimode fibre induced by temperature variations has no significant modification on the transmitted beam due to an extremely small change in refractive index and insignificantly modified transmission distance of the perturbed fibre. Overall, it must be concluded that a high quality self-imaging is restricted by the fibre perturbation to periodically reproduce the spatial input channels as well as the consistency in the formation of the self-imaging distances.

Tables of Contents

List of Abbreviations

AM	amplitude modulation
ASK	amplitude shift keying
APD	avalanche photodiode
BER	bit error rate
BPSK	binary phase-shift keying
DOF	depth of focus
DWDM	dense wavelength division multiplexing
DSDM	dense spatial/space division multiplexing
DMGD	differential modal group delay
DGD	difference group dispersion
DSF	dispersion-shifted fibre
DSP	digital signal processing
DPSK	differential phase shift keying
DQPSK	differential quadrature phase shift keying
DRS	double ring structure
EDFA	erbium-doped fibre amplifiers
FDE	frequency domain equalisation
FDM	frequency domain multiplexing
FDTD	finite difference time domain
FMF	few-mode fibre
FRT	fractional Fourier transform
FSK	frequency shift keying
FTTH	fibre to the home
GI50	a 50 μm core diameter graded index fibre

GI62.5	a 62.5 μm core diameter graded index fibre
GI100	a 100 μm core diameter graded index fibre
GI200, GI200/400	a 200 μm core with a 400 μm cladding in diameter graded index fibre
GI-MMF	graded/gradient index multimode fibres
GRIN	quadratic gradient index medium
GVD	group velocity dispersion
HG	Hermite-Gaussian functions
IM-DD	intensity modulation/direct detection
IF	intermediate frequency
IL	insertion loss
LCOS	liquid crystal on silicon
LP	linearly polarised
ISI	inter-symbol interference
MC-EDFA	multicore erbium-doped fibre amplifiers
MCF	multi-core fibre
MDG	modal differential gain
MDL	modal differential loss
MDM	mode division multiplexing
MFD	mode field diameter
MG	mode group
MIMO	multiple-input-multiple-output
MMF	multimode fibre
MM-EDFA	multimode erbium-doped fibre amplifiers
MMI	multimode interference
NA	numerical aperture
OOK	ON-OFF-keying
PCM	pulse-code modulation

PL	photonic lantern
PolSK	polarisation shift keying
PML	perfectly matched layers
PSK	phase shift keying
QAM	quadrature amplitude modulation
QPSK	quadrature phase shift keying
ROI	regions of interest
RL	radiation loss
S-DEMUX	space-demultiplexer
S-M-S	single-mode-multimode-single-mode
S-M-M	single-mode-multimode-multimode
S-MUX	space-multiplexer
SDM	spatial/space division multiplexing
SI-MMF	step index multimode fibres
SI50	a 50 μm core diameter step index fibre
SMF	single-mode fibre
SNR	signal to noise ratio
SRS	single ring structure
TDE	time-domain equalisation
TDM	time division multiplexing
TIR	total internal reflection
WDM	wavelength division multiplexing
XT	crosstalk

List of Symbols

a	fibre core radius
b	normalised propagation constant
c	velocity of light in a vacuum
c_i	amplitude coefficient of each Eigenmode
f	focal length of the lens
k_0	wave propagation constant in a vacuum
m	radial mode number, number of maxima of the field
n	refractive index of the medium, number of field maxima around the fibre radius, number of transformations to reproduce the input signal, beam/channel number
n_1	higher refractive index of a medium
n_2	lower refractive index of a medium
n_{eff}	effective refractive index
$n(T)$	refractive index changes for different environmental temperatures
$n(T_o)$	refractive index of the fibre at ambient temperature
(x_n, y_n)	Gaussian beam coordinates where subscript n denotes the beam number
or^{th}	degree of fractional Fourier transform order
or_g^{th}	arbitrary angle between a frequency and space domain
r	radial distance of the beam from the fibre axis
t	time constant
v	cut-off frequency
v_p	phase velocity

v^{th}	mode number
w	angular frequency, Gaussian beam radius
z	propagation distance
z_0	position where the beam starts to diffract from the plane wavefront
z_R	Rayleigh length
Δz	change in length z of the fibre with temperature.
B	magnetic flux density
D	electric flux density
E	electric field
E_0	optical energy
H	magnetic field
I	optical intensity distribution
I_0	maximum optical intensity
J	Bessel function
$J_m(U)$	Bessel function of the first kind, of order m
K	modified Bessel function
$K_m(W)$	modified second kind of Bessel function of order m
L	length of fibre, the Fourier distance
L_f	the final section length of the fibre
L_π	beat length
L_{img}	self-imaging length interval
M	number of modes, number of output channel
M_g	number of guided modes in graded index fibre
$M_{g,straight}$	number of modes before the fibre is bent in graded index fibre
$M_{g,bend}$	number of modes in a bent fibre

M_s	number of guided modes in step index fibre
N	number of transmitter, number of input optical channel
P	electric power in the beam
P_{core}	power propagating in the core
P_{cladd}	power propagating in the cladding
P_{output}	optical output power
$P_{launched}$	optical input/launched optical power into a fibre
$P_{\sin gle}$	optical power of the transmission signal in a single beam
$P_{multiple}$	optical power collected from the multiple channel transmissions
R	curvature radius of a bent fibre
R_c	radial distance inside the cladding of a fibre bend
T	temperature of the environment in Celsius
T_o	ambient temperature (25°C)
$\frac{dn}{dT}$	thermo-optic coefficient
U	Eigenvalue of the fibre core
V	normalised frequency of the fibre, V-number
W	Eigenvalue of the fibre cladding
XT_n	optical channel crosstalk in channel number n
θ_1	angle of incidence
θ_{air}	angle in the air
θ_{core}	acceptance angle in a core region
θ_c	fibre critical angle
$\theta_{\max}$	fibre maximum acceptable angle to the axis which is usually the half angle of an acceptance cone

α	index profile of fibre
$\alpha_{thermal}$	thermal-expansion coefficient
β	propagation constant
β_z	propagation constant in *z*-direction
$\Delta\beta$	separation distance of the propagation constant
Δ	relative refractive index difference between the core and cladding
Δn	index differences between the n_1 and n_2
∇	vector operator
∇^2	Laplacian operator
λ	optical wavelength
λ_0	free space wavelength of light
λ_c	cut-off wavelength
$\Im$	conventional Fourier transformation
$\Im^2$	second application of the Fourier transformation
$\Im^3$	third application of the Fourier transformation
$\Im^4$	self-transformation, the four applications of the Fourier transform
$\Im^{a^{th}}\{f(x,y)\}$ or $\Im^{a^{th}} f$	the fractional Fourier transform of a function *f*(*x*,*y*)
μ	magnetic permeability
ε	dielectric permittivity
ζ	thermal electronic polarizability coefficient
ψ	scalar component representing $\boldsymbol{E}$ or $\boldsymbol{H}$ field
Ψ_{mn}	two-dimensional Eigenmode
$\Psi(x,0)$	initial field profile

$\Psi(x,z)$	field distribution profile at some particular z-distance
$\Psi(x,L)$	field distribution profile at L-distance
(x,y,z)	rectangular Cartesian coordinates
(r,ϕ,z)	cylindrical coordinates
(r',θ,z')	cylindrical local coordinate for the bent fibre.

List of Figures

List of Tables

Chapter 1

Introduction

1.1 Motivation

The internet is dominating modern communication, with long-haul transmission being implemented via fibre optic network technology. There is wide demand for internet use, high power consumption and the need for ever increasing bandwidth requirements. One of the main goals is expanding capacity to allow enormous communication bandwidths for a range of successful commercial applications such as high definition video-on-demand, file sharing and the increasing move to cloud computing [1]. In order to provide the transmission of huge amounts of information and the needs for different types of communication such as images and speech, substantial bandwidth capacity will be required, which clearly effects the demand for the large communication capacity, i.e. up to 100 Gigabit per second nowadays and a growth into the range of 100 Tbit/s per fibre with the possibility of achieving up to 1 Pbit/s and further in the near future [2,3].

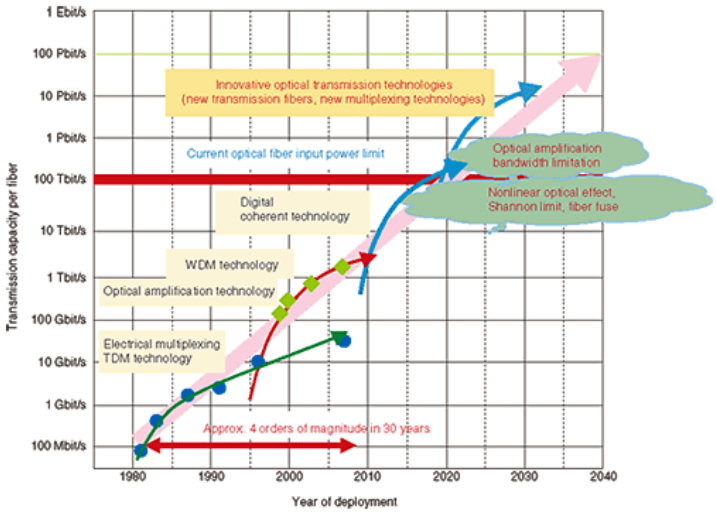

Figure 1.1: The evolution of optical fibre technology in the next step change of transmission capacity [5].

Due to the exponentially increasing demand of global social information and the demand of worldwide communications, we are rapidly moving and driving toward higher network capacity than the standard systems can handle and creating many new challenges and limiting factors for the required network infrastructure. The development of new optical transmission technologies has been occurring rapidly through three main innovations, namely, time division multiplexing (TDM) based on electrical multiplexing; wavelength division multiplexing (WDM) with optical amplification technology; and digital coherent techniques, as illustrated in Figure 1.1. These optical transmission technologies are currently developed and searching for a way to increase the transmission capacity that has been continuously invented over the last several decades to achieve a bandwidth capability per fibre [3].

1.2 Limit of current single mode fibre transmission

Currently, the traffic growing capacity demand rate is around 30% to 40% increase per year [4, 5, 6]. Indeed, the trend of progressively increasing the communication capacity, has achieved more than 100 Tbit/s in a system using the existing multiplexing technologies over standard fibre systems employing single mode fibres. However, these transmission technologies are facing their limits; they are close to the theoretical limits of the Shannon theorem and near limits due to the degradation of the signal from the Kerr fibre nonlinearity. Much work has indicated that single mode fibre may not support the future demand of high data rate and high speed demand as it is approaching full capacity in the existing infrastructures. Transmitting information in an optical fibre at higher bit rate is physically difficult because the optical signal is attenuated by several factors, for example, waveform distortion, caused by the high instantaneous power of the optical signal. However, the need for increased capacity of the network is still the major challenge and is difficult to achieve using standard single mode fibre. A newly proposed technique, exploiting a multimode fibre to increase the capacity is one of the existing solutions. Recent work has indicated

that the use of multimode fibres has become attractive in networks as they can propagate simultaneously up to 100 modes, realising optical fibres with an increased capacity [7].

In order to deal with the huge amount of signal transmission over thousands of kilometres, one of the most significant solutions is thus based on optical fibre communications. To cope with an increasing bandwidth problems, the use of wavelength multiplexing techniques, with first wavelength division multiplexing and then dense wavelength division multiplexing (DWDM), being implemented. Hence many relevant techniques have been developed to obtain such higher bandwidths. It is evident that these techniques have been developed over the last thirty years to progressively increase the network capacity [2, 6, 7, and 10]. However, DWDM implementations, which are suitable for long haul fibre connection, tend to be too costly for data centre applications and so alternative methods for more cost effectively increasing short haul bandwidths are actively being sought.

1.3 Current technologies

Several technologies have been used to increase capacity in the last three decades and have been evolved through the use of division multiplexing of different types of degrees of freedom as shown in Figure 1.2 [8-11]. Many studies have intensively focused on the four degrees of freedom that have been used in long haul transmission to maximise capacity. Therefore, we need new multiplexing technologies as a new path for utilising and increasing the transmission capacity by making use of a last option (i.e. space) which is known as space/spatial division multiplexing (SDM) in the new optical fibres [12].

This is accomplished by multiplexing optical signals using unique spatial modes or several fibre cores beyond the limitation of a standard fibre system. A number of modulated signals may be combined into multichannel signals by being multiplexed on to the same fibre for communication transmission using a new multiplexing technique. This multiplexing technology, employed in SDM

systems, can obviously support the multiple numbers of mode channels, and optical amplifiers operating with optical connectors and space-(de)multiplexers (S-MUX, S-DEMUX) used with multimode fibres. The SDM approach aims to increase the capacity by the number of modes (i.e. a mode division multiplexing (MDM) [68]) or the number of spatial input channels in which there are great advantages over the existing approaches, i.e. time or wavelength, promising the potential for a reduction in cost and providing more energy efficiency per bit transmitted [13].

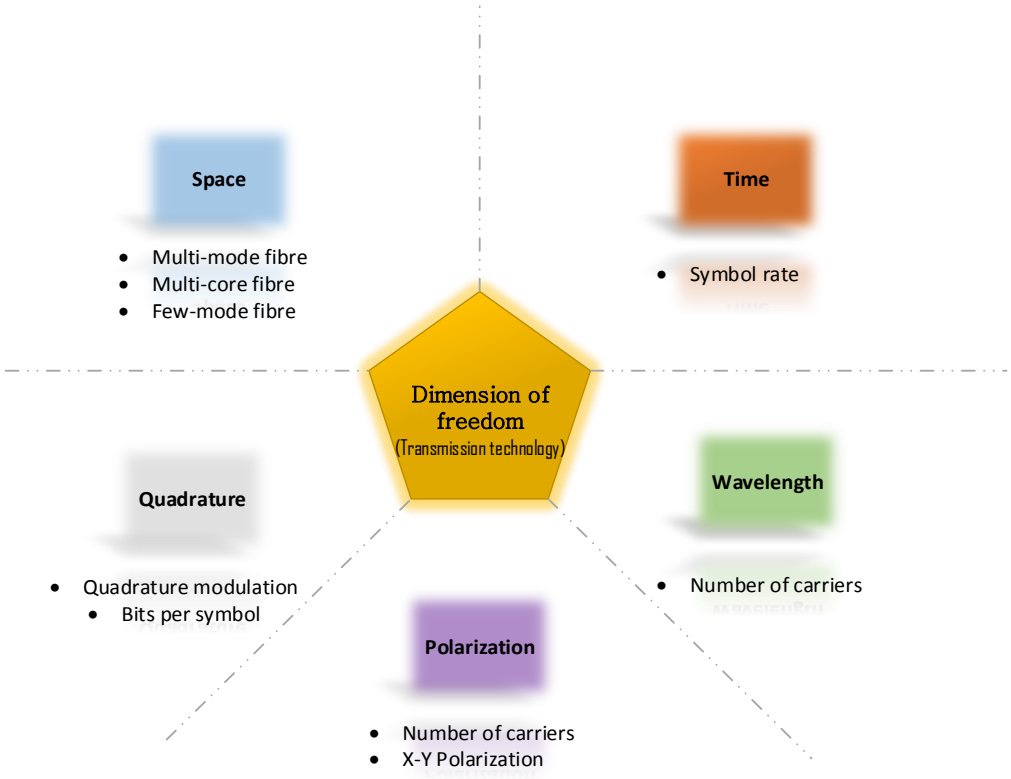

Figure 1.2: The five physical dimensions for increasing data transmission capacity.

Through using SDM, including mode-division multiplexing (MDM) as a subset of SDM using a new optical fibre that has high power tolerance and suppresses undesired optical non-linear effects, a multimode fibre (MMF) can be used to map signal channels onto different transmission modes of a single fibre. This is now being thought of as a new way of increasing the capacity by using the multiple numbers of modes, channels, and cores (i.e. MCF). It is available to

be implemented in either free space (by multiple beams) [14] or guided media [15, 16]. However, there is the need to overcome the major limitation of bandwidth that is brought about by modal dispersion in a MMF and the critical issue of modal crosstalk that has required digital signal processing (DSP) techniques to compensate for unwanted linear distortion and multiple-input-multiple-output (MIMO) techniques, as employed in wireless communication, at the receiver to equalise the signal [17]. At the receiver end, the different group dispersion (DGD) affects the original signal so that it cannot maintain its shape which will eventually result in more difficulties for the DSP-MIMO equaliser. Therefore, it is necessary to minimise the distortion by measuring each mode coherently across the beam and sending these modes to the DSP-MIMO that can unscramble the signal and equalise the group delay and hence be able to reconstruct the input field. These are the reasons why today researches have been intensively investigating SDM along with the new transmission fibre types to maximise the capacity and degrade nonlinear optical effects.

1.4 Statement of research topic

This project will extend the use of wavelength multiplexing techniques that was implemented to increase the capacity of communications using an existing single-mode fibre optic system. The study of the spatial multiplexing scheme as an additional transmission path for fibre optic communications has been reviewed in parallel with the current technologies based on this scheme. The reason for this is because the number of multiple modes or cores are now seen as a way of increasing the communication-carrying bandwidth capacity of a MMF through a new multiplexing technique (i.e. SDM). The idea of multi-channel transmission can be adapted from the space division multiplexing, i.e. a number of independent channels are sent into the same fibre in which each of these channels carries unique information. We, therefore, propose an alternative method to allow multi-channel transmission down a single fibre to progressively increase the bandwidth capacity.

Our greatest concern is to overcome the limited transmission capacity of current existing optical fibre systems and can be achieved by transmitting a multiplicity of channels down a single fibre to progressively increase the bandwidth capacity whilst achieving a reduction of cost. The specific method will require the use of graded index fibre (GI-MMF) with a large core diameter to multiplex more than one channel, defined as an input Gaussian beam from a number of sources that carries independent information. Thus a single fibre core is used, rather than increasing the modulation rate of the optical source to allow enormous communication bandwidths for a range of short haul communications. In this way, a number of channels can be simultaneously propagated through the fibre, providing the potential to increase the capacity beyond that of current existing optical fibre systems based on a single mode fibre, so achieving a reduction of cost. In addition, this fibre type is already commonly used in local area networks (LANs) [1, 2, 18, 19 and 20]. As data centres expand, there should be no impediment to replacing multimode fibre with GI profile fibre since the cost increases would not be prohibitive.

In order to make a model of the propagation through sections of a quadratic graded index multimode fibre (GI-MMF), the properties of the fractional Fourier transform (FRT) [21-28] is investigated to study the propagation of a single channel and multi-channel transmission by providing an analytical model in addition to a numerical simulation to model the greater information-carrying bandwidth capability. This generalisation of the Fourier transform (FT), i.e. the FRT, can be used to model the propagation of wave fronts in an optical system having a graded index profile since a quadratic graded index medium has a direct relationship with the FRT.

One of the main tasks is to optimise and adjust the fibre parameters, such as mode diameter, the number of beams from the laser sources, the influence of core/cladding diameters, and the appropriate length of fibre, which will allow an effective periodic reconstruction of the original multi-channel source along the length of propagation. Thus the research has modelled the propagation

characteristics of a multimode fibre. The major obstacles during the transmission of multiple channels, such as channel variations, modal crosstalk from adjacent spatial channels, and environmental effects is investigated in detail to realise a higher communication bandwidth capacity. Once the relevant design parameters are determined, the experimental investigations of the proposed method will be made. This can be done at modest cost using a single modulator and detector at relatively low bandwidth together with spatial relocation in the fibre coupling zone.

Our proposed method has a particular requirement to allow multiple channel transmission down a single graded index fibre for high communication bandwidth over several meters. Thus this research focuses on the carrying capacity of short haul fibre connections for short distances as required in data centres.

1.5 The basic physical configuration

The physical configuration is that a number of *N*-channel signals (e.g. from an array of individual modulators) can be individually modulated, resulting in a two dimensional (2-D) spatial domain intensity distribution. An individual channel transmits each of the signals separately which is then mapped to a specific mode. The spatially multiplexed signals are coupled into a graded index fibre (GI-MMF) which can then be recovered from the end of the fibre over any number of specified intervals of distance. This is because the GI-MMF has the effect of forming a continuous 2-D fractional Fourier transform of the input intensity distribution so that the field is progressively transformed to a Fourier transform plane, i.e. a 2-D spatial frequency spectrum, and back again to the original 2-D spatial domain intensity distribution.

After an arbitrary number of transformations between spatial frequency and spatial domains, the signal emerging from the end of the GI fibre will be a preserved 2-D spatial intensity distribution, with each pixel temporally modulated. The modulated light distributions may then be imaged to a 2-D

photodiode detector array, so allowing the (periodic) reconstruction of the individually modulated *N*-channel signals. According to the studies reported in references [21-35], the graded index medium can be used to implement a cascading fractional Fourier transform (FRT) to produce a perfect optical imaging system. It has been shown that a piece of GI fibre of the proper length can generate a Fourier transform and cutting the piece of GI fibre into fractional pieces will correspond to an implementation of the FRT. To further extend the concept of transmission by using a GI-MMF system, it can be shown to perform a fractional Fourier transform (FRT) to a full Fourier transform (FT) over a certain length of the fibre.

Thus the investigation will be focused on the profile of graded index fibres to determine the optimal profile to create propagation conditions where the image can go between the Fourier plane and reconstruction plane. Additionally, the modal dispersion will be investigated at various points to see where the signal is dispersed or undispersed. This can be done by developing a Fourier based analytical model and modifying the refractive index profile of the fibre in order to manipulate and improve the propagation effects. We need to see how pulses of light with, for instance, a simple Gaussian shape, spread out as they propagate down a fibre when there is a continuous graded index. It has been shown that by employing the graded index profile to transmitted pulses, pulse spreading and diffraction is minimised. Therefore, we need to observe these effects by modelling to support the theoretical explanation that the light pulses are re-imaged at the planes where $z = 2L$ where L is known as the Fourier distance.

1.6 Achievements of the research

The aim of the thesis research was to investigate and design a multiplicity of channels for transmission down a large graded index core multimode fibre which could increase the carrying capacity of existing short haul communications. A high density transmission was simulated for spatial input channels in a 200/400 μm core/cladding graded index fibre with a numerical aperture of 0.132. Eight independent channels positioned 45º from the neighbouring channels with a 60 μm separation from the centre of the fibre, and launched with an equivalent 10 μm beam diameter, were used to achieve a crosstalk tolerance on a level of approximately -30 dB at the working wavelength of 1.55 μm. The coupling from each channel into adjacent channels gave approximately equal radiation at the self-imaging length intervals. As a group of beams simultaneously propagate into the proposed large graded GI-MMF along the transmission length, the formation of replicas of the launched beams were realised and were shown to occur at the theoretical predicted self-imaging planes.

Perturbations of the fibre induced by bending and temperature fluctuation was used to study the behaviour of light propagation by transmitting a single channel and multi channels. The study was completed successfully and the proposed 5º bend fibre gave a typical bending loss of around 6.27 dB at wavelength of 1.55 μm for the four excited spatial beams and a typical sensitivity to bending was 0.75 dB for a single channel transmission under the same curvature radius of 400 mm. The reproduction pattern of multiple initial beams has been investigated as the fibre undergoes perturbations. It was found that a good quality reconstruction of the input beams is restricted by the fibre perturbation which thus affects the periodic reproduction at the self-imaging planes.

1.7 Organisation of this dissertation

Chapter 2 introduces a brief literature review on the characteristics of pulse propagation and the physical transmission impairments in optical fibres. A full explanation of an implementation of a fractional Fourier transform in graded index media to produce a perfect optical imaging system is presented at the end of the Chapter.

Chapter 3 covers the design concepts and analysis of an optical pulse in graded index multimode fibres with different fibre parameters and physical configurations. Various electromagnetic field distributions in different commercial fibres having a parabolic index profile are compared for analysis of the reconstruction performance of a specific excitation Gaussian beam. Lastly, the self-imaging effect was demonstrated for different fibres with various specifications to determine the longest reproduction length interval of an initial beam. Chapter 4 continues with a theoretical background of SDM transmission systems followed by the principles of coupling and the design of spatial channels in a single core fibre with different design arrangements at the centre of the fibre core. The analysis of channel crosstalk for each of the independent channels is investigated at different self-imaging planes for an 8-spatial channel.

Next, the bending and temperature effects are presented in Chapter 5 and Chapter 6, respectively. Chapter 5 starts with an introduction to the propagation characteristics in the bent fibre, the design considerations of various bending conditions, and then the discussion of the bending losses in a GI200 fibre with a single channel transmission and four spatial channel transmission with a single bend section between perfectly straight fibres at both ends, and then with two consecutive bend sections (i.e. a downward bend and an upward bend) under various bending angles.

Chapter 6 focuses on the temperature effects on a commercial GI62.5 multimode fibre. A change in optical path length of the fibre and its refractive index profile are demonstrated in addition to the self-imaging phenomenon in

the perturbed fibre at various surrounding temperature conditions. Finally, a discussion of several issues of the current research together with concluding remarks and future work are provided in Chapter 7. The future section work includes the design of an ultra-small rib silicon photonics waveguide and the study of the light propagation through the waveguide.

Chapter 2

General Background

2.1 Fundamentals of optical fibres

2.1.1 Optical transmission systems

There are a number of methods for developing an optical communication system, starting from a simple propagation of the light beam through free-space (for instance, by a light beam carrying encoded information as orbital angular momentum states [14]) or an optical fibre. These types of transmission can propagate the laser source over great distances; however, when sending the signals through the atmosphere unexpected weather conditions can be encountered. Thus long haul communication is unlikely to be suited to this simple method but for short range of communication within few tens of meters it is more feasible. For these reasons, an alternative transmission line method via optical fibres is the chosen method. There are several advantages in the use of fibre for optical communication over other waveguide systems. Clearly, the fibre is much more robust and flexible. It has low loss over various ranges of wavelength and also a huge bandwidth is possible [1, 36, 37, and 38].

Fundamentally, communication via an optical fibre is a communication system that transmits via light waves, signals or information a user would like to send from one point to another point. Basically, there are three major components representing part of the communication system: transmitter, communication channel or guiding medium and receiver. The channel is normally the fibre optic that acts as a guiding medium for light waves to travel from the transmitter to the receiver. The electrical signal is converted into an optical signal by the transmitter which is addressed by a drive signal, which varies the irradiance of the source as a function of time so producing a modulated

signal, which is either analogue or digital. In general, the transmission of information is made as a series of pulses using digital pulse-code modulation (PCM). The signal is coupled into a fibre and can propagate along the total length of the fibre. After arriving at the fibre end, the light is detected by an optical intensity detector which can be either a semiconductor PIN diode or an avalanche photodiode (APD) which can achieve high bandwidth detection [36, 37].

A number of information channels can be encoded in an optical fibre communication system employing intensity modulation/direct detection (IM-DD). In this case, each of these signal channels is modulated onto different carriers in order to be transmitted through the optical source as an electrical signal that has been multiplexed onto a single fibre link. However, it is necessary to modulate an incoming information signal and, at present, the use of intensity modulation (IM), as shown in Figure 2.1, is widely implemented with the available sources (i.e. LED and lasers), to then be used with a direct detection (DD) system at the receiver. This system is essentially based on the number of photons counted which is eventually transformed into a number of electron-hole pairs in the PIN photodetector. The phase and polarisation of the signal are not employed in a direct detection receiver. However, receiver sensitivity is poor and no improvement in signal to noise ratio (SNR) is possible. In contrast, coherent detection techniques employing both homodyne and heterodyne detection provide a higher detection sensitivity. Similar modulation techniques to those employed in intensity modulation can be easily applied to a coherent optical signal detection system but binary phase, rather than amplitude modulation is employed. The transmitted optical signals are converted into an electrical signal by a photodetector which does introduce signal distortion. Hence, to compensate for the distortion and to recover the original transmitted signal, an equaliser and filter are included as the final stage of the receiver terminal [38].

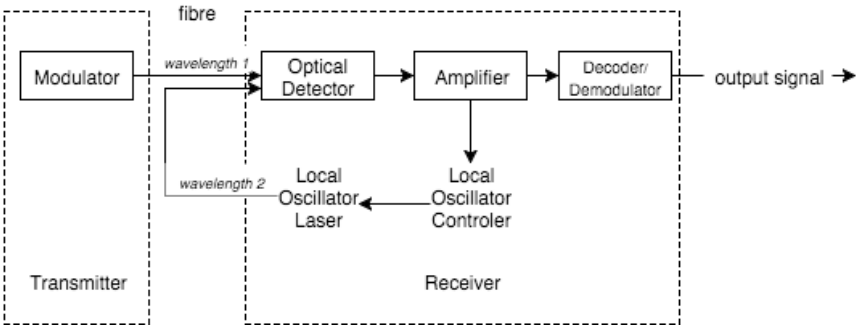

Figure 2.1: The coherent optical system [38].

From the transmission point of view, the pulses are modulated to generate a binary modulation which could be amplitude modulation (AM) with a simple square shape (or sometimes slightly rounded at the edge due to a limited bandwidth switching in ON-OFF keying). Also, there is a possibility of doing just phase modulation, flipping the phase between 0^0 and 180^0 whilst maintaining a continuous amplitude wave. However, there are other possible modulation techniques which are mainly binary keying, i.e. on-off small modulation depth pulses. At the receiver side, it is possible to have a coherent detection system which can detect the amplitude and phase of the wave front rather than a simple intensity detector such as a photodiode.

In IM/DD the intensity of the optical signal is directly detected and the phase and wavelength cannot be detected or measured by this technique. However, this limitation is overcome by a coherent system which is shown schematically in Figure 2.1, where the low level of an incoming signal is mixed with a larger electromagnetic reference field coming from the laser local oscillator. The output between these two mixed signals is only then forwarded to the detector. This is known as a homodyne receiver if the wavelength from the two signals is equal. The phase of signal is then estimated by using a phase-locking technique between the local oscillator and incoming signal before the detected signal is recovered into the original baseband signal [38]. On the other hand, in heterodyne detection, the local oscillator frequency is not identical to the incoming signal frequency, and therefore the difference signal, normally

referred to an intermediate frequency (IF), which is derived from the output of the photodetector can be forwarded to the demodulation process. Further, the demodulation process can be realised by either synchronous (coherent) or nonsynchronous (non-coherent) schemes.

2.1.2 Modulation formats

Modulation techniques, which can be utilised with either digital or analog subcarrier signals employ different modulation schemes such as: amplitude shift keying (ASK); frequency shift keying (FSK); phase shift keying (PSK); or polarisation shift keying (PolSK). Each of these signals is transmitted on its own fibre within a fibre bundle. Furthermore, by increasing the number of bits per symbol one can increase the transmission rate. The traditional scheme is the ON-OFF-keying (OOK) format, sometimes referred to ASK where the amplitude of the waveform is switched on and off between a binary bit 1 and 0. Then direct detection can be used to detect the amplitude of information. The information is coded in the amplitude and there is no phase modulation. In binary phase-shift keying (BPSK), there are two phase shifts separated between 0° and 180°. The amplitude in this format is constant while the phase modulation carries the information. The downside of BPSK over OOK is that it requires the more complicated coherent detection method to determine the phase of the signal. However, it is more immune against noise and distortion than OOK. The several extensions of the PSK format, e.g. differential phase shift keying (DPSK), quadrature phase shift keying (QPSK) and differential quadrature phase shift keying (DQPSK) have been utilised as modulation formats. The need for coherent detection can be avoided in a DPSK and DQPSK based system since the signal can be detected with just a photodetector as in direct detection. Nevertheless, these formats are uncommon in optical fibre networks because they are less dispersion tolerant. A data rate of 400Gbps and above is possible with amplitude and phase shift keying schemes known as quadrature amplitude modulation (QAM). The M-QAM format, where M is a number of bits per symbol

such as 16-QAM (4 bit/symbol), 64-QAM or 256-QAM is preferable in fibre optics with high data rate demands due to its tolerance to dispersion and the ease of implementation [1,38].

2.2 Pulse propagation in optical fibres

2.2.1 Light guiding in optical fibres

The phenomenon of total internal reflection (TIR) describes the propagation of light when it is injected into an optical fibre. The basic structure of an optical fibre consists of the core, located in the central region, having a higher refractive index, n_1. It is surrounded by the cladding, that is made of material of lower refractive index, n_2 to permit the total internal reflection at the core and cladding boundary, as illustrated in Figure 2.2.

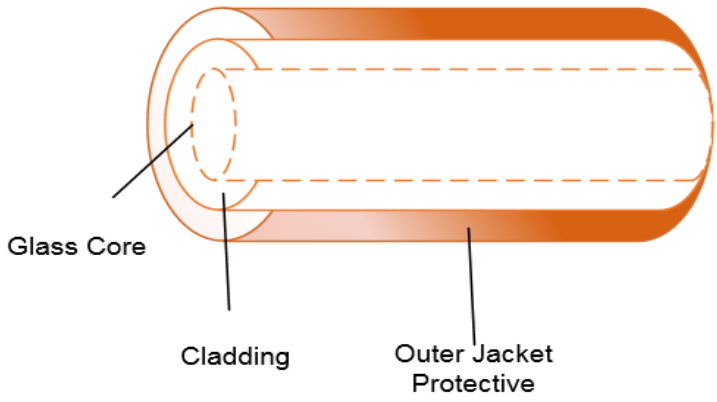

Figure 2.2: Basic structure of an optical fibre.

Let us first consider the case when the ray partly goes into the region having a lower refractive index, n_2 and reflection at the interface takes place. Some rays partially internal reflect back into the higher index region, n_1 and are eventually lost by radiation and so leak out of the fibre. Thus the total internal reflection will no longer take place along the direction of propagation. The incident ray at an angle θ_1 illustrates this situation in Figure 2.3 when θ_2 is greater than θ_{max} (where θ_{max} is defined as the maximum acceptable angle to the

axis which is usually the half angle of an acceptance cone), it is reflected into cladding region [1, 38].

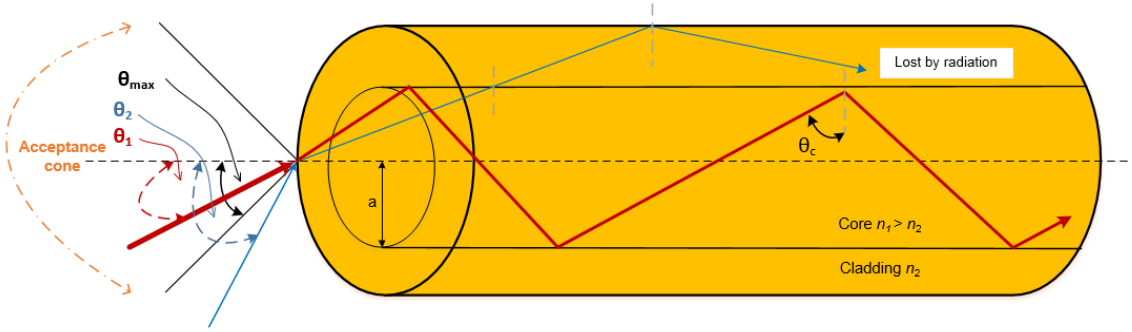

Figure 2.3: Light propagation in an optical fibre (adapted from [38]).

As soon as the light ray is injected into an optical fibre, it enters the denser medium, corresponding to the inner core of the fibre. When the light ray travels from the higher to lower refractive index, it arrives at the boundary between the core and cladding at an angle of incidence θ_1 (incident within θ_{max}). As θ_1 becomes greater than the critical angle θ_c (i.e. the largest incidence angle θ_1 for which the reflection can take place), all rays bounces back and forth displaying the phenomenon known as total internal reflection (TIR)[1, 38]. This takes place for the condition:

$$\theta_1 > \theta_c = \sin^{-1}\frac{n_2}{n_1} = \sqrt{\left[1-\left(\frac{n_2}{n_1}\right)^2\right]} \approx \sqrt{(2\Delta)} \qquad (2.1)$$

where Δ is the relative refractive index difference between the core and cladding which is sometimes is referred to as the fractional relative refractive index difference and is given by [38]:

$$\Delta \approx \frac{n_1 - n_2}{n_1} \qquad (2.2)$$

The angle of incidence is always equal to the reflection angle. There is no refracted ray and so no energy is lost by refraction and the ray is totally reflected back into the core and continues bouncing along the length of the fibre. It should be noted that at every position, the light ray travels from the denser medium to the lower refractive index medium so that the values of the total internal reflection angles remain the same.

2.2.2 Numerical Aperture

The refractive index difference between the fibre core and cladding will cause any arriving ray to be reflected. The numerical aperture (NA) is a parameter used to describe the light gathering capacity at the input to the fibre (see equation (2.5) for the definition of NA). However, there is an acceptance critical cone angle which is used to indicate the maximum amount of light entering into a fibre core and the light must be within $\theta_{\max}$, a half of an acceptance cone angle. When the light is injected at an angle greater than half the acceptance angle then some fraction of the light travels into the cladding region and will be guided for a short distance only and be lost, as illustrated in Figure 2.3. On the other hand, the incident light at the fibre core within the local numerical aperture NA of the fibre will propagate as a guided mode (i.e. the modes propagate around the fibre axis) along the length of the fibre.

From Snell's law at the air-core boundary, θ_{air} is an angle in the air and θ_{core} is an acceptance angle in a core region:

$$1 \times \sin\theta_{air} = n_1 \times \sin\theta_{core} \tag{2.3}$$

$$\sin\theta_{air} = n_1 \times \sqrt{1-\cos^2\theta_{core}}$$

$$= n_1 \times \sqrt{1-\left(\frac{n_2}{n_1}\right)^2}$$

$$= \sqrt{n_1^2 - n_2^2}$$

$$\theta_{air} = \sin^{-1}\sqrt{n_1^{\,2} - n_2^{\,2}} = \sin^{-1}\times[\mathrm{NA}] \tag{2.4}$$

where:

$$\mathrm{NA} = \sqrt{n_1^{\,2} - n_2^{\,2}} = n_1\left[\sqrt{2\Delta}\right] \tag{2.5}$$

where n_1 is the refractive index of the core, n_2 is the refractive index of the cladding and Δ is defined in the equation (2.2)

It is clear that the NA can be thought of as an indicator of an angle contained within the acceptance cone. However, the higher the value of NA the higher the number of modes can be propagated and the less critical is the fibre alignment as compared with the smaller NA for a single mode fibre. Moreover, the efficiency of an optical fibre is directly proportional to the amount of light entering the core since the more light reaches the receiver end and so a lower the bit error rate (BER) can be achieved. Conversely, the NA is indirectly proportional to the attenuation of the light ray propagating in the fibre. A larger number of modes propagating in a multimode fibre leads to higher dispersion and greater attenuation which results in a lower data rate and so speed of the signal transmission. The typical value of the NA for a single-mode fibre is 0.1, whereas for a multimode fibre it is about 0.2 and up to 0.3 for a very large core diameter. Usually, the typical value of the fractional refractive index difference between core and cladding should be much less than unity ($\Delta \ll 1$), and is denoted as the weak guiding approximation (i.e. $n_1 \approx n_2$). Accordingly, the linearly polarised group of modes (LP modes) can be generated for which each of the same group of modes has an identical value of the propagation constant β [1, 38, and 49].

2.2.3 Normalised frequency number

By solving Maxwell's equations, the propagation characteristics of an optical fibre can be obtained by treating it as a cylindrical waveguide and so can be solved for the guided modes propagating in the fibre. In order to characterise the guided modes that propagate in a cylindrical waveguide structure, the *V*-number is an important parameter for each distinct normalised frequency of each of the modes and gives an indication of an allowance number for the modes, which is given by:

$$V = \frac{2\pi a}{\lambda_0} \times \mathrm{NA} \tag{2.6}$$

where $\frac{2\pi}{\lambda_0}$ is the free-space wave number (λ_0 is the free space wavelength of light), and a is a core radius. The value at which $V < 2.405$ allows only one single mode (LP_{01} or HE_{11}) to propagate in the fibre.

2.2.4 Cut-off wavelength

The cut-off wavelength is defined as the wavelength at which a certain single mode only occurs and propagates through the fibre above the cut-off wavelength λ_c; therefore that mode is said to be a single longitudinal mode. However, below this theoretical wavelength, the fibre becomes multimode, with propagation in higher order modes, i.e. LP_{11}, LP_{21} etc. The cut-off wavelength λ_c is given by:

$$\lambda_c = \frac{2\pi a}{V_c} \times \mathrm{NA} \tag{2.7}$$

2.2.5 Types of fibre

There are basically three classes of optical fibre, characterised by the way the light wave propagates along the fibre, as shown in Figure 2.4. These are:

- Single mode fibres (SMF)
- Step index multimode fibres (SI-MMF)
- Graded index multimode fibres (GI-MMF)

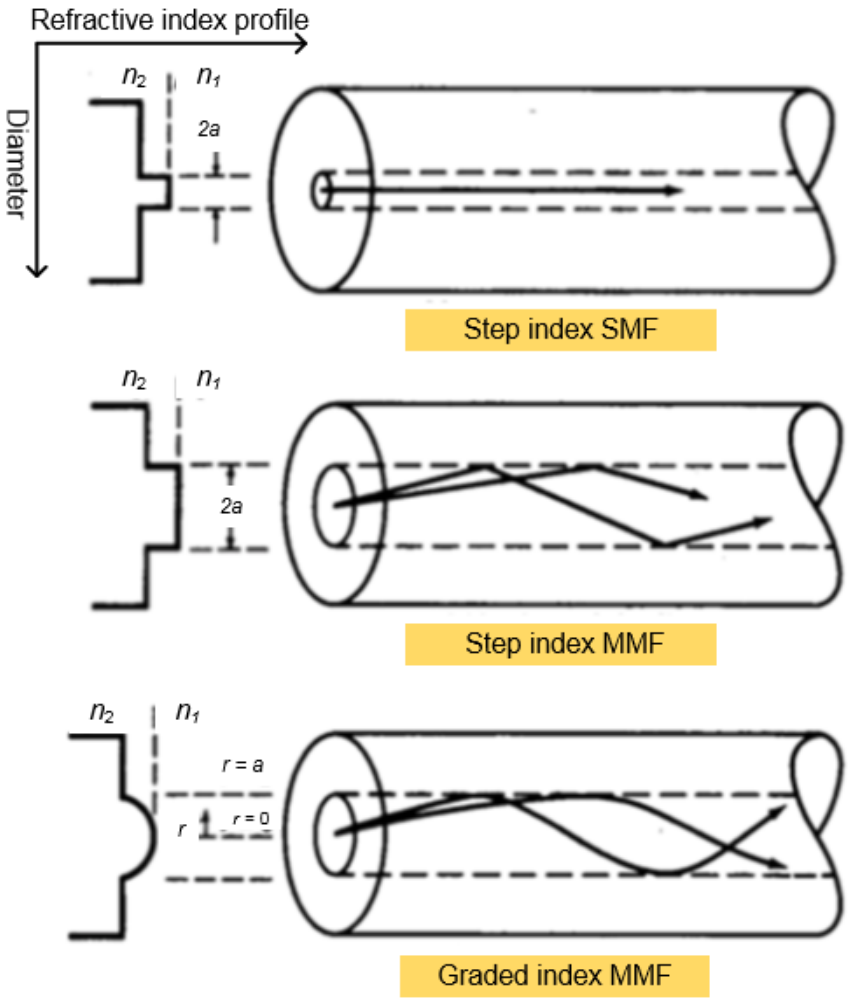

Figure 2.4: Propagation modes in different fibre types [1].

2.2.5.1 Single mode fibre

SMF has many advantages such as a very large transmission bandwidth, no exhibition of intermodal dispersion and no delay difference in mode propagation. Since all energy is confined to a single ray and no energy is lost into the cladding, the fibre has low attenuation and dispersion rate. Thus, due to the small difference in refractive index between the core and cladding, this type of fibre has a lower attenuation and not any reflection from the core-cladding boundary. Therefore, this fibre is suitable for long distance communication due to its advantages over multimode fibre. Thus it can be used in many modern communication systems. However, it does not have superior performance in all respects because the small core diameter creates physical problems when coupling and splicing.

2.2.5.2 Step index fibre

SI-MMF has a uniform profile inside the core area. One of the disadvantages of step-index multimode fibre is its small transmission bandwidth. This is because various numbers of bouncing rays propagate into the core region at different angles and so take different path lengths and so reach the end of the fibre at different times resulting in light pulse broadening, known as dispersion, when the output pulse is reconstructed. This major obstacle restricts the propagation distance that a pulse can be sent over the fibre and also limits the speed at which the fibre can operate.

The refractive index in a step-index profile remains constant in the fibre core region [38] and thus:

$$n^2(r) = n_1^2 \ldots \text{for } r \leq a \tag{2.8}$$

$$n^2(r) = n_2^2 \ldots \text{for } r > a \tag{2.9}$$

where a is a fibre core radius

2.2.5.3 Graded index fibre

Multimode graded index fibre has a refractive index in the core that changes gradually as it extends from the axis outward. The light traveling further from the optical axis propagates faster than that travelling along the optical axis. Due to the refractive index profile the rays propagating along the fibre axis in the core region have a shorter distance but are traveling at a lower speed since the refractive index is highest in the centre of the core. In another way of visualising the propagation, light rays travel away from the core axis where they travel faster due to the lower refractive index of the core near the cladding boundary, as shown in Figure 2.5. Even though all the travelling light waves take different paths, they reach the detector approximately at about the same time. As a consequence, pulse broadening and differences in the group velocities are minimised.

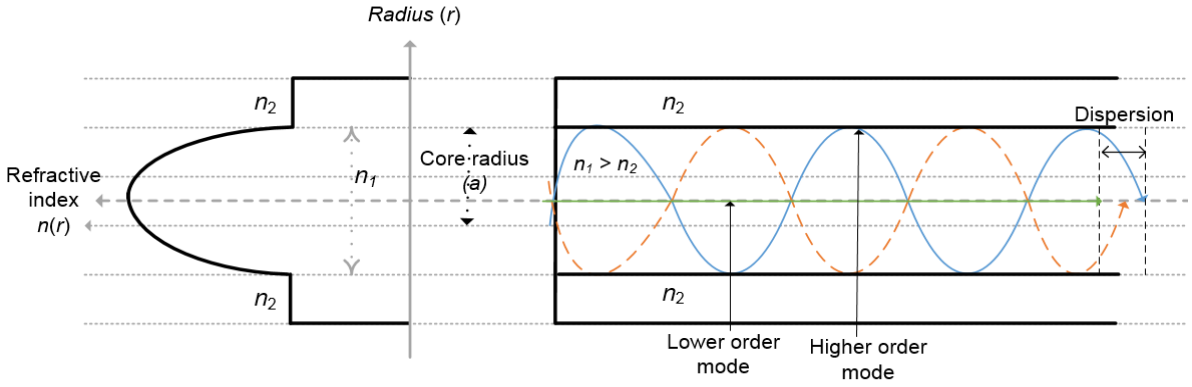

Figure 2.5: Schematic diagram showing light propagation in multimode graded index fibre. A parabolic refractive index profile ($\alpha = 2$) with a maximum at the fibre core axis is shown at the left of a figure and ray paths having different speeds and travelling along the fibre core, having radius *a,* which follow sinusoidal trajectories are shown at the right of the figure (adapted from [1]).

2.2.5.4 Refractive index profile of GI-profile

When a graded index (GI) fibre is used, there is the possibility of an increased bandwidth. The refractive index of the core follows a graded profile and continuously decreases away from the fibre axis to the cladding. The light rays traveling in a GI-MMF do not propagate in straight lines like in an SI-MMF but are constantly changing direction as they propagate. The refractive index profile $n(r)$ can be expressed as:

$$n^2(r) = n_1^2\left[1-2\Delta\left(\frac{r}{a}\right)^{\alpha}\right] \text{..... for } r \le a \tag{2.10}$$

$$n^2(r) = n_2^2 \text{ ..... for } r > a \tag{2.11}$$

where α is an index profile parameter which determines the steepness of the profile. We can characterise the refractive index profile exponent, as illustrated in Figure 2.6, into distinct cases.

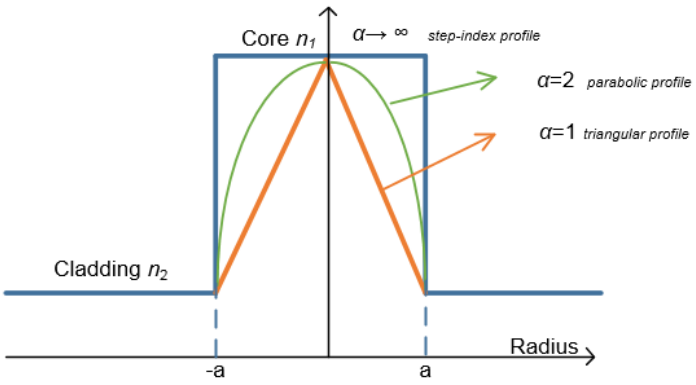

Figure 2.6: Refractive index profiles of GI-MMF fibres.

It is desirable to minimise the intermodal dispersion in a GI-MMF by careful design of the refractive index profile to create an optimum value of the graded profile parameter. This is because the GI-MMF can have a profile close to a parabolic shape which can be used to compensate the differences in path length so that each group velocity of each mode is nearly the same and so has the same propagation constant. This is the case, for example, when the graded

profile exponent is close to 2, resulting in the best profile for the reduction of modal dispersion [39].

2.2.6 The number of guided modes

The total number of bounded modes supported in a graded index fibre structure is expressed as [39]:

$$M_g = \frac{\alpha}{\alpha+2}\alpha^2 k^2 {n_1}^2 \Delta \tag{2.12}$$

$$M_g = \frac{\alpha}{\alpha+2}\frac{V^2}{2} \tag{2.13}$$

where α, as above, is the parameter that defines a characteristic refractive index profile.

Suppose $\alpha \approx 2$, the number of modes then becomes:

$$M_g \approx \frac{V^2}{4} \tag{2.14}$$

which is half the number of modes supported by a step-index fibre. In the case where $\alpha = \infty$ the number of modes in a step-index fibre is 0.5 times greater than that in a graded index fibre and so is related to the *V*-number by:

$$M_s \approx \frac{V^2}{2} \tag{2.15}$$

2.3 Physical transmission impairments in optical fibres

2.3.1 Types of dispersion

The bandwidth and dispersion are two main parameters that are strongly related due to the fact that the modal dispersion and attenuation have great impact on the achievable bandwidth as well as the distance the pulse can be transmitted. Dispersion, as a limiting factor in light-carrying capacity, can be categorised, as shown in Figure 2.7, into intermodal and intramodal dispersion. The intermodal dispersion, as its name suggests, is the difference in propagation between different modes having different group velocities and, due to their reaching the detector at different times, causing the pulse to broaden. The dispersion occurring within a single mode fibre is known as intramodal dispersion. It occurs due to the different colours of light travellings at different speeds in the material regions of the fibre [38, 40].

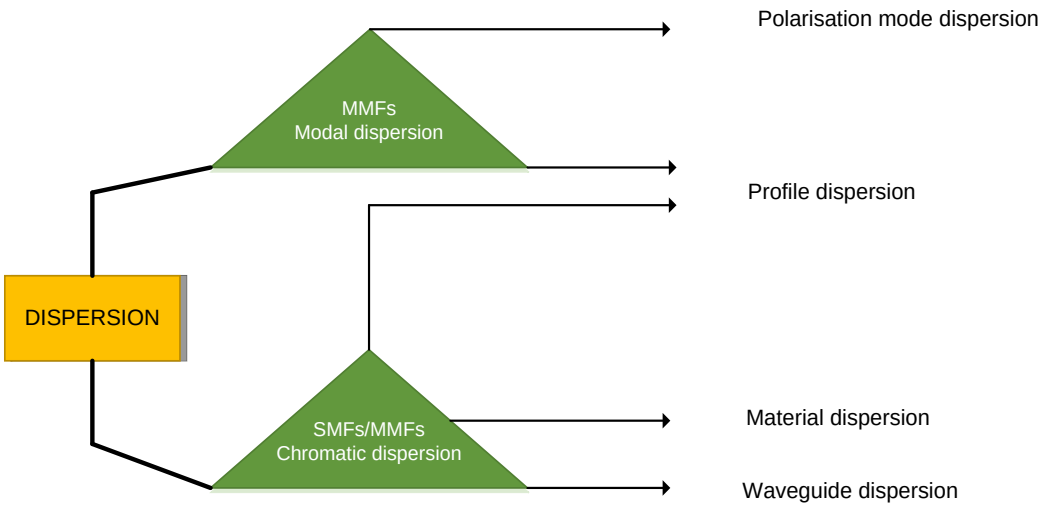

Figure 2.7: Summary the different types of dispersion in an optical fibre communication system.

The degradation of an optical signal in a fibre optic system is characterised by factors which include: signal optical attenuation; interference; and modal dispersion. The attenuation (a limiting factor in the transmission distance of light pulses) can be separated into two main categories which are intrinsic and extrinsic attenuation. Intrinsic attenuation is caused by impurities in the material of the fibre that are hard to eliminate during the manufacturing process. There are two main effects resulting from intrinsic attenuation which are: material absorption, resulting in absorption of photons as a result of imperfections and impurities in the fibre; and there is also Rayleigh scattering which is the dominant attenuation in optical fibres, accounting for 96% of the attenuation. Extrinsic attenuation can be caused by bending of the optical fibre and causes a reduction in optical power transmitted. The effects of bending have an influence on the light travelling within a fibre core and can cause ray paths to refract out of the fibre during their propagation. Thus the light moves from low-order modes to high-order modes, and is eventually radiated out of the fibre.

Modal dispersion is caused by various transverse modes with different group velocities arriving at the receiver at different times in a multimode fibre. The direct effects of this phenomenon are limitation of bandwidth and information-carrying capacity, whereas transmission length per bit rate is limited by the attenuation. Thus modal dispersion leads to an inter-symbol interference (ISI) and modal crosstalk and so must be minimised. The purpose of using GI-MMF is to overcome modal dispersion by equalising the transmission times for numerous modes. Thus the value of the refractive index profile of the fibre core must be carefully designed to produce the correct graded index profile and so the total transmission bandwidth can be increased over given transmission lengths. By working with a longer wavelength, around 1550 nm, it is possible to reduce the attenuation from 2.5 dB/km, that occurs in the 850 nm wavelength band, to 0.25 dB/km [38].

2.3.2 Key design features of fibres in order to compensate modal coupling

The independent signals are transmitted over various paths or modes and can be considered as independent channels. There is a chance of mode coupling among each mode; however, the major obstacles for MDM are differential modal group delay (DMGD) and modal coupling which are both proportional to the fibre length. Therefore, a proper design of the fibre must be addressed to overcome these unwanted effects. The optical fibres must be designed with special features in order to obtain a reduction in modal coupling and to simultaneously increase the fibre bandwidth as much as possible.

By using an appropriate spatial index profile for the fibre, particularly a parabolic shape, the DMGD can be significantly minimised for the greater number of modes being supported. It was demonstrated in experiments [15, 75] that a GI profile can reduce DMGD between the fastest and slowest modes by two orders of magnitude as compared to step-index fibres. Another approach to design an appropriate fibre is to have a strong MMF coupling between each mode to significantly reduce group delay spread. All independent data paths have an approximately equal amount of delay by travelling on the fastest and slowest modes.

To summarise, in the strong coupling regime, the DMGDs have a temporal spread scaled by the square root of the propagation distance because of a strong coupling between all propagating modes [76]. Therefore, the strong mode coupling offers several advantages in comparison with weak mode coupling in the reduction of modal group delay (MGD) spread and mode-dependent loss (MDL). By implementing the fibre with a graded index profile, and so minimising the modal dispersion effect, can thereby increase the bandwidth capacity of a multimode fibre because of a small difference in the arrival times for each of the modes. In conclusion, a GI profile of a fibre can be used to reduce DMGD between the fastest and slowest modes by two orders of magnitude as compared to step-index fibres [76, 77].

2.4 Fractional Fourier transforms

2.4.1 General background to the Fourier transform

One of the most important mathematical operators is the Fourier transform, which is used in many areas of study such as in optical physics, optical information processing and linear systems theory. In the study of linear systems, the Fourier transform is widely used for modelling optical information systems and also in image processing. In so-called Fourier optics, the optical system is analysed by Fourier methods to model geometrical optics, Fresnel diffraction, propagation by plane wave expansion, Hermite-Gaussian beams, and the fractional Fourier transform [25, 26]. The fractional Fourier transform, and its inverse transform, as a function of a continuous-time aperiodic signal can be expressed as:

$$X(f) = \int_{-\infty}^{\infty} x(t)\exp(-j2\pi ft)dt \tag{2.16}$$

$$x(t) = \int_{-\infty}^{\infty} X(f)\exp(j2\pi ft)df \tag{2.17}$$

The major significance is that the Fourier transform based on this definition can be developed to fractional orders. This extension of the Fourier transform allows application to quadratic phase systems, i.e. a quadratic graded index (GRIN) medium. Generally speaking, by using fundamental properties of the Fourier transform, we can derive a function for the case when the or^{th} order is equivalent to an integer order.

The zero order Fourier transform, denoted as $\Im^0$, corresponds to the original function or so a null transformation in the ordinary space domain. In addition to this, the first Fourier transform $\Im^1$ is what we call the conventional Fourier transform, in other words, the self-Fourier function in the spatial frequency domain. The second Fourier transform $\Im^2$ arises from the Fourier transform of the first Fourier transform, and is the same as the original function but with reversed coordinates in the space/time domain. However, in contrast,

the third Fourier transform $\Im^3$ corresponds to the same function but with reversed frequency coordinates. A self-transformation or self-reciprocal property that is equivalent to four applications of the Fourier transform operator, corresponding to its initial function, is represented as $\Im^4$ [26].

Let $f(x,y)$ be an initial function. Then we can summarise the or^{th} Fourier transform if the or^{th} order is limited in an interval [-2, 2) by the following:

$$\Im^0\{f(x,y)\} = f(x,y) \tag{2.18}$$

$$\Im^1\{f(x,y)\} = \Im\{f(x,y)\} \text{ (Common FT)} \tag{2.19}$$

$$\Im^2\{f(x,y)\} = \Im\Im\{f(x,y)\} = f(-x,-y) \tag{2.20}$$

$$\Im^4\{f(x,y)\} = \Im^2\Im^2\{f(x,y)\} = \Im^2\{f(-x,y-)\} = f(x,y) \tag{2.21}$$

2.4.2 Introduction to the fractional Fourier transform (FRT)

The basic theory of the FRT has been presented by Namias [28]. The FRT can be understood from a physical and optical viewpoint [21, 22 and 28]. It is well known as a generalisation of the classical or conventional Fourier transform with a degree of order, denoted by the or^{th} fractional transform [34, 35] where the small order or^{th} fraction is continuously increasing from zero at intermediate planes. The Fourier transform has major significance in spatial domain signal processing, and thus has a relationship with the fractional Fourier transform [28].

The conceptual ideas of the FRT have been discussed in many areas related to optical signal processing [30-35]. This is because of the fundamental Fourier transform of an object plane to a spatial frequency plane. The FRT of some fractional distance can be considered as a linear transformation in the same manner, whose angle is rotated by a degree of freedom $\frac{or_g^{th}\pi}{2}$ where or_g^{th} represents any arbitrary angle between a frequency and space domain [21]. The signal in the space domain is rotated by an angle of 90° degree into the frequency

domain where the first full Fourier transform is performed to a conventional 2*f* Fourier transform plane. A comparison between the FRT and imaging systems is described at the end of this Chapter and is illustrated in Figure 2.8.

A class of quadratic-phase systems usually has a relationship with various optical systems. The extension of an ordinary Fourier transform can be optically realised in many different configurations such as the system involving the combination of an arbitrary number of lenses separated by a sequence of free-space propagation distances or a quadratic graded index medium of a certain length [23, 35]. Moreover, it is possible to use the concept of Fresnel diffraction in order to obtain the amplitude field distribution during wave propagation through a sequence of free-space propagations between the input spatial domain and the Fourier domain; however, this approach is difficult when the medium has a variable refractive index.

The propagation of a light distribution through sections of a quadratic graded index (GRIN) medium, having a refractive index profile of the medium in a parabolic form [23, 24], must thus be treated in a different way. The amplitude field distribution at different planes can be observed through the use of the fractional Fourier transform of different fractional orders as the wavefront propagates throughout the GRIN medium. This implies that the field distributions of an input object can be investigated at many short distances during the propagation inside a quadratic GRIN medium by applying the FRT operation of an increasing order as a function of the propagation in the *z*-direction (from zero) at the input plane.

2.4.3 Notations used in the fractional Fourier transform

Generally, a FRT can be defined in mathematical terms with the GRIN medium as a physical interpretation of its use to visualise the propagation of a wavefront in an optical system. The mathematical definition also has a direct relationship to its physical meaning, in which each of the self-modes of a quadratic GRIN

medium are members of a set of the 2-D Hermite-Gaussian (HG) functions as a mode of propagation in a quadratic medium [21].

The fractional Fourier transform (FRT), a generalisation of the conventional Fourier transform, is a linear transformation that has recently been applied to optical systems. The fractional Fourier transform with an order of $or^{th} = 1$ is defined as the common Fourier transform. The or^{th} order fractional Fourier transform of a function $f(x,y)$ is denoted as $\Im^{or^{th}}\{f(x,y)\}$ or $\Im^{or^{th}} f$ in short, where the order of the transformation increases linearly with the distance of propagation. By performing a set of fractional Fourier transforms in cascade a perfect imaging system can be obtained if the initial amplitude distribution has no phase term present [21].

The FRT of an or^{th} order can be written in mathematical expression as:

$$\Im^{or^{th}}[f(x)] = \sum_m A_m \Psi_m(x) \exp(i\beta_m z) \tag{2.22}$$

where A_m is the amplitude coefficient, β_m is the propagation constant for each of the modes, z is the propagation distance (defined in the equation 2.28 below), and $\Psi_m(x)$ is the eigenmode of GI medium, and is given by:

$$\Psi_m(x) = H_m\left(\frac{\sqrt{2}x}{w}\right)\exp\left(-\frac{x^2}{w^2}\right) \tag{2.23}$$

where H_m is a Hermite polynomial of order m and w is a constant parameters associated with the quadratic GI medium, described as:

$$w = \sqrt{\frac{\lambda}{\pi}}\left(\frac{n_1}{n_2}\right)^{1/4} \tag{2.24}$$

It is interesting to discuss some boundary properties and characteristics of the fractional Fourier transform of any arbitrary order [26, 27]:

a) The fractional Fourier transform is a linear transformation operator, the same as the Fourier transform.

b) The Fourier property: the FRT is considered to be the first Fourier transform at an ordinary frequency domain if its order is equivalent to one ($\Im^{or^{th}} f$ where the or^{th} order = 1), and is defined as:

$$\left(\Im^{1} f(x,y)\right)(x',y') = \int_{-\infty}^{\infty}\int_{-\infty}^{\infty} f(x,y)\exp\left[\frac{-i2\pi(xx'+yy')}{s^{2}}\right]dxdy \tag{2.25}$$

where all variables have the dimension of length and $s^2 = \lambda f$. The λ is the wavelength of the illuminating wavefront and f is the focal length of the lens in a $2f$ optical system. In addition to this, the $\Im^{0} f(x,y)$ corresponds to the zero order of a given function or the original function at an ordinary space domain plane.

c) The index additive property (the semigroup property) is:

$$\Im^{a1}\Im^{a2} f(x) = \Im^{a1+a2} f(x) = \Im^{a2}\Im^{a1} f(x) \tag{2.26}$$

For example, a 0.3rd FRT of a 0.5th FRT is equal to a 0.8th FRT or, as another example, a 2.1st of a 1.6th of a 0.4th FRT is equal to a 4.1st FRT that is equivalent to 0.1st FRT, where the 4th FRT or $\Im^{4}\{f(x)\} = f(x)$.

d) The negative order (-or^{th}) is a conjugate of the kernel of its positive order (+or^{th}) transform such that:

$$B^{-or}(x,x') = B^{+or}(x,x') \tag{2.27}$$

2.4.4 The fractional Fourier transform in optics

Due to the properties of the GRIN medium, combining self-focusing and propagation, the input signal is repeated over an arbitrary distance that is identical to the repeated application of a Fourier transform four times to reproduce a real image [26] and one quarter of this propagation distance one observe the Fourier plane [30]. In addition to this, a 2-D Fourier transform of an input field corresponds to the field amplitude observed at multiple distances of a desired Fourier length of the propagation. The propagation of a parallel bundle rays in a quadratic graded index media usually exhibit circular trajectories in the phase space domain.

Mendlovic and Ozaktas [21, 22] defined a FRT as a new mathematical tool in optics by its use as a means of calculating propagation in a quadratic GRIN medium, in which a continuous fractional Fourier transform can be implemented in an optical system. A physical interpretation of the FRT can be obtained and developed to explain the propagation of a wave in such a medium. A non-integer order of FRT at each small distance within a graded (GRIN) medium, where its refractive index varies from point to point, can be found in the plane between the spatial domain and the ordinary Fourier transform plane so allowing one to observe what happens between these planes. When the light propagates inside a quadratic GRIN medium, an input field distribution will perform a common Fourier transform at a specific length of graded index fibre. This thus results in the same distribution as in the far-field free-space diffraction.

A continuous monotonically evolving FRT can be thought of as the solution of the wave propagation problem. The evolution of the light as it propagates through an optical system can in general be realised by the generalisation of the Fourier transform of a fractional order, which increases linearly with the propagation distance. As the light propagates, one can observe the field pattern at closer distances in the form of a FRT of a diffracting object while in the far-field of the diffraction pattern one can observe the Fourier transform of the diffracting object (where the or^{th} order is 1). In general, the FRT

can be achieved by means of the wave propagation through a graded (GRIN) medium with variation of index of refraction. Moreover, the ordinary Fourier transform is accomplished at a certain distance as the light evolves and the amplitude field distributions at any particular plans are effectively obtained from the FRT method between the input plane and Fourier plane along the GRIN medium at different transform orders.

To fully exploit the FRT of fractional order or^{th}, the length of the fibre is sectioned into small pieces of length L. Throughout the system, one observes first an ordinary Fourier transform at the length L of the medium since the medium is uniform in the direction of propagation. Then one observes an inverted image at length $2L$, then an inverted Fourier transform at $3L$ and finally an erect image will be observed at a length of $4L$ from an input plane. This concept is similar to the operation of the Fourier transform as discussed in Section 2.4.1. Such amplitude field distributions appear in between these planes, where the numbers 2, 3 and 4 correspond to a fractional order a, at different points along the optical axis throughout the system at multiple lengths of L. It is concluded that the diffraction pattern of an or^{th} order FRT from 0 to 1 is observed within a distance L from the diffracting aperture at a reference plane where the distance of propagation increases from zero to infinity (i.e. the length of the medium).

2.4.5 Self-imaging length intervals

An inhomogeneous medium has a refractive index which is constantly changing which results in propagating beam delays all the way along the fibre. Conversely, for a propagation through a section of free-space, the calculations do not have to take account of refractive index changing since it is constant. For all these reasons, we assume that the refractive index profile is constant for a short distance and continuously modify the refractive index after each step to calculate an approximation to the FRT. The index profile of the fibre is applied on the wavefront which is then propagated in a small step, and therefore an approximation can be made at each point as the beam propagates. The process

is repeated again by taking a new step forward and applying the refractive index profile again.

The properties of the wave front propagation in the GRIN medium can be examined by means of its fractional transforming property. Self-focusing, propagation and re-focusing are properties that can be investigated within the medium. The self-imaging of the system can be understood through a series of applications of the FRT. This is because a quadratic graded index fibre is optically aligned along the propagation direction of the guided wavefront that gives a physical interpretation of the FRT in optical communication systems [21-24]. As the light propagates, it is simply fractionally Fourier transformed resulting in a fractional transform of order or^{th}, increasing with the direction of propagation. The amplitude field distributions can be observed in any fractional plane, described as:

$$z = (or^{th})L \tag{2.28}$$

where L is the physical length of a quadratic GRIN medium that results in a Fourier transformation, and is given by:

$$L = \frac{\pi}{2}\sqrt{\frac{n_2}{n_1}} \tag{2.29}$$

where n_1 and n_2 are the refractive indices of the fibre core.

This implies that the propagation inside a GRIN fibre performs a fractional transform until a parallel bundle of light can be observed at the ordinary Fourier transform plane where or^{th} is equivalent to one. A full Fourier transform of an input object, i.e. a distance of $z = L$ from the input plane, corresponds to a rotation of an input object by $\frac{\pi}{2}$, in which the field is uniformly distributed throughout the system [21, 22].

The physical interpretation of light propagation is that an input object is coupled into a GI-MMF at certain distances. During the propagation inside a quadratic GRIN medium, the FRT operation is applied, and the field distribution

of an input object is coupled out again at the end of the fibre. As presented in Figure 2.8 (a), the input image will go through a frequency plane at some point over a distance, $z = or^{th}L$ where L can be determined from (2.26), and over another distance, $z = or^{th}L$, be returned to the spatial domain, i.e. an image plane (but with reversed axes); thus the image reconstruction should be recovered again at twice the Fourier length of propagation, i.e. $z = 2L$ and the process repeats again for the total length of $2Ln$ of the fibre, where n is a number of transformations where the light rays will be focused to reproduce the input signal. The field incident upon the Fourier plane is basically a Fourier transform of the incident electromagnetic field from the source. The field incident upon the imaging plane can be thought of as a Fourier transform of the spatially modulation of field distribution in the Fourier plane. In order to obtain a reconstruction of an image (a reciprocal image), it is therefore necessary to arrange the fibre to be multiple of the length $2L$.

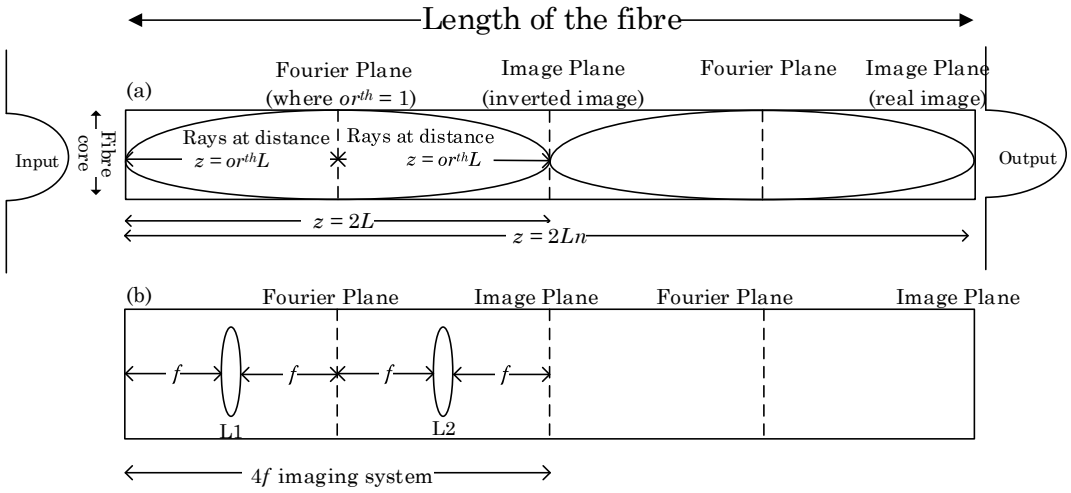

Figure 2.8: Physical configurations of light propagation for: (a) the transformation of the spatially multiplexed signal inside a quadratic graded index medium; and (b) the operation of wave evolution in a 4*f*-imaging system. L1 and L2 represent the first and second lens, respectively.

To compare the behaviour of light propagation with a conventional imaging system, as shown in Figure 2.8 (b), the FRT of fractional distances can be considered as a linear transformation in the same manner, whose angle is rotated by a degree of freedom $\frac{(or_g^{th})\pi}{2}$, where or_g^{th} represents any arbitrary number or fractional order between a frequency and space domain and increases with the propagation distance [14].

Table 2.1

Summary of the self-imaging length intervals for wave propagation in a quadratic graded index medium and in conventional imaging systems.

Propagation distance	**Periods over axial distance**	**The region represented in a 4*f* Fourier-transforming system**
$z = L$	$\frac{\pi}{2}$	$z = 2f$
$z = 2L$	π	$z = 4f$
$z = 4L$	2π (a full wave period)	$z = 8f$

The self-imaging length intervals that appear in a traditional imaging system and in a quadratic graded index medium are summarised in Table 2.1. For a propagation distance to a $2f$ distance, at which the light rays are focused by the lens, corresponds to a distance where the field inside a GI medium has undergone the first full Fourier transform (i.e. where $z = L$) with a uniform distribution throughout the system. Thus the reconstruction of the original object inside a GI medium (i.e. at the imaging plane where $z = 2L$) is equivalent to a $4f$-Fourier transforming distance with passage through the two Fourier lenses.

Chapter 3

Model analysis and excitation with different fibre parameters

3.1 Introduction

In this section, we describe the design concepts and analysis of graded index fibre. One of the most effective index profiles, to realise the reconstruction of an initial input beam distribution and light guiding along the optical axis, is a quadratic refractive index profile (lens-like structure). A reproduction of the beam arrives in a natural way periodically at the optimum distance through a parabolic graded index profile structure. The self-imaging distance will be explored in more detail later in the chapter whilst discussing the fractional Fourier transform.

We modelled commercial available optical fibres using the FIMMWAVE mode solver by PhotonDesign™ to evaluate the modes of a multimode fibre from the calculated effective refractive index and normalised propagation constant of the particular modes. Then the analysis of an optical pulse was performed using the FIMMPROP program to visualise the excited modes inside the MMFs. In our simulations, we assign different types of fibres according to their specifications. Table 3.1 shows the key multimode fibres with a quadratic index profile and a step index profile at a 1.55 μm operating wavelength. These fibres are excited with the same launching condition where the initial beam widths are calculated analytically to support different fibre interfaces.

Table 3.1

The specific parameters of multimode fibres used in the simulations at λ = 1.55 μm

	Geometrical Specification			
Fiber Name	GIF50C	GIF625	F-MLD	FG050LGA
Manufaturer	Thorlabs	Thorlabs	Newport	Thorlabs
Index Profile	Graded	Graded	Graded	Stepped
Fibre Type	MMF	MMF	MMF	MMF
Core diameter	50 ± 2.5 μm	62.5 ± 2.5μm	100 ± 4 μm	50 ± 2%
Cladding diamter	125 ± 1 μm	125 ± 1 μm	140 ± 3 μm	125 ± 1 μm
Numerical Aperture	0.2	0.275	0.29	0.22

3.2 Basic electromagnetic wave

Light is referred to as an electromagnetic spectrum due to the fact that it propagates in the form of two vector fields, namely the electric E and magnetic H field. An electromagnetic wave mode theory is considered as a model for light propagation in an optical fibre. Maxwell's equations allow solution of the electromagnetic wave propagation problem in optics. The relationship between four vector fields as curl equations is given by Maxwell's equations in vector form [38]:

$$\nabla \times E = \frac{-\partial B}{\partial t} \tag{3.1}$$

$$\nabla \times H = \frac{\partial D}{\partial t} \tag{3.2}$$

$$D = \varepsilon E \tag{3.3}$$

$$B = \mu H \tag{3.4}$$

where D is the electric flux density, B is the magnetic flux density, ε is the dielectric permittivity and μ is the magnetic permeability.

Substituting from the vector identity: $\nabla \times (\nabla \times E) = \nabla(\nabla \cdot E) - \nabla^2 E$ we have:

$$\nabla \times (\nabla \times E) = -\mu\varepsilon \frac{\partial^2 E}{\partial t^2} \tag{3.5}$$

$$\nabla \times (\nabla \times H) = -\mu\varepsilon \frac{\partial^2 H}{\partial t^2} \tag{3.6}$$

then Eq. 3.5 and 3.6 can be written as a non-dispersive wave equation:

$$\nabla^2 E = \mu\varepsilon \frac{\partial^2 E}{\partial t^2} \tag{3.7}$$

$$\nabla^2 H = \mu\varepsilon \frac{\partial^2 H}{\partial t^2} \tag{3.8}$$

The scalar wave equation is given by:

$$\nabla^2 \psi = \frac{1}{v_p^{\,2}} \frac{\partial^2 \psi}{\partial t^2} \tag{3.9}$$

where ψ is a component of the electric and magnetic fields and the phase velocity is:

$$v_p = \frac{1}{\sqrt{\mu\varepsilon}} \tag{3.10}$$

$$c = \frac{1}{\sqrt{\mu_0 \varepsilon_0}} \tag{3.11}$$

Rearranging:

$$\left(\nabla^2 - \frac{1}{c}\frac{\partial^2}{\partial t^2}\right)\psi(r,t) = 0 \tag{3.12}$$

where $\psi(r,t) = \mathrm{Re}\{\psi(r)\exp(-jwt)\}$ and substituting $w^2 = c^2 k_0^2$, where w is an angular frequency of the field and k_0 is defined as the propagation vector or the rate of change of the phase with distance r at a point where the field is observed.

It is also referred to as the free-space wave number or propagation constant for light in a vacuum and is defined by:

$$k_o = \frac{2\pi}{\lambda_0} = \frac{w}{c} \tag{3.13}$$

Then the time invariant Helmholtz equation can be derived which depends on the position of r:

$$(\nabla^2 + k^2)\psi(r) = 0 \tag{3.14}$$

For a planar waveguide, which can be described by both rectangular and cylindrical polar coordinates, the Laplacian operator ∇^2 takes the following forms.

For rectangular Cartesian coordinates (x, y, z):

$$\nabla^2\psi = \frac{\partial^2\psi}{\partial x^2} + \frac{\partial^2\psi}{\partial y^2} + \frac{\partial^2\psi}{\partial z^2} \tag{3.15}$$

For cylindrical polar coordinates (r, ϕ, z):

$$\nabla^2\psi = \frac{\partial^2\psi}{\partial r^2} + \frac{1}{r}\frac{\partial\psi}{\partial r} + \frac{1}{r^2}\frac{\partial^2\psi}{\partial \phi^2} + \frac{\partial^2\psi}{\partial z^2} \tag{3.16}$$

The plane wave is guided along the direction of propagation in the z-direction. As the mode propagates along the z-direction, it has a periodic form of $\exp(-j\beta_z z)$ where β_z is the phase propagation constant in the z-direction, and is the time dependence for the electromagnetic field of the form $\exp(jwt)$. The mode can then be described by $\exp(j(wt - \beta_z z))$.

Referring to a cylindrical polar coordinate waveguide, the scalar wave equation can be written in the form of [1, 38, 49]:

$$\frac{\partial^2\psi}{\partial r^2} + \frac{1}{r}\frac{\partial\psi}{\partial r} + \frac{1}{r^2}\frac{\partial^2\psi}{\partial \phi^2} + (n_1^2 k^2 - \beta^2)\psi = 0 \tag{3.17}$$

where n_1 is the refractive index of the core. A number of guided modes can be viewed as a ray of light, dependent on both the physical parameters (variation of refractive indices, core radius etc.) and wavelength to be guided through the core region over the entire fibre length.

3.3 Mathematical model for guided modes in optical fibres

The linearly polarised (LP) modes are transverse modes in both polarisations and are two complete independent set of modes in the *x* and *y* directions. An Eigenvalue equation for the characteristic equation of a weakly guiding fibre (i.e. $\Delta<<1$) can be written in the form [50]:

$$U\left[\frac{J_{m\pm1}(U)}{J_m(U)}\right] = \pm W\left[\frac{K_{m\pm1}(W)}{K_m(W)}\right] \qquad \begin{cases} \dfrac{J_{m+1}(U)}{J_m(U)}, 0 \le r \le a \\ \dfrac{K_{m+1}(W)}{J_m(W)}, r > a \end{cases} \tag{3.18}$$

where $U = V\sqrt{1-b}$ and (3.19)

$$W = V\sqrt{b} \tag{3.20}$$

The parameter V is defined in equation (2.6) as a normalised frequency. The $J_m(U)$ describes the propagating field within a core of the fibre as a Bessel function of the first kind, of order *m* and $K_m(W)$ is the modified second kind of Bessel function of order *m*, describing the field distribution within the cladding which monotonically decreases as the radial distance increases further away from the axis with faster velocity [1, 38, 50].

Substituting equation (2.6) in (3.19) and (3.20) and rearranging equation (3.18) to derive the solution of various modes:

$$V(\sqrt{1-b})\left[\frac{J_1\left(V(\sqrt{1-b})\right)}{J_0\left(V(\sqrt{1-b})\right)}\right] = \pm V\sqrt{b}\left[\frac{K_1\left(V(\sqrt{b})\right)}{K_0\left(V(\sqrt{b})\right)}\right] \ldots\ldots\ldots\ldots\ldots\ldots m = 0 \qquad (3.21)$$

for a fundamental mode, and:

$$V(\sqrt{1-b})\left[\frac{J_{m-1}\left(V(\sqrt{1-b})\right)}{J_m\left(V(\sqrt{1-b})\right)}\right] = \pm V\sqrt{b}\left[\frac{K_{m-1}\left(V(\sqrt{b})\right)}{K_m\left(V(\sqrt{b})\right)}\right] \ldots\ldots\ldots\ldots\ldots\ldots m > 1 \qquad (3.22)$$

for higher-order modes.

Since the relative refractive index difference between the media is relatively small ($\Delta << 1$) in a weakly guiding approximation of an optical fibre, the modes are expected to travel along the core and this guiding condition is said to be totally internally reflected. The value of Δ is typically less than 0.03 (3%) for communications in optical fibre systems. Assuming that multiple guided modes undergo total internal reflection, any set of conventional modes (HE, EH, TE and TM) that have an identical propagation constant and effective refractive index can be grouped together as a single mode. Thus, the degeneracy between modes exists in which these groups of modes travel with the same speed. It is, therefore, convenient to represent these degenerate modes of electromagnetic fields in the form of the linearly polarised (LP_{mn}) modes. The subscripts *m* and *n* are regarded as the electric field around the core circumference and in the radial direction, respectively. In Table 3.2 below is shown a comparison between the traditional designation modes and the linearly polarised modes, together with the number of degenerate modes for the first ten lower-order modes [1, 38, 49].

The rules for grouping these conventional modes to LP modes are as follows [50, 51]:

$$LP_{0n}\ (m = 0) = HE_{m+1,n} \tag{3.23}$$

$$LP_{mn}\ (m = 1) = HE_{m+1,n}\ ,\ TE_{0,n}\ \text{ and } TM_{0,n} \tag{3.24}$$

$$LP_{mn}\ (m > 1)\ = HE_{m+1,n}\ ,\ EH_{m-1,n} \tag{3.25}$$

Table 3.2

A comparison between the traditional designation modes and the linearly polarised modes

Designation of LP_{lm} modes	Designation of conventional mode	Degenerate modes
LP_{01}	HE_{11}	2
LP_{11}	HE_{21} , TE_{01} , TM_{01}	4
LP_{21}	HE_{31} , EH_{11}	4
LP_{02}	HE_{12}	2
LP_{31}	HE_{41} , EH_{21}	4
LP_{12}	HE_{22} , TE_{02} , TM_{02}	4
LP_{41}	HE_{51} , EH_{31}	4
LP_{22}	HE_{32} , EH_{12}	4
LP_{03}	HE_{13}	2
LP_{51}	HE_{61} , EH_{41}	4

Based on the fact that n_1 approaches n_2, each of the degenerate modes is formed into one single linearly polarised mode. The LP_{mn} modes can also be considered an alternative way for naming the group of modes, propagating into an optical fibre where the fields are polarised linearly with the same polarisation orientations. The solutions of a propagation constant β can be determined analytically from the effective refractive index n_{eff} by:

$$\beta = \frac{n_{eff}^2 - n_{clad}^2}{NA^2} \tag{3.26}$$

For the requirement of the propagation modes guided in the core and minimising the radiation modes, the normalised propagation constant should satisfy the following boundary condition:

$$n_{clad}k_0 \leq \beta \leq n_{core}k_0$$

$$n_{clad} \leq n_{eff} \leq n_{core} \tag{3.27}$$

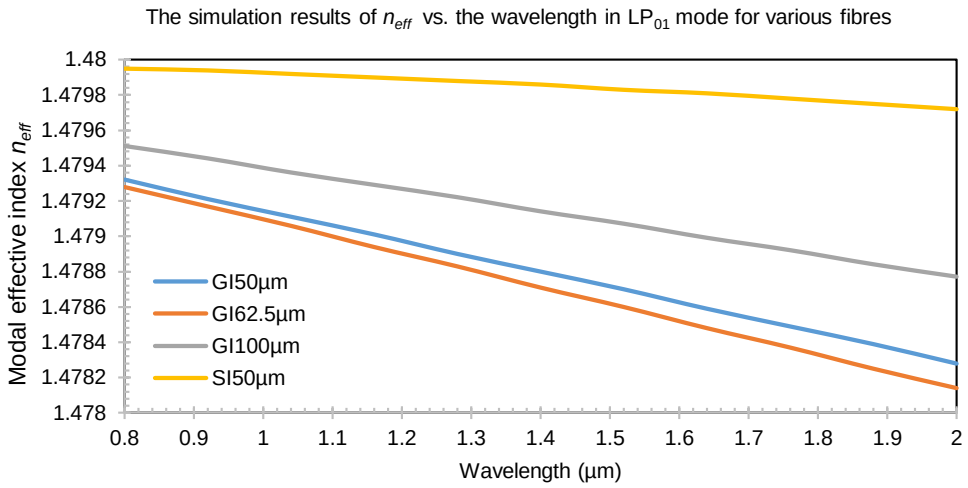

Figure 3.1: Modal effective index n_{eff} as a function of the wavelength for the fundamental mode LP_{01} in various fibres at different core diameters and index types in a range from 800 nm to 2000 nm.

The graph in Figure 3.1 shows the results of the simulations that are in agreement with the theoretical studies in that the value of relative refractive index n_{eff} of the mode is inversely proportional to wavelength. We see that the n_{eff} values tend to decrease at the higher wavelengths. However, as indicated in equation (3.27), the lowest value of n_{eff} should be kept in the range of the index of the lowest medium in order to avoid the unguided modes.

Thus light is guided by the total internal reflection (TIR) inside a fibre core with a higher index. The guided modes are totally internally reflected at the core-cladding boundary with a different propagation constant β that is defined as the product of the index of refraction and the light propagation constant in vacuum $k_0 \left(\beta = n_1 k_0\right)$ and is used to determine the variation of light in both amplitude and phase in the *z*-direction of propagation. The spatial modes are considered as the number of *M* modes in a fibre corresponding to $\frac{M}{2}$ linearly polarised modes (LP) in the weakly guiding approximation. As mentioned, the larger number of modes can be accommodated with an increasing cross-sectional area which will support the fundamental mode, LP_{01}, and other degenerate modes.

In order to generate higher order modes, the fibre diameter is increased up to a point above the single-mode condition with the normalised frequency *V* of 2.405. The MMF can support three spatial modes, namely LP_{01}, LP_{11a} and LP_{11b} if the light is guided with no more than the triple-mode condition below the normalised frequency of 3.8. The LP_{mn} modes in principle each have two-fold degeneracy of polarisation mode in *x* and *y*. The number of maxima of the field corresponds to the subscript $2m$ around the circumference of the fibre core whereas the subscript n ($n \neq 0$) is used to label the number of field maxima around the fibre radius [38]. For LP_{mn} (m>1), there are four degenerate modes, namely $LP_{mn,a}$ and $LP_{mn,b}$ in both parallel and perpendicular polarisation, respectively [41].

More fundamentally, the main issues of using multimode fibres in a system is that various modes have their own propagation constant and result in a transmission delay. However, there is an exception for a special characteristic of fibres with a graded index profile ($\alpha = 2$). In such a fibre system a desired LP_{mn} modes can be grouped into the same principle mode groups (MG), sharing almost identical degenerate phase constants and propagation delays. The mode group of order MG fulfils the following order [41]:

$$MG = m+2n+1 \tag{3.28}$$

Table 3.3

Principle of spatial groups of modes MG having two polarisations

Mode Group (MG)	**Modes**
3	LP_{01}
4	LP_{11a} , LP_{11b}
5	LP_{02} , LP_{21a} , LP_{21b}
6	LP_{12a} , LP_{12b} , LP_{31a} , LP_{31b}
7	LP_{03} , LP_{22a} , LP_{22b} , LP_{41a} , LP_{41b}
8	LP_{13a} , LP_{13b} , LP_{32a} , LP_{32b}, LP_{51a} , LP_{51b}
9	LP_{04} , LP_{23a} , LP_{23b} , LP_{42a}, LP_{42b} , LP_{61a}, LP_{61b}

Table 3.3 shows the list of degenerate modes, which can be grouped together for the first seven groups of modes MG = 3 to MG = 9 of a preferably parabolic graded index multimode fibre. Because each of the modes has the same propagation constant value, then they can be grouped together within the same mode group MG, experiencing approximately the same propagation delay for realising high communication bandwidth performance.

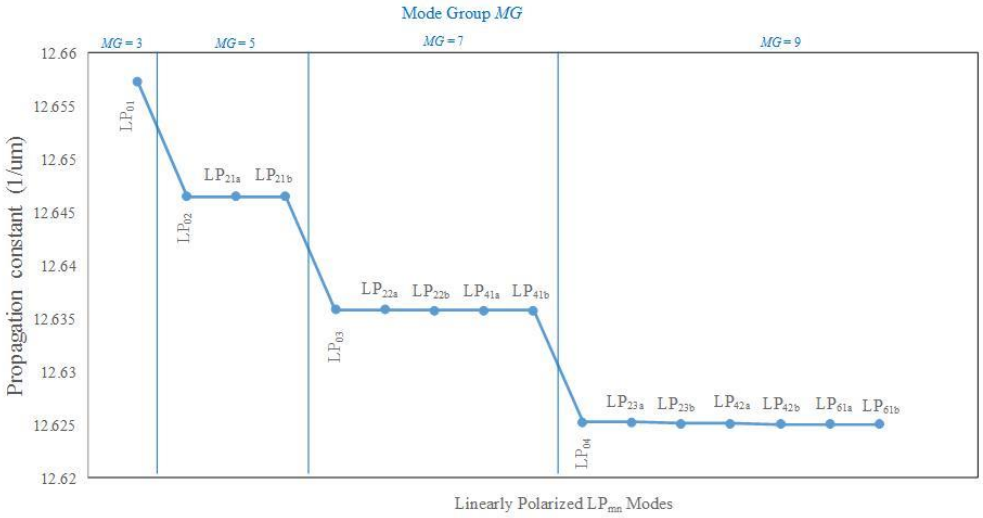

Figure 3.2: The propagation constant of the first seven LP_{mn} modes and their correspondence mode group number, simulated using a standard commercial GI50µm fibre at a wavelength of 1550 nm.

The simulation graph shown in Figure 3.2, obtained from the transmission of a GI50µm operating at a 1.55 µm wavelength, clearly shows the theoretical prediction (as shown in Table 3.3) of the first seven LP_{mn} modes. It can be seen that all the degenerate modes having an identical phase constant can be combined together into the same principal mode groups (MG), corresponding to an MG of 3, 5, 7 and 9. For instance, the MG = 5 contains 3 spatial orthogonal modes, which comprise all degeneracies and both polarisations (parallel and perpendicular) in the modes of LP_{02}, LP_{21a}, and LP_{21b}. This corresponds to a total of six data streams, which could provide a relatively high transmission bandwidth if employed together [41].

The modes within the same MG are strongly coupled to each other due to the identical propagation constant (small $\Delta\beta$), while the modes in different MGs are weakly coupled since the propagation constant spacing between each MG is relatively large (large $\Delta\beta$). As a result of strong coupling of the modes in the same MG, the maximum power can be achieved after propagating for a short distance. This is because if we selectively launched any particular mode, more power will be coupled to other modes within the same group of the modes [17]. Moreover,

there also exists the solution to enhance the capacity of the optical fibre by selectively exciting groups of modes as spatially separated transmission channels. It is expected that by increasing a number of spatial modes in a few-mode fibre, the channel capacity can be potentially maximised by a factor proportional to the number of modes [42-45].

3.4 Modal excitation condition

There are a number of ways to couple the light in multimode fibre systems, for example, based on multimode interference MMI devices (see the detail in section 3.7.1) or by directly launching onto the front face of a device. The former case is effective for use in self-imaging by using a coherent light source [46, 47] in which the device has N input guides and M output guides for launch and recovery onto a central multimode waveguide. However, in our case, we will examine the latter case, assuming that the beam is well aligned with the fibre axis. The variation of the electric field in a Gaussian beam is given by [38]:

$$E = E_0 \exp\left(-\frac{r^2}{w^2}\right) \tag{3.29}$$

where r is a distance from the centre of the beam to the propagation axis. The parameter w is defined as the beam radius at which the field amplitude drops to the 1/e point from its maximum peak on-axis amplitude. This parameter is also known as the beam waist or radius of the beam, measuring from the waist of the beam at which the phase of the wavefront is plane.

The beam width or radius $w(z)$ at any z-position is given by:

$$w(z)^2 = w^2\left[1+\left(\frac{\lambda z}{\pi n w^2}\right)\right] = w_o{}^2\left[1+\left(\frac{z}{z_o}\right)^2\right] \tag{3.30}$$

where n is the refractive index in the medium the beam is propagating through and z_0 is a point where the beam starts to diffract from the plane phase wavefront which is defined as:

$$z_0 = \frac{\pi n w^2}{\lambda} \tag{3.31}$$

Close to the beam waist the beam does not spread out greatly. The distance from the waist to the Rayleigh length, z_R, the width of the beam along the propagation direction increases by a factor of $\sqrt{2}$, i.e. $w(z) \cong \sqrt{2}w$.

From equations (3.28-3.30), we can determine the radius of curvature as:

$$R(z) = z\left[1 + \left(\frac{\pi n w^2}{\lambda z}\right)^2\right] = z\left[1 + \left(\frac{z_o}{z}\right)^2\right] \tag{3.32}$$

Now we wish to find the amount light that propagates along an optical axis, by defining a Gaussian intensity distribution of the source as shown in Figure 3.3, and expressed by the following equation:

$$I(r) = I_o \exp\left(-\frac{2r^2}{w^2}\right) = \frac{2P}{\pi w^2}\exp\left(-\frac{2r^2}{w^2}\right) \tag{3.33}$$

where P is the total power in the beam and w in this expression is defined as the beam radius at which the intensity has dropped to the $1/e^2$ point of its peak value or approximately to 13.5% of the peak power on the propagation axis.

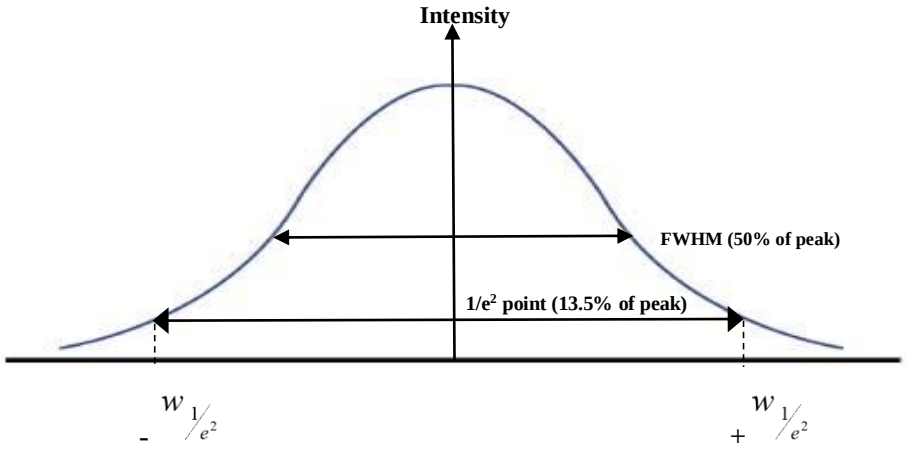

Figure 3.3: Gaussian beam intensity profile

The radius of the beam waist is sometimes measured at different levels, and is represented as:

$$w(1/2) = 0.588 \times w(1/e^2)$$

$$w(1/e) = 0.707 \times w(1/e^2) \tag{3.34}$$

The parameter $w(1/e)$ is referred to a radius at which the intensity has decreased to 0.707 at the 1/e point, and $w(1/2)$ is known as the intensity at the half width at half maximum point. The beam diameter at the $1/e^2$ intensity point is 10 μm for all the simulations conducted in this thesis.

3.5 The transmission analysis in MMF structures

The analysis of electromagnetic fields in MMF structures of all modes will be exploited, by assuming that only the guided modes will be excited in the structure. Each mode is a pattern of the electric and magnetic field distributions, which are repeated periodically along the direction of propagation at equal intervals, corresponding to a self-imaging of the intensity pattern of light. The repetition of the field in graded index fibres is defined as a self-imaging characteristic of an input intensity pattern, which propagates along the length of the fibre. In fact, each mode has its own propagation constant and it

propagates at different velocities. However, because of an oscillatory behaviour between different modes each of which propagate with different propagation constants, they interfere with each other as a result of multimode interference inside the fibre [47].

We use the modal field derived in references [48, 49, 50, and 51] for a two-dimensional Eigenmode that propagates in the *z*-direction with its corresponding propagation constant for each propagation mode:

$$\Psi_{mn}(x,y,z) = \sum_{v=1}^{N} c_v \Psi_v(x,y) \exp(i\beta_v z) \tag{3.35}$$

where c_i is the amplitude coefficient of each Eigenmode and N is the number of Eigenmodes. Equation (3.35) shows the solution of Maxwell's equation in the form of a modal cross-section describing the guided and radiation modes within a waveguide. The modal profile $\Psi_v(x,y)$ is said to be the Eigenfunction while the Eigenvalue describes the propagation constant in the modal field.

The initial field profile $\Psi(x,0)$ at distance $z = 0$ is decomposed into a sum of individual modal field distributions $\Psi_v(x)$ of all guided modes:

$$\Psi(x,0) = \sum_{v=1}^{V\max} c_v \Psi_v(x) \tag{3.36}$$

where c_v is the coefficient of the field excitation with v^{th} number of guided modes with $v = 1,....,V_{\max}$. We assume that the input field $\Psi(x,0)$ is decomposed only for the guided modes which can be written as:

$$c_v = \frac{\int \Psi(x,0)\Psi_v(x)dx}{\sqrt{\int \Psi_v^2(x)dx}} \tag{3.37}$$

The field distribution profile at some particular distance *z* can be written as:

$$\Psi(x,z) = \sum_{v=0}^{V\max-1} c_v \Psi_v(x) \exp\left[j(\beta_0 - \beta_v)z\right] \tag{3.38}$$

From the explanation in references 47 and 52, the propagation constant spacing between the different modes can be written as:

$$\beta_0 - \beta_v \approx \frac{v(v+2)\pi}{3L_\pi} \tag{3.39}$$

where the propagation constant of mode v is in the form:

$$\beta_v \approx k_0 n_1 - \frac{(v+1)^2 \pi \lambda_0}{4 n_1 \phi_{core}^2} \tag{3.40}$$

where the beat length L_π is defined as:

$$L_\pi \approx \frac{4 n_1 \phi_{core}^2}{3\lambda_0} \tag{3.41}$$

The initial field at $z = 0$ will be reimaged at some distance $z = 2L$ and then the field becomes:

$$\Psi(x, L) = \sum_{v=0}^{V\max -1} c_v \Psi_v(x) \exp\left[j(\beta_0 - \beta_v)L\right] \tag{3.42}$$

It is clearly seen from the field distribution at $z = L$ that the input field will be regenerated if the condition obeys:

$$\exp\left[j(\beta_0 - \beta_v)L\right] = 1 \tag{3.43}$$

The input field is reproduced at a specific length inside a multimode fibre as long as the condition between the two excited modes is satisfied by:

$$(\beta_0 - \beta_v)L_{img} = m_v 2\pi \tag{3.44}$$

where m_v is an integer.

Thus the initial amplitude and phase between guided modes will be retrieved at the fibre locations at which the self-imaging peaks are observed, and then self-imaging appears at the position [52]:

$$L_{img} = \pi \frac{n_{core} a}{\sqrt{n_{core}^2 - n_{clad}^2}} \tag{3.45}$$

where a is the core radius of the fibre. The term in (3.45) satisfies the self-imaging condition for the excitations of modal fields in a parabolic index fibre. A periodic reimaging thus occurs, in which an input field is duplicated at specific positions repeating along the length of propagation in the multimode fibre. Based on the study of self-imaging in the transverse plane, our proposed configurations, with different numbers of optical sources, are thus investigated with the emphasis being on graded index optical fibres where the image reconstruction is dependent upon the refractive index profile of the guiding medium.

3.5.1 Variation of the intensity distributions in multimode fibres

The beam can be described in terms of the propagating field inside the fibre. In order to simulate the propagation beam inside a single core multimode fibre, we assume that an initial beam is launched onto the face of the fibre on the optical axis and we observe several LP_{mn} modes transmitted in a section of the multimode fibre.

Table 3.4

The comparison of a number of modes in different commercial fibres

Index Type	Graded	Graded	Graded	Step
Core Diameter	50µm	62.5µm	100µm	50µm
NA	0.2	0.275	0.29	0.22
Normalised frequency, V	20.26	34.82	58.75	22.28
Number of modes, M	103	303	863	248

The maximum number of allowed modes, M, that can be propagated with different fibre core diameters, is calculated numerically in Table 3.4 using equations (2.14) for graded index (GI) fibre and (2.15) for step-index (SI) fibres. There are more than twice the number of modes in a SI fibre as compared to a GI type, with similar core size. Moreover, it is evidently shown that the dependence of the number of propagation modes on the normalised frequency (*V*-number) is linearly proportional to the core diameter size. The larger the size of a core, the greater the number of modes that can be transmitted through a fibre. The study by Fertman and Yelin [53] shows the effects of increasing the number of modes in a multimode fibre. It shows that fine details of a transmitted image and its quality would be possible with a larger diameter fibre because the high spatial frequencies are found in the higher order modes.

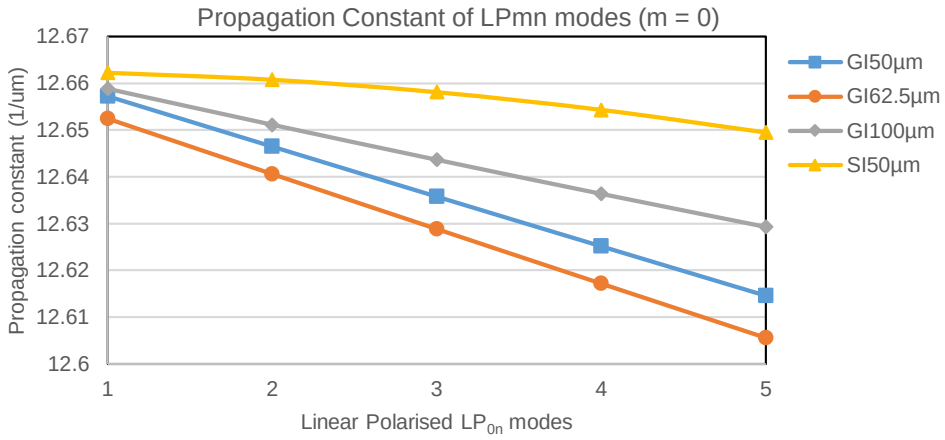

Figure 3.4: A comparison of the propagation constants for the scalar mode groups in four different commercial fibres with a variety index types and core dimensions at a 1.55 µm wavelength.

Due to the similarity of the propagation constant between some of the modes, the degeneracy modes can be formed as a single transverse mode (LP mode). The simulated propagation constants of the first LP_{0n} modes where n is 1, 2,…,5 are plotted in Figure 3.4 for three different graded index fibres, with different core diameters and in comparison with a step index fibre with a 50 µm core diameter.

Notice that the propagation constants of fibres with the same index characterisation (i.e. graded index) are equally separated and do follow similar linear trend lines, whereas in a step index type the curve is arched as the beam propagates further. As shown in the graph, the propagation constants of the lower order modes of the first vector mode group are slightly distinguished between these fibres. However, as the light propagates further, the difference of the between these fibres are clearly apparent.

3.5.2 The differences in the fundamental modes in commercially available fibres

The number of various fibre modes that are excited depends upon the geometry of a fibre to give certain field distributions. The simulated fibres are analysed with a fixed wavelength of 1.55 µm. The intensity field profiles of the fundamental (lowest-order) linearly polarised LP_{01} mode in the transverse plane are shown in Figure 3.5 (a) - (d) for three different core diameters and two different index types, labelled as GI50µm, GI62.5µm, GI100µm and SI50µm respectively, which were investigated.

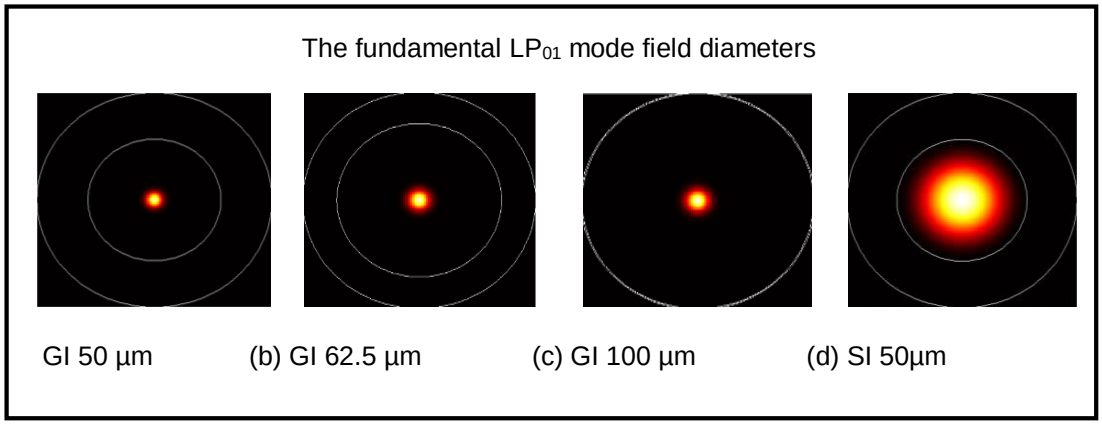

Figure 3.5: A comparison of various multimode fibres showing the cross-section of the intensity field profile for the fundamental (lowest-order) LP_{01} mode in a transverse plane. The generated transverse intensity distributions are compatible for graded index fibres with a 50µm, 62.5µm and 100µm core diameter as shown in (a) - (c), respectively. The right of the Figure shows the beam profile of a step-index fibre over the region of a fibre core. Note that the inner and outer white circles indicate the edge of the core and cladding, respectively.

It is clearly seen that the intensity field distributions are centred in the middle of the fibres (assuming a straight fibre). They are indistinguishable in the fibre with a curved index profile, and the mode field areas are not much different in size. The cross-sectional intensity distributions in the GI-MMFs remain almost unaltered, as the physical characteristics of the fibres have changed. However, for a uniform refractive index in a SI50µm fibre whose index profile is constant in the middle, the transverse field of the LP_{01} mode noticeably fills the whole fibre core. This is because the light rays take different paths to travel down the fibre. As a result, the beam profile is larger than that in a parabolic index profile.

One can see the effect of an increasing number of modes in multimode step index fibres, which induces a modal dispersion as different modes take different paths to travel through the fibre axis with different angles and velocities. This has led to the development of graded index fibres to compensate for this effect. Therefore, this is one of major reasons an optical fibre with a graded index profile is chosen in our further simulation work.

Table 3.5

The comparison of measured sizes of the MFD for the lowest-order LP_{01} mode

GI50µm	GI62.5µm	GI100µm	SI50µm
15.72 µm	15 µm	18.46 µm	38.05 µm

It should be noted that the MFD is a function of index difference and the multimode fibre structure, i.e. a core radius. Thus, the mode field diameters of the LP_{01} mode are dissimilar for different tested fibres as one can see from the comparison shown in table 3.5 above.

3.5.3 The transverse intensity distributions of higher-order modes

We show the difference in the intensity patterns of higher-order modes in a multimode fibre in Figure 3.6 with a parabolic index profile ($\alpha = 2$), having a 62.5μm core diameter. The fibre under test has a numerical aperture of 0.275 operating with a 1.48 core refractive index. According to the field profiles of the fibre modes, we can see that the mode size is dependent upon the characteristic of the index profile of the medium and its fibre core size which the beam propagates through. As the core size is increased, the number of transverse modes becomes multimode and, eventually, several higher-order modes propagate in the fibre.

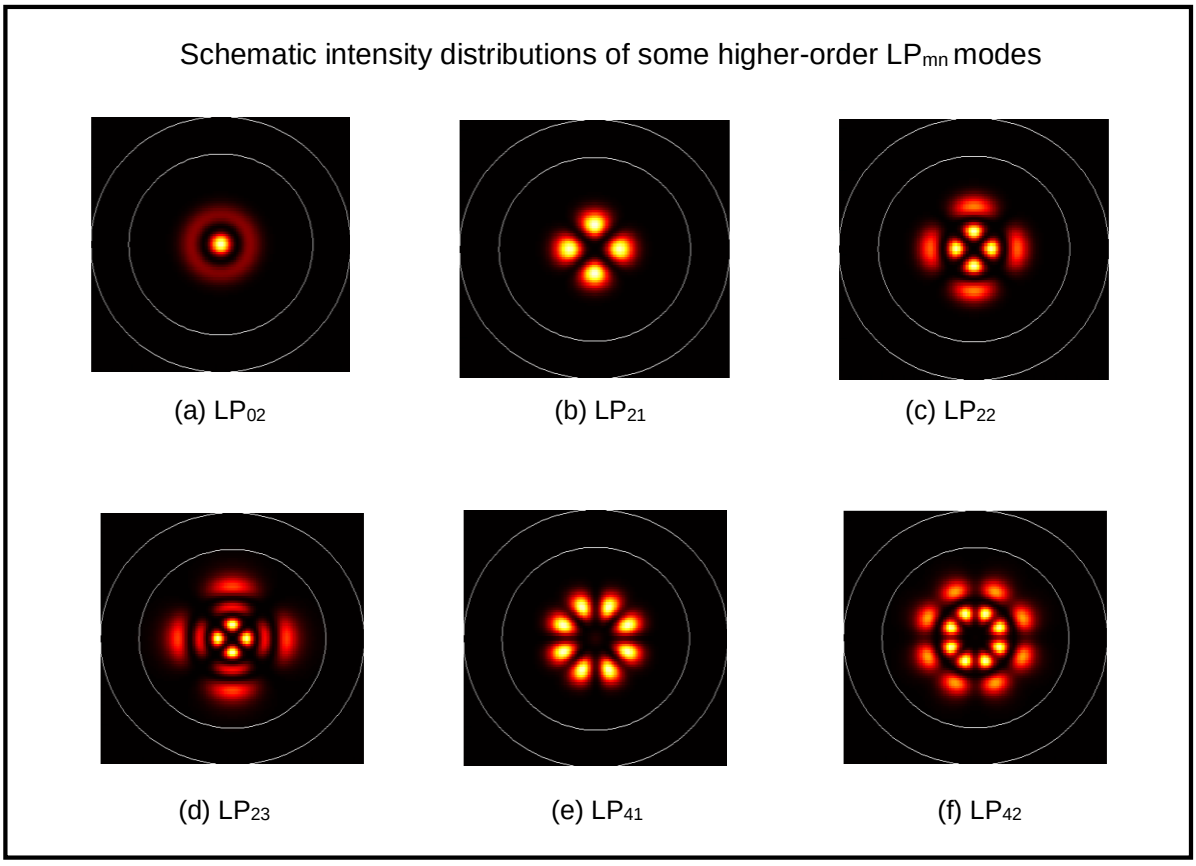

Figure 3.6: The schematic intensity distributions of some LPmn modes obtained from the GI62.5μm, simulated with the FIMMPROP software. Figure 2(a)-2(f) shows the transverse field distributions of higher-order modes for LP_{02}, LP_{21}, LP_{22}, LP_{23}, LP_{41} and the LP_{42} mode, respectively. The uniform input beam was injected into a fibre with 62.5μm graded-index profile and an NA of 0.275 where n_1 is 1.48. The cross-sectional beams profiles are obtained with a fixed wavelength at 1.55μm.

From the observations, it is confirmed that the propagating beam (excited into the fibre axis) is effectively confined along the optical axis, and the core region is fully filled with all guided modes. However, in principle the intensity of higher-order modes can significantly distribute into the cladding (but with a weak intensity field far from the core) and this leads to the radiation of higher-order modes at the interface between the core and cladding. This is very important when imperfections of the fibre are considered, such as bending and temperature variations. These radiation modes will be eventually lost during the propagation into the cladding region. We shall see later that the modal power distributions will be coupled into different modes, especially in a step-index fibre; some of them are guided inside the core and some of them are radiation modes.

3.6 The contribution of modal power through a section of multimode fibre

3.6.1 Concept and analysis

The importance of the relative modal power contributions in different core sizes of fibre makes it beneficial to study the number of guided modes and radiation loss to the cladding modes at a given operating wavelength. Additionally, there are a number of studies on the power distribution in various fibre types with different dimensions of core and cladding used for medical imaging purposes. Using derivations from equations (3.19) and (3.20), the amount of power propagating in the core and cladding is given by Gloge [49]:

$$\frac{P_{core}}{P} = 1 - \left(\frac{U^2}{V^2}\right)\left(V^2 - (2v)^{\frac{1}{2}}\right)^{-\frac{1}{2}}$$
$$\frac{P_{clad}}{P} = \left(\frac{U^2}{V^2}\right)\left(V^2 - (2v)^{\frac{1}{2}}\right)^{-\frac{1}{2}} \tag{3.46}$$

where V is the cutoff frequency of the v^{th} mode and P is equal to $P_{core} + P_{clad}$ which is the total power.

Writing equation (3.46) in terms of the overall M modes:

$$P_{core} = 1 - \frac{Pv}{M(2M - 2v)^{\frac{1}{2}}}$$
$$P_{clad} = \frac{Pv}{M(2M - 2v)^{\frac{1}{2}}} \tag{3.47}$$

where the number of total M modes is defined differently in step-index and graded index fibres from equations (2.14) and (2.15). The dependence of the average power propagating in the cladding on the transmitted modes, derived from equation (3.47), can be rearranged:

$$\frac{P_{clad}}{P} = \frac{4}{3} M^{\frac{-1}{2}} \tag{3.48}$$

This is of great importance in considerations of novel methods to maximise coupling of the transmission power to a particular mode or group of modes, especially for fibres with different physical characterisations. In our simulations, launching of the light can be achieved through using a Gaussian beam approximation interfacing to the fibre end as an initial transmitting beam. A Gaussian beam was simulated with a 10 μm-beam diameter at the $1/e^2$ intensity point. The beam was injected into the fibre axis (assuming no tilt). It follows that the effective index n_{eff} for different modes is different, i.e. these modes have different β values.

3.6.2 The distribution of power in different modes in multimode fibres

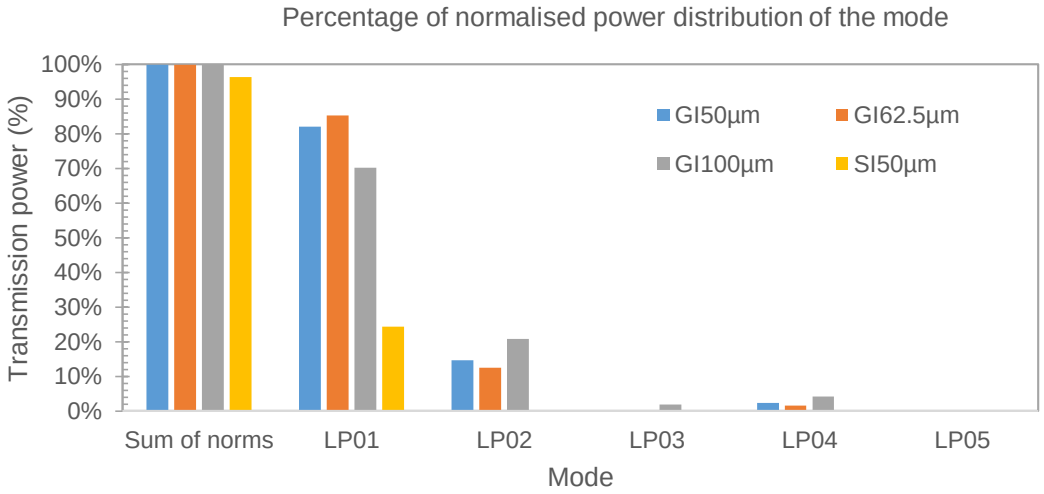

Figure 3.7: The comparison of modal power distributions contained in each scalar linearly polarised LP_{0n} mode and the total percentage of power transmission in GI-MMF and SI-MMF.

We simulate, as shown in Figure 3.7, the modal power distribution of the LP_{0n} modes in various fibres (where n varies from 1-5), i.e. the LP_{01}, LP_{02}, LP_{03}, LP_{04} and LP_{05} modes. The sum of the mode powers is almost 99% (only 1% of the power is missing) for all cases. It can thus be considered that almost all of the total power is effectively coupled and transmitted to the multimode fibre. The distributions of the modal fields are coupled to the lower-order modes, i.e. the modes propagate slower near the centre core of the fibre, and the largest contributions of the power are mainly contained in the fundamental modes. It is worth noting that there will be some level of power transfer losses that make the total power coupling less than a 100% from the beam to the fibre during launching (such as Fresnel reflections at the fibre interface).

Nevertheless, as the beam evolves along the length of the fibre, the light is coupled to some higher-order modes. It can be seen from Figure 3.7 that the highest percentage of power is transferred to the LP_{01} mode, with approximately 85% of the total power being in this mode for GI62.5µm, the remaining power being distributed into the higher-order mode region where the light is exponentially decaying to the cladding. In comparison, in the largest core diameter fibre GI100µm, the percentage of power contributing to the LP_{01} mode drops by almost 15% compared to fibres having similar index profiles, but with smaller core radii, operating at the same wavelengths. As the number of modes and the cut-off frequency increase, these amounts of power are distributed to several higher-order modes.

According to the bar chart presented above, the percentage of transmission power with the same core dimension was significantly greater in the GI50µm over the SI50µm fibre. This can be explained by the fact that only about 25% of the transmitted power is in the fundamental mode of the SI50 µm fibre, compared with the power transmitted in the GI50µm fibre which is approximately 82% of the transmission power. Likewise, we can see the modal power of the higher-order mode in the SI50µm fibre is barely retrieved.

Table 3.6

The percentage of power contributions in the cladding for different fibres

GI50µm	GI62.5µm	GI100µm	SI50µm
13.13%	7.66%	4.53%	8.47%

Using the average percentage of power flow in the cladding derived from equation (3.48), the results in Table 3.6 imply that some of the power contributions are due to those present in the cladding region, leading to roughly 13% of the beam power being distributed into the cladding of the GI50µm fibre

while 7.66% is distributed into the cladding in a GI62.5μm fibre. From this, we see that the power flow in the cladding is inversely proportional to the size of the fibre core diameter, a higher number of modes being present in the core for the larger diameter fibres. Likewise, the normalised power distribution also depends on the design structure of the multimode fibres. Thus increasing the core diameter is beneficial to raising the modal power contributions in the core area and lowering the amount of power contributing to the cladding region. This property is thus useful for applications involving high power laser transmission.

3.7 The reconstruction performance in unperturbed fibres

3.7.1 Principle of reconstruction in optical fibres

In the following section, we will demonstrate the evolution of light propagating in optical fibres by assuming that there are no fibre impairments, such as bending, during the transmission. An initial Gaussian beam with a $1/e^2$ diameter of 10 μm with a wavelength of 1.55 μm was directly coupled into the centre core of the fibres. The effects of multimode interference in the fibres has been examined with several fibres tested in this study. The propagation of the light depends on the excitation conditions of the input beam profile, which also relies on the characteristics of the fibre. The physical properties of fibres and the fibre impairment conditions such as microbending and temperature variation of the fibres have significant effects on the output beam profile.

In the graded index fibres, the phenomenon of self-reproduction of the input field occurs at a periodic interval as a result of the interference between propagating guided modes in an optical waveguide. The concept of self-imaging was first investigated extensively by Allison *et al*. [54] to demonstrate the propagation effects in optical fibres transmitting a coherent light source. The applications based on multimode interference (MMI) effects can be found in optical communication systems [55-57] and several implementations in optical sensing, utilising bending and temperature effects [58-61].

We have previously mentioned in Section 3.5 that the propagation constant values are distinct in different modes, in such a way that the changes of β strongly induce the interference patterns at the re-imaging distances over the transmission length of the fibres. A reproduction of an input image in the multimode fibre appears by means of significant changes in β between guided modes and the oscillatory nature of the independent phases of the propagating fields.

Figure 3.8: Schematic of a cascaded fibre structure (not to scale) showing: (a) a single-mode-multimode-single-mode MMI device; (b) a single-mode-multimode-multimode device; and (c) a single section of a multimode configuration device as used in our design structure for a graded-index profile.

The original design for an MMI device is realised by the cascading of a number of inputs N and a number of outputs M ($N \times M$ devices) where the multimode waveguide is located in the middle section for the design demonstration. The configuration of the MMI devices (as shown in Figure 3.8) is usually in the form of a single-mode-multimode-single-mode (S-M-S) structure, or the form of single-mode-multimode-multimode (S-M-M) which has also received much attention in the design literature [62]. However, our approach is to employ the simplest method of coupling by using a section of single multimode fibre with an appropriate length of transmission in the structure.

As has been emphasised previously, a periodic reimaging can be generated in which an input field is duplicated at specific positions occurring along the length of propagation in multimode fibre. Based on the study of self-imaging in the transverse plane, our proposed designs are investigated with most of the emphasis being on graded index optical fibres where the image reconstruction is

dependent upon the refractive index profile of the guided medium. A self-imaging property in a quadratic graded index medium occurs perfectly in a natural way at a periodic interval, leading to the repetition of the original image along the optical fibre axis [54, 62-65].

3.8 Simulation results of the variation of the self-imaging effects with different fibre specifications

3.8.1 Introduction

A set of Eigenmodes is excited when an input field is coupled into the single front face of multimode fibres. The self-imaging of a transmitted input field profile is obtained due to the interference between the excited modes and thus the change of the intensity profile inside the fibre [54]. It is worth noting that the occurrence of reconstructions of an input field profile can happen when the phase difference between two guided modes is an integer multiple of 2π, i.e. the excited modes are in-phase. The Eigenmode expansion is used to calculate the results of modal analysis where Maxwell's equations are numerically solved on a cross-sectional mesh of the fibres.

Thus an investigation has been made of the variation of an electromagnetic field inside the MMFs along the propagation distance. To investigate the results of propagating all the first 30 guided modes, we calculate and then visualise the evolution of the intensity field for each of the commercial fibres tested. By measuring the intensity profile across the beam, the reconstruction of the electromagnetic field can be retrieved at the desired propagation length. Thus the input modal distribution is guided along the fibre axis within the region of higher refractive index of the graded index fibre. Generally speaking, the original beam is expected to reproduce (an inverted image) of itself at twice the focal distance when propagating within a quadratic index profile of graded fibre. The interference and self-imaging effects are different for each fibre and depend strongly on their characteristics. In this section, the phenomenon of light propagation inside the fibres is investigated.

The light is confined to a medium which has a graded index refractive index profile, leading to the phenomenon of light interference in that medium and hence the propagation results in a self-imaging effect. However, it is also found that decreasing the index difference (Δn) between the core and cladding results in increases of the self-imaging length which shall be demonstrated in Section 3.8.4.

3.8.2 Influence of fibre specifications

We investigated the influence of fibre specifications such as core diameter and the index profile of the fibre. Figure 3.9 shows the intensity patterns of a transmitted Gaussian beam inside the fibres. The simulation is for the beam being guided a short distance along a 2 mm length of propagation from the original input field, for the three examples of the GI-MMFs examined. The results obtained show that a replica of an initial beam profile occurs due to the oscillatory nature of the guided modes in all the GI-MMFs. The different modes interfere, leading to an interference pattern of several modes that periodically regenerates the initial beam distribution.

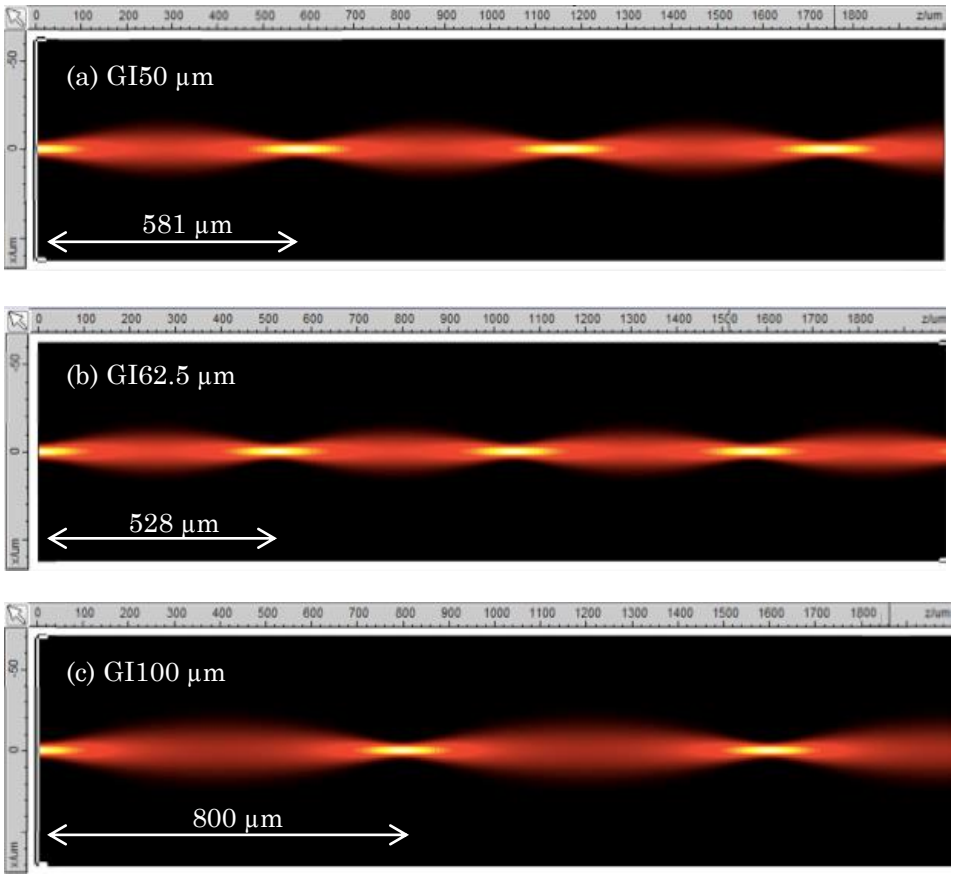

Figure 3.9: The evolution of the intensity profile inside the tested graded index multimode fibres at a fixed 1.55 µm wavelength is shown for: (a) GI50µm; (b) GI62.5µm; and (c) GI100µm fibres for a distance of 2 mm. The light transmission varies according to the specifications of fibres and only a small amount of light is lost to the cladding. The interference pattern between guided modes results in self-imaging at certain lengths down the fibres (where the FIMMPROP software was used to simulate the evolution of the intensity for the different fibres).

All the guided modes in the graded index fibres propagate with different velocities at specific values of propagation constant. The characteristics of multimode interference between these guided modes correspond to the phenomenon of self-imaging occurring during the light propagation. It is this phenomenon that allows the original phase and field distribution to be retrieved. In Figure 3.9, the light evolution in different commercial GI-MMFs is demonstrated to compare the self-imaging properties. The initial phase is recovered in the fibres with a parabolic index profile; however, the positions at which the original input beam is reconstructed are different. According to Figure 3.9, the self-imaging length depends strongly on the fibre parameters such as

the core diameter and the NA of the fibre. The self-imaging lengths with smaller core diameters shown in Figures 3.9 (a) and 3.9 (b) appear within a few µm length after propagating through GI50µm and GI62.5µm, respectively, whereas, as shown in Figure 3.9 (c), several higher order modes are excited in GI100µm leading to the self-imaging distance being almost doubled.

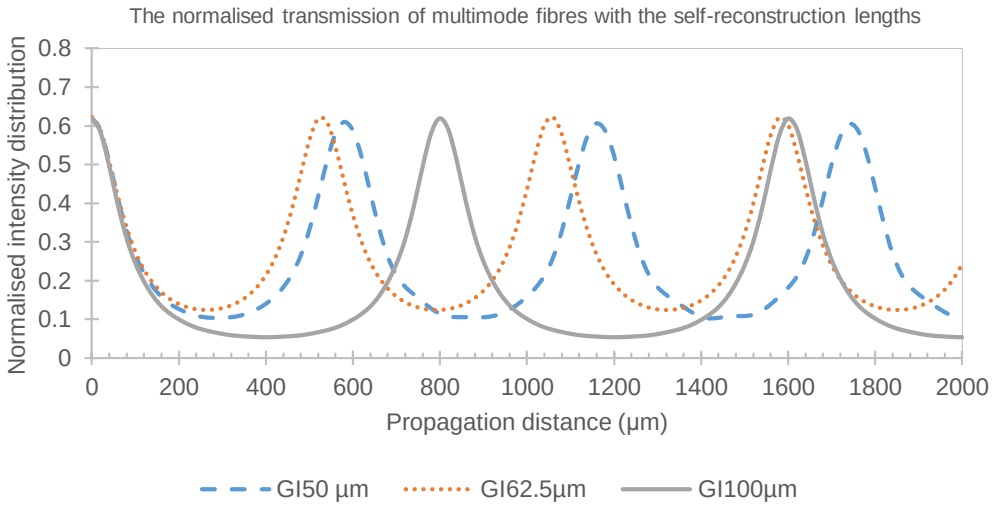

Figure 3.10: The intensity distribution of the reconstructed beam as it propagates along the length of three GI-MMFs with different core diameters and NA. The highest transmission peaks correspond to the reproduction of an initial phase and intensity distribution and occur at various propagation lengths along the fibre.

The graphs in Figure 3.10 show that the intensity of the original beam profile comes back nicely at the highest transmission peak positions with almost unchanged beam profile (e.g. a MFD). By considering the multimode interference pattern in GI50µm, as shown in Figure 3.9 (a), the first highest transmission peak is at a position 581 µm away from the source. The reconstruction of an initial transverse field is repeated at every 581µm interval. For the transmission of a Gaussian beam in GI50µm at z = 0 µm, we see that the second and third peaks are at lengths of 1162 µm and 1743 µm, respectively, and we were able to achieve approximately the same size of the beam diameters at these planes.

In addition, the periodic interference pattern of the excited beam for GI62.5μm, shown in Figure 3.9 (b) and the orange coloured curve in Figure 3.10, occurs after transmission of the fields to a propagation length of 528 μm for the first reconstruction position. At the propagation distances of z = 1056 μm and 1584 μm, the second and third self-imaging peaks are generated, respectively. It can be seen that the transmission peaks in GI50μm are formed farther apart than in GI62.5μm, by approximately 60 μm. In GI100μm the difference in the guided modes leads to a much further distance at which the transmission peak is recovered; for this fibre diameter a propagation distance of 800 μm is required for the first duplication of the incident field. Thus we conclude that the self-imaging length of GI-MMFs is an increasing function of core diameter and the NA of the fibre, for a specific wavelength.

A Gaussian beam propagation with $\alpha = \infty$ in a SI50μm fibre is shown in Figure 3.11 (a). The field distribution is unevenly spaced and evolves in a complex way from the input transverse plane along the length of the fibre. It is hard to specify the position of any reconstruction of the originally excited input field where the guided modes interfere in phase along the step-index fibre. The fields along the z-axis at z = 2420 μm and 5672 μm in Figure 3.11 (b) do not imply self-reproductions of the initial field distribution, although they are the locations at which the maxima of the intensity distributions are present across the plane.

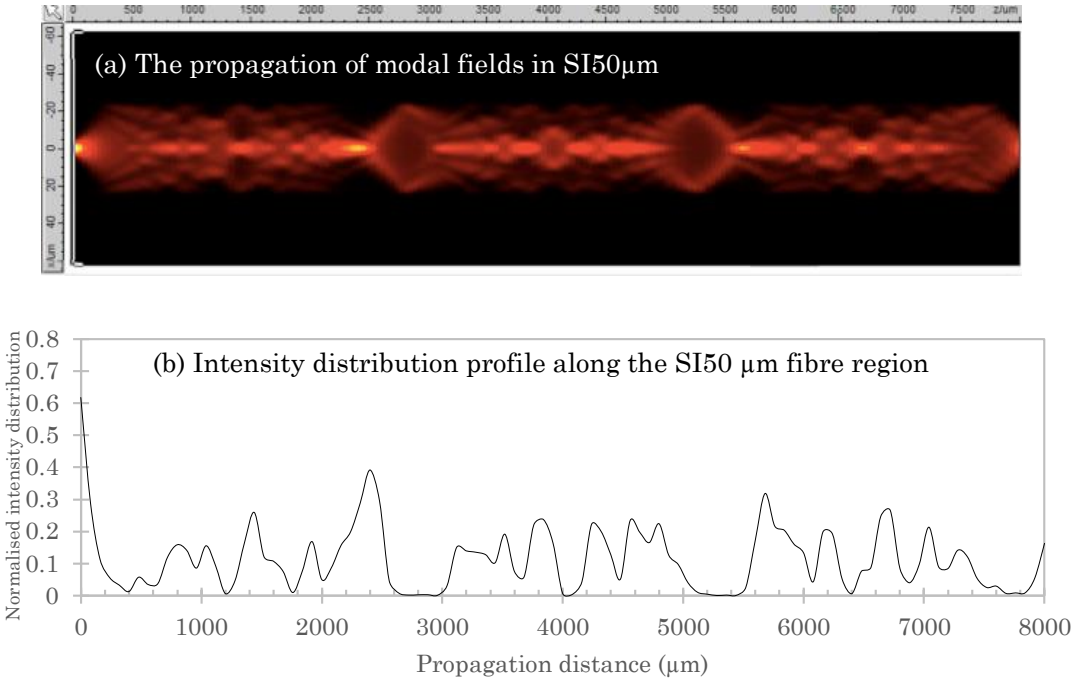

Figure 3.11: The evolution of the propagation through a step-index multimode fibre from $z = 0$ to $z = 8$ mm: (a) beam intensity in the fibre; and (b) the normalised intensity of the propagated beam profile showing the locations where the intensity distribution peaks. However, the effect of self-imaging is not evident due to numerous number of modes that are excited.

There is a large variation of the intensity pattern in a multimode step-index fibre as compared to when the light propagates within a graded index profiled fibre. In principle, the formation of an interference pattern arises from the fact that light enters into the fibre with different paths. They follow different ray trajectories with different phase constants and they interfere with each other. These rays converge at a desired position with similar phases, and thus generate the observed reconstruction of an initial field distribution.

To conclude, we have found that the propagating modes in GI-MMFs tend to concentrate near the optical axis. The reproductions of the initial excitation field are regenerated along the core of the fibre. Excellent results have been obtained for the re-imaging lengths at which the excited beam is repeated periodically within optical fibres structured with graded index profiles. When employing a constant wavelength of 1.55 μm the distance between the generated

intensity peaks varies for the four different fibres tested. The results show the longest reconstruction distance of an initial excitation field can be obtained in the case of GI100μm with the largest NA and core size. Regarding the location of the reconstructed beam, one can determine this by looking at the transmission peak associated with a specific mode in any transverse plane. The highest peaks (i.e. the maxima along the propagation length) indicate the positions where the light is most highly concentrated. However, in some cases, especially for the SI50μm fibre, these positions do not indicate the exact position of a duplicated input field but only show in general the locations of the highest intensity concentrations of the beam profile.

3.8.3 Influence of the operating wavelength

We have examined the dependence of the self-imaging length in GI fibres with different specification parameters such as the core diameter and numerical aperture; however, in this section, we will demonstrate the effect of variations of the wavelength on the reconstruction and modal propagation in the GI fibre. To examine this effect, the core diameter of the multimode fibre was fixed to be equal to 62.5 μm, and a refractive index difference (delta value) of 0.0176 was used at a fixed 0.275 numerical aperture. The light propagation in GI62.5μm with the lower dispersion ranges at wavelengths of 850 nm, 1300 nm and 1550 nm (i.e. the three lowest attenuation wavelength regions) has been explored.

In Figure 3.12 (a) – (c) we present the results of the evolution of the electromagnetic fields inside GI62.5μm, performed for fibres with three different operating wavelengths at 0.85 μm, 1.3 μm and 1.55 μm, respectively. We compare the mode field diameters of three directly launched 10 μm Gaussian beams for a GI62.5μm fibre and examine the three intensity peaks after equal lengths of propagation of 2 mm. The mode field diameters (MFD), measured at the $1/e^2$ points from the intensity peak, are the same when the operating wavelength is changed from 1.55 μm to 1.3 μm and 0.85 μm.

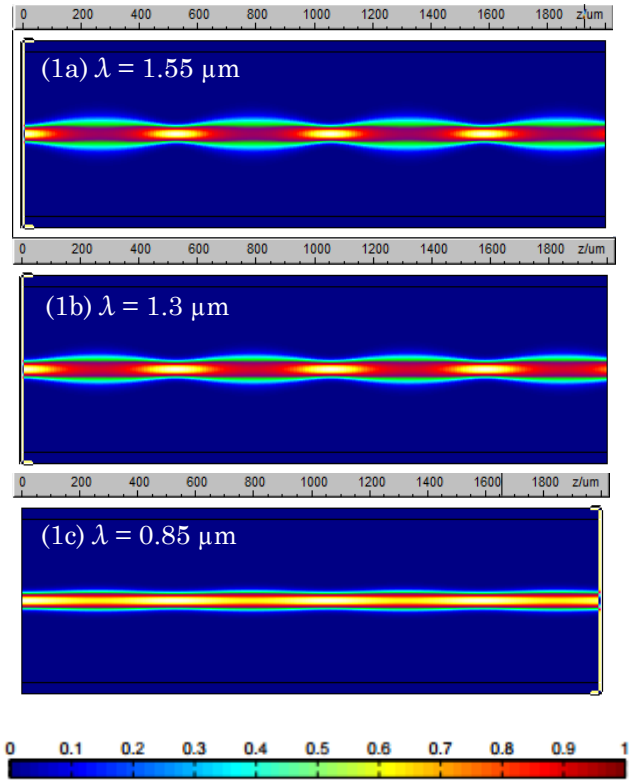

Figure 3.12: The dependence of field distributions upon the wavelength for the propagation of an incident Gaussian beam with a beam diameter of 10 µm in a GI62.5 fibre: (1a) 1.55µm; (1b) 1.3µm; and (1c) 0.85µm.

It can be seen from Figure 3.12 that the beam diffracts to a greater extent over the fibre core beyond its minimum waist position when the system is operated with a longer wavelength. Conversely, a smaller diffraction of the beam is observed in the fibre when operating with the shorter wavelength. This can be explained from the Huygens-Fresnel principle [64, 65]. It is well known that the amount of a light wave's diffraction depends on the wavelength of light. Accordingly, a strongly diffracted beam is more observable with longer wavelength radiation as compared to that in a shorter wavelength region.

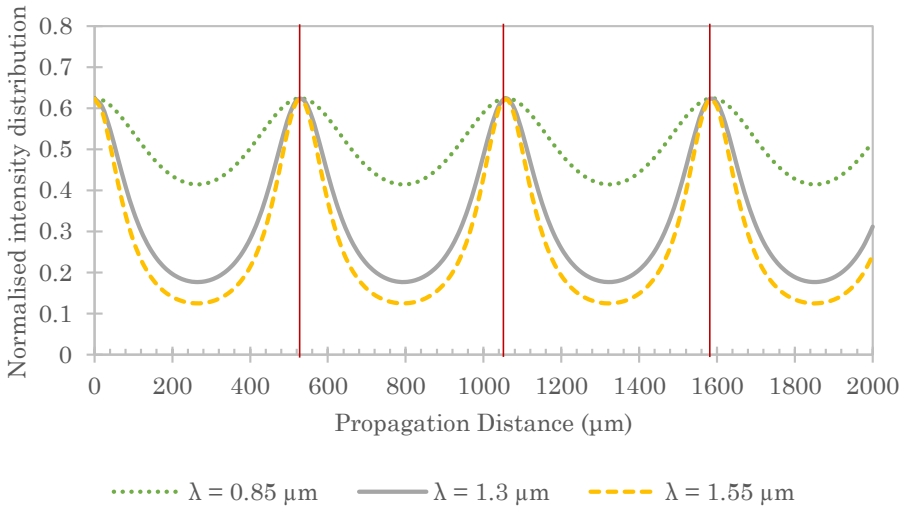

Figure 3.13: The normalised intensity profiles of the propagating fields from the planes at $z = 0$ to $z = 2000$ μm for a GI62.5μm as a function of the various wavelengths employed. The red lines represent the self-imaging peaks.

The normalised distributions of the intensity for various wavelengths at a wavelength of 1.55 μm, 1.3 μm, and 0.85 μm are plotted in Figure 3.13. At the wavelengths of 1.3 μm and 1.55 μm, the intensity distribution obtained exhibits almost the same pattern. We see that the interference between the higher-order modes is excited strongly, as indicated by the bottom peak (nearly zero) of the graph shown in Figure 3.13, particularly for the wavelength of 1.55 μm. In contrast, as the signal wavelength changes to 0.85 μm, we observe that the fundamental mode carries the most significant power. At this wavelength, the fundamental mode is predominantly excited, among higher-order modes, as shown in Figure 3.12(c).

Moreover, it is interesting to note the effect of wavelength on the self-imaging phenomenon in that the re-imaging length interval of the incident beam operated at different wavelengths comes to focus at the same plane. The maxima of the transmission peaks (self-imaging peaks) occur at approximately the same positions inside the GI62.5μm multimode fibre. We, therefore, observe that the re-imaging length is wavelength independent since the self-imaging length will

be generated at very nearly the same position for different wavelengths of light in the fibres [66].

3.8.4 Influence of the relative refractive index differences

In the previous section, we have determined the excitation of an input field by directly coupling a beam along the optical axis of a single strand multimode fibre. It has been shown that by suitably choosing the length and the index profile of the fibre in the design, multimode fibres (especially GI-MMFs) can be used to image the original intensity beam profile at certain distances. To investigate this further, we have performed an examination of the effects of propagation along the total length of the fibre. It was determined that the fibre specifications, i.e. the fibre core dimensions and the operating wavelengths, influence strongly on the evolution of an initial beam profile as it propagates through the fibre to replicate an optical source. We found that the initial intensity and phase of the original beam are then regenerated, resulting in maxima in intensity at periodic locations down the fibre length, each produced by the interference pattern generated inside the optical fibre.

In this section, the influence of the relative refractive index differences between the core and surrounding medium has been investigated. Launching conditions such as, for example, the NA and the delta fractional index difference (%Δ) of the fibre also depend strongly on the imaging position of the original beam. We maintain the initial beam size of 10 μm, a wavelength of 1.55 μm and an index of the core, n_1, of 1.48 and examine a GI62.5μm commercially available fibre of 3 mm length. However, the index of the cladding is adjusted to obtain a smaller value of the fractional index differences.

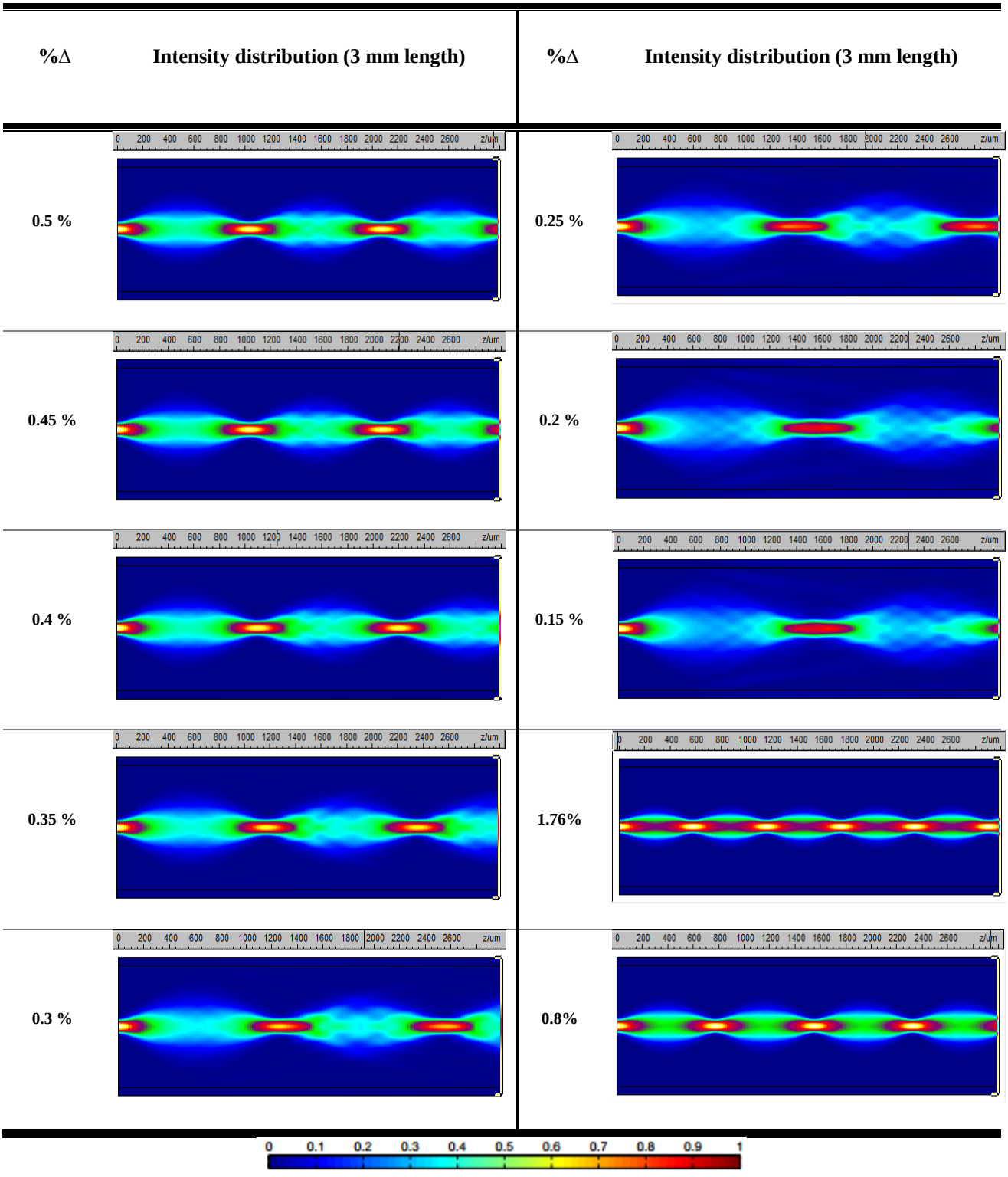

Figure 3.14: The simulated light propagation in a graded index profile multimode optical fibre with a 62.5 µm core diameter and 3000 µm length. The modal propagating fields are at 1.55 µm wavelength with various fractional relative refractive index differences (%Δ) shown between core and cladding, ranging from 0.5% to 0.15% with increments of 0.05. Also shown are the best reimaging quality fibres with Δ of 1.76% and 0.8%.

The reimaging of an initial beam profile after propagation along the fibre length occurs when there is a fractional index difference between the fibre core and cladding that is greater than or equal to 0.8%, which is suitable for a high quality of self-imaging since the beam spot size is very similar to the commercial GI62.5 fibre and the MFDs remain the same at different peak positions along the propagation distance. However, we cannot achieve a perfect self-imaging quality when the $\Delta < 0.8\%$, as shown in Figure 3.14. This is because of the dissimilarity of the mode field diameters at the maxima, which means that a perfect input profile can never be reproduced at the duplicate imaging locations. For the propagation characteristics shown in the above figures, light interference is clearly seen in the fibres but we see that as the Δ is made smaller, the reduction in the number of propagating modes results in a deterioration in the quality of the input image replicas produced by the self-imaging effect in the fibre. When the Δ is less than 0.3%, more light propagates through the cladding region, resulting in the loss of clear reproduction of the initial fields.

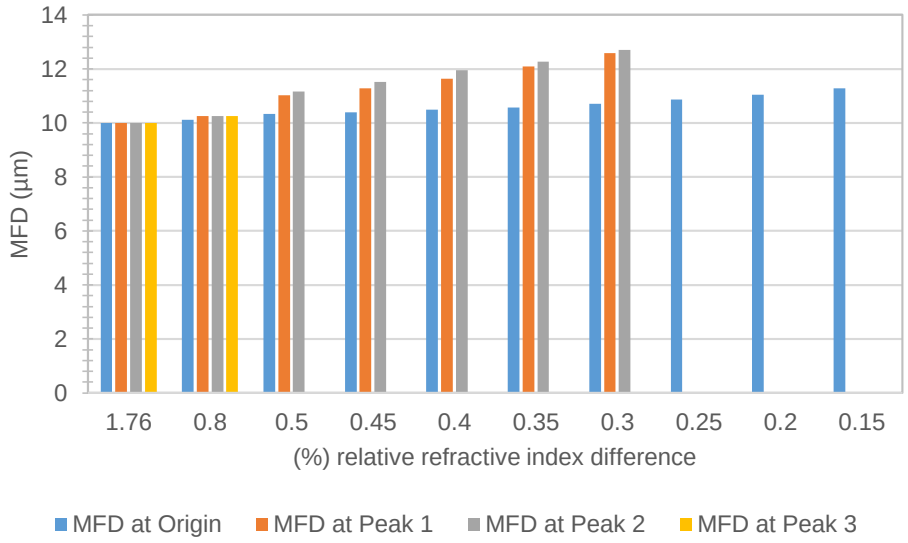

Figure 3.15: The bar chart shows the mode field diameters as a function of percentage of the relative refractive index difference (%Δ), measured at the $1/e^2$ intensity point, that alter with fractional index differences for particular transmission peaks.

The bar chart in Figure 3.15 shows the difference of the MFDs, measured at the $1/e^2$ intensity point, at the indicated self-imaging positions for different relative refractive indices. For a fibre length of 3000 µm, there are five replicas of the initial beam (i.e. the peak intensity position) for a Δ of 1.76% and three duplicated beams for a Δ of 0.8%, while the remaining fractional index differences do not show the same MFD at different maxima points. However, this is in contrast with Δ of 1.76% (the value in a commercial GI-MMF and a Δ of 0.8%, which are able to achieve perfectly high quality re-imaging. However, when we reduce the value of the fractional index difference from these values, the imperfect beam re-imaging results in their MFDs not being identical with the original at $z = 0$ µm.

Even though the MFDs are dissimilar to that of the input modal excitation at the fibre face, we can consider the highest transmission peaks as the locations where the reconstruction of the input optical field occurs (whose normalised intensity values are relatively larger than their surrounding fields). Clearly, the power is distributed over the entire cross-sectional core area of the multimode fibre. We have explored the effects of duplicating the original beam profile with particular fractional index differences (less than 1%) in the multimode fibres. Although the self-imaging length increases with the relatively smaller fractional index differences, we notice that it was difficult to achieve 100% replicas of the initial image in these fibres. About 0.3% relative refractive index difference between the fibre edge and core is required to achieve a longer re-imaging distance in a GI62.5µm, neglecting the image quality.

3.8.5 Influence of the lower the refractive index in the core

In Section 3.8.4 we have explored the effect of lower fractional index differences by keeping the same refractive index in the cores. It showed that self-imaging positions were different for different relative refractive indices. However, in this section the results of the reconstruction lengths of lowering the refractive index of the fibre in the cores with a fixed cladding index (at n_2 = 1.454 as used for a GI62.5µm in our previous simulation tests). By lowering the index n_1 in the core, the index differences (Δn)between n_1 and n_2 are clearly decreased as depicted in Figure 3.16 below.

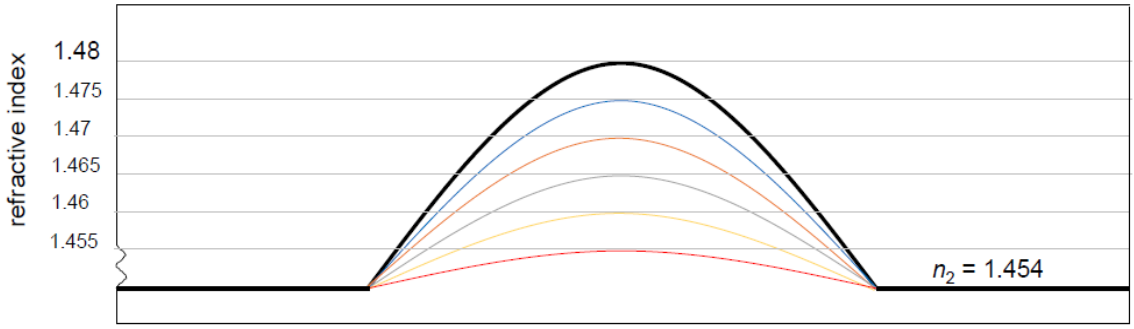

Figure 3.16: Design of a graded index fibre for different refractive index of the cores.

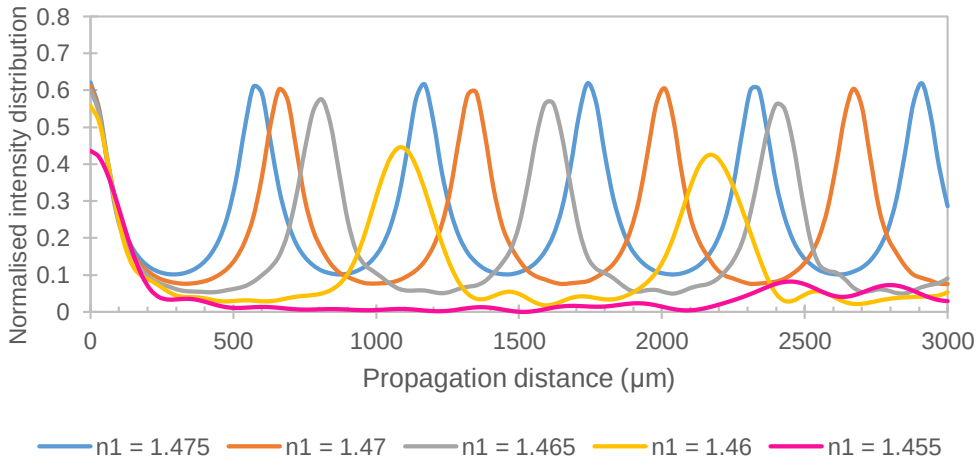

Figure 3.17: The normalised intensity profiles of the propagating fields with various smaller refractive of the core n_1 (with its corresponding colour of graph) inside a GI62.5µm, operating at a 1.55 µm wavelength with a beam diameter of 10 µm when the fibre length is 3000 µm.

The corresponding normalised peak intensity for each profile varying along the propagation direction is shown in Figure 3.17, for the transverse intensity distributions for each GI62.5μm fibre with various values of the core's refractive index (lower than that of the previous simulations with $n_1 = 1.48$). The intensity profiles of the duplicated input beam reduces when the core's refractive index is decreased. Most specially, the dispersion has significant effects on the self-imaging length. Clearly, the reduction in the peak intensity is especially significant as the light pulses propagate further away from the fibre facet. Although the light does propagate further away from an input beam with the various desired intensity pattern along the length of the fibre, it tends to continuously disperse with the lower index n_1 of the core (such as the intensity profile shown in yellow in Figure 3.17). From this interesting phenomenon, we can draw a conclusion that the dispersion effects are strongly related to the self-imaging location and the corresponding reduction of the intensity distributions. It is obvious that the power intensity is spread out more over the wider depth of focus (DOF) with the decreasing core index; therefore, the peak intensity has reduced significantly with the longer focusing distance (i.e. self-imaging position). On the contrary, the DOF is narrower for the higher intensity peak because the spreading of the power is much lower. For this reason, the repetition in imaging of the input beam can be found at shorter distances (with a definite DOF) after propagating from the fibre front facet.

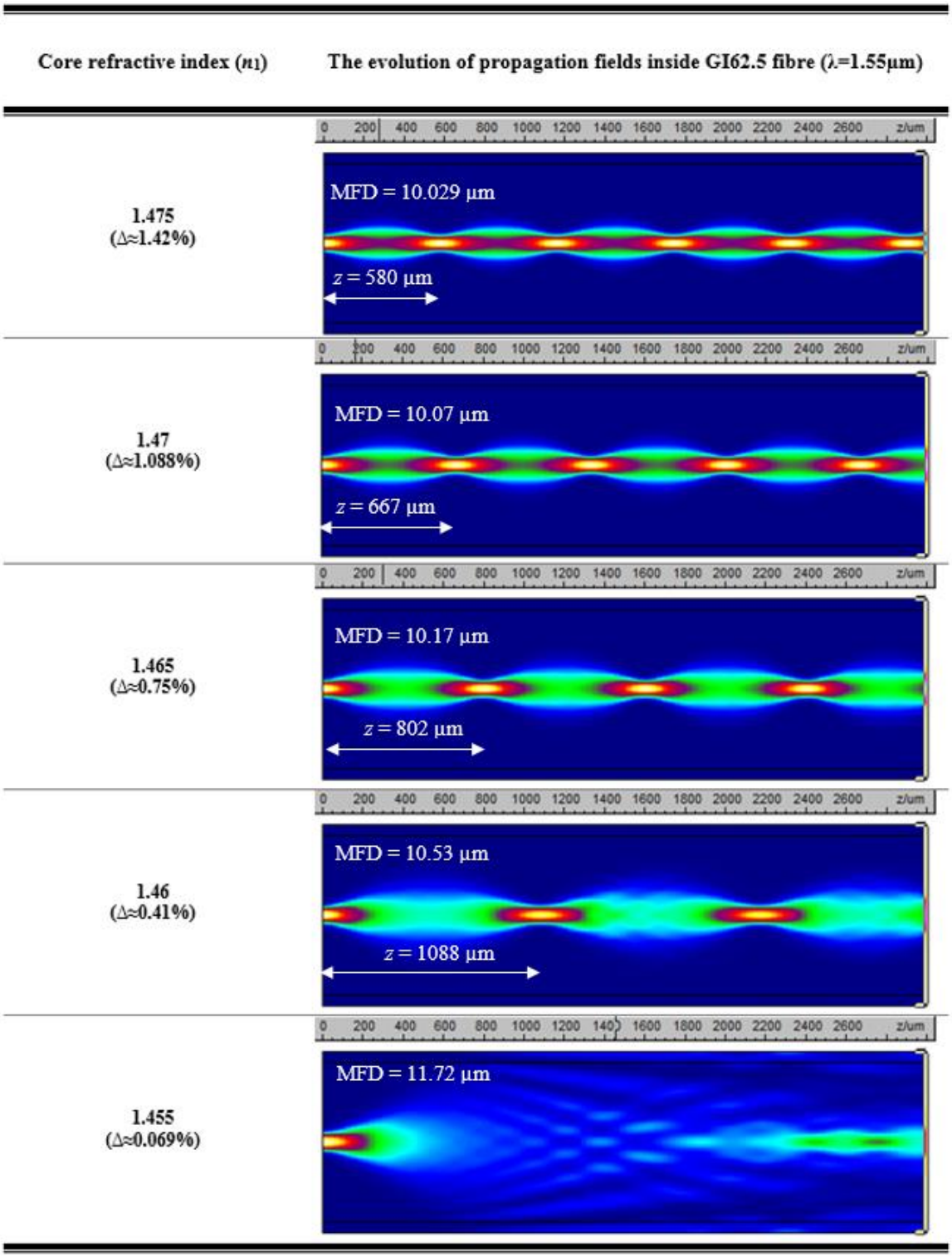

Figure 3.18: The simulated light propagation in a graded index profile multimode optical fibre with a 62.5 μm core diameter and 3000 μm length. The modal propagating fields are at 1.55 μm wavelength with various refractive indices, n_1 , of the cores, reducing from 1.48 with decrements of 0.005 to almost 1.454 of the cladding index. The mode field diameter of an initial input Gaussian beam was 10 μm at the $1/e^2$ point (measured at z = 0 μm).

It can be seen that by minimising the n_1, the self-reproduction lengths of the input Gaussian beam appear at longer distances in a GI62.5 μm fibre (with a larger DOF). By decreasing the index of the core to 1.46, as shown in Figure 3.18, the input beam is reconstructed at the plane z = 1088 μm which is more than double that which occurs in the commercial fibre with n_1 = 1.48 (shown in Figure 3.9b). Additionally, there is a trade-off between the beam size and the position of the redistribution of an incident field. The MFD of the incident beam at position z = 0 is closer to that of the reference Gaussian beam (before coupling to the fibre) for a fibre with significantly larger values of NA and index difference in comparison with a fibre with a smaller value of n_1 in the core (i.e. only a slight difference of refractive indices between the core and cladding). Even though the reconstruction distances of the input field are shorter than in a fibre with a low index differences, the power is spread out less than in a fibre with a lower n_1 value in which the beam is not as strongly focused.

The reason why the MFD at the plane z = 0 is larger than that for a lower core diameter, is because most of the power tends to spread out towards the sides of the fibre and thus the initial beam is focused further away with a broadened intensity peak.

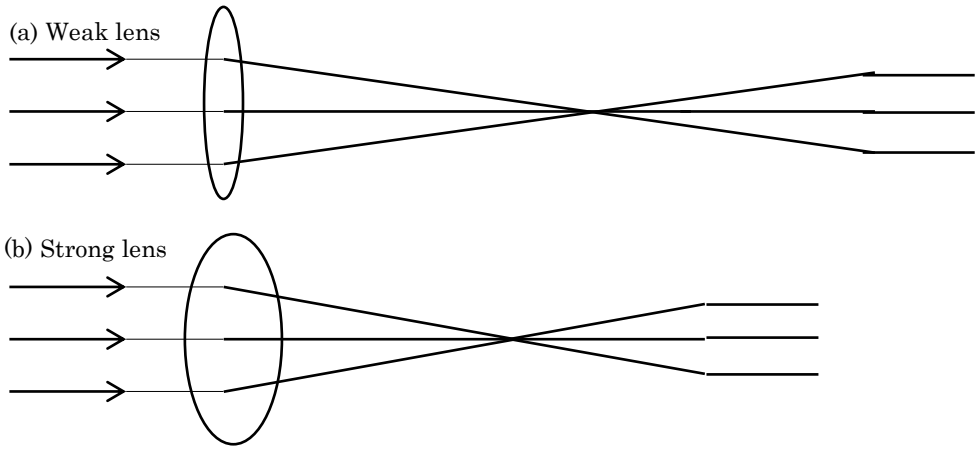

Figure 3.19: The difference of focal distance between a weak lens and a strong lens: (a) the incoming rays pass through the thin lens (weak lens) and the light rays are focused at a longer distance away from the lens, while in (b) the focal length is much shorter after the beams pass through the stronger lens (thick lens).

As depicted in Figure 3.18 above for different values of n_1, the concept of the stronger or weaker lens (as shown in Figure 3.19) can be applied to this effect. Thus the higher n_1 can be thought of as the stronger lens which has a shorter focal length. This is opposed to the lower n_1 in which the formation of the reconstructed beam can be thought of as resulting from a weaker lens-like structure, where the image reconstructed lengths appear at longer distances [67]. Thus the repetition of an input beam occurs at further distances away from an input plane in a fibre with a lower n_1. On the other hand, for those fibres with higher n_1 values, the self-imaging length appears at shorter distances. For example, the first duplication of the original beam was at a distance of 1088 µm for the value n_1 of 1.46, whereas the first intensity peak was found at the position z = 580 µm with a fibre with an n_1 of 1.475.

It is, therefore, shown that in order to achieve a longer reimaging distance, the recommended fibre should have a much lower refractive index of the core since we have found that the self-imaging length interval is inversely proportional to index difference between n_1 and n_2. Based on our investigations, we conclude that the core refractive index and Δ both have a significant influence on the self-reproduction length interval of the original input beam.

3.8.6 Influence of fibre geometry with a fixed NA of the fibre

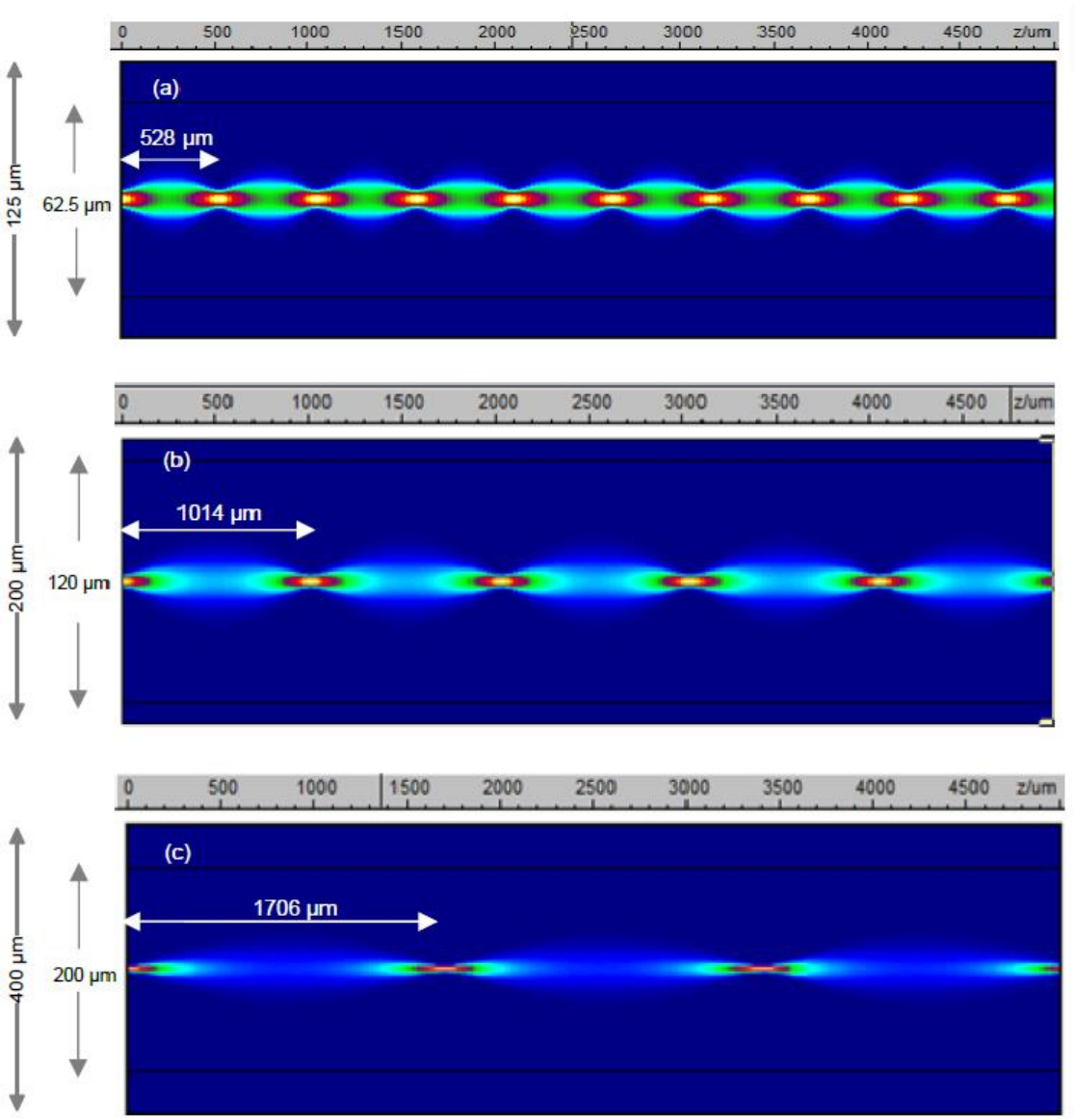

Figure 3.20: The characteristics of an incident Gaussian beam (MFD of 10 µm) within a 5 mm long section of GI-MMFs with a variety of core/cladding diameters of: (a) a 62.5/125 µm, (b) a 120/200 µm, and (c) a 200/400 µm. The fibre is operated at a 1.55 µm wavelength and the refractive indices of the core and cladding are n_1 = 1.48 and n_2 = 1.454, respectively.The NA is 0.275 for all three fibres.

A visualisation of the propagated 10 µm beam with different core/cladding diameters of the GI-MMFs, i.e. 62.5/125 µm, 120/200 µm, and 200/400 µm, together with their first self-imaging locations are depicted in Figure 3.20 (a) – 3.20 (c), respectively. The fields are propagated in GI-MMFs for a distance of 5 mm, with core and cladding refractive indices of n_1 = 1.48 and n_2 = 1.454, respectively. Considering the length of the duplicated incident beam inside the fibre, our results show that the target location of a transmitted Gaussian beam with a 10 µm diameter seems to increase with larger core sizes. It is found that the most effective way of increasing the focal distance seems to be to increase the fibre diameter. Comparison of the focal distances in these fibres, showed the effects of increasing the fibre dimensions on increasing the length at which the input field is redistributed. After propagating about 0.528 mm distance away from the input plane, the Gaussian beam distribution is displayed inside a 62.5/125 µm dimension fibre in Figure 3.20 (a). The excited modes interfere with each other at a longer distance (by more than three times of the re-imaged length occurring in a 62.5/125 µm fibre) from a front facet of the fibre when the generated Gaussian beam is directly launched to a larger core size, i.e. in a 200/400 µm fibre. As discussed above, when a larger core size is used the beam experiences more dispersion; however, the collimated input Gaussian beam can be reproduced further from the plane of the incident beam.

3.8.7 Influence of fibre geometry with lower index of the fibre core

Our simulation results reveal that we have coupled about 96% of the total transmitted power into the modes in the guided fibre section and the significant power was transmitted to the fundamental mode of the fibre, whereas the remaining power is distributed into a large number of higher output modes.

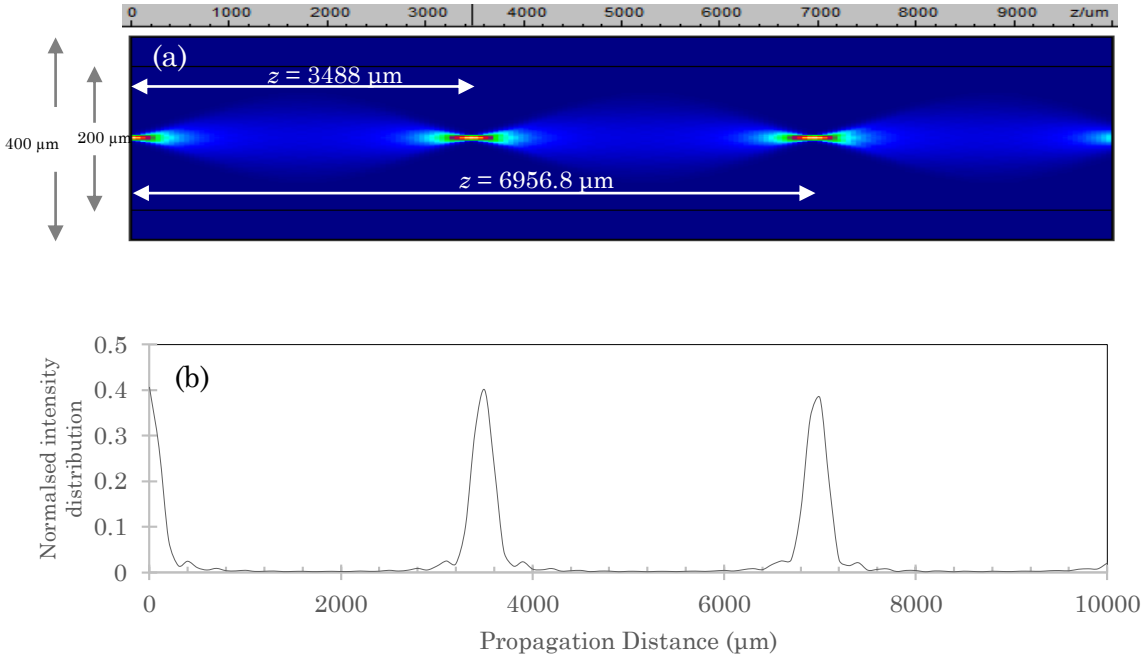

Figure 3.21: (a) The numerical simulation results of the light propagation along a transmission distance in a GI-MMF of 10 mm length with the core and cladding refractive indices of n_1 = 1.46 and n_2 = 1.454, respectively. An incident Gaussian beam, with a 10 µm beam diameter, is introduced into a fibre with the core/cladding diameter of a 200/400 µm, with a wavelength of 1.55 µm and (b) the corresponding normalised intensity profile of the propagation beam.

According to our previous investigations of the characteristic propagation of an optical field along the GI-MMFs with an optimum parabolic index profile, we obtained a number of useful and interesting results to achieve a longer reimaging distance of an input field profile. Furthermore, it is of interest to propose a new technique by taking advantage of our previous numerical simulation results to exploit the optimum distance for which we can obtain a high quality of reproduction the original input field profile. However, an additional concern is the effect on the beam propagation of having a fibre with greater diameter with less index difference.

The optical field distribution in *x-z* cross-sections along a GI-MMF with a larger core and cladding of 200/400 µm are presented in Figure 3.21 (a) along with the corresponding normalised intensity profile in Figure 3.21 (b) of the propagated beam with an MFD of 10 µm at the $1/e^2$ value of maximum on the beam axis. The fibre is operated at a 1.55 µm wavelength and the refractive indices of the core and cladding are n_1= 1.46 and n_2 = 1.454, respectively. Although the refractive index of the core is made smaller, the light is mostly maintained in the core region and propagates with the total internal reflection (TIR) phenomenon through the fibre.

The simulation results in Figure 3.21 (a) show the results of increasing the inner and outer geometry of the fibre for a 10 mm length of transmission. We found that after propagating the original input image through nearly z = 3.48 mm in the proposed fibre, the transmitted incident Gaussian beam were completely retrieved (an inverted image based on the fractional Fourier transform). This reproduction length interval is twice the first self-imaging distance of a fibre with similar geometry (as shown in Figure 3.20 (c) of section 3.8.6), but slightly higher index of the core (n_1 = 1.48). By lowering the index differences between the core and cladding to its minimum point, an input beam is reconstructed (i.e. an actual image) at almost 7 mm, which is where $z = 4L$ (with the Fourier length L being 1.75 mm).

It is clearly evident that using the fibre with a lower index difference for a given refractive index, the power is distributed to the side of the structure over a large area of the cross-section but experience longer self-imaging distances at the re-imaging planes. Thus one way to extend the formation of an imaging to longer lengths is to use the GI-MMFs with less index differences and large fibre geometries. Thus this fibre design can effectively expand the self-imaging lengths, with a real image being formed at a distance of 7 mm away from an input plane.

3.9 Conclusion

Throughout the simulation presented in this section, we have investigated a beam of light transmitting in MMFs with different fibre specifications, dimensions and index profiles (but at the same operating wavelength). It has been shown that is possible to periodically fully recover the input beam, and hence the data or information carried by modulation of this beam. We also show their relationship to length of the image reconstruction at the desired plane.

Thus the initial phase pattern and the beam amplitude profile at the source are reconstructed at some particular planes along the length of the fibre. These positions are the so-called the self-imaging planes where the interference of the excited modes has converged. It is possible to observe the interference patterns over the cross section of the fibre and the characteristics of the light propagation in different locations because of the distribution of the excited modes, i.e. each of the modes travel with different speeds and phase constants. We have designed a new optical fibre architecture to couple one spatial channel of the beam passing through a single strand GI-MMF. In the simulation results, our approach allows the input beam to be reconstructed periodically at longer distances, such that one can easily optimise the distance of the image reconstruction for an input image by carefully designing the fibre parameters.

Chapter 4

High-density multi-channel transmission in graded index fibre

4.1 Introduction

A plurality of spatially independent channels is seen as a way to increase the capacity of a fibre by transmitting a number of input Gaussian profile beams [68, 87, 95], operating in the same wavelength region within a single multimode fibre. Multiplexing a number of communication channels is our greatest concern in this chapter to overcome the limited transmission capacity and maximise the data rate. Another important factor that needs to be investigated is the degradation of the optical signal due to perturbation effects within the fibre. This is because this affects the maximum number of channels that can be transmitted in the system. Our primary objective in this chapter is to demonstrate the number of multiplexed optical sources in the system by illuminating multiple numbers of Gaussian beams onto the centre fibre, which has been proposed in Chapter 3. In this work, we define the channel as an input Gaussian beam, propagating from a number of sources that is carrying independent information down to a single multimode fibre core. We show the potential to increase the capacity of a fibre employing a SDM technique, which is multi-channel transmission down a single core of a GI-MMF. However, there are several challenges that need to be considered with the design of such a system, for example, the arrangement of the optical sources and the packing of the number of optical channels that can be simultaneously accommodated in the GI-MMF. Later in this chapter, we investigate the influence of the excitation conditions, i.e. the separation distance and the physical arrangement of the optical

channels, on the strength of coupling between adjacent channels (beams), and then estimate the channel crosstalk.

4.2 General background of SDM

The crosstalk between channels is an obvious drawback in SDM and is the main challenge when using multimode or few-mode fibres. This is because the spatial channels in either the modes or cores are packed tightly inside the optical fibre. Hence there is the need for electronic post processing, namely multiple-input-multiple-output (MIMO) at the receiver to subtract out and equalise the mode crosstalk. However, the management of differential modal group delay and strong coupling effects have created difficulties for MIMO in equalising the channel crosstalk. Over the last two decades, using wavelength division multiplexing (WDM) as a multiplexing technology has increased the transmission capacity by two orders of magnitude which has met the growth in capacity demand [68]. Most recently, increasing the capacity of optical fibres using coherent detection methods rather than direct detection has been used to achieve higher spectral efficiency (SE) with the maximisation of SNR [11]. Clearly, high SNR values mean that more power of the signal must be employed and as such requires more energy per bit transmitted and so can limit the traffic demand.

As a more recent technology, SDM has been heavily investigated as a new way to further increase the transmission per bit and has promising potential to provide a reduction of cost per transmission bit and be more energy efficient with the use of in-line amplifiers. The systems using SDM are categorised into two fibre types (see Figure 4.1) as candidates to transmit signals having the same wavelength, i.e. multi-core fibre (MCF) and multimode fibre (MMF) or few-mode fibre (FMF). In principle these fibres can support more than one transverse mode. The MCF has the potential to transmit data with a high spatial density of cores in a single cladding. However, the multiple independent cores have to be sufficiently well separated with the properly sized distances to minimise

crosstalk. Another fibre type utilises MMF or FMF transmission using mode-division multiplexing (MDM) to spatially multiplex multiple distinguishable modes with sufficiently different propagation constants between each spatial mode guided. By doing so, the reduction of crosstalk between each mode and the suppression of linear coupling are possible. As has been described in the literature, an SDM fibre that supports a large number of spatial modes, N, can be used to increase the transmission capacity by a factor of N times over that of a single mode fibre [68]. However, the number of modes transmitted is restricted by the dimension of the core and the maximum number of an acceptance angles and/or the numerical aperture.

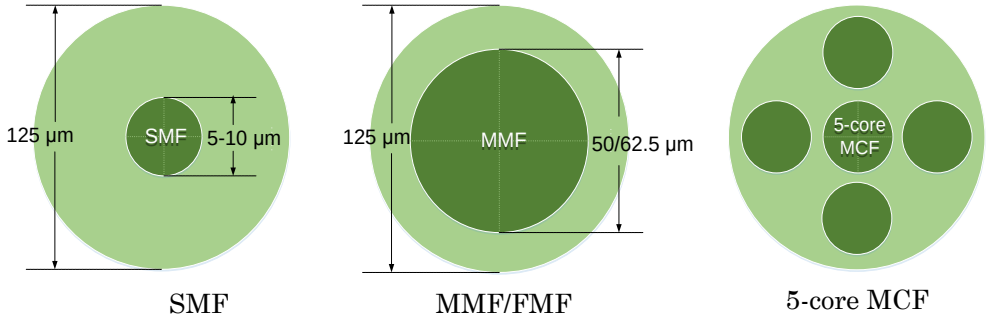

Figure 4.1: Summary the different types of optical fibre used in communication systems (adapted from [68]).

The current challenge in designing a fibre is to have the maximum number of spatial modes whilst making sure that the linear mode coupling and modal dispersion are suppressed since these are the main obstacles to achieving a higher transmission bandwidth [68]. Therefore, there are possibilities that the different modes will exhibit fibre impairments, i.e. there will be detrimental effects due to the differential modal group delay (DMGD), modal differential loss (MDL) and gain (MDG), mode-coupling, crosstalk from one mode to an adjacent mode and inter-symbol interference (ISI) in modes that have different group velocities.

To achieve more transmission capacity per bit, it is essential to compensate these impairments by introducing electronic or optical compensating techniques. To date it can be clearly seen that utilising traditional MMFs can support more numbers of modes with different core and cladding diameter designs (core/cladding size), e.g. 50/125 µm and 62.5/125 µm. However, these experience high DMGDs and it is difficult to specify them individually. Nevertheless, the recent fibre technologies of FMF, supporting only a small number of modes, have led to significant developments due to their low DMGD and so can largely reduce the system level complexities required in previous multi-core designs [15, 69, 70].

4.2.1 SDM transmission system architecture

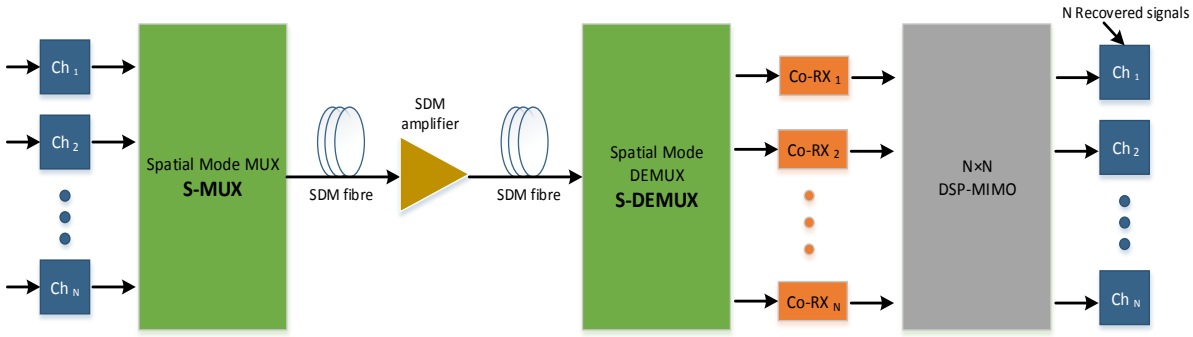

Figure 4.2: Architecture of an $N \times N$ SDM transmission system utilising coherent MIMO digital signal processing. MUX/DEMUX: multiplexer/demultiplexer, Co-Rx: coherent receiver (adapted from [43]).

The major key elements for the full realisation of the SDM architecture (see Figure 4.2) for an $N \times N$ channel system comprise:

- N transmitters
- space-multiplexer (S-MUX)
- SDM fibres
- SDM optical amplifiers
- space-(de) multiplexer (S-DEMUX)
- Mode generators
- N coherent receivers

By using MDM, the multiple channels are used as multiple independent modes to further increase the capacity. The S-MUX is used to couple the light carried from different spatial modes into SDM fibres, i.e. MCF, MMF/FMF. It is noted that all the modes propagate with the same wavelength. The SDM signals are amplified, added and dropped at the same time. The received signals are demultiplexed at the end of the SDM fibre and *N* channels are ready to be detected by coherent receivers to convert from an optical domain to an electrical domain, and electrical signals are processed with a DSP-MIMO algorithm to minimise the channel impairments such as mode coupling and crosstalk between each mode [12, 71, and 72].

The first proposed method using the refractive index profile of a graded index fibre core design to realise the MDM concept was reported in 1982 by Berdague and Facq [69] to launch and recover the two independent modes using spatial filtering techniques for short-haul transmission up to a ten kilometres. Gruner-Nielsen *et al*. [70] have also recently experimentally demonstrated a reduction of DMGD, a low insertion loss as well as lower coupling between each mode for transmission supporting LP_{01} and LP_{11} guided modes.

4.2.2 Impact on MDM in optical fibres

Modes in fibres are said to be orthogonal to each other as long as their spatial amplitude and phase stay the same during their propagation in the fibre. However, the orthogonality of modes is destroyed if a coupling level exists in the fibre and also due to crosstalk among each mode caused by imperfections of the fibre such as bending. Thus this main challenge has placed a limitation to achieving higher capacity and long transmission distances of communications.

Since the degenerate modes have the same propagation constant, they will couple with each other and so mode coupling and crosstalk are introduced between the degenerate modes. The input independent data stream will be dispersed at the receiver; in other words the signal is spread and it is not easy to characterise the channels individually due to the modal dispersion which

causes the signal to arrive at the receiver with different modal group delays. According to [13, 15], mode coupling can be compensated in order to achieve greater modulation bandwidth within the available optical power budget. This effect, however, seems to be contradictory if the loss is suffered by transferring the optical power into radiating modes.

The coupling between degenerate modes of different paths must be undone to fully recover the original transmitted data stream. The method used in wireless communication, namely, the MIMO transmission system, can be exploited to equalise the mode crosstalk in a SDM system. In general, there are two main equalisation techniques: time-domain equalization (TDE), reported in [71-73], and adaptive frequency-domain equalization (FDE) [74, 75]. It is observed in [15] that the BER performance in an adaptive FDE reduces the complexity more for each spatial mode than that in adaptive TDE.

4.2.3 SDM components

The components in SDM systems are classified into passive and active devices, which will be covered in this sub-section.

4.2.3.1 Passive fibre components

These offer an option to be highly integrated with the SDM system and be able to convert a multiple single mode signal into a multimode light signal and vice versa. The mode-division multiplexer has to map one single mode input signal to one mode of the multimode output signal at the other end face of the fibre. With inputs to the fibre having different propagation constants, the mode selectivity can be performed, meaning that each input mode is mapped into one particular output mode. The passive components for mode MUX and DEMUX comprise of the following:

Mode conversion methods are based on the use of phase plates, a bulk phase mask device, or tuneable spatial light modulators (SLM) such as liquid crystal on silicon panels (LCOS). Phase plates are capable of matching the fundamental mode profile LP_{01} into higher order modes and to excite mode

guides in MMF. However, the drawback of this multiplexer is the high insertion loss (IL) and the number of modes is limited since the insertion losses are mode dependent and scale with the number of modes.

Spot-based multiplexers are seen as a way to improve an increasing IL with multiplexing a high number of modes that are imaged onto the MMF/FMF facet [15, 68]. These spot multiplexers can excite a linear combination of modes and match each spot profile to a near group of SMFs. The addition of an adiabatic transition region in a so-called photonic lantern (PL), is an extension of the spot-based multiplexer; the input signals have a potential to transmit with a large number of modes over MMF/FMF within the transition region (see Figure 4.3). The input signals are coupled to more than one mode group making the mode selectivity feature possible and the ability to excite only one mode group per fibre.

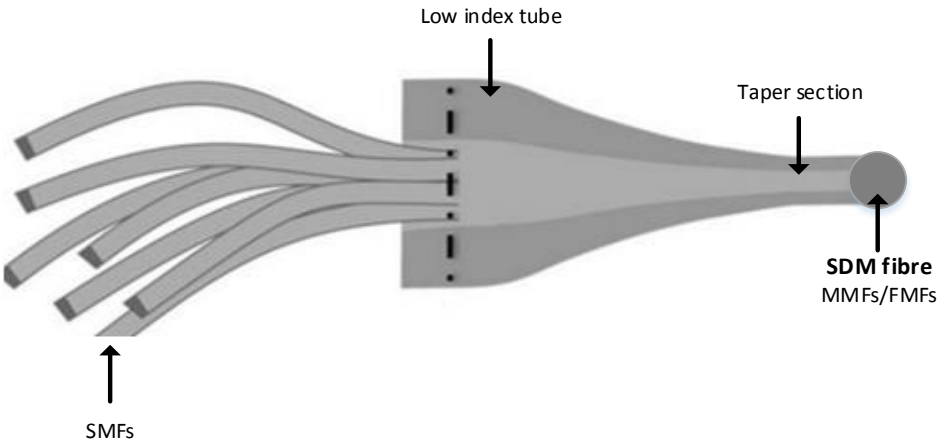

Figure 4.3: Passive component in SDM systems (adapted from [68])

4.2.3.2 Active fibre components

Multimode amplifiers are essential in long distance SDM transmission to boost the power and compensate for losses. The key recent technologies in amplification for SDM systems are multimode erbium-doped fibre amplifiers (MM-EDFA) and multimode Raman amplifiers. Currently, multicore EDFA (MC-EDFA) has been demonstrated that has the potential to amplify multiple spatially separated channels with a low core-to-core crosstalk for achieving long distance communication in a weakly coupled transmission [78].

For a MM-EDFA, the main concept is that each mode needs to manage its power loss and the associated signals within each mode must have enough gain to amplify the signals. It is essential to minimise mode-dependent gain (MDG) and to control distribution of power in a signal mode [15]. From the theory of MM-EDFA, there are basically two main approaches to equalise MDG: pump-mode control and doping-profile control. In the pump-mode control approach the power distribution depends upon the desired pump intensity profile in which it is generated from the pump source and is controlled by attenuators. Then the pump source, generated by a laser diode, is first separated into a number of different paths and the mode converter is used to convert from low-order modes to high-order modes and vice versa. Each mode generated from a pump source is then combined with the field distributions of signals guided by the MMF via a dichroic mirror (Figure 4.4).

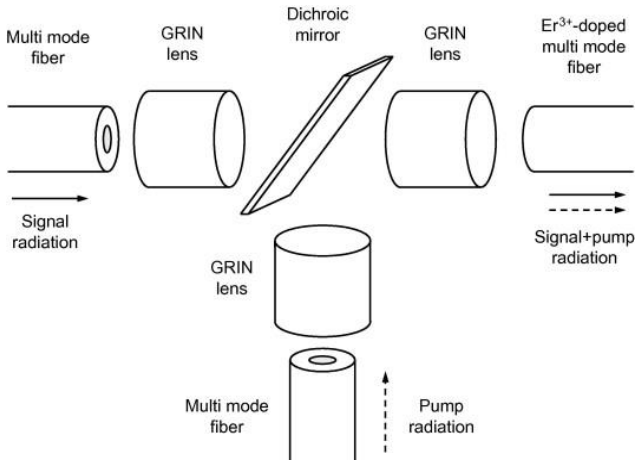

Figure 4.4: Pump signal combiner concept for single multimode core fibres [12].

The dichroic mirror is used to reflect the pump radiation and also can be used to transmit the signal from the MMF. The combined signals are fed into a MMF and focused into a MMF EDFA module [15, 68]. Another MM-EDFA approach is doping-profile control in which all signal modes receive the same gain level and use a refractive index profile to control the modal gain by having a ring profile shape. The latter method can amplify significantly four nondegenerate mode groups and has been experimentally demonstrated elsewhere [79].

Another frequently used MMF amplifier is the distributed Raman amplifier. A flat Raman gain derives from the transfer power from multiple pump radiations of different modes to multiple signal radiations along the transmission path. In comparison with MMF-EDFA, the Raman amplifier requires more pump power density at longer lengths of the fibre. It is shown in [12] that the total power pump level in the case of MMF-EDFA is less than that for the distributed Raman amplification and has the possibility to gain better power efficiency.

4.2.4 The progress in SDM transmission system experiments

The long transmission distance in a graded index FMF-MDM system consisting of 6 spatial modes has been reported in [80] over a 1200 km length with 30 km spans. The crosstalk was suppressed by using coherent 12×12 DSP-MIMO processing using the work of Ryf *et al*. [81], where a record was achieved for the highest number of 6 spatial modes (LP_{01}, LP_{11a}, LP_{11b}, LP_{21a}, LP_{21b}, and LP_{02}), considered as multiple separated data channels.

To date, the developments of SDM transmission have shown a net total capacity of more than 1.01 Pb/s by utilising a 12-single mode MCF and a MCF which has been demonstrated by Takara *et al*. [82] over a distance of 52 km in a single span. In the experiment by Igarashi and co-workers [83], a transmission distance over 7326 km with a 45.5 km span length achieved a record 1030.8 Pb/s × km of capacity-distance product with a 7-core fibre. In order to gain further significant increases in the capacity it is possible to utilise a hybrid of the MCF and FMF concept. Recent developments by Qian, *et al*. [84], have achieved the highest record capacity so far which is now approaching 1.05 Pb/s with a hybrid of 12 single-mode cores and 2 few-mode cores supporting 3 spatial modes but at only 3 km distance. However, the net spectral efficiency is by far the highest, leading to 109 bit/s/Hz as the initial achievement. The current transmission systems are moving forward into a region that provides high spatial multiplicity of more than 30 spatial channels [155] and dense space division multiplexing (DSDM) by utilising multi-core and multimode fibre as the transmission medium to triple the current capacity per fibre of 1 Pb/s in SDM systems [156, 157].

In our proposed system, the light exiting from the same laser source with the same wavelength was launched as spatially modulated channels into a single fibre. An output in the form of circular rings is obtained at the end of the fibre corresponding to the modulated channels. The channels are then directed to a number of detectors. The output intensity profiles of the beam are visualised to determine the interference pattern and crosstalk during propagation between channels. The SDM channels use a laser source to transmit different channels

of the same wavelength with each channel being specified by its own spatial location. The channels are transmitted on separate spatial modes/routes and then routed together into a standard graded index multimode fibre with a well-defined core/cladding diameter. The ring shape output pattern can be used to determine the density of SDM channels supported inside the fibre core from its total thickness [85]. Most importantly, this will allow the bandwidth of existing systems using one fibre core to be improved by more than 10 times in the near future [86].

4.3 Principles of coupling between spatial channels in the fibre

When two or more input channels are multiplexed in the same fibre, there is a possibility that an undesired optical power from one channel will transfer into another channel and an amount of signal power is coupled from one channel into other channels. That signal then becomes the noise of another channel such that this fraction of unwanted signal is known as crosstalk [87-89]. The main sources of contribution to the crosstalk between channels are from the effects of scattering (i.e. from one beam into the neighbouring beams) and the diffraction of light during propagation.

It is important to minimise the exchange of unwanted signal between adjacent channels and reduce the chance of interference with an inflow of unwanted signal; therefore, arranging the channels with sufficiently spaced distance is key to providing a solution to guarantee acceptable crosstalk levels of the signal from one channel into another channel. If, however, the channels were physically placed close to each other below the optimum separation distance, this in turn would give rise to increased channel crosstalk. To meet the higher bandwidth requirements for future communications by employing multi-channel propagation, it would be useful to increase the density of the packed channels and simultaneously propagate them within the same fibre. However, there is a trade-off between the crosstalk levels, and achieving the maximum number of

input channels over a length of transmission because the higher the channel density, the larger the crosstalk between multiple channels. Thus, maximising the distance between these channels is seen as a way to overcome the power coupling present between the neighbouring channels, although the number of multiplexed channels is limited in such a way.

Many SDM transmission systems based on multi-core (MCF) and multimode (MMF) or few-mode (FMF) fibre usually employ a DSP-MIMO to equalise the crosstalk level and to spatially de-multiplex the transmitted data at the receiving end. Nonetheless, the complexity of DSP-MIMO can be neglected if the crosstalk between adjacent data streams that arises from the extraneous optical power from the other channels during propagation can be reduced with a proper channel design arrangement in which each of these channels are spaced equally with an optimum distance. According to the studies in [90, 91], a tolerable inter-channel crosstalk levels of -10 dB for a power penalty of 0.5 dB is required for a digital signal over a short reach communication system. However, for a power penalty of about 1 dB, a typical crosstalk of less than -25 dB is appropriate for the in-band channel crosstalk for long haul transmission greater than about 100 km [92-94].

4.4 Design of multiple spatial channel transmission

4.4.1 Optical channel arrangement

To realise such a plurality of transmission channels, the combination of multiple Gaussian beams can be utilised as input optical light sources in the fibre. In the simulation model, we set the launched beams with an equivalent spot size w_n of 5 μm (the beam diameter $2w_n$ = 10 μm). The model that is being investigated comprises of four, seven and eight independent beams, which are arranged over the cross section of the fibre as displayed in Figure 4.5(a) – 4.5(c), respectively. We decompose the input Gaussian beams in the GI-MMF, which supports a multi-channel transmission as has been proposed in the previous chapter. The optical beams are injected onto the centre of a GI-MMF structured with 200/400 μm (core/cladding) diameters with a low index difference (Δn_1 = 0.6%), with a refractive index in the core axis n_1 of 1.46 and surrounded by a lower cladding refractive index n_2 of 1.454. The transmitted beams are coupled through the optical transmission system at the wavelength λ of 1.55 μm. To make a fair comparison, these input beams have the same physical parameters, i.e. the same beam spot sizes. Here, the Gaussian beams used in our model are defined by the following equation:

$$E(x_n, y_n) = \exp\left[\frac{-(x-x_n)^2 + (y-y_n)^2}{{w_n}^2}\right] \tag{4.1}$$

where the subscript n denotes the beam number.

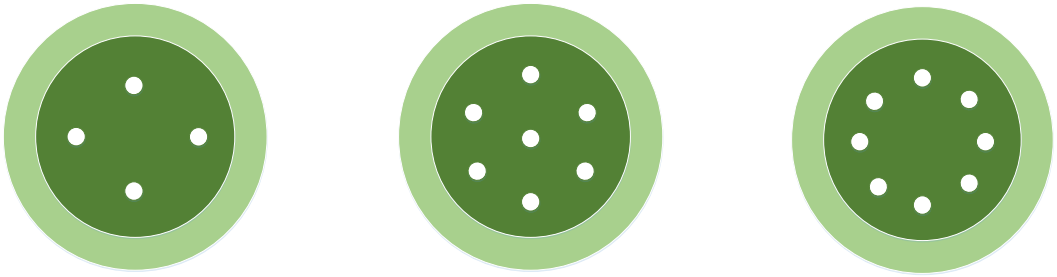

(a) 4-channel arrangement (b) 7-channel arrangement (c) 8-channel arrangement

Figure 4.5: A schematic view of the multiple beam arrangement in a GI-MMF for: (a) 4-channel; (b) 7-channel; and (c) 8-channel configurations.

4.4.2 Design structure of multi-channel transmission in optical fibre

The study of independent transmission channel arrangements with a high number of transmitting channels per fibre core has been investigated from the viewpoint of crosstalk analysis between the channels in order to progressively increase the channel capacity in the SDM transmission. In this work, we have demonstrated the coupling of different channels with a 4-channel, 6-channel, 7-channel and 8-channel arrangement. It is worth noting that we should get the same coupling phenomenon between the neighbouring channels since each beam has the same properties and they are equally separated from each other. For simplicity and ease of the launching condition, it is reasonable to assume that the separation distances between the beams are equal and by a sufficient distance from the centre of one beam to adjacent beams. To further explain the design, the centre of the fibre is located at the (0,0) coordinate and each channel is assigned at different positions in x_n and y_n coordinates, which depend on the design configuration. To begin with, we have characterised the impact of inter-channel crosstalk between a 4 beam spatial channel at a close spacing distance between the beams of 45 µm, and consequently a high density of beams has been packed in the proposed fibre. Then, we further increase the spacing distance between the channels and find that the best optimum distance where the beams can be positioned is around 60 µm from the centre of the structure. It is

demonstrated that increasing the spacing distance further away from the optimum range, the beams tend to lose their power to the lower refractive index region and it is impossible to maintain good quality Gaussian beams.

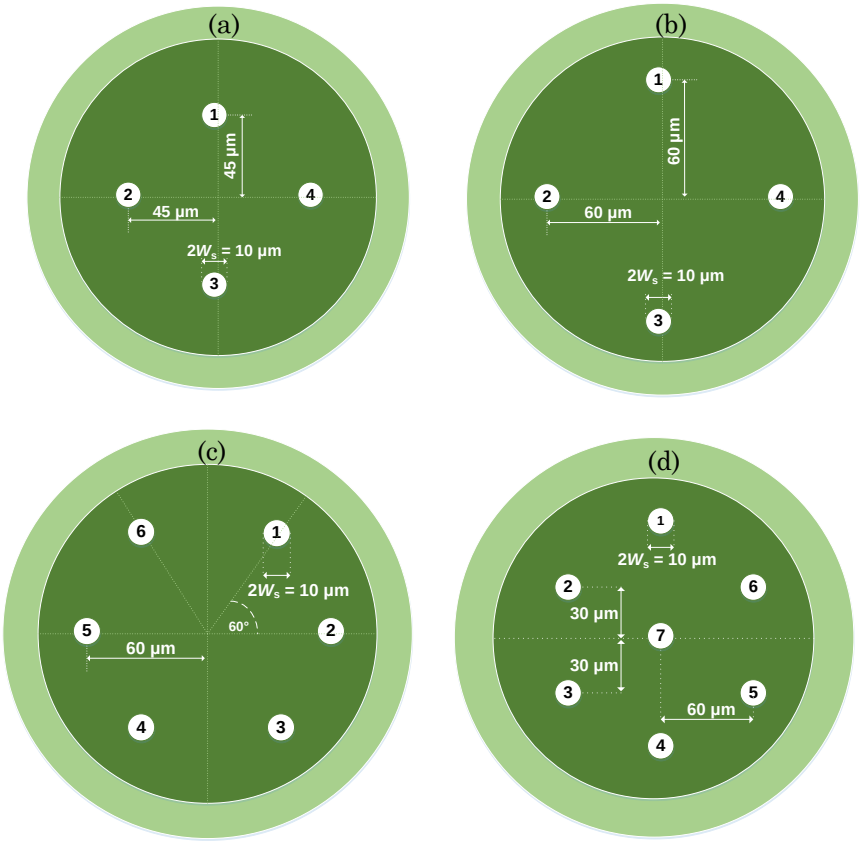

Figure 4.6: A schematic view of different beam arrangements and the associated optical parameters of: (a) 4-channel transmission with a 45 µm spacing distance, (b) 4-channel transmission with a 60 µm spacing distance, (c) 6-channel transmission with 60° spacing distance between adjacent channels; and (d) 7-channel transmission.

Later we will show that arranging the beam in a circular ring-like structure can ensure a tolerable crosstalk level and make use of the total available capacity in the fibre. In other words, the power coupling of each channel in this design, as shown in Figure 4.6 (a) - (c), receives approximately the same amount of additional power from the two adjacent channels, while the hexagonal structure in Figure 4.6 (d) is not quite an optimum arrangement. The

reason is that the central beam is surrounded by six outer channels and so suffers significant scattered signal from all the neighbouring channels.

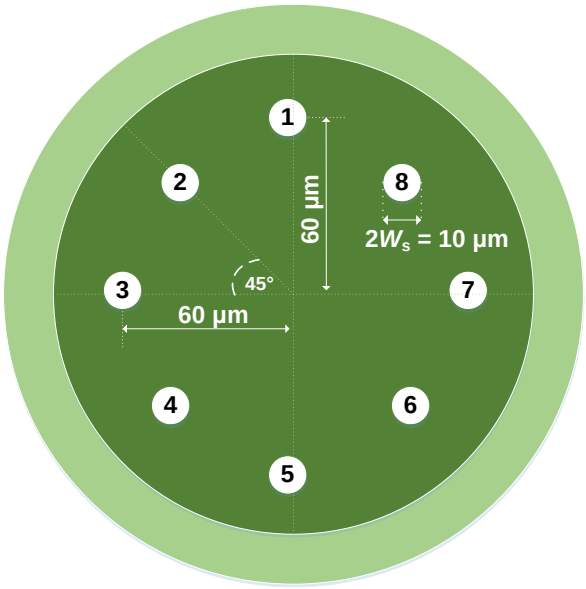

Figure 4.7: The structure of eight independent spatial channels is well separated by the angle $\theta = 45°$ between adjacent channels.

Let us consider the beam arrangement in Fig. 4.7 for an 8-channel configuration where each beam is spaced by the angle $\theta = 45°$. Obviously, the total number of spatial channels that can be packed in the fibre core increases with a decreasing angle between adjacent beams, but the overlapping area occupied by the detector at the central location of each beam will receive a significant portion of the transferred power from the near channels and hence introduce large amounts of beam coupling. Furthermore, it is seen that the number of channels that can be simultaneously multiplexed in a large fibre core diameter increases with a decreasing angle θ between the channels. Nevertheless, the maximum number of communication channels and the minimum separation distance are limited since it depends upon the tolerable crosstalk levels between nearby channels as mentioned in Section 4.3.

4.5 Measurement method for channel crosstalk

4.5.1 Metrics for measuring the crosstalk

The crosstalk in fibre optics is a measure of the amount of an undesired transmitted signal from one channel that is picked up by another channel. A relation of the optical power at the transmitting end and the power at the receiving end usually defines the crosstalk. However, in our crosstalk evaluation, the channel crosstalk XT in channel number n is estimated from the ratio of the signal and crosstalk optical power that has fallen into the detector space and is determined by using the relation:

$$XT_n = \frac{P_{\text{sin}\,gle,n}}{P_{multiple,n} - P_{\text{sin}\,gle,n}} \tag{4.2}$$

where $P_{\text{single,n}}$ is the optical power of the transmission signal in a single beam and $P_{\text{multiple,n}}$ is the optical power collected from the multiple channel transmissions that occur at the same time, as shown in Fig. 4.8 (a) and (b), respectively, as an example of a 6-channel transmission for the beam located in the top right of the structure. Generally, $P_{\text{single,n}}$ is always less than $P_{\text{multiple,n}}$ because there is the leakage of signal crosstalk from adjacent channels.

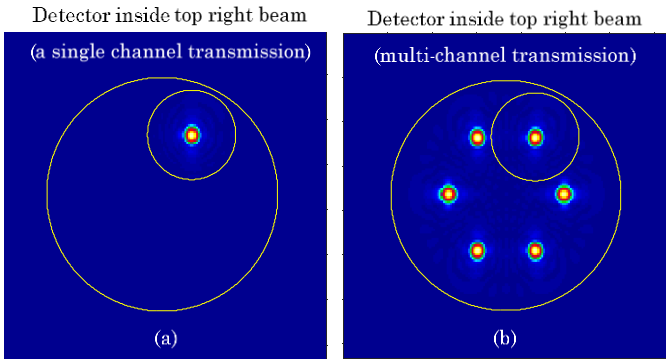

Figure 4.8: The XT_n evaluation of the top right beam for: (a) $P_{\text{single,top right}}$ the optical signal of the beam; and (b) $P_{\text{multiple,top right}}$ the optical signal of the top right beam with associated crosstalk. The small circular region located in the middle of the beam denotes the area of the detector and the bigger circle represents the boundary of the fibre core size.

To analyse the beam crosstalk in a multi-channel transmission configuration, initially we run a simulation for a single channel transmission with each simulation being launched with a Gaussian input beam positioned exactly at the same coordinates as the beam would be in a given multi-channel arrangement, in which the detector size and its position are kept the same for both the single and multiple beam transmission, i.e. centered on the beam re-imaging position. A reasonable circular size of the detector can be made to cover most of the propagated field of a single beam. Overlaps of the multiple beams onto that detector are determined by measuring the optical power within a surrounding circular area of a single channel transmission, and then comparing the occupied optical power in multi-channel transmission so allowing the power coupling to be analysed. Thus to assist in crosstalk reduction, we would prefer to have a detector size as small as possible in order to prevent the undesired signal being coupled from the neighbouring beams [95]. However, it is not the best option to keep the crosstalk below the tolerance levels simply by reducing the detector size. The reason is because the optical fields during the transmission will be lost in the surrounding area. Rather than decreasing the detector size, there exist other solutions to further reduction of the crosstalk by optimising the channel spacing and arranging the multiple beams to be accommodated in the core area.

4.5.2 Algorithm for evaluating the multi-channel crosstalk

As the beams propagate in the fibre, they overlap with the neighbouring beams in a certain circular area. In order to take account of the amount of additional signals coming from other beams, it is essential to set the boundary regions of interest (ROIs) for each channel. The occupied circular area of the ROI can be thought of as the detector size, i.e. the photodiode. Moreover, there is no particular rule for the size of the detector (indicated as a circular shape), but it should be large enough to collect most of the optical power in one channel and a minimum amount of light from the other beams. To optimise the influence of crosstalk on the multiple beam transmission, it has been suggested by Gloge [95] that at least 75% of total distribution power should be received within the detector region. Consequently, the unwanted signal crosstalk received from other channels can be suppressed. Also, it is stated in the same source that any beams that are equivalent in size and spacing between nearby channels should have a similar amount of scattering.

In the following, we explain in detail the measurement methods to evaluate the channel crosstalk from each of the transmitted Gaussian beams. The data extraction process for each of the beam profiles is given in the flow chart shown in Figure 4.9, which comprise three main steps as follows:

1) Obtain the image response at the image plane for the transmission of one channel;

2) Address the location for the centre of the detector array where the spot intensity level is maximised as the region of interest;

3) Determine the optical power falling into each of the circular regions.

We perform these steps again for the different coordinates of the beam profiles.

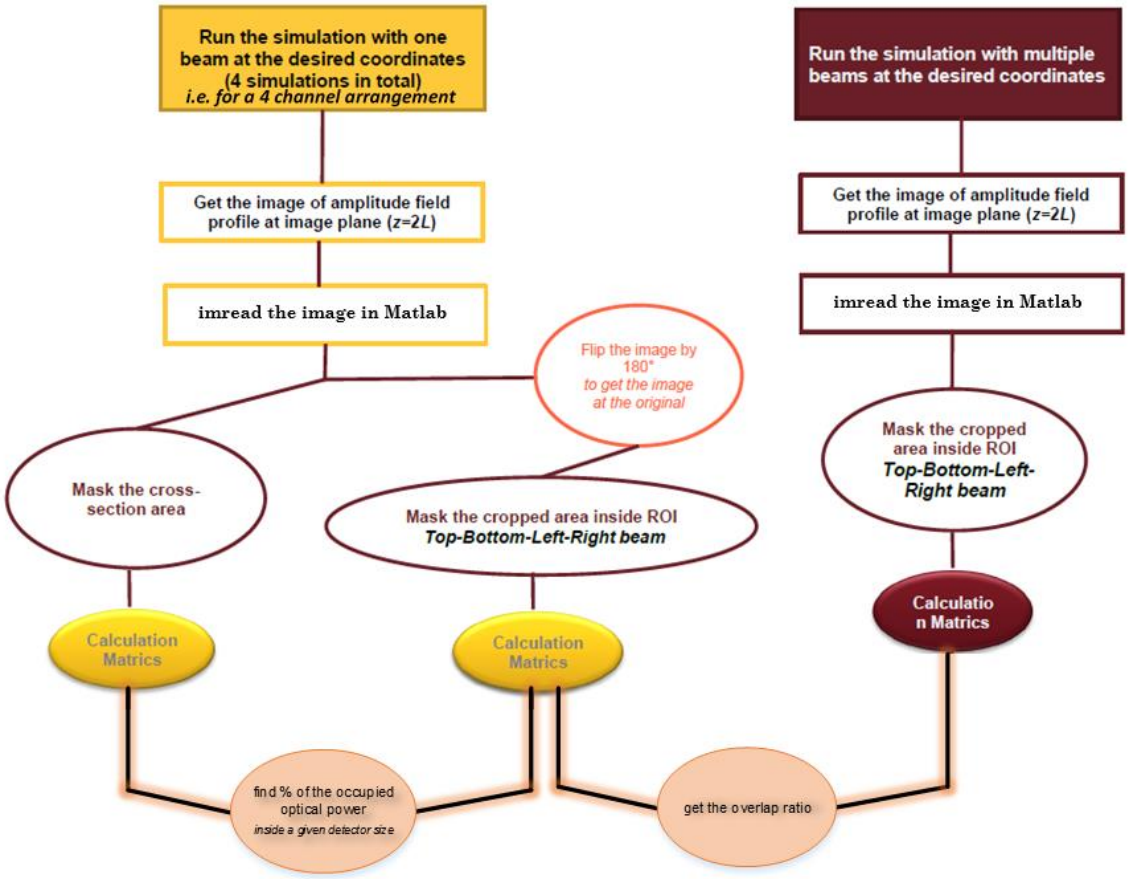

Figure 4.9: The flow chart diagram displays a process for the measurement of the associated signal of the beam ROI and ratio of overlapping power.

This process is repeated again with the reproduction of the input beam profile that is taken in the imaging plane of the multi-channel transmission. The increments of the overlapping area were measured by the difference of the associated optical signal between the individual beams and the multiple beam transmissions at the segmented ROI. Our proposed algorithm can be adapted to any number of beams with no restriction on the pattern of the launching beams at the fibre cross section.

Subsequently, the study of linear effects is determined when multiple channels are multiplexed and propagated in the same fibre. However, it becomes incredibly challenging to extract the light that propagates at the same wavelength from one of the several Gaussian beams. Therefore, we run a

simulation for a single channel transmission, and each simulation was launched with a Gaussian input beam positioned exactly at the same coordinates as the beam would be in multi-channel transmission. After running the numerical simulation for a single channel transmission, the next step is to multiplex several input channels with the same spacing between adjacent beams at the same time through the optical fibre.

Let us assume that we have chosen the size (in diameter) and the position (in the middle of the beam) of the detector and know the associated signal falling on the detector and then that amount will be squared to obtain the collected optical power for each of the beams. It is now a simple calculation to get the portion of scattered beam power outside of the detector area in order to determine the percentage of power collected by the detector. This was calculated in a single channel transmission by subtracting from the full amount of the optical power that is collected by the large detector region (i.e. within the total fibre cross sectional area) and the optical power that enters onto the defined detector region, as shown in in Figure 4.10 (a) – (d). This is done for the position of the masked circular detector for each beam for a 4-channel transmission located at the top, bottom, left and right, respectively.

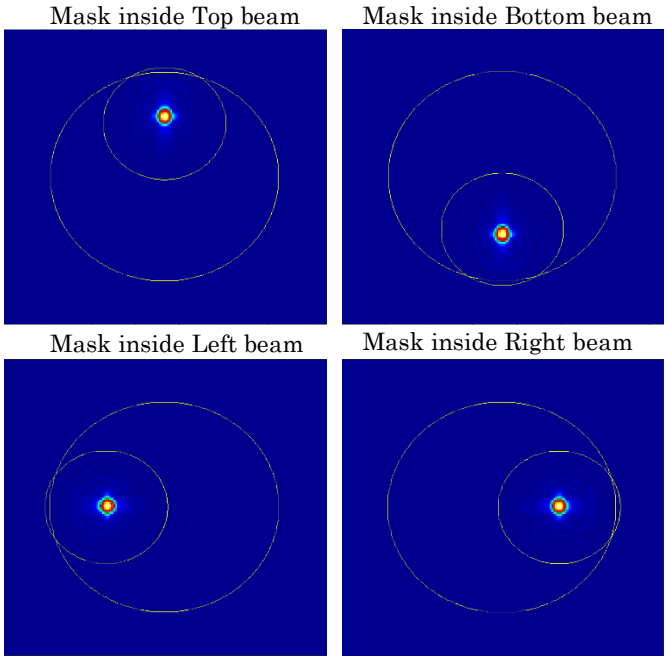

Figure 4.10: The numerical simulation of amplitude Gaussian beam profiles with their circular masks located at the centre of the beam coordinates for the beams arranged at the top, bottom, left and right positions.

The first step in performing a crosstalk analysis is to gather the amplitude field distribution from both the single and multi-channel propagation at the reconstructed plane $z = 2L$, i.e. twice the Fourier length in the fibre.

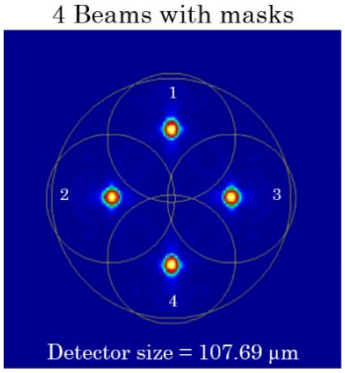

Figure 4.11: The amplitude beam profiles of the four-beam transmission with their circular detectors located at the centre of each beam at their different coordinates.

To determine the area overlapping from the nearby channel, we repeat the same boundary addressing process as described in Figure 4.9. We can see from Figure 4.11 that the detector is located in the middle of the beam to estimate the undesired signals from the other beams. Note that the size of the detector is identical between the different channels. Lastly, the coupling level, i.e. the unwanted signals of a channel, can be characterised by comparing the overall optical power with the power falling on the detector between the single channel and multi-channel simulation runs at the same input coordinates.

4.6 Simulation results

4.6.1 Results and Discussion

As the beams propagates along a 10 mm length of the fibre, it is clearly seen in Figure 4.12 that the first reproduction position of the multiple input beams was found at a distance z = 3488 µm. In addition, one can see that when multiple channels are simultaneously propagated in a GI-MMF, a significant amount of power is still coupled into the centre of the fibre. There is not much of the power that has been transferred into a lower refractive index region. In addition, a group of beams come to focus at the same position and arrange themselves periodically along the fibre in a multi-channel transmission.

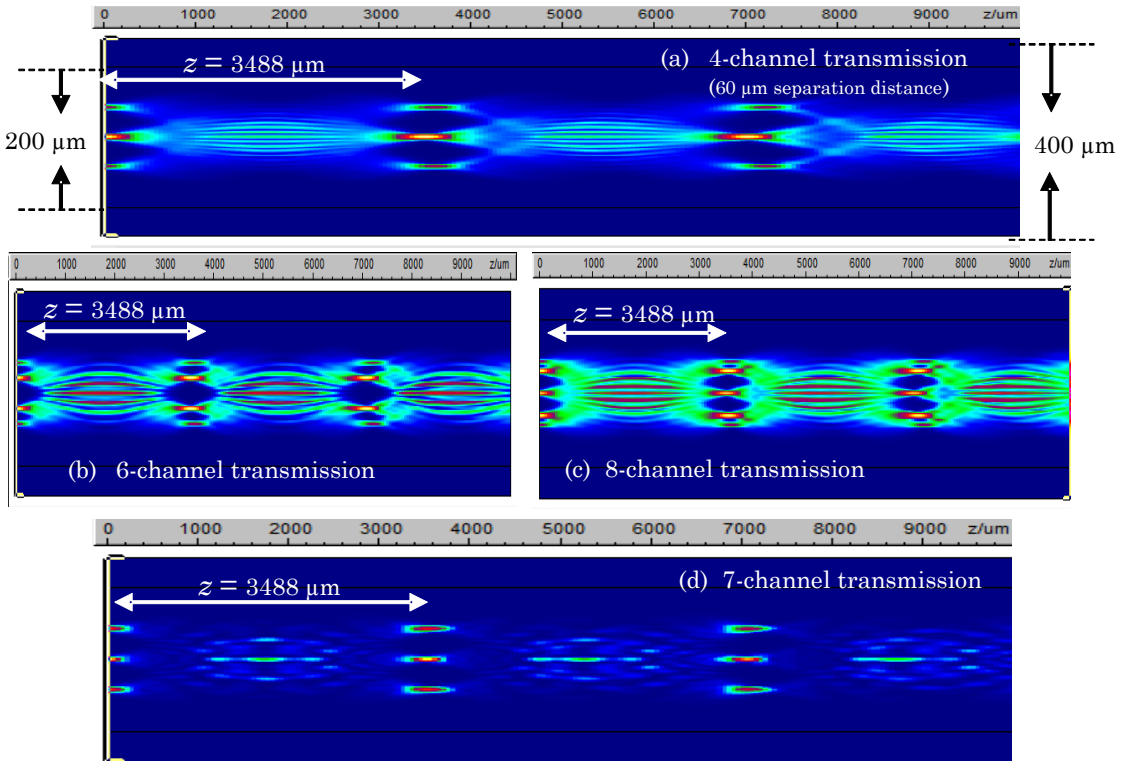

Figure 4.12: Side view of the propagation of the Gaussian beams multiplexed in the GI200/400 µm fibre operated with λ =1.55 µm for a propagation distance of 10 mm with: (a) the four Gaussian multiplexed beams; (b) the six Gaussian multiplexed beams; (c) an eight Gaussian multiplexed beams; and (d) the seven Gaussian multiplexed beams.

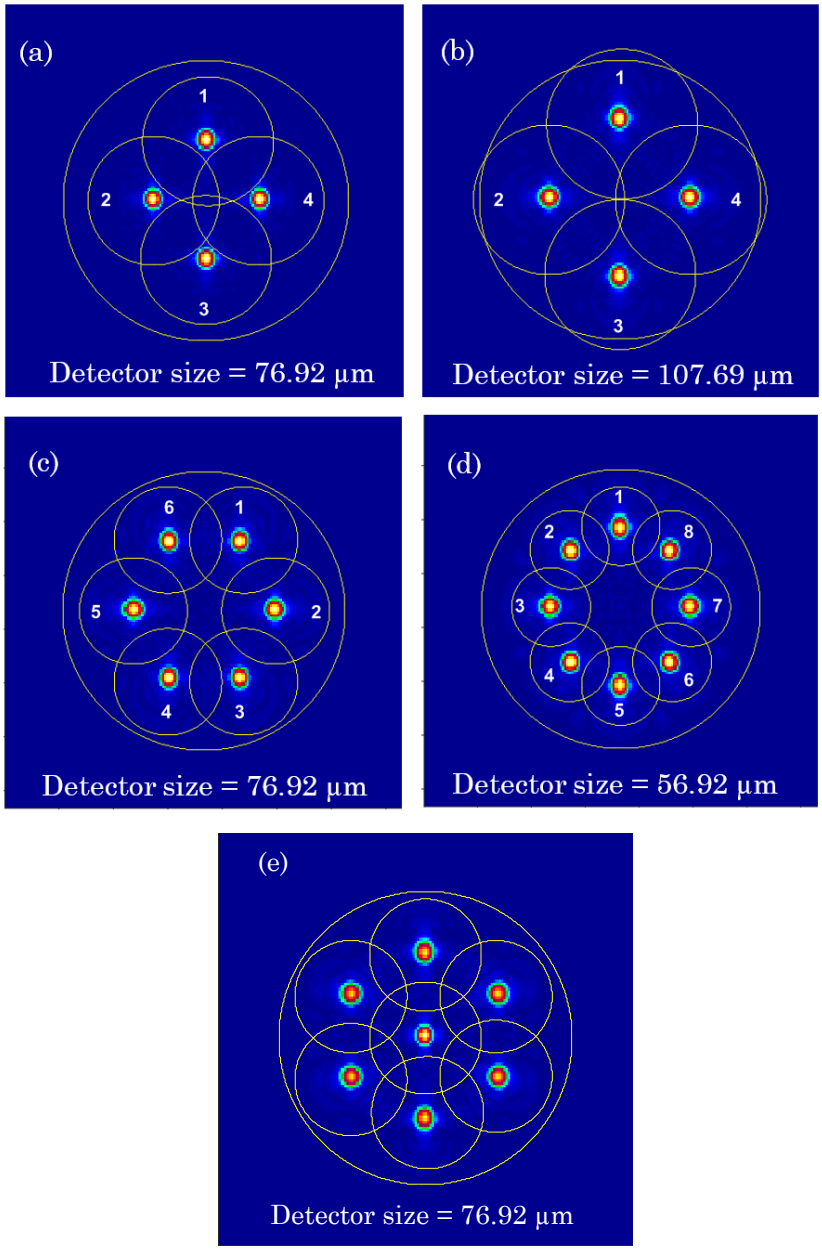

Figure 4.13: The amplitude field distribution of each of the physical channel arrangements and the detector's position with the marked channel number on the circular detectors (measured in diameter) for different types of SDM transmission system: (a) 4-channel (a 45 µm separation distance); (b) 4-channel (a 60 µm separation distance); (c) 6-channel with 60° spacing distance between adjacent channels; (d) 8-channel with 45° spacing distance between adjacent channels; and (e) 7-channel configurations with a 60µm spacing distance.

We measure that about 90% of the power is coupled into a GI200/400 µm fibre when the channels are distributed in a single ring structure for 4, 6, and 8 transmission channels, as depicted in Figure 4.13 (a) - (d), respectively. On the other hand, nearly 88.50% of the power is fully transmitted into the fibre when 7 optical channels are packed together in a hexagonal shape as shown in Figure 4.13 (e). Consequently, we can conclude that a ring-like channel arrangement is an optimum design configuration since the total available channels at a cross-section of the fibre receive approximately equivalent amounts of coupling and a high percentage of the power can be coupled in the fibre.

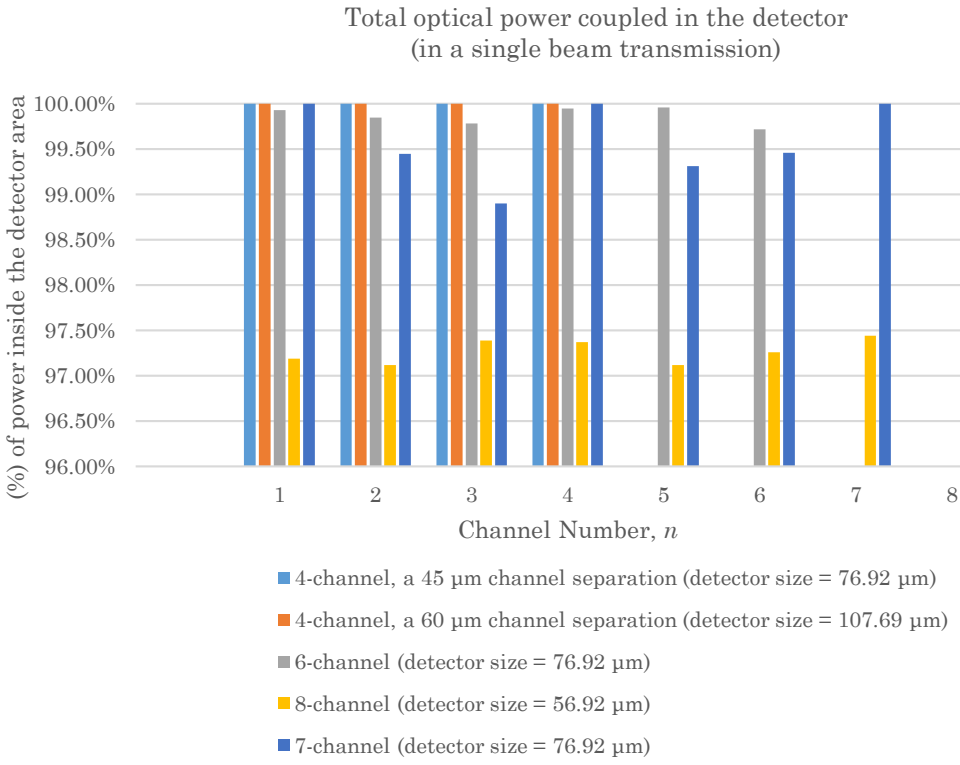

Figure 4.14: The percentage of the power coupled into the detector area (in diameter) for each beam position when a single beam is transmitted in the fibre.

Using the measurement metric for channel crosstalk given in Section 4.5.2, the graph in Figure 4.14 shows us that the detected optical power in a detector is greater than 75% of the total optical power transmitted from each beam [95]. Notice that the percentages of optical power collected in each detector are different between the several designs because the detector sizes are modified, which depend on the position, the number of channels and arrangement of the beams. We have therefore shown that the greater the spacing between the beams, the bigger can be the detector size. The reason for this is that the detector should collect the beam signal as much as possible in order not to lose the optical signal to the surrounding area outside the ROI. However, as the number of channels expand, the detector area should be kept as small as possible such that the percentage of extra power from the surrounding channels is diminished. Approximately 100% of the total power is received within the detector for all of the beams for 4 channel transmission, whereas in the 7 and 8 spatial channel transmission, we can achieve roughly 97% of the total power detected onto the face of a circular detector. The reason for this decrease in percentage of received beam signal is the reduction in size of the detectors due to a high number of multiplexed channels being transmitted.

4.6.2 Channel crosstalk measurement

The total crosstalk calculated for multiple channels in each channel structure was evaluated using the equation (4.2) and the results are represented in Figure 4.15. The graph shows the outcome of the channel crosstalk calculations that results from undesirable signal overlaps from neighbouring channels, for different numbers of spatial channels. It is clearly seen that a minimum channel crosstalk of approximately -30 dB is achieved when a 200 µm fibre core diameter is used as a medium to support 8 separated channels with an optimal channel spacing of 60 µm from the fibre axis. It can be confirmed from the work of Gloge and Weiner [87] that the fraction of coupled optical signal from channel No. 1 to channel No. 2 should be identical to the power coupled from channel No. 2 to

channel No. 1, and it will be approximately of the same amount with other channels. Generally speaking, the maximum level of crosstalk arises with increasing the number of packed optical channels in a fibre, and hence diminishes the ability to achieve an acceptable multi-channel fibre performance.

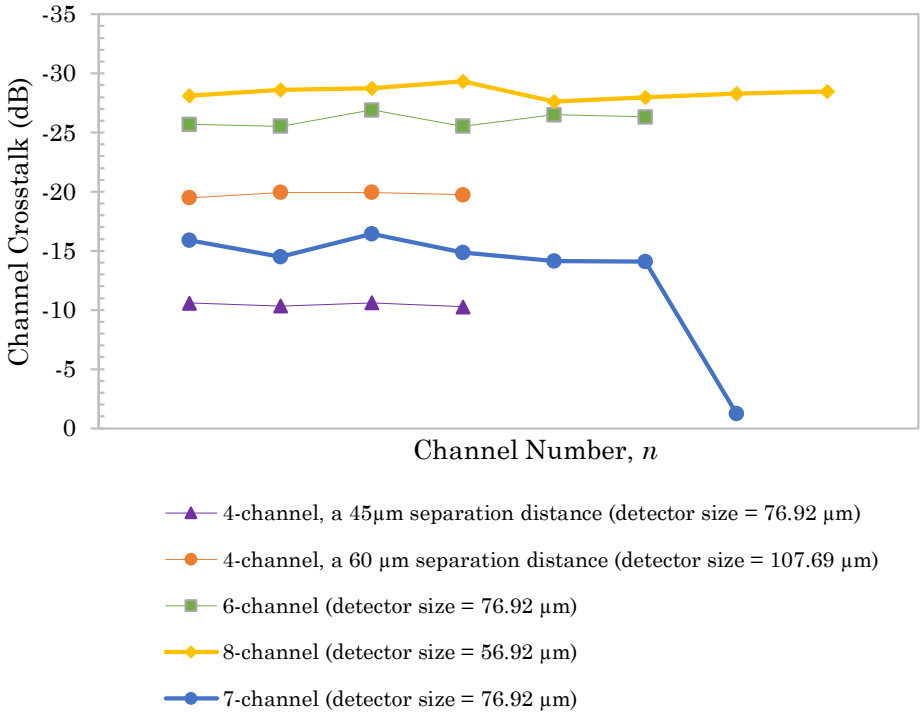

Figure 4.15: Calculated results for channel crosstalk with multiplexed 4, 6, 7 and 8 optical channels with distinct channel separations for a 200 µm fibre core diameter at the first reproduction plane where $z = 2L$.

In a single ring geometric structure of the 4-spatial channel arrangement, we observe that a channel crosstalk of approximately -10 dB is possible from each channel when the spacing distance was reduced to be as close as 45 µm from the centre of the fibre. On the other hand, we notice that by increasing the channel spacing in the design to a separation distance of 60 µm between each of the four channels and the fibre centre, the effective crosstalk decreases to -20 dB even with the larger detector size.

Moreover, the maximum crosstalk in the six channel configuration, at the level of -25 dB, occurs for all channels since these suffer undesired beam power

crosstalk from the two neighbouring channels. The overlapping area occupied by the detectors will receive a lower proportion of the transferred power from the nearby channels because of the smaller detector sizes and hence introduce relatively low amounts of beam coupling. Furthermore, when the channel spacing and detector size appears optimum, we observe that the tolerable crosstalk levels reach a maximum of nearly -30 dB, for a 1 dB power penalty, by increasing the number of transmission channels to 8 spatially independent channels. Hence, these calculated results show that a separation distance with an angle θ of 45° between beams and an optimum detector size can still maintain good crosstalk levels even with a dense multiplexing of transmission channels.

However, in the seven channel case, because some channels are spaced with an optimum separation distance, we can achieve the lowest crosstalk value of roughly -15 dB from the six outer channels of the seven channels. Moreover, the maximum crosstalk in this configuration, at the level of -1.3 dB, occurs for channel No. 7 since this suffers undesired crosstalk from all the six surrounding channels and as such we have seen that the hexagonal channel arrangement is not the optimum design for multi-channel transmission. It can be seen that by using well separated spacing distances between the channels in the design, the crosstalk is suppressed significantly even with the larger number of channels. The reason for this is because the overlapping area occupied by the detector will receive less portion of the transferred power from the near channels due to the smaller detector size, and hence introduce relatively low amounts of beam coupling. Clearly, the fibre of 200 μm diameter can well support the larger number of multiplexed channels by reducing the angle θ between two adjacent channels in a ring-like channel arrangement. As the crosstalk is a function of channel separation, the tolerable crosstalk could be increased with a narrower spacing distance and hence further increase the density of optical channels.

4.6.3 Channel crosstalk measurement of 8 independent channels at different planes

The graphs in Figure 4.16 show the measured sensitivity of the crosstalk channel for a group of the beams located at different planes, slightly before and after the imaging plane, for $z = 1.9L$, $z = 1.95\ L$, $z = 2.05L$ and $z = 2.1L$ µm in a fibre with a 200 µm core diameter, operated at a wavelength of 1.55 µm.

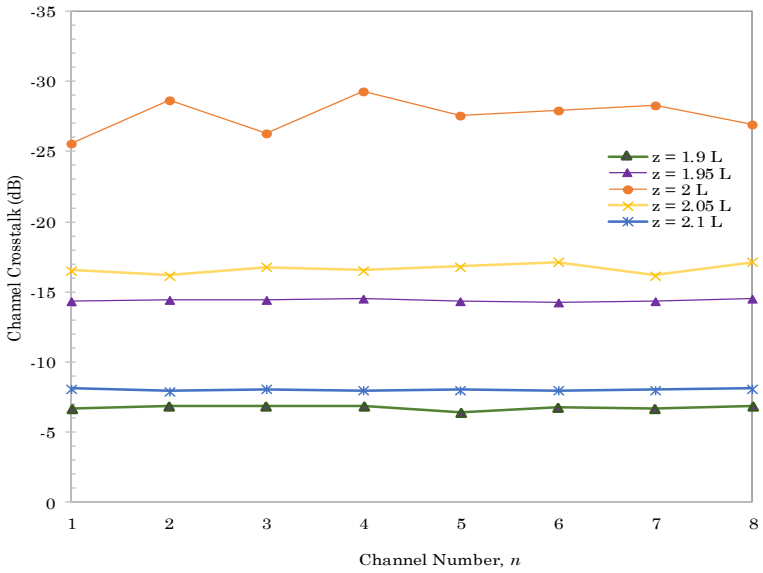

Figure 4.16: Comparison of the calculated results for channel crosstalk with 8 multiplexed optical channels with the same detector size of 56.92 µm, measured at different planes for $z = 1.9L$, $z = 1.95\ L$, $z = 2.05L$ and $z = 2.1L$ µm for a 200 µm fibre core diameter.

It is clear from the graph that at the positions further from the image plane, the beam crosstalk sensitivity increased to approximately -8 dB and -7 dB, measured from the worst channel crosstalk in the plane $z = 1.9L$ µm and $z = 2.1L$ µm, respectively. On the other hand, the sensitivity to crosstalk is improved when the position of these channels is close to the focal distance. Indeed, a channel crosstalk of about -15 dB to -18 dB can be achieved from the transmission of 8 independent channels when the detectors' positions are located on the plane $z = 1.95L$ µm and $z = 2.05L$ µm, respectively. Besides, it is interesting to mention that the planes just after the focal distance (i.e. $z = 2.05L$

μm and $z = 2.1L$ μm) have better insensitivity to the multi-channel crosstalk than that of the planes located before the imaging plane.

4.7 12-channel transmission with different design arrangements

In this section the analysis is further extended from that in the previous section in which a few numbers of channels were investigated. In this section, we progressively implement the transmission up to 12 channels through the GI-MMF. This has a large core diameter of 200 μm with low index differences. The channels are distributed over a cross section of the fibre in two dissimilar channel arrangements, namely a single ring structure (SRS) and a double ring structure (DRS), as presented in Figure 4.17 (a) and (b), respectively.

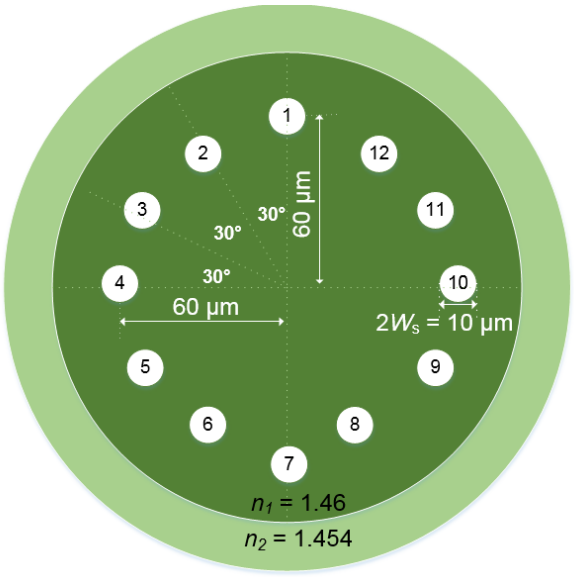

(a1) Single ring structure (SRS)

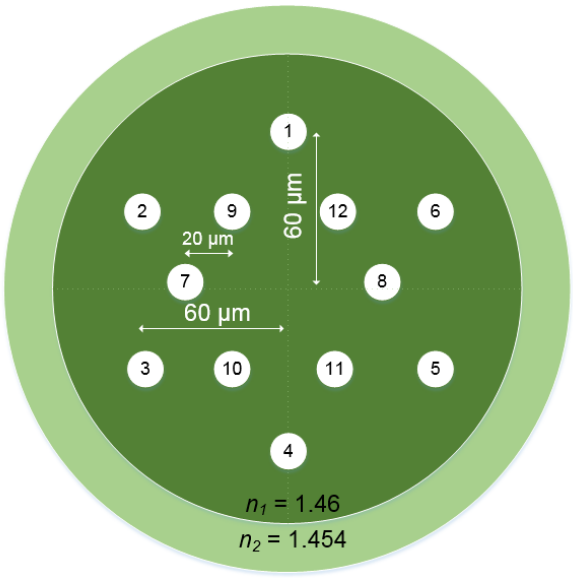

(b1) Double ring structure (DRS)

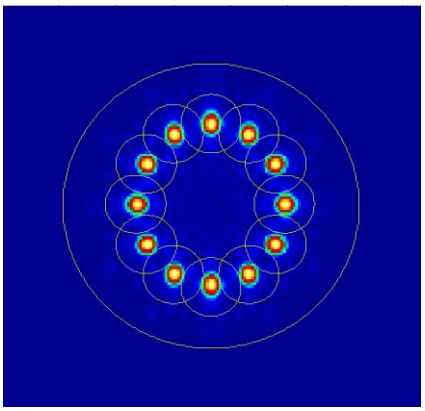

(a2) The amplitude field distribution of 12 input channels in SRS design with a circular detector size of 41.54 µm for each of the beam

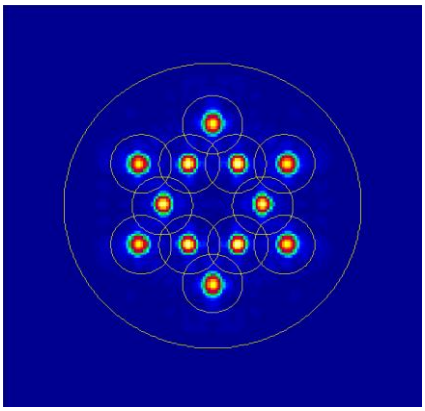

(b2) The amplitude field distribution of 12 input channels in DRS design with a circular detector size of 41.54 µm for each of the beam

Figure 4.17: Schematic cross sectional view of a 12-beam multimode fibre in (a1) for the SRS design and (b1) for the DRS design. The field amplitude distribution of 12 input beams is shown in (a2) and (b2) for the SRS and DRS design structure, respectively with a 41.54 µm detector diameter for each beam.

A 12-channel configuration was multiplexed onto the GI-MMF, with a SRS design, in which these channels are assigned with an equal distance from adjacent channels by using a 30° angular separation with a circular detector size of 41.54 μm for each of the beams. It is to be noted that an equal strength input signal was launched into the different channels. The graphs in Figure 4.18 show the results of the aggregated channel crosstalk of the two different channel structures. We see that we can easily obtain a tolerable channel crosstalk of approximately -9 dB from a 12-beam configuration based on the SRS structure. The reason for a relatively high crosstalk is because of an increase in the number of optical channels with a minimum channel separation between them. Therefore, it is unexpected that the effective crosstalk remains low as the number of channel increases.

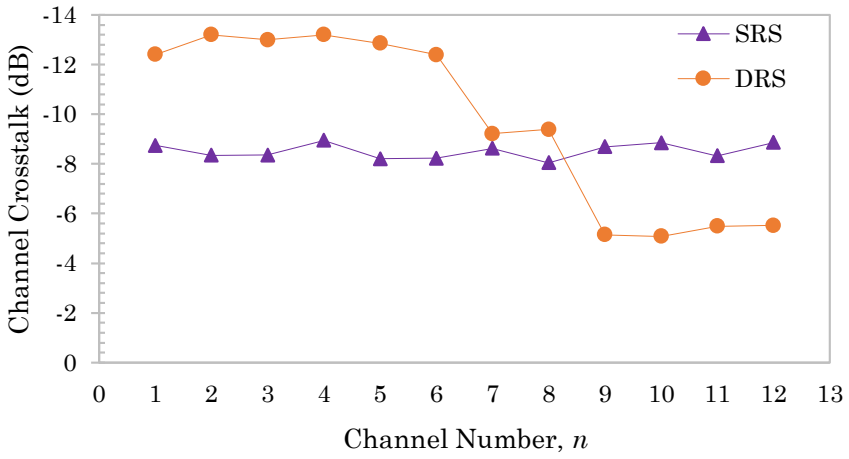

Figure 4.18: Measured channel crosstalk of twelve multiplexed channels with a single ring structure (in closed purple triangle) and double ring structure (in closed orange circle).

For the purpose of crosstalk reduction, a choice of channel arrangement is considered in the design of a multiple number of channels that are packed in a fibre. Another view point of the SDM approach based on a multi-core transmission, it has been reported by Sano *et al.* [96] which has a heterogeneous 12-core fibre (i.e. different core structures between adjacent cores). The DRS

design can overcome the problem of excessive crosstalk, as a result of enlarged core-to-core separation, compared to that of a SRS with the same number of cores and similar conditions as proposed by Matsuo *et al*. [97]. The simulation work reported in this section has adapted the core arrangement in a DRS configuration displayed in Figure 4.17 (b1, b2) with the transmission of 12 beams per fibre core. The results are depicted on the same graph, and show a channel crosstalk of less than -12 dB can be achieved for an SDM system with this structure. Also from this analysis, it is shown that a further improvement in channel crosstalk can be obtained for the channels positioned in the outer ring of the structure because of a larger channel spacing.

However, the drawback of this geometric design is an excessive crosstalk for the channels located in the inner ring of the structure. We observe a significant increase of the crosstalk channel of beam No.7 and beam No.8 at a value of -9 dB, and beam No.9 to beam No.12, at roughly -5 dB. The reason behind this is because the inner channels experience overlap from of the undesired signals from neighbouring channels. The conclusion to be drawn from these results is that even if we use a different design structure with extremely large spatial channels (e.g. a DRS), then only the channels with fewer numbers of nearby neighbours can achieve a slight improvement in crosstalk, while the others are affected by an increase in the quantity of input channels. From comparison of the channel crosstalk performance between a hexagonal beam transmission and twelve channel transmission based on DRS, we can see that the estimation of channel crosstalk for the inner beams in the 12 channel configuration exhibits similar performance due to the design of the channel arrangement. We can draw the conclusion that crosstalk between the channels is one of the key limiting factors in substantially reducing the per-fibre capacity and limits the transmission over greater distances in the multiple channel transmission. Therefore, it would be of great interest to apply an effective crosstalk management technique in the design. Additionally, it is necessary to have a relatively large separation distance between the multiplexed channels

even though the number of channels would be limited. In summary, the number of neighbouring channels and the geometric arrangements have to be taken into account since the channel crosstalk is related to the surrounding number of channels.

4.8 Conclusion

We have designed and simulated an SDM transmission system by spatially multiplexing a plurality of optical channels in a proposed large core graded index fibre by employing different geometries of the physical channel arrangement to exploit a greater information-carrying capacity. It was found in this work that the beam arrangements over the fibre cross-section, the spacing distance from the centre-to-centre of adjacent channels and the number of multiplexed channels have an enormous influence on the performance of crosstalk between closely spaced channels. The simulation results indicated that there was a trade-off between getting the maximum number of independent channels on the one hand, and reducing the crosstalk levels on the other. However, it was proved that the larger the channel positioning, the better the improvement in the channel coupling, but loss in the ability to realise a greater channel capacity in spatial division multiplexing employing multi-channel transmission. In addition this, the periodic re-imaging property of the graded index fibre has been exploited to recover the independent channels.

To achieve a coupling lower than -25 dB for a short haul communications system, the minimum separation distance between the channels that can be used to pack at least four spatially independent channels should be, approximately, at most 60 μm away from the fibre centre. Nonetheless, it could be more beneficial to reduce the channel separation within the optimum ranges for better crosstalk performance among the channels. It can be concluded that channel coupling in a spatially multiplexed system, which is a key restrictive issue to an increases in the density of accommodated channels with a ring-like

arrangement, must therefore be suppressed to as low a value as possible to transmit the multiple data information efficiently at greater capacities.

From our study of the independent parallel transmission channels in a single fibre to achieve a greater per-fibre capacity, we have seen that effective solutions exist, such as increasing the optical bandwidth of the fibre, maximising the spectral efficiency and exploiting a multiplicity in SDM transmission paths. These are the important optical properties in need of concern for the optical design in order to realise a higher capacity per cross sectional area of the fibre. The development of multiple distinct spatial information channels was successfully accomplished by optimising the signal degradation challenges.

Indeed, it is possible to increase the fibre capacity beyond the current scaling of 1Pbit/s through the use of low loss and low crosstalk levels between spatial channels of multimode fibre with the highly packed communication channels contained in the SDM transmission configuration. Since the transmission with a multimode fibre introduces a time delay difference, which can corrupt and spread the optical signals into the nearby channels during the propagation, this results in modal dispersion and the overlapping between the spatial channels, and eventually becomes a significant problem. These effects can be compensated through the use of a graded index profile. In addition, one way to mitigate the linear impairments is to detect the received signal coherently and employ an electronic DSP-MIMO mechanism to effectively distinguish the coupled information channel at the transmission end. This is, however, not an ideal solution since the crosstalk rises as the amount of multiplexed channels increase in the design and thus the complexity of the DSP-MIMO would also be increased.

Chapter 5

The effects of light propagation in a curved graded index fibre

5.1 Introduction

In the previous chapter, we discussed the required conditions to further increase the total carrying capacity of the fibre systems considered. To achieve this in optical fibre communications, it is beneficial to equalise the differential modal group delay and thereby minimise modal coupling between adjacent modes through the use of a low loss graded index multimode fibre. However, in this chapter, we discuss another key challenge in the design of the fibre optics, which are bending losses from a single and multiple bends of the fibre. An overview of the evolution of light propagating in curved graded index multimode fibre is presented. In addition to the capacity enhancement, the efficiency and system performance of the optical fibre in multi-channel transmission are examined for the bend-optimised fibre. The first part of this chapter reviews the transmission along the fibre with the bending condition, and then we briefly introduce the background theory of the bent fibre. The characteristics of the bend-insensitive fibre were examined in detail under various fibre conditions, which should be carefully designed to ensure a reduction of bending losses. A low bending loss bend-optimised fibre should meet all the criteria required to produce a high-capacity bend-tolerant fibre using a parabolic index profile. Finally, the capability of the bent fibre to fully reproduce a single and multi-channel transmission are discussed in the last part of the Chapter.

5.2 Propagation characteristics in the bent fibre

The propagation of optical light in the waveguide is expected to encounter some perturbations; for example, bending the fibre, heating and pressure variations along the transmission path. Bending is one of the common effects of an optical fibre since it degrades the system performance due to a leakage of the guided light through the bend. When the fibre is bent, the propagating fields from a straight fibre through to a curved fibre region are stripped out of the fibre core in the bent section and subsequently transfer their energy to the cladding modes, which eventually leak out of the fibre in the form of radiation losses. Thus, because of bending in an optical fibre, the guiding of light from the input straight fibre, through the bend, to the fibre output is reduced, especially for the modes travelling with a faster speed near the core-cladding boundary (i.e. the higher-order modes) which are thus the most sensitive to the bend.

Furthermore, there are many factors contributing to bending losses, such as a tighter bend, a deformation of the fibre, disruptions during the cabling design and errors from the manufacturing processes [98-101]. These factors contribute to the bending losses of the transmitted light in optical fibres. However, the bending effects can be minimised by designing the bent fibre with the appropriate fibre and bending properties. Thus, the transmitted light in the fibre core can be maintained with an increasing radius of curvature, such that the transmission capacity of multimode GI fibres is improved with superior bandwidth performance, thereby enhancing the probability of receiving the correct transmission signals at the channel end, without leaving any additional losses in the fibre. Figure 5.1 illustrates wave propagation in the cylindrical coordinates (r,ϕ,z) and local coordinate (r',θ,z') system for the bent fibre.

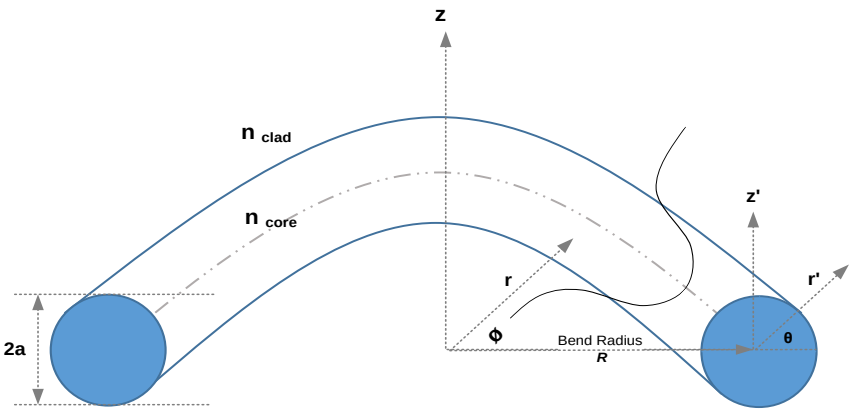

Figure 5.1: Schematic of the bent fibre with a curvature radius R and bending angle (adapted from [109]).

Let us recall the electromagnetic wave $\boldsymbol{E}$ for propagation in a fibre in a cylindrical coordinate (r, ϕ, z) system:

$$\frac{d^2E}{dr^2}+\frac{1}{r}\frac{dE}{dr}+\frac{1}{r^2}\frac{d^2E}{d\phi^2}+\frac{d^2E}{dz^2}+n^2k^2E=0 \tag{5.1}$$

The equation of light propagation in the local coordinate system (r', θ, z') of a bent fibre can be expressed as the following [101]:

$$\frac{d^2E}{dr'^2}+\frac{1}{r'}\frac{dE}{dr'}+\frac{1}{r'^2}\frac{d^2E}{d\theta^2}+\left[n^2\left(1+2\frac{r'}{R}\cos\theta\right)k^2-\beta^2\right]E=0 \tag{5.2}$$

where β is the propagation constant and k is the wave number.

The radius of curvature R in a bent fibre is defined as a distance of the bend origin measured to the centre point of the fibre. The principle of light propagation in the bent fibre can be explained in a similar manner as that in a straight fibre, but from equation (5.2) the propagation characteristics of an electromagnetic wave in the bends is changed in accordance with the effective refractive index distribution n_{eff}, depending on the radius of curvature R:

$$n_{eff}^2=n^2\left(1+2\frac{r'}{R}\cos\theta\right) \tag{5.3}$$

When the fibre is bent, the refractive index of a straight fibre is modified and, therefore, the total internal reflection (TIR) of the light wave inside the core is disrupted since the incident angle of the input light rays is less than the critical angle. Part of the section length in a bent fibre is stretched out, leading to an increase in the speed of the light of the guided modes at local coordinates outside of the curve, i.e. in the cladding region. Subsequently, the transmitted light is stripped out of the core and output power is lost during the transmission [102,109]. The propagation constant at the local coordinates r' in Figure 5.1 can be described by:

$$\beta_{r'} = \frac{R}{r'}\beta(R) \tag{5.4}$$

where, as before, R is the radius of curvature, measured from the centre of the curve.

The propagation constant of the guided modes is gradually decreased when their speed of propagation is increased proportionally to the transmission distance from the optical axis. As depicted in Figure 5.2, the light located at a radial position $\left(R_c = R + r'\right)$ inside the cladding part diverges into two different directions. Some of the rays bounce back into the core whereas the others are shifted out of the core to form a so-called radiation wave which results in light escaping from the fibre.

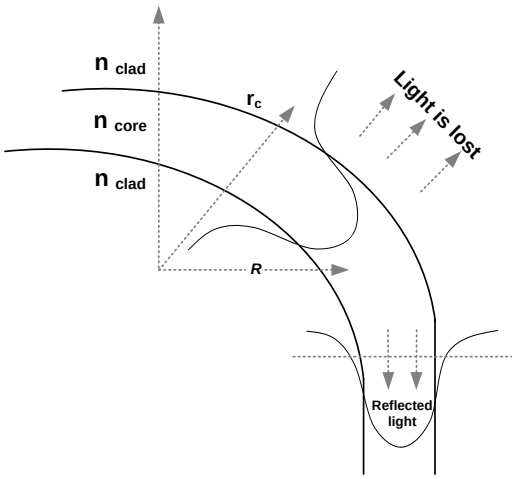

Figure 5.2: A graphical explanation of the effects in a curved fibre.

The modified propagation constant of the modes located at the radial position, r_c, can be written as:

$$\beta(r_c) = \frac{R}{r_c}\beta(R) \tag{5.5}$$

The propagation constant in equation (5.5) can be written in the form of an effective refractive index of the mode as:

$$k_o n_{clad} = \frac{R}{r_c}\beta(R)$$

$$r_c = \frac{R}{k_o n_{clad}}\beta(R)$$

Therefore,

$$r_c = \frac{n_{eff}}{n_{clad}}R \tag{5.6}$$

From equations (5.4 - 5.6), the propagation constant of a modal wavefront at the outside of the bend is directly proportional to the radius of curvature. This means that the bent fibre can be optimised by increasing the curvature radius R due to a reduction of modal coupling among the propagating modes because of the increasing separation of their propagation constants. On the other hand, increasing the radial distance toward the bend decreases the phase constant of the guided modes; as a consequence, several higher order guided modes are excited because of a modification of the index profile and so the intensity distribution is altered as compared to the straight fibre. It is worth mentioning that the phenomenon of total internal reflection of the guided modes in which the light bounces inside the higher refractive index medium no longer exists if the modes travel with a speed greater than or equal to that of the cladding modes, especially those propagating near the boundaries. Then most of the energy leaks out of the transmission direction.

Let us recall the equation of the guided mode in a graded index fibre $(\alpha \approx 2)$; the total propagating mode before the fibre is bent is written as:

$$M_{g,straight} = \frac{\alpha}{\alpha + 2}\left(\frac{V^2}{2}\right) \approx \frac{V^2}{4} \tag{5.7}$$

After bending, the number of propagating modes that can be simultaneously transmitted over the fibre length is decreased because of the change of the index profile of the fibre. The total mode volume in a bent fibre can be written as [102]:

$$M_{g,bend} = \frac{\alpha(R)}{\alpha(R) + 2}\left(\frac{V^2}{2}\right) \tag{5.8}$$

As we can see from the derivative equations in (5.7) and (5.8), the $M_{g,bend}$ is much less than $M_{g,straight}$ because the radius of curvature is involved in the modification of the index profile.

5.3 Characteristics of bending

As mentioned previously, recently a number of research studies have investigated an enhancement of transmission capacity of fibres, in particular with low bending losses. The optical losses caused by the bends have great impacts from the communications point of view, e.g. the ability to achieve superior bandwidth performance. According to the transformation of the fibre structure after bending, the losses in the bent fibre can be classified as resulting from two major mechanisms contributing to bending losses, which are microbending and macrobending, which should be considered separately to allow flexibility in order to optimise the fibre with high bend tolerance.

5.3.1 Microbending in a curved fibre

The losses caused by microbending arise from the deformation of the fibre's surface during the cabling process due to the application of stress onto the fibre. A small force or pressure can be applied at the interface or the boundaries between the core and cladding, leading to an imperfection of the perfectly straight fibre, e.g. a surface roughness, contributing to the coupling of energy from the guided lower order mode to higher order modes and, subsequently, strike out of the fibre as depicted in Figure 5.3.

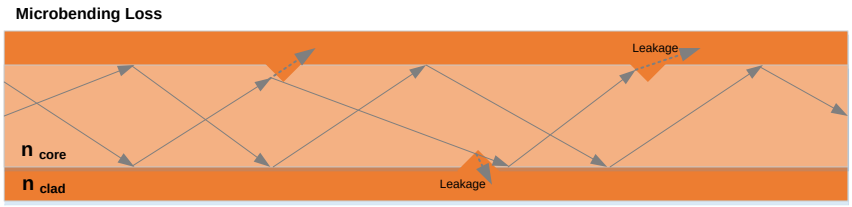

Figure 5.3: Schematic diagram of microbending of a multimode fibre.

The launching condition is one of the key solutions needed to take into consideration when designing microbend resistive fibre to assure an acceptable level of microbending losses. This is because microbending loss is dependent on the separation distance between adjacent modes so that the propagation

constant of the modes must be well spaced with a sufficient distance between them [99,100, 101,102, and 103]. If the difference in the phase constant of neighbouring modes is too narrow, it is likely to produce significant microbending losses. However, the microbending loss will be insignificant when a small force is exerted on the surface of a straight fibre.

Gloge [104] has shown that fibre with a parabolic index profile is not to be preferred in a bent fibre, even though the modal distortion occurring from multi-transmission paths can be minimised through the use of this index graded profile. The significant bending loss in the bent graded index fibre is typically greater than that of a step-index profile due to the limitation of the number of guided modes. However, the bent graded index fibre will have the same bending behaviour as in the step index profile if the relative refractive index difference of the bent GI fibre is doubled, since then the number of the associated modes in the bent GI fibre is identical to that of a constant index fibre.

5.3.2 Macrobending in a curved fibre

The second bending mechanism, which can be easily seen with the naked eye, is so-called macrobending. When the fibre is physically bent, the geometrical specification of the fibre is changed, leading to an escape of light into the cladding. In addition, the fraction of refracted light depends strongly on the fibre's parameters and bending radius. A schematic of a substantial bend is shown in Figure 5.4 to illustrate macrobending. A large portion of the guided modes are stripped off the fibre if the fibre is subjected to bending with a minimum radius of curvature. In general, the manufacturer usually recommends the minimum bend radius of the fibre.

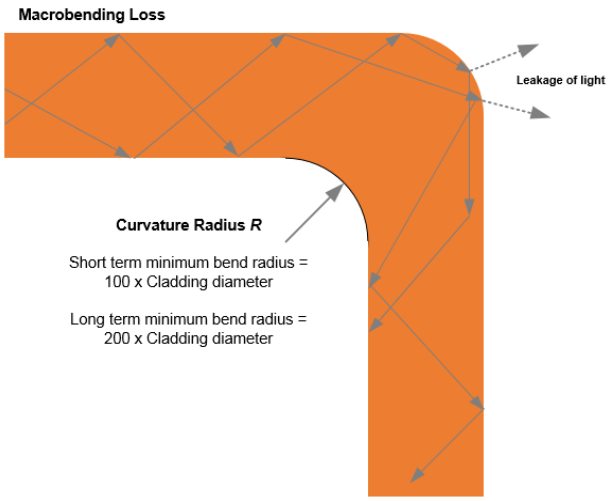

Figure 5.4: An illustration of macrobending at a bend in multimode fibre. Part of the emitted light rays from a straight section are diverted into two transmission parts at the corner of a bend. On the one hand, the light radiates out of the core, the amount of light escaping depending on the size of the bend radius, whilst the remaining light is still guided along the propagation direction.

5.3.3 Losses in macrobending

Macrobending results in four losses, which comprise the transition loss, pure bend loss, scattering loss and material absorption loss [105]. The total losses of the fibre and the variation of the output intensity that occur from the physical bending can be largely accounted for from the first two sources. Thus, as illustrated in Figure 5.5, the transition loss and the pure bending loss are the main contributors to the bending losses of the optical fibre, originating from two different regions and should be taken into consideration individually.

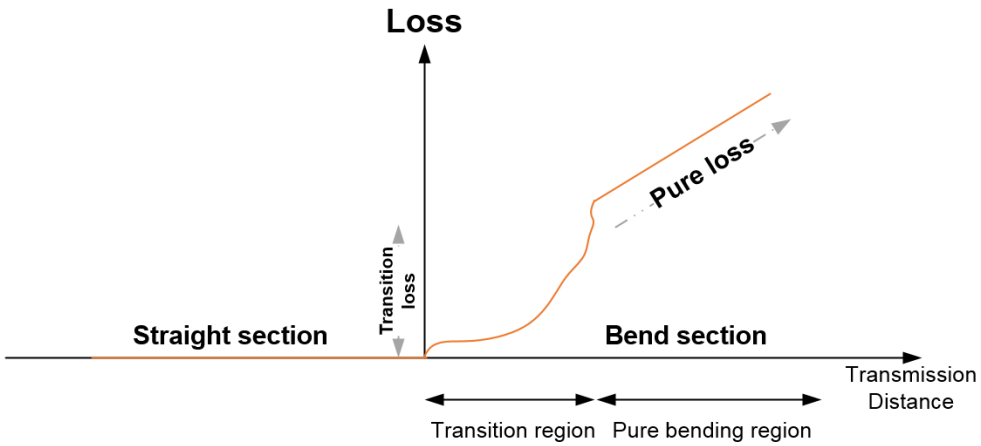

Figure 5.5: Diagram illustrating the two bending losses in different regions of a bent fibre: transition loss and pure bend loss (adapted from [106]).

(a) Transition loss

To begin with, the first region to consider after the fibre's geometry is suddenly changed is the transition region. It can be found at the junction between the straight fibre and the bend section. The attributed loss in this region is the so-called transition loss or insertion loss, arising from the fact that only a portion of light from a straight fibre is coupled to a bent section. The remaining optical power excited to the guided modes (i.e. near the fibre axis) is progressively emanated to that of radiation modes as the field propagates to the curved section [106]. It should be emphasised here that the length of the transition section increases with the bending radius R, even though the field intensity produced in this region fluctuates, as a result of the exchange of the incident power between the guided modes and radiation modes [107, 108].

(b) Pure bending loss

On the other hand, the pure bending loss arises in the following region. In general, the light is totally internally reflected down the fibre core if the propagating modes keep their speed of travel below the velocity of the cladding modes. However, once the local phase velocity of the modes, located just outside the fibre core, becomes comparable to the velocity of light in the cladding modes the guiding light is radiated away from the fibre.

It is very challenging to preserve most of the propagating light inside the fibre core since its velocity is equal to that in the lower index region. This results in a drastically greater amount of escaping light rays and radiating of the light rays away throughout the bend. The lower the proportion of the transition loss and the pure bending loss, the lesser the fraction of the radiated wave will be transmitted out of the fibre but if, and only if, the fibre is flexible enough to bend at a larger radius.

5.4 Design considerations

It is well known that the light propagating outside of the fibre core exponentially decays; however, some portion of the light rays might reflect back into the core once they hit the coating-air interface. This is because the coating has a slightly higher refractive index than the air outside of the jacket [114] and, accordingly, the refracted light rays are bounced back into the core owing to the TIR phenomenon.

Recently, a number of research studies have carried out research into the development of bend-insensitive fibre with low bending loss characteristics which are becoming increasingly important in many applications due to their superior performance in many application environments e.g. in medical applications [110, 111], fibre sensing [100, 102, 112, 113], under tighter bend conditions, and finally in optical communication transmission paths for either short haul or long haul communications. Therefore, many researchers and also fibre manufacturers are finding effective solutions in order to cope with the leakage of light from the propagation medium caused by bending. A well-known method for dealing with fibre bending is to add a lower-index trench having a refractive index smaller than the cladding medium in order to trap a weak signal, thereby ensuring the minimum leakage of light rays from the fibre [115] and raised velocity of the cladding modes [116]. Another successful improvement has been achieved by employing a translucent material within the fibre identification hardware having a refractive index approximately comparable to the coating layer. As a consequence, the escaped light rays are trapped within the translucent region before scattering into the air. Subsequently, a fraction of this weak signal will thus be reported as it arrives at the detector [117]. The advantages of the bent fibre identification hardware are the improvement of the quality of the service and also the ease of design and engineering maintainability.

For all the above reasons, our initial reasoning for the design of bend-insensitive fibre is that increased values of the bend radius will be beneficial to improving the bending losses allowing the possibility to further increase the transmission capacity. Therefore, it is meaningful to investigate the characteristics of light wave propagation in a bent graded index multimode fibre, experiencing a single bend or multiple bends with a uniform radius of curvature at different bending angles, to find effective ways of reducing the losses from the bend-sensitive fibre. Later on, we will show how the bending influences the oscillatory behaviour of the output intensity distribution. Similarly, the dependence of the bending losses on the angular bend and the geometric specifications of the fibre will be investigated as the GI-MMF is subjected to a tight bend radius.

The effect of bending caused by the asymmetry configuration of the structure on the propagation down the bent fibre is modelled to determine the losses of power at the output after bending. As soon as the light rays reach the bend section, the pattern of the propagating fields diverges into different directions, resulting in a radiation or leakage of the optical signals. Some of the light hits the boundaries and continues to propagate down the bent fibre; however, some of the rays might refract out of the fibre and be coupled back to the core. Therefore, it is important to compensate the refracted light coupled into the propagation direction by adding additional absorbing layers i.e. Perfectly Matched Layers (PMLs) at boundaries of the simulation windows with a thickness of 1 μm each side. The advantage of using the PMLs at the boundaries is to avoid the reflected light coupled back into the structure. From the simulation point of view, the PMLs are helpful tools to indicate the amount of radiated losses out of the fibre.

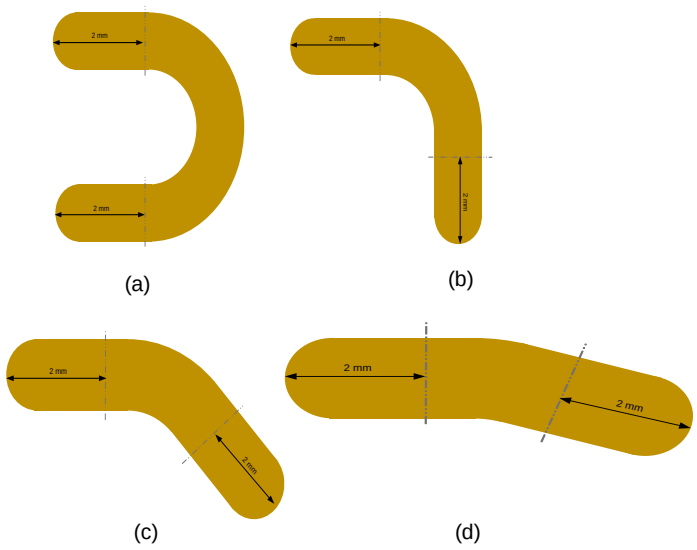

Figure 5.6: Schematic model structures of the macrobending of fibre for: (a) U-bend (180°); (b) L-bend (90°); (c) 45°; and (d) 10° degree, angular bend.

We propose model structures of bent fibre with a specified radius of curvature with a variety of bending angles. The overall structure is of a singular bend comprised of 3 successive sections with the bend section in between the two straight sections at both ends. The straight fibres consist of a 2 mm length of transmission where the optical source is launched to the input end of the first straight section, and then the light is propagated through the bend section. Some of the propagating light will be coupled out of the propagation direction, and some will be continuously transmitted to the output end of the straight section. In Figure 5.6 (a) – (d) are displayed the schematic structures of a U-bend (180°), L-bend (90°), 45° bend and 10° degree bending angle, respectively.

5.5 Simulation of the bending losses for a single bend of fibre

5.5.1 Influence of the radius of curvature and the angular bending

5.5.1.1 Optical source and model structure

This section aims to study the evolution of electromagnetic fields when GI62.5 fibre is bent with distinct properties (i.e. radius of curvature and bend angle). The implementation of an appropriate design models the effect of bending losses of the propagating modes as an input beam is transmitted through a fibre undergoing a fixed bend radius and angular bend. The bending loss of a multimode graded fibre with a core diameter of 62.5 µm is measured with different model structures, as shown in Figure 5.6. The curved radius of the bent section is adjusted from a 5 mm to a 30 mm radius in which the length of the arc is varied, depending on the bend radius.

In the simulation, an input Gaussian beam having a beam radius of 5 µm is introduced through a 2 mm length of the first straight GI62.5 fibre from the input end. The simulated fibre has a core index of 1.48 and a NA of 0.275, transmitting with an operating wavelength of 1.55 µm. After passing through the fibre for a length of 2 mm, the optical signal is propagated through the bent fibre experiencing different bending conditions, and then the amount of power that is lost through the bend is measured as the radiation loss. As explained in detail in section 5.3.3 concerning the major sources of bending losses, an insertion loss is evaluated at the joints between the two different geometrical shapes of the fibre (i.e. at the junction between the straight and the bent sections).

For simplicity in the simulation, the non-guided modes are excluded in the transmission; only the first 30 guided modes are included in all simulations presented here. However, it has been shown by the simulations that these 30 modes are sufficient to investigate the coupling to high order modes, ensuring the minimum of unwanted coupling between different modes. In addition, it has

also been confirmed by simulations that more than 99% of the power is predominantly allocated to the guided modes, especially in the fundamental mode of a GI62.5, even under a tight bend radius of 5 mm, from all the differently designed configurations. It is found that the total transmitted power from a 10 μm diameter Gaussian beam to the first 30 propagating modes of a GI62.5 μm does not change much with variations of bend profiles when the beam is coupled into the guided modes.

5.5.1.2 The electromagnetic field intensity distributions

Comprehensive studies were carried out to investigate the distribution of the propagation field along the transmission distance. It has been observed from the simulations that the propagation of the optical fields is dramatically changed from the input section of the fibre as soon as the physical shape of the fibre is simultaneously transformed to various shapes, depending on the bend radius and a given bend angle.

Figures 5.7 (a) – (d) show the distribution of intensity between the modes with a uniform bend angle and radius in the direction of propagation in the *x*-*z* plane. It is quite clear that the propagation of light is coupled to the radiation and the characteristics of the propagation fields show an irregular fluctuation of the intensity field distribution along the length of the arc for the Gaussian input beam in the bent section. This can be explained by the fact that the higher guided modes interfere with the other modes due to the interference effects between the bend modes and the propagation constant of the guided modes which are not properly separated.

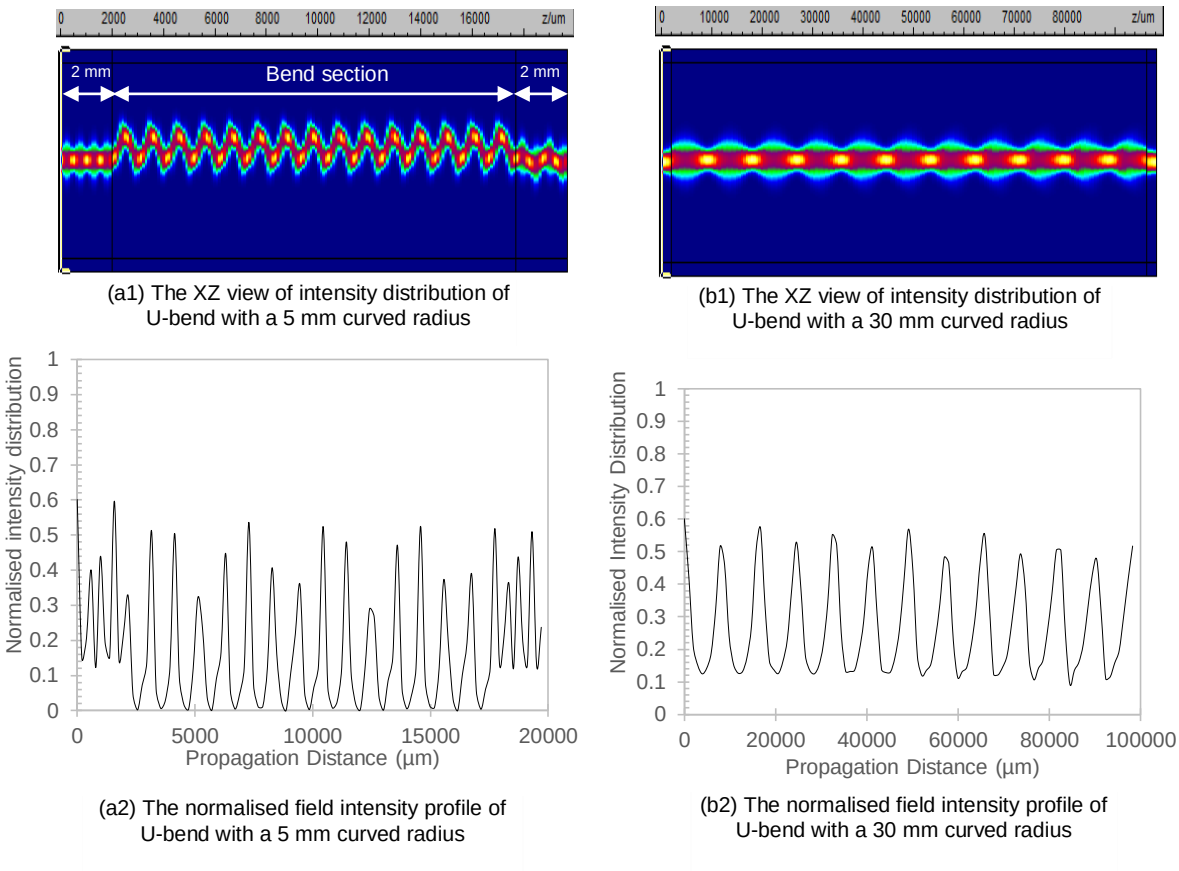

(a1) The XZ view of intensity distribution of U-bend with a 5 mm curved radius

(b1) The XZ view of intensity distribution of U-bend with a 30 mm curved radius

(a2) The normalised field intensity profile of U-bend with a 5 mm curved radius

(b2) The normalised field intensity profile of U-bend with a 30 mm curved radius

Figure 5.7: The propagating field evolution through a U-bend of GI62.5 multimode fibre for a transmission length of z = 19.70 mm and z = 98.25 mm with a fixed 5 mm and 30 mm bending radius in (a) and (b), respectively: (a1, b1) the x-z view of the beam intensity distribution of the reconstructed beam in the fibre; and (a2, b2) the normalised intensity of the propagated beam profile, showing the locations where mode coupling strongly affects the propagation.

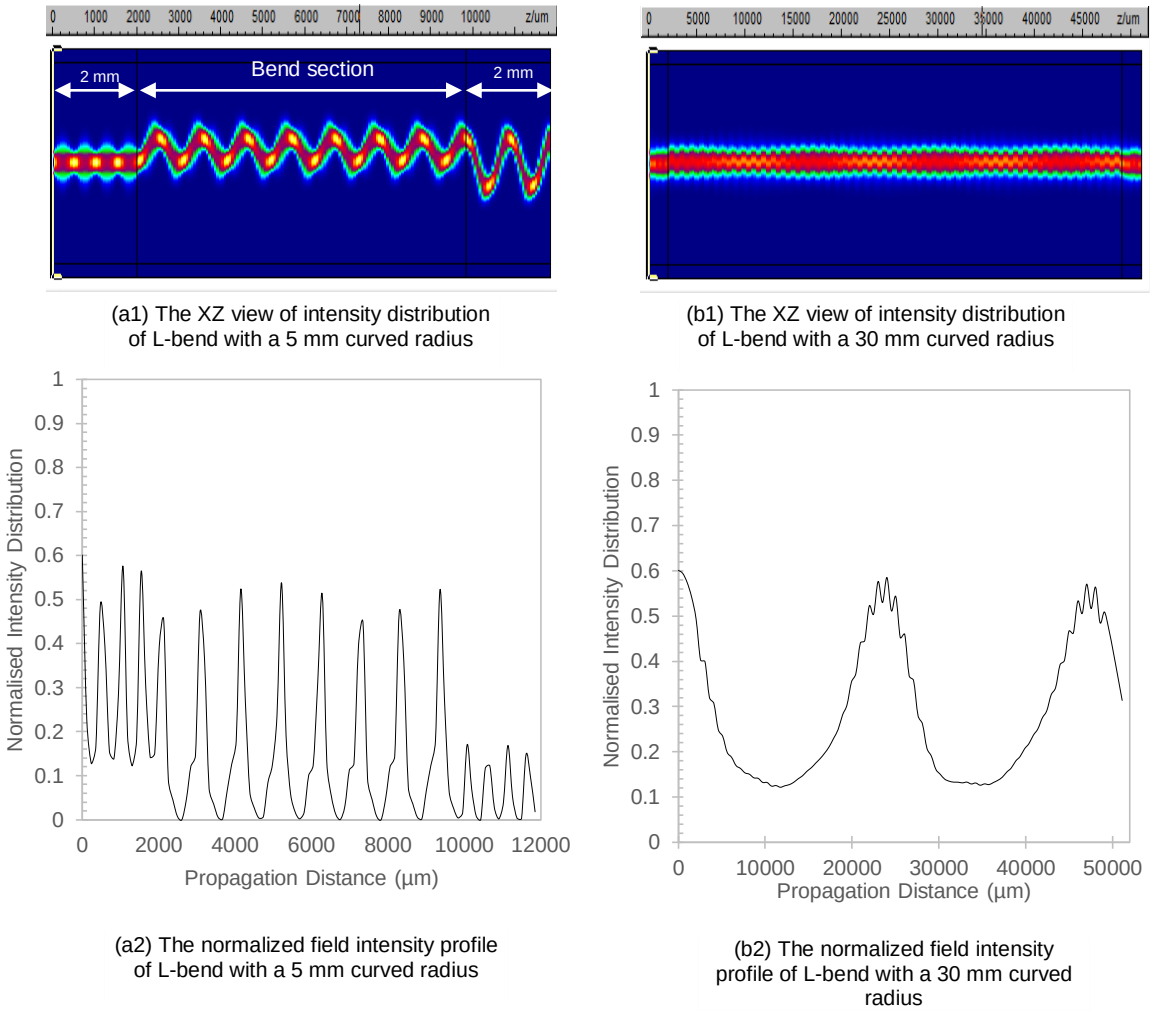

(a1) The XZ view of intensity distribution of L-bend with a 5 mm curved radius

(b1) The XZ view of intensity distribution of L-bend with a 30 mm curved radius

(a2) The normalized field intensity profile of L-bend with a 5 mm curved radius

(b2) The normalized field intensity profile of L-bend with a 30 mm curved radius

Figure 5.8: The propagating field evolution through an L-bend of GI62.5 multimode fibre for a transmission length of z = 11.85 mm and z = 51.12 mm with a fixed 5 mm and 30 mm bending radius in (a) and (b), respectively: (a1, b1) the x-z view of the beam intensity distribution of the reconstructed beam in the fibre; and (a2, b2) the normalised intensity of the propagated beam profile, showing the locations where mode coupling strongly affects the propagation.

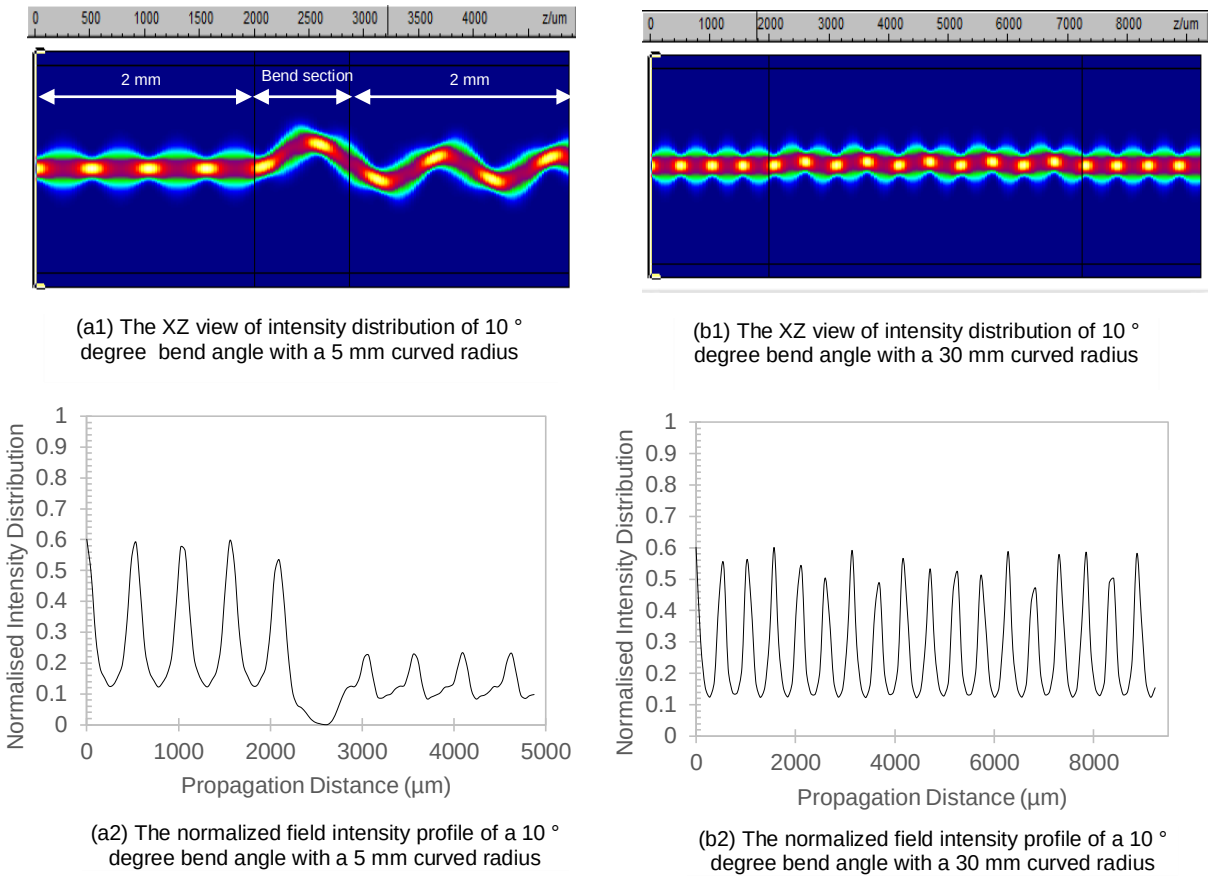

Figure 5.9: The propagating field evolution through a 10° degree bending angle of GI62.5 multimode fibre for a transmission length of z = 4.87 mm and z = 9.24 mm with a fixed 5 mm and 30 mm bending radius in (a) and (b), respectively: (a1, b1) the x-z view of the beam intensity distribution of the reconstructed beam in the fibre; and (a2, b2) the normalised intensity of the propagated beam profile, showing the locations where mode coupling strongly affects the propagation.

The amount of power coupled to the given modes varies greatly at the output of the straight section owing to the interference between the modes of that section and the bend modes, such that the power at the output drops significantly with a tighter bend radius. A very strong oscillation of the intensity distribution can be seen in a GI62.5 µm fibre when a drastic decrease of bending radius is applied to the structure, as shown in Figure 5.7 (a1, a2), Figure 5.8 (a1, a2) and Figure 5.9 (a1, a2) with respect to a U-bend, L-bend and 10° bend structure with a curvature radius of 5 mm. As explained, the optical power

becomes more scattered and more oscillatory over the section length of a reduced bending radius of the fibre when the number of the radiative modes increases.

Moreover, it can be seen that the bend affects the output of the intensity field profile, which can produce coupling between the modes by changing the distribution of the input field profile [118, 119, 120, 121]. Multiple guided modes cause the interference patterns between these modes at the output of the straight fibre. This effect is as theoretically expected since the characteristics of a GI62.5 μm fibre are as a multimode structure that can simultaneously transmit several guided modes. It is, therefore, impossible to preserve a spatial periodicity of the input power throughout the direction of propagation since the intensity profile of the launched optical power is strongly modified within a tight bend condition. Nevertheless, these strong fluctuations of intensity for the guided modes at the output of a straight fibre, or even at the bend section, can be reduced if the curvature radius is large enough. This is demonstrated by the simulation results shown in Figure 5.7 (b1, b2), Figure 5.8 (b1, b2) and Figure 5.9 (b1, b2) for the U-bend, L-bend and 10° bend fibre with a sufficiently large bend radius of 30 mm that minimises the amount of the mode/power coupling. Furthermore, it can be confirmed from the study of Gambling [107] that the conversion of the modes from the straight and the bent section, in particular at the transition region, becomes more steady until it reaches the radiation region (i.e. pure bend region), as clearly seen in Figure 5.8 (b2).

To conclude, it is clear that the length of oscillations (i.e. the beat length) in the bent section with different bend angles typically depends on the length of the arc, which changes linearly with the bending angle. After multiple successive internal reflections, we observe that the distribution of the rays inside the core does not follow the same propagation pattern as they do at the entrance of the straight section, as a consequence of the modification of the geometry of the fibre introduced by the bending. Therefore, the radius of curvature has a great impact on the intensity distribution and the output power. The larger the radius of curvature, the lesser variation of power density among the modes, so that the

fluctuations steadily decrease with the number of bend modes in the bent section with increasing bend radius.

5.5.1.3 Loss analysis

It is also interesting to examine the macrobending losses of the GI62.5 fibre under various bending conditions. The impacts of the bent fibre on the losses have been demonstrated by varying the radius of curvature and bend angle. It should be emphasised that the optical power that is left from the fundamental mode could be coupled to high order modes and be dissipated into the two major sources of loss in the bend region of the fibre, as explained in section 5.3.3.

To explore the bending losses of the fibres, we measure not only the radiation losses (RL) from the bend section but also the insertion losses at the first joint (IL_1) and second joint (IL_2) of the structure between the straight sections and bend section, which is caused by the mismatch between the modes when the geometry of the structure is dissimilar. Note that the results of bending losses are calculated by means of the coupling ratio of the output power to the launched power in dB, which can be expressed as:

$$\text{Bending losses (dB)} = -10\log_{10}\left(\frac{P_{output}}{P_{launched}}\right) \tag{5.9}$$

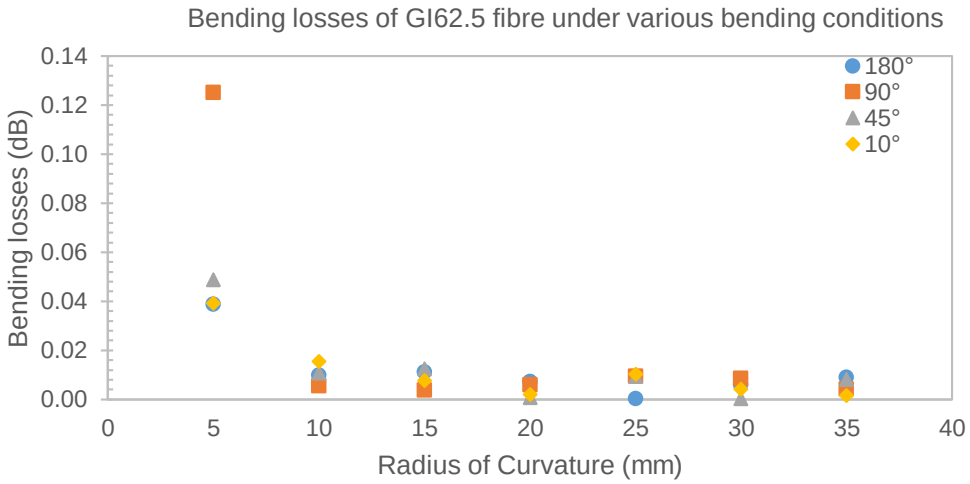

Figure 5.10: Simulation results of the bending losses as a function of bend radius for GI62.5 µm fibre with different angular bends. The optical source is a single Gaussian beam with a radius of 5 µm at a wavelength of a 1.55 µm.

The simulation results of the macrobending losses for GI62.5 fibre are shown in Figure 5.10 as a function of the curvature radius, ranging from 5 mm to 35 mm with an increment of 5 mm under various bending shapes. At the minimum bending radius of 5 mm, the GI62.5 fibre with an L-bend shape seems to be the most bend-sensitive structure, in which the response to the bending loss exhibits a value of more than 0.12 dB/90° bend angle, compared to approximately 0.04 dB from a U-bend and a 10° bend, and just under 0.05 dB/45° bend angle. The minimum bending losses below 0.02 dB can be realised when a GI62.5 fibre is bent with a radius of curvature of more than 20 mm at the bent section of the structure for all differently configured structures.

The simulations show that different types of bend structure experience characteristic bending losses with a similar trend. It can be observed from Figure 5.10 that the bending losses are continuously reduced with an increasing bending radius of the waveguides. However, the behaviour of propagation in all the structures fluctuates after the fibre is bent with a significant radius of curvature, especially after the fibre is bent with a radius of curvature beyond 20

mm at the bend section and becomes too small to be precisely measured. More interestingly, investigation has shown that the insertion losses play a significant role in contributing to the bending losses, specifically at the first joint (IL_1) of the structure. This is because of the power coupling to high order radiation modes and the mismatch between the modes of dissimilar curvature (i.e. the mode orthogonality) between two structures [120, 121]. However, the radiation loss in the bent sections does not influence the total losses of the fibre. We assume that the radiation loss is almost negligible for the larger core size although the fibre is tightly bent. This is because the input end of the straight section is launched with a few guided modes and therefore the signal leakage due to the coupling into higher-order guided modes at the output section of the fibre does not produce a high bending loss.

To accomplish a minimum bending loss for the structure, the bending losses (i.e. insertion loss, radiation loss) of the structure is expected to decrease if a significant portion of the launched power is distributed into the first few lower order guided modes rather than the higher order modes. As a consequence, the unwanted modal coupling is diminished with the suppression of optical losses. Furthermore, we have seen that the characteristics of bending losses are strongly dependent on the curvature radius of the bend rather than the bend shape. For this reason, increasing the bending radius would be one of the solutions to effectively ensure minimal disruption to the beam propagation in the fibre.

5.5.2 Influence of the fibre dimensions

To explore the sensitivity of the fibre to the bending losses due to its physical properties, the fibres we examine are based on the geometrical specifications of commercially available fibres as summarised in Table 5.1. The comparison is made with various commercial GI-MMFs as a function of various design parameters (e.g. the core diameters, cladding diameters and the NAs) under the same bend angles with an increment of radius of curvature, ranging from 5 mm to 35 mm.

Table 5.1

Properties of tested commercial fibres for various NA and Δ values

Fibre Name.	Δ	**NA**	**Core index n_1**
GI50	0.00913	0. 2	1.48
GI62.5	0.0176	0.275	1.48
GI100	0.01919	0.29	1.48

However, it has been shown from the previous section that bending losses are independent on the shape of the bend, except for some cases with numerical errors due to a very small loss. The circular arc of a 90° bend is assumed in this study due to its importance in many applications such as, for example, in the design of fibre to the home (FTTH) when the fibre is required to be bent in a 90° bend with a desired radius of curvature at the corner of a domestic room. Therefore, the L-bend configuration is considered in the study of bending loss behaviour with different fibre specifications. The bending losses for various commercially available fibres are compared as a function of the core sizes and radius of curvature with the same operating wavelength of 1.55 μm. The simulation results are given in Figure 5.11, comparing the impact of different fibre conditions on the bending loss performance.

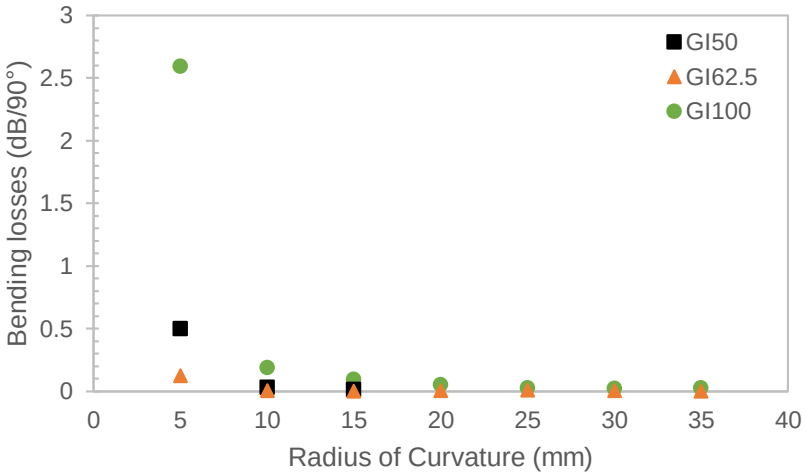

Figure 5.11: The bending losses as a function of curvature radius of commercially available fibres with different specifications, obtained by applying a ¼ turn (90° bend) in the middle section of the fibres.

The highest optical losses induced by the macrobending can be seen to have a value of 2.6 dB/90° bend at the minimum recommended bend radius of a 5 mm with the GI100 fibre, having a larger Δ and NA than that of the GI50 and GI62.5 fibres. On the other hand, bending losses below 0.3 dB/90° can be achieved with GI50 and GI62.5µm core diameters at a circular bend radius larger than 10 mm. The maximum bend radius of the GI50 fibre is not specified in the technical data sheet from the Thorlabs manufacturer [122]. However, it has been determined from the simulations that the bending losses for this fibre cannot be measured accurately when the bend radius is beyond 15 mm because of an apparent increase of the output power after bending, which is clearly anomalous.

The results are a good indication that a bend-improved fibre can be designed by employing a smaller core diameter with larger bending radius [123]. Thus we have seen that it is important not only to consider the geometrical specifications but also other relevant parameters in order to ensure a fibre can withstand a tighter bend. As the core diameter becomes larger, the portion of power is steadily transferred from the lower order modes to higher order modes

owing to the generation of several excited modes along the propagation direction, caused by the modal coupling. It is well known that multiple higher order modes are more likely to leak out of the fibre than the lower order modes. Moreover, the modes propagating near the boundaries are easily radiated off the core, in particular with the bending conditions contributing additional losses. Our simulations are in good agreement with theoretical and experimental investigations. We have demonstrated that a relatively small size of core diameter is preferable in order to effectively optimise the bend sensitivity compared to a larger core diameter. The simulations show the profound effect of changing the fibre geometry in achieving an improvement of the transmission efficiency and the ability to withstand macrobending.

5.5.3 Influence of the index contrast and NA on GI62.5 fibre

In this section another property of the fibre affecting the bending loss behaviour is investigated in detail by varying the relative refractive index contrast of the waveguide. For a fair comparison, it is assumed that the core diameter of the tested GI fibre is fixed with a diameter of 62.5 µm, operating at a wavelength of 1.55 µm where an optical source of 10 µm Gaussian beam diameter is launched into the first straight section of the structure, and is propagated for a distance of 2 mm before the fibre is bent with a 90° bend. The simulated bending losses were performed for different bending radii, ranging from 5 mm to 30 mm, with an increment of 5 mm with 6 distinct ratios of relative index difference (Δ%), as given in Table 5.2.

Table 5.2

Properties of GI62.5 fibre for various values of Δ

Fibre No.	**Δ (%)**	**Core index n_1**	**Cladding index n_2**	**Remark**
1	2.08 %	1.485	1.454	
2	1.76 %	1.48	1.454	*Commercial fibre*
3	1.42 %	1.475	1.454	
4	0.75 %	1.465	1.454	
5	0.41 %	1.46	1.454	
6	0.07 %	1.455	1.454	

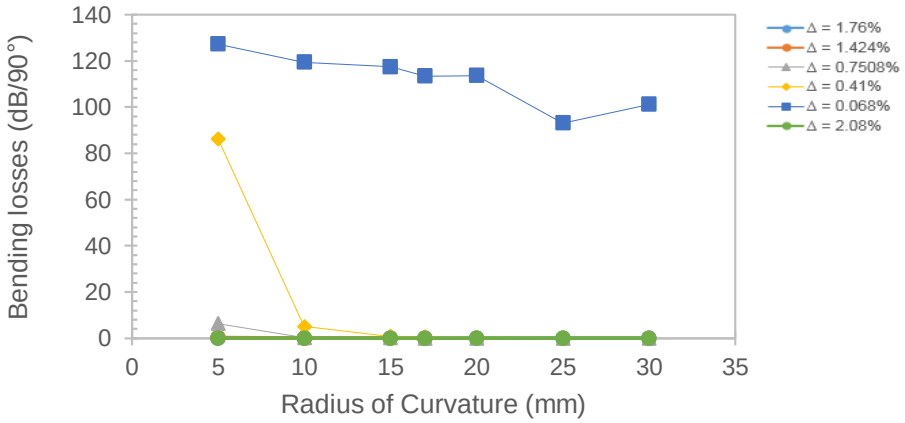

Figure 5.12: Bending losses as a function of curvature radius in dB/90° bend for GI62.5 fibres with different index contrast.

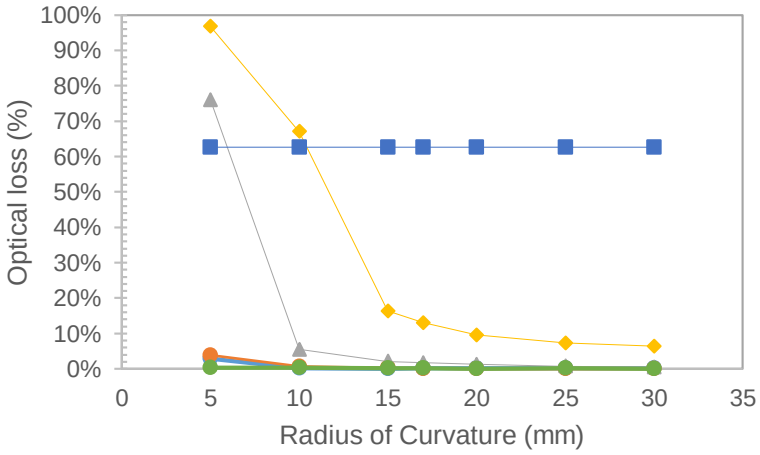

Figure 5.13: The total optical losses (IL_1, IL_2 and the RL) in percentages as a function of bending radius of GI62.5 with an L-bend section with distinct ratios of relative refractive index differences.

The optical bending losses induced by a ¼ turn macrobending on the GI62.5 fibre shown in Figure 5.12 are determined using the coupling ratio as the fraction of output power to the power at injection, whereas the percentages of optical losses, given in Figure 5.13, are analysed by adding three losses, i.e. the IL_1, IL_2 and the RL of the bent fibre from the different locations. It can be determined from the graphs that the modification of the index differences, Δn_1, have strongly influenced the behaviour of bending loss of the optical fibre. The total bending losses are apparently increased with a decrease of the index contrast between the core and cladding, in particular when the light propagates in a fibre with a tighter bend radius. The numerical simulation results show how the losses remained constant in the L-bend fibre having Δ equal to 0.068%. The reason why the total loss remains the same as the bend radii increase is due to the very small relative refractive index difference in this case. In contrast, under the same bending conditions, significantly larger losses can be seen in fibres with a Δ of 0.41% and 0.7508%. In particular, the former dissipates almost all its optical signal when it is bent excessively.

Nonetheless, it is noticeable that the losses suddenly drop to a minimum value as the radius of curvature is increased beyond its minimum recommended value. It should be emphasised that the bending losses of the GI62.5 fibre with a Δ of 1.424% reaches its minimum losses at an enlarged bend radius of 17 mm, and this bend radius would be sufficient to drastically improve the bending losses of this fibre specification. It has been determined that the maximum bending radius of the fibre with a Δ of 1.424% cannot be extended beyond a 17 mm radius because of numerical errors in simulation of the fibre since it produces a greater output power after transmission without any optical repeaters which is clearly erroneous. The simulations results are as expected. A well-optimised bend-insensitive fibre can be realised by increasing the index contrast, in particular with sufficiently large circular bend radius. This study should be a good indication of the influence of varying Δ on the characteristics of

bending losses. Therefore, it seems to be predicted that the effect of macrobending can be further suppressed by increasing the Δ and NA of the fibre.

Accordingly, more propagating light would be confined in the core, less amount of modal power being stripped out of the propagation direction. Besides the properties of the fibre, a sufficiently large curvature radius should be assured in order to maximise the total power coupled to transmitted modes at the output throughout a bend in the fibre and thereby optimise bending loss behaviour. The reason of such a good enhancement could be explained by the fact that by increasing the index difference the separation distance of the propagation constant, $\Delta\beta$, between neighbouring modes is increased [108, 120]. Subsequently, the number of excited modes and the mode coupling are decreased without creating any additional losses in the fibre [104, 124].

5.5.4 Propagation inside the bend region of a graded index multimode fibre with a small index contrast and large core

From our previous studies, we demonstrated the sensitivity of the fibres to bending using the main parameters, such as the NA and core sizes to characterise the bending of multimode graded index fibre. Bending is of particular importance to most optical links since it affects the transmission capabilities of the systems. Likewise, the coupling efficiency of light is one of the most important factors contributing to the optical losses. Launching of light rays using a small NA and a larger core diameter would be beneficial for splicing and installation of the fibre. However, there is a trade-off between these fibre specifications and the transmission performance, with such fibres suffering from a high attenuation due to fibre perturbations. In order to enhance the transmission efficiency with superior bandwidth performance, only existing solutions can be considered which involve the mechanical properties of relatively large core GI-MMFs. In practice, bending normally occurs in the middle of a transmission link during fibre installation or maintenance.

To illustrate the effects of bending, and in particular the sensitivity to macrobending, on a large core fibre with a small relative refractive index difference, an optical input Gaussian beam with a 10 µm beam diameter was launched into a GI200 graded index multimode fibre having a core diameter of 200 µm with a small refractive index contrast between the materials, corresponding to an NA of 0.132. The light propagation was modelled for an operating wavelength of 1.55 µm. It is found that a small amount of the guiding light is lost during the launching into the GI200 fibre. Part of the launched power could indeed be lost at the interface due to Fresnel reflections. In general, the effects of reflections at the interface will be accounted for by approximately a 4% loss per interface, which typically depends on the refractive index difference of the medium [125, 126]. We thus observe approximately 96% of the maximum transmission is coupled to the entrance end of the GI200 fibre, propagating with a number of guided modes. Measurements of bending losses for a 10° and a 90° bend of the GI200 fibre are shown in Figure 5.14 as a function of bending radius from 40 mm to 400 mm.

As expected, a large core-low NA fibre exhibits much more bending loss as compared to the standard commercially available fibres with a relatively small core diameter and large index contrast.

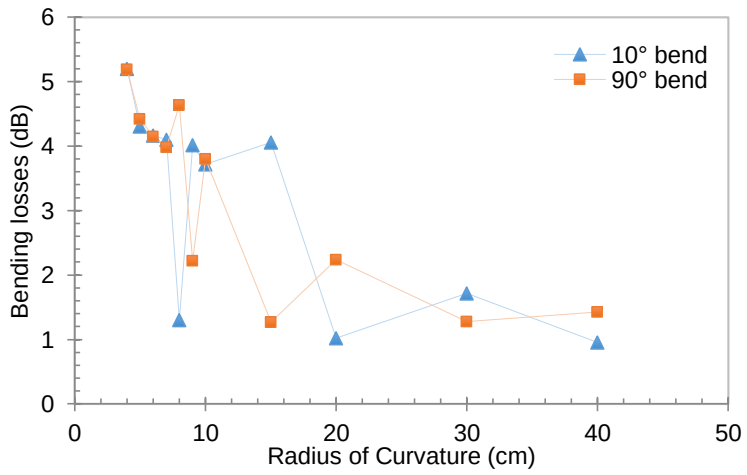

Figure 5.14: Losses of GI200 fibre for a 10° bend and 90° bend

The sensitivity to the bending losses of the proposed fibre drastically increases when the fibre is bent excessively with the minimum bend radius. This is due to the change of the fibre specifications, which has more influence on the bending losses. At the critical tight bend radius of 40 mm, the GI200 fibre exhibits a 5 dB loss for the 10° and 90° bends (with comparable NA in both cases). The GI200 fibre with the 10° and 90° bends has similar high bending losses at a curvature radius below 80 mand experiences different bending performance with an increase of circular arc radius. Comparing the characteristics of bending for the different angular changes it is found that the bending losses of 4.6 dB/90° bend is larger compared to a smaller bend angle with the same radius of bending (where R = 9 cm) for which the losses suddenly drop to the minimum value of 1.3 dB/10° bend, propagating for a distance of z = 145 mm and z = 180 mm, respectively.

More interestingly, the effect of bending losses in a 10° bend of GI200 fibre greatly improve with superior bend resistance with a tighter bend of the order of 80 mm. This can be explained using the investigation results to understand that the fundamental mode carries most of the fractional power compared with only 66.16% of the light being coupled to the first order mode in a 90° bend fibre. In addition, it can be seen from the numerical results that the losses appear to fluctuate after increasing the radius of curvature. The reasons for this bending characteristic is dependent on the amount of transmitted light to the first few guided modes. The higher the fractional power remaining in the low order modes, the less the sensitivity to bending. Nonetheless, it was assumed that working with the bend radius beyond 200 mm and 300 mm would be sufficient to improve the bending losses of GI200 fibre for a 10° bend and 90° bend angle, respectively.

The corresponding normalised intensity distributions for the GI200 fibre are compared for different stress properties as shown in Figure 5.15 for: (a) a 10° bend with R = 80 mm; (b) a 90° bend with R = 80 mm; and (c) a 10° bend with R = 400 mm.

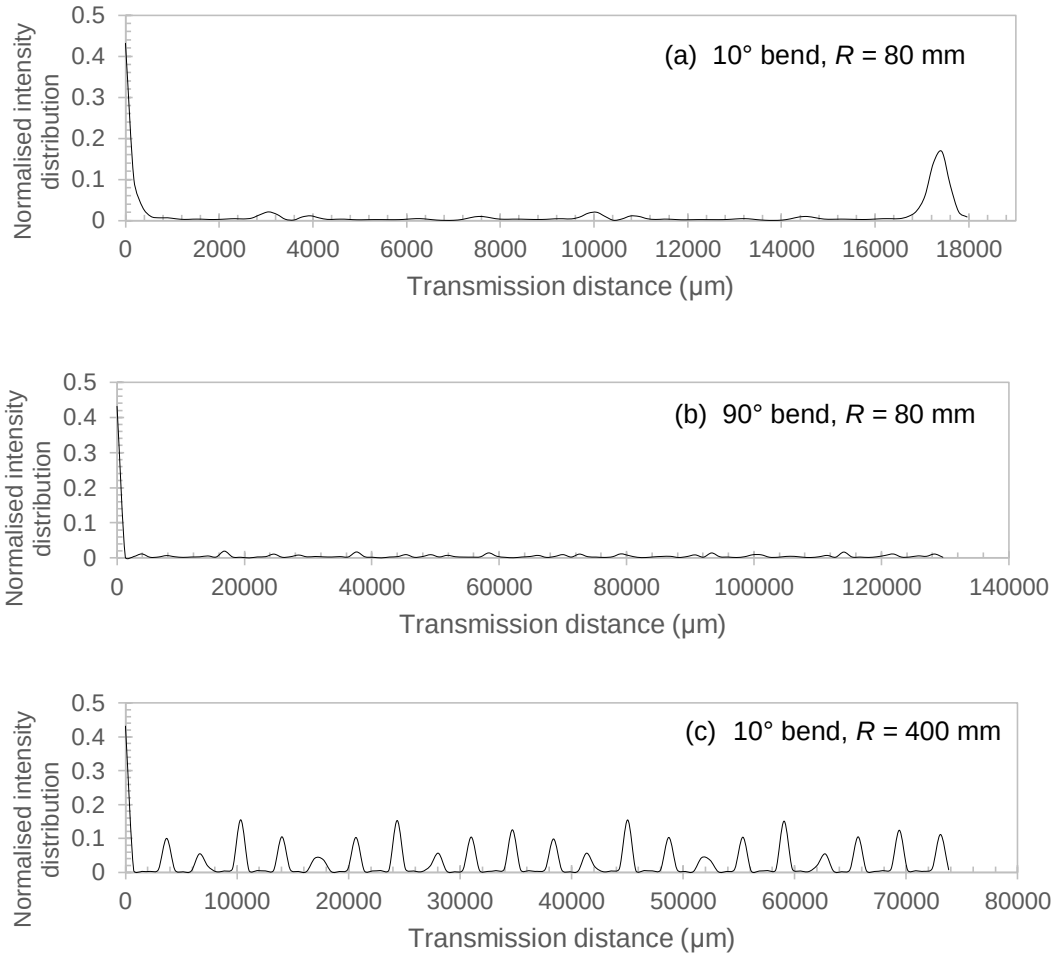

Figure 5.15: Normalised intensity distributions after propagating through the bent GI200 fibre under various mechanical conditions for: (a) a 10° bend with R = 80 mm; (b) a 90° bend with R = 80 mm; and (c) a 10° bend with R = 400 mm.

It is apparent in Figure 5.15 (a) that the maximum transmission through a smaller 10° bend with a sharply bent fibre can be achieved at the fibre output after travelling for a distance of z = 18 mm, even though the propagation inside the bent section is relatively small. For this reason, the GI200 fibre having a 10° bend and R = 80 mm shows better macrobending performance with about 1 dB loss compared with the larger bend angle shown in Figure 5.15 (b) with the same a circular radius.

Thus the conclusion must be drawn that after propagating a certain length along the bent fibre, the reconstruction of the incident beam is barely retrieved at the length intervals. In Figure 5.15 (c), the degree of random periodicities of light propagation can be seen along the z-direction for a distance of 74 mm after increasing the curvature radius R to the order of 400 mm. The reason can be explained by the fact that the propagation constants are unevenly spaced between the excited modes. For that reason, it is assumed that it is appropriate that the GI200 fibre be bent in a circular radius of R = 400 mm, which can then be used to further investigate the oscillatory behaviour of an incident light beam in the fibre under bending conditions in the next section.

5.5.5 Characteristics of the interference pattern of a single channel in a single bend of a GI200 fibre

The details presented in this section focus on the phenomenon of the multiple interference pattern between several guided modes along the length of the bent GI200 fibre. Optical fibre has become increasingly used in many related fields of applications, e.g. for transferring images, diagnostic instruments in the biomedical industry and in communications fields, including signal delivery systems. A variety of applications could be based on the phenomenon of the self-imaging properties in fibres but should be tolerant to the bending configurations. We have demonstrated the behaviour of light propagation in a perfectly straight graded-index fibre to reproduce the original beam periodically along the distance of propagation. The simulations in this section present the effect of the interference pattern generated between a number of excited modes as the fibre undergoes perturbation.

To quantify the superiority of the self-imaging at each periodic length interval along a large core and low NA curved fibre, the measurements were performed with a single Gaussian input beam with a diameter of 10 μm that is launched into a piece of 5 mm straight section of GI200 fibre at a wavelength of 1.55 μm before coupling through approximately a 35 mm curved section with a fixed bend radius R of the order of 400 mm. The orange lines shown in Figure 5.16 (b) indicate the boundaries between the two successive straight and bent sections. The corresponding bend angle of this fibre configuration is changed to a 5° bend, to ensure the optimum self-imaging distance and the minimum bending losses.

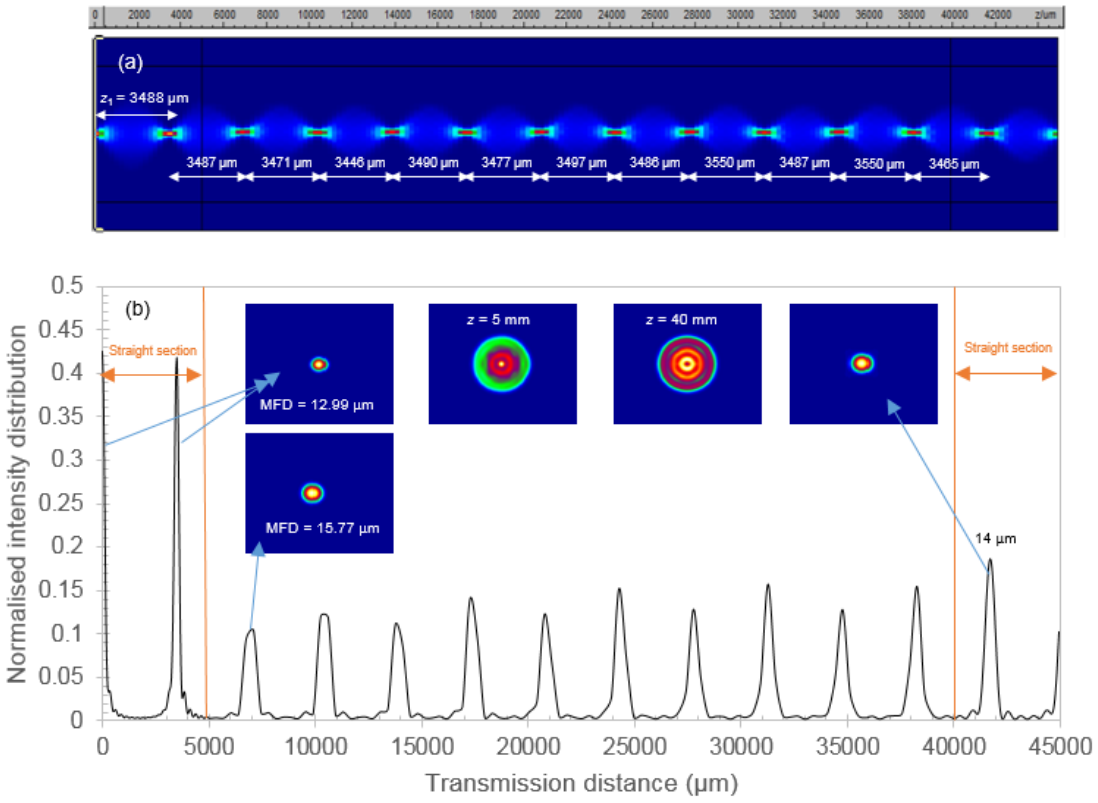

Figure 5.16: (a) The output intensity profile and the field propagation inside a 5° bent GI200 fibre with R = 400 mm, transmitting with a single Gaussian beam diameter of 10 µm at the operating wavelength of 1.55 µm for a distance of z = 45 mm. The inset in (b) shows the beam profile at the first reproduction length of an input beam after propagating for z = 3.48 mm.

The simulated propagation of the electromagnetic field inside the bent GI200 fibre along the transmission length of the order of z = 45 mm is presented in Figure 5.16 (a). It can be noticeably seen that the first optimum distance, at which the initial field is regenerated, occurs after propagating for a distance of z = 3.48 mm through the first straight section of the fibre. In addition, a perfect duplication of the initial Gaussian beam was preserved at this self-reconstruction position with an equivalent mode field diameter, as depicted in the inset of Figure 5.16 (b). Since more than 99% of the power was retained in the first order mode, the bending sensitivity of this fibre was greatly improved with minimum losses below 0.75 dB.

The interesting numerical result shows perfect beam spots at different locations after propagation of the beam through the modified fibre geometry with a small 5° tilt, even though the mode field diameter at the peak transmission occurrence is larger than that of the launched input beam. It can be seen from the characteristics of the multimode interference patterns that the repetition of the single incident beam cannot be recovered periodically along the propagation *z*-direction for which, in principle, the image reconstruction should be recovered again at twofold the Fourier length in a general graded index fibre. Furthermore, the reproduction of an initial phase relation is hardly visible after the light is coupled to the bent section. Consequently, a spatially periodic length interval becomes impossible to create at the same locations where the initial beam should be recovered.

It should be emphasised that the self-imaging does not appear within the fibre length after bending, but only the blurred output beam where its maximum transmission occurs at a periodic length interval. The positions at which the peak power appears are slightly shifted to approximately 50-65 μm from where the reproduction of an image is supposed to be recovered. This is because of the effects of the unequal distribution of the propagation constants among the excited modes, leading to a modification of the self-reconstruction length intervals and the deterioration of the quality of the image reconstruction. Due to the asymmetric interference pattern of the multiple excited modes, the reconstruction of a periodic object cannot be observed in multiple fractional Fourier planes and so no longer exists at a multiple of the Fourier distance [21, 22, 127]. Therefore, in this special case, we might assume that the position where the focusing of the input fields takes place, with a maximum coupling efficiency (i.e. the planes in which the light field is most concentrated), can be considered as the fractional plane [128].

5.5.6 Characteristics of single bend in a GI200 fibre with a four channel spatial input

In this section, we present comprehensive investigations into the multiple channel propagation inside a small NA, large core diameter GI200 fibre under different bending conditions. The optical sources are launched from the entrance of the first straight section and comprise four Gaussian beams with each of the beams having a diameter of 10 μm and an operating wavelength of 1.55μm. The fibre structures consisted of the bent section in the middle between straight pieces of input and output GI200 fibre, in which the bend angles are varied with a fixed curvature radius. The effects of bending on a small NA, large core fibre can be seen in Figure 5.17.

As expected, the efficiency of self-imaging is significantly degraded after bending because of a permanent change in the fibre configuration. In Figure 5.17 (a) and (b) are shown the propagation characteristics and the corresponding normalised intensity distribution of a GI200 fibre in which the bent section undergoes a 5° curve angle with a radius R of 400 mm. After propagating the four spatial beams through an 8 mm long section of the straight fibre, the output intensity profiles of the duplicated beams (i.e. an inverted image) are observed at the first reproduction plane at a distance of $z = 2L = 3.48$ mm where L denotes the Fourier length interval. As the beams are further propagated, the second reconstructed beams (i.e. uninverted image) can be recovered at the desired distance where $z = 4L = 6.96$ mm, inside the first straight section of the fibre. The output cross sectional views of the duplicated incident four channels are shown in Figure 5.17 (c) at their self-imaging positions.

Furthermore, the multimode interference pattern has been thoroughly investigated in the bent fibre section. A good quality of the reconstructed input channels cannot be obtained in GI200 fibre under certain bending conditions. It can be seen in Figure 5.17 (d) that the self-imaging phenomenon is barely visible after the external perturbation is exerted for a short distance on the fibre. The modified shapes of the duplicated incident beams can be observed at the optimal positions where we believe that the best quality of the reproduced fields are visible even though they are surrounded by several unwanted field perturbations. However, a group of beams cannot come to sharp foci and arrange themselves periodically at the self-imaging length intervals along the fibre after propagating through the bent fibre.

Due to the bends, the characteristics of the propagation constants between the guided modes are changed and not evenly spaced due to modification of the refractive index of the fibre. This in turn affects the appearance of the reproduced initial beam profile, which is dependent on the difference in propagation constants [38], such that the formation of the images at the Fourier length intervals to the next self-imaging length location is changed. Nevertheless, the aberrated images can be reconstructed at certain imaging planes after propagating along the output straight fibre as shown on the right in Figure 5.17 (e).

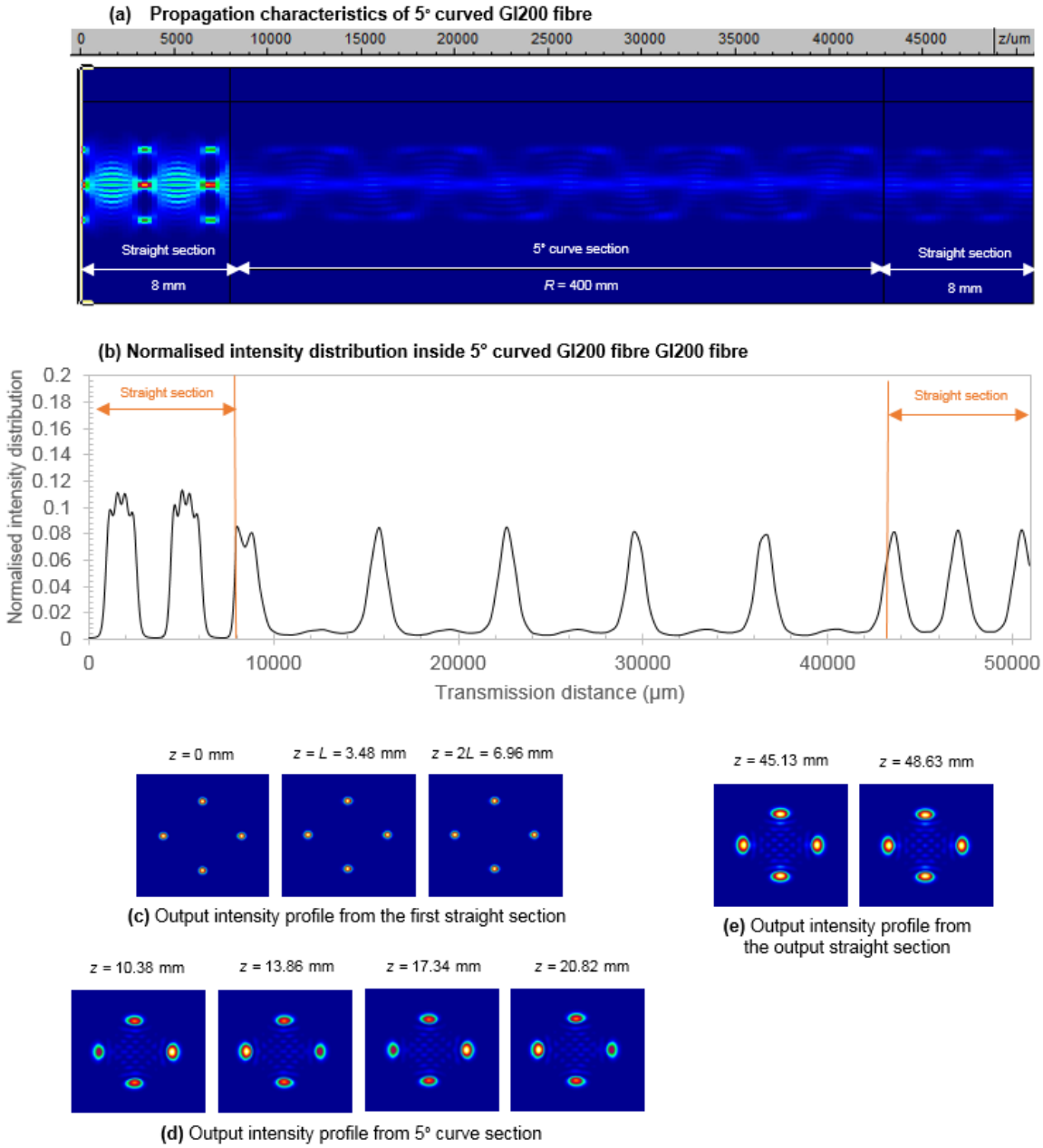

Figure 5.17: (a) The propagation characteristics inside GI200 fibre having a 5° curve section with a circular radius R of 400 mm, propagating for a distance of 50 mm from the straight fibre facet; (b) the corresponding field intensity distribution and (c) – (e) the cross sectional views of the intensity profile for the four input Gaussian beams of the first straight section, 5° curve section and the output straight section at the indicated optimal self-imaging locations.

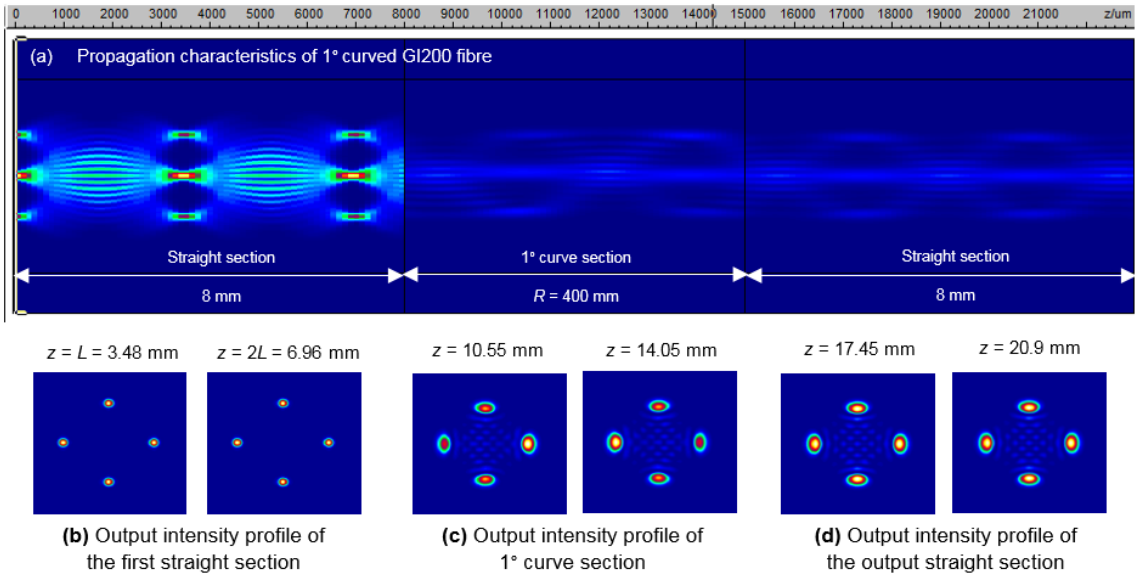

Figure 5.18: (a) The propagation characteristics inside GI200 fibre having a 1° curve section with a circular radius R of 400 mm, propagating for a distance of 23 mm from the straight fibre facet, and the cross sectional view of the intensity profile for the four input Gaussian beams at different locations and (b) – (d) the cross sectional view of the intensity profile for the four input Gaussian beams from the first straight section, 1° curve section, and the output straight section at different optimal self-imaging locations.

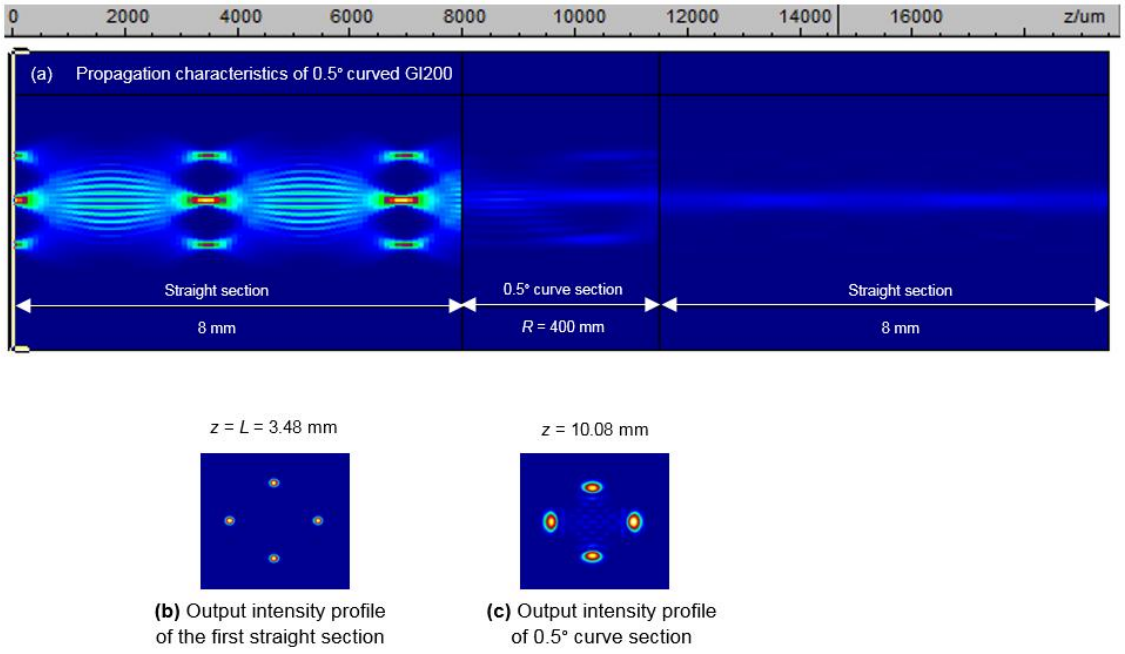

Figure 5.19: (a) The propagation characteristics inside GI200 fibre having a 0.5° curve section with a circular radius R of 400 mm, propagating for a distance of 19.50 mm from the entrance fibre, (b) the cross sectional view of the intensity profile for the reproduction of four input Gaussian beams from the first straight section and (c) the intensity profile at the optimal self-imaging locations inside 0.5° curve section.

According to the numerical simulations in the above figures, it can be seen that a strong concentration of the excited beams can be observed within the bend region in different observation planes. However, there are present the effects of aberrations on the self-imaging reconstructions in different fractional planes. It should be emphasised that even though the distribution of the incident light does not repeat at multiples of the Fourier distances away from the front surface of the fibre, the images are formed at regular distances in the fractional planes along the bend waveguide. This means that the separation distance of each of these planes occurs at every period of the fractional distance.

Indeed, as depicted in Figure 5.19 for the simulated results of a half degree bend of fibre, it is clearly seen in the bend section that there is an enhancement in the quality of the reconstructed images compared to those with larger bend angles. However, a group of imaged beams cannot be apparently identified in the fractional plane as the beams propagate further through the output straight fibre. Due to the mismatch between the fibre geometries, the fractional power drastically drops from 90% to approximately 25% after a group of incident beams are simultaneously propagated down a 5° degree and a 1^{o} bend of the fibre. However, a significant amount of the power loss is leakage out of the direction of propagation with less than 12% of the power being coupled onto the output section as the fibre undergoes even half a degree of bending. For tighter bends, a much lower fraction of power is coupled to the output fibre due to a rapid change of the structure and the consequent very short period of the arc length in the bent section. For this reason, the light rays are hardly recombined in the fractional planes even for a small degree of bend in the fibre.

5.5.7 Characteristics of multiple bends in GI200 fibre with a four channel spatial input

After examining the propagation of multiple input channels in a single bend of GI200 fibre, we further investigate the sensitivity to bending on the reproduction of the excited fields with a multi-bend structure. To examine this effect, the four spatial beams, each with an equivalent beam diameter of 10 μm, are launched into an 8 mm piece of GI200 straight fibre that is spliced to two consecutive bends in opposite directions.

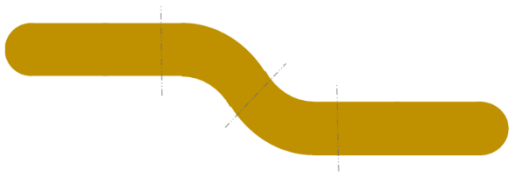

Figure 5.20: Schematic diagram of two successive bends of the fibre

The design of this bend structure is schematically shown in Figure 5.20. The radius of curvature is fixed at R equal to 400 mm for both of the two different bend angles. After passing the curved sections, multiple propagation modes are coupled to another piece of an 8 mm long section of straight fibre. The numerical results are illustrated in Figure 5.21 and 5.22 for a 5° bend and a 1° degree bend.

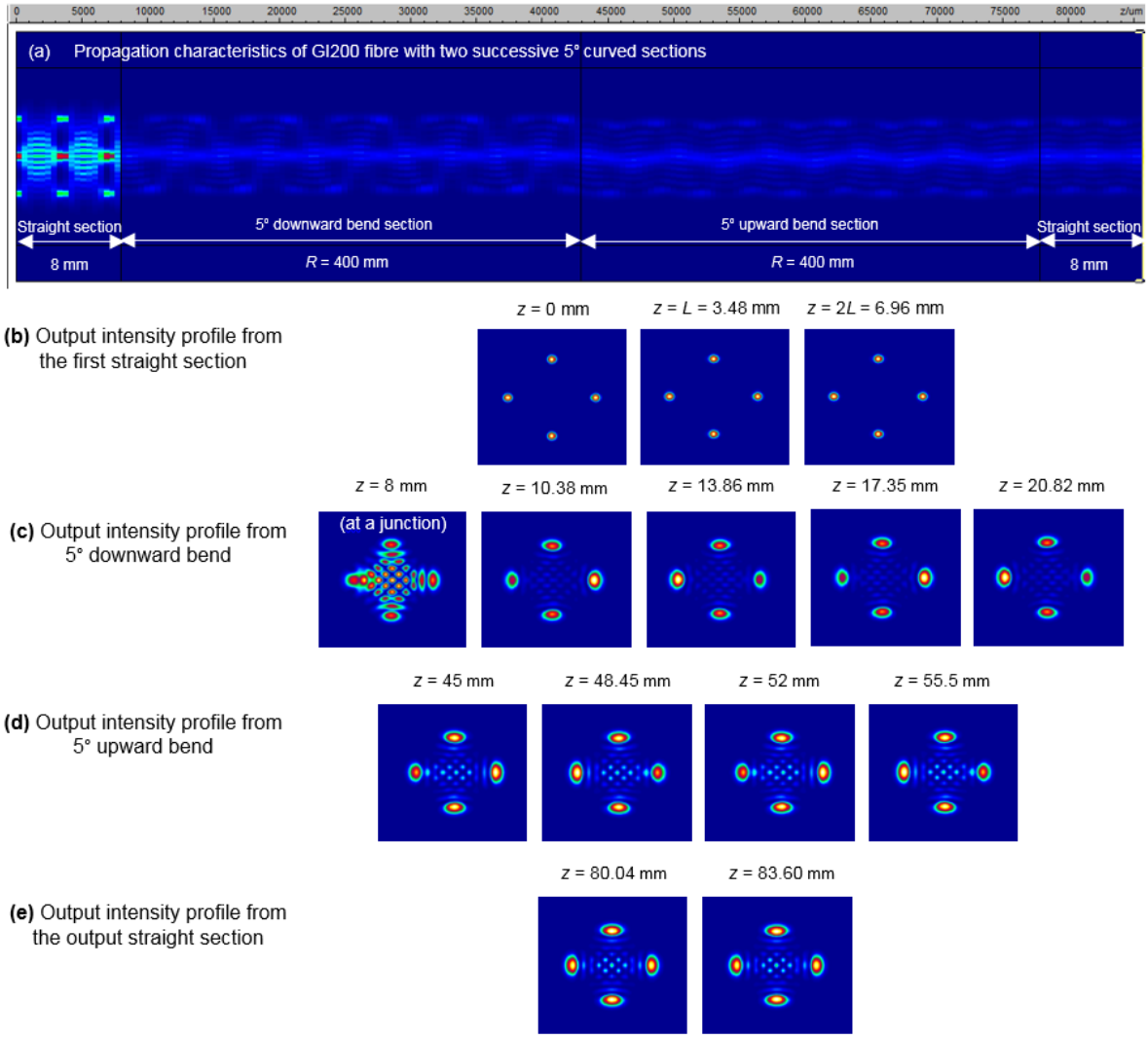

Figure 5.21: (a) The propagation characteristics inside GI200 fibre with two consecutive 5° bends with a circular radius R of 400 mm, propagating for a distance of 85.81 mm from the fibre facet and (b) – (e) the cross sectional views of the intensity profile for the four input Gaussian beams from the first straight section, 5° downward bend, 5° upward bend and the output straight section at different optimal self-imaging locations.

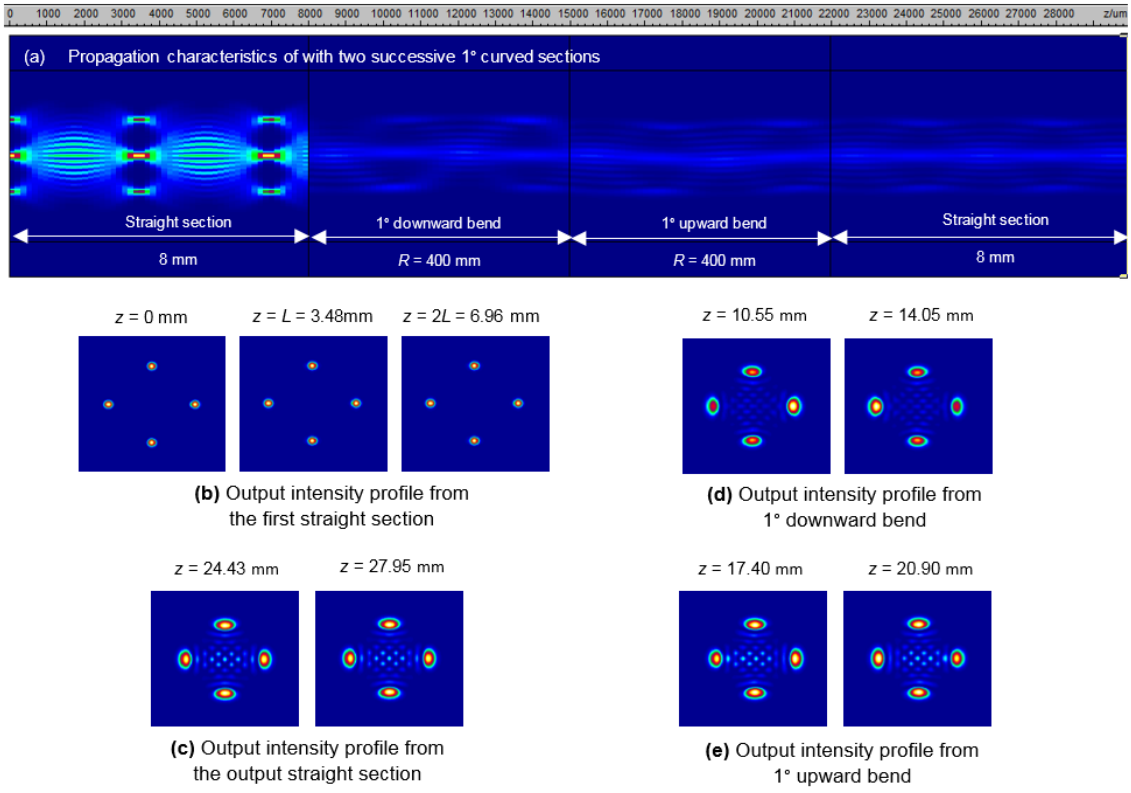

Figure 5.22: (a) The propagation characteristics inside GI200 fibre with two successive 1° bends with a circular radius R of 400 mm, propagating approximately a distance of 30 mm from the fibre facet and (b) – (e) the cross sectional views of the intensity profile for the four input Gaussian beams from the first straight section, 1° downward bend, 1° upward bend and the output straight section at different optimal self-imaging locations.

It is clearly seen that an enhanced self-imaging quality can be observed along the optimal fractional distances when two bend sections are adjacent and in precisely opposite directions. Correspondingly, the aberrations of the reconstructed beams in a 1° degree bend angle of the fibre are much better-quality than for the 5° bends with the beam profiles at the fractional planes of the bend section being comparable to that of the output straight fibre, as depicted in Figure 5.21 and Figure 5.22. Also, it may have been expected that by increasing the arc length of the bends further, a higher quality of self-imaging might be observed by adjusting the curvature radius R maybe to the order of 1000 mm. However, the effect of increasing R for a certain constant bend angle does not appear to be effective in improving the self-imaging quality but, rather,

leads to a greater bending sensitivity of the fibres since the beam has a much greater propagation distance through the curved region of the fibre.

Table 5.3

Summary of the propagation loss induced by bending for different fibre configurations and bending conditions. The results are for a spatial input of four channels with Gaussian beam diameters of 10 μm as the optical sources, transmitting at the wavelength of 1.55 μm inside a 200 μm core diameter fibre with an NA of 0.132 at a fixed bend radius of 400 mm.

Configurations of the fibre	A single bend			2 consecutive bends				
	R = 400 mm			R = 400 mm		R = 1000 mm		
	5° bend	1° bend	0.5° bend	5° bend	1° bend	5° bend	1° bend	0.5° bend
Propagation loss (dB)	6.27 dB	6.25 dB	8.77 dB	6.44 dB	6.43 dB	7.60 dB	7.98 dB	8.50 dB

As shown by the analysis conducted, the propagation loss will increase in comparison to the core diameter, but is less dependent on the number of bend sections in the structure as shown in the results given in Table 5.3. This summarises the impact of bending on the propagation for the different fibre configurations. The results reveal that the sensitivity to the bending for a single bend structure is very similar to the bending behaviour for that of the two consecutive bend configuration with only a slightly increased propagation loss in the latter. Also, the transmission within a single bend shape with half a degree of bend is the most sensitive to the bend as compared to the larger bending angle because less output power from the bend is coupled into the last section of the straight fibre. This is mainly because of the very short section length of the bend (for more detail the reader is referred to section 5.5.6). Thus, overall, it can be concluded that the transmission efficiency and capability of the fibre to periodically reproduce high quality self-imaging are restricted by fibre perturbations.

Above all, this study has emphasised that the bends do not only affect the re-imaging of the excited beams in the bent fibres but also alter the self-reproduction length intervals, which in a straight fibre will be repeated at intervals of twice the Fourier length. This is due to a rapid decrease of the transmitted power, so that the fibre exhibits much more loss, especially the transition losses at the interface where there is a sudden change of the fibre geometry, which is the most significant contribution to the total propagation losses. For this reason, the GI200 fibre loses much of its effectiveness in its unique property to fully recover the incident fields at periodic distance intervals along the direction of propagation.

5.6 Conclusion

The propagation characteristics of excited single channel and multiple channels have been studied in a large core-small numerical aperture multimode bent fibre. The formation of reproductions of the incident field has been investigated and its corresponding self-imaging distance has been examined for different sections of the fibre. As a result of bending, the direction of light paths is modified and portions of light are lost during the propagation, generating additional losses in the optical fibre. The numerical simulations have shown that the increased optical losses are directly related to the core diameter and inversely to the index differences between the core and cladding. As a result of our simulations, our proposed multi-channel fibre with a small NA of 0.132 and 200μm in core diameter has been shown to be less sensitive to bending effects for single channel transmission with a low propagation loss of 0.75 dB/5° bend. A typical sensitivity to bending of approximately 6.27 dB/5° bend was achieved when four spatial channels were transmitted in the same fibre under the same curvature radius of 400 mm.

This study has emphasised the formation of reproductions of the incident field and its corresponding self-imaging distance for different sections of the fibre. As can be seen, the bends have a great influence not only on the transmission efficiency, but also affect the quality of the reconstructed beams as well as the consistency of the formation of the self-imaging distances. Thus, overall, it must be concluded that the transmission efficiency and capability of the fibre to periodically reproduce high quality self-imaging is restricted by the fibre perturbation since the fibre is compromised in much of its effectiveness in its unique property to fully recover the incident fields as well as the consistency in the formation of the self-imaging distances. However, the analyses can be used as a guideline to optimise a new bend resistant fibre having a large core-small index contrast without trade-off of optical performance to meet current demands of high bandwidths with improved transmission capacity. Nevertheless, any practical application based on such a fibre system will have to ensure minimum perturbations to the fibre path and possibly accommodate required changes of direction with out-of-fibre reflective optical components.

Chapter 6

The effect of temperature on a multimode graded index fibre

6.1 Introduction

The use of optical fibres as a transmission medium is being progressively enhanced for deployment in ever-wider applications due to their excellent features. Thus in addition to losses and degradation of the transmitted optical signals caused predominantly from mechanical defects and deformations, maybe due to human errors during their installation or maintenance, another key factor that imposes a risk of effecting performance is the temperature dependence of the optical fibre. The sensitivity of a fibre to temperature can possibly pose a significant impact on the optical performance, causing damage to the fibre when the outer layer of the fibre absorbs a large amount of leakage light, specifically under tight bend conditions. For this reason, it is, therefore, meaningful to estimate the effect of temperature variations over a reasonable operating range of temperatures, and hence provide an indication for the fibre's capability in a transmission system when designing temperature tolerant fibres. In the previous Chapter, we have demonstrated the bend sensitivity of optical fibres under different bending conditions, resulting in a degradation of the propagation signals to the fibre output. This Chapter gives an analysis of optical fibre performance under varying temperature conditions. We investigate how the temperature changes the transmission characteristics with which light propagates through the fibre by varying the range of temperature but without bending effects on the fibre. Additionally, we use this modelling to investigate the optical performance of the perturbed fibre under different temperature

conditions when employed to reproduce an input beam profile periodically along the length of the fibre.

6.2 Temperature effect in a fibre

Due to a rapid growth of network demands, additional optical amplification techniques, such as EDFA and Raman amplification, have been employed within optical communication systems to enable high carrying capacity. Accordingly, a large optical loss is expected to be produced with an increase of the power levels during propagation, leading to damage of the fibre. Moreover, key challenges exist in the design of high optical transmission systems that are capable of a large carrying capacity and operating in harsh environmental conditions, in particular at both high and low extremes of temperature.

Recently, a number of research studies have focused their interest on the ability of optical fibres to withstand additional transmission link losses. In addition, investigations of refractive index changes in combination with bending effects have been reported by many authors [129, 130, and 131]. It has been shown that a change in refractive index with temperature has a great impact on optical systems under bending conditions, causing more scattering of light in the fibre glass. Under tight bend conditions, high bending losses can possibly produce significant damage to optical cables when a large amount of leakage light is absorbed by the coating layer, eventually causing burning to the fibre.

The optical path length of a fibre is subjected to change in accordance with the surrounding's temperature, and subsequently undergoes changes in the physical properties of the fibre. It is well known that a decrease in temperature will result in contraction of the actual fibre length, whereas the optical path length is expanded with a rise in temperature. In this section, the aim is to study the dependence of thermal properties of the fibre materials, such as the thermo-optic coefficient and the effective thermal expansion coefficient, on the optical fibre path length. To study the dependency of temperature on the optical fibre

path length, the changes in both the refractive index, n, and the length of a fibre, z, need to be determined from these thermal properties.

As we have emphasised, the light propagation in an optical fibre is based on the phenomenon of total internal reflection, in which the light rays bounce between the boundaries of the core and cladding all the way throughout the transmission path. However, the direction of propagation is altered if the fibre undergoes some of unwanted perturbations during the transmission. Consequently, this leads to a significant increase in the transmission link losses, and hence changes in the output of light intensity since some of the optical signal leaks from the guided core and can be transferred to the surrounding layer. The scattered light rays are then converted into heat, leading to an increase in the coating temperature [132-134]. Also, with changes in the temperature surrounding the fibre, its physical properties will be changed, so affecting the transmission characteristics and obviously the optical path length of the fibre.

Since the variation of refractive index is a typical function of both temperature and wavelength, the temperature-dependence optical fibre is of great importance in various areas of studies. A number of theoretical and experimental studies have investigated the temperature effect on propagation behaviour in optical fibre under various environmental conditions. Soares and Dantas [135] have demonstrated that the refractive index changes of the cladding material can lead to a modification of output power and, therefore, contribute significant losses. Recent advances in optical fibre temperature sensors are increasingly being made for biomedical applications based on several methods [136]. Scheggi *et al*. [137] have initiated a new area of study by investigating a fibre temperature sensor based on light intensity modulation, caused by the thermo-sensitivity of the materials employed. In fact, the modifications of the transmission path length and refractive index of optical fibre are generally dependent on the thermal properties of the fibre that in turn can be determined from its chemical compositions.

6.2.1 Change in optical transmission length and the refractive index of a fibre

The local refractive index is a function of the changes in the temperature of the optical medium, ΔT, in which the light is propagating. This can be described using the temperature coefficient of refractive index or thermo-optic coefficient, $\frac{dn}{dT}$ and can be written as [102]:

$$\frac{dn}{dT} = \frac{\Delta n}{n\Delta T} \tag{6.1}$$

From equation (6.1), the refractive index changes with temperature of the environment, T, is thus given by:

$$n(T) = n(T_0) + \frac{dn}{dT}(T - T_0) \tag{6.2}$$

where $n(T_o)$ is the refractive index of the fibre at ambient temperature, $T_o = 25°C$.

According to the study by Prod'homme [138], the thermo-optic coefficient $\frac{dn}{dT}$ of the fibre can be alternatively derived from two contributing factors: the thermal electronic polarizability coefficient (ζ); and the linear thermal-expansion coefficient $(\alpha_{thermal})$ of the material observed at room temperature, and is expressed as:

$$\frac{dn}{dT} = \frac{(n^2 - 1)(n^2 + 2)}{6n} \times (\xi - 3\alpha_{thermal}) \tag{6.3}$$

From the above equations, it can be seen that the temperature dependence of the optical fibre path length has a significant effect on the changes in refractive index and physical length of the light guided medium. In addition to the change in refractive index profile, the fractional change in the length of a fibre resulting from changes in temperature can be determined from the thermal expansion coefficient, $\alpha_{thermal}$, which is given by [154]:

$$\alpha_{thermal} = \frac{\Delta z}{z\Delta T} \tag{6.4}$$

where Δz is the change in length z of the fibre with temperature.

Thus, equations (6.1) and (6.4) can be combined to give the temperature coefficient of changes in optical path length ΔL:

$$\alpha_{thermal} + \frac{dn}{dT} = \frac{1}{\Delta T}\left(\frac{\Delta z}{z} + \frac{\Delta n}{n}\right) \tag{6.5}$$

$$\alpha_{thermal} + \frac{dn}{dT} = \frac{1}{\Delta T}\left(\frac{\Delta L}{L}\right) \tag{6.6}$$

where L is the original length of the fibre at room temperature T_o and:

$$\frac{\Delta L}{L} = \Delta T\left(\alpha_{thermal} + \frac{dn}{dT}\right) \tag{6.7}$$

Hence the entire transmission length of the fibre, or the final section length of the fibre, L_f, that is subjected to environmental temperature changes, is simply determined by adding the actual length interval, L, to the change in optical path length of the fibre, ΔL, for various temperature conditions.

6.3 Analysis of temperature effects on the refractive index of the fibre modes

As a result of a change in refractive index of the optical fibre and scattering of light out of the transmission direction, the propagation characteristics of optical communication signals is expected to change along the transmission path. In this section, the temperature-dependence of refractive index for GI62.5 multimode fibres has been investigated using various recommended ranges of temperature without considering an additional mechanical stress effect on the fibre. The fibre chosen for our simulations is a graded index fibre consisting of a fused silica Ge-doped core (GeO_2-SiO_2) and silica cladding (SiO_2). The core and cladding diameters are: 62.5, and 125 μm respectively, with a core refractive index of 1.48 and a numerical aperture equal to 0.275 (abbreviated to GI62.5 fibre). For this study, an input Gaussian beam with a 10 μm diameter was launched into a piece of 10 mm length of fibre at the operating wavelength of 1.55 μm.

It is noted that fused silica Ge-doped glass is often the most preferable dopant composition for optimising the functionality and performance of optical fibres in telecommunication systems or other related fields because of its excellent features, such as supporting high fibre temperature tolerance, and hence improved thermal stability, and low scattering losses [38, 139]. Thus for the higher refractive index of the fused silica fibre core, a germanium (Ge) compound is used as a core dopant with an acrylate composition for the coating material whose refractive index is set to approach that of the cladding giving a number of advantages for optical communication system usage [140]. For example, the leakage of energy can be trapped within the cladding region instead of entering the coating and reflecting back into the propagation direction. Another benefit is to overcome the effects of heating due to significantly reducing the absorption of light within the coating and so increasing the temperature of the coating layer, resulting in a degradation of the lifetime usage and reliability

of the fibre. This is of particular importance for a fibre operating with a tight bend condition.

To begin with, the thermal properties of the optical fibre need to be determined in order to study a significant change in both the refractive index, n, and the length of a fibre, z, generated by the surrounding temperature variations. Using equation (6.2) with a thermo-optic coefficient $\frac{dn}{dT}$ of the GeO_2-SiO_2 fibre core with a value of approximately 8.6 x10^{-6}/°C and a value of 10 x10^{-6}/°C for the SiO_2 cladding [141, 142], one can determine temperature dependence of the refractive index changes for different environmental temperatures, $n(T)$, with respect to the index of refraction at a room temperature T_0 of 25°C. The calculated refractive index changes of the fibre core and cladding as a function of the entire simulated range of temperature T from 0°C to 80°C with increments of 10°C are graphically presented in Figures 6.1 and 6.2, respectively.

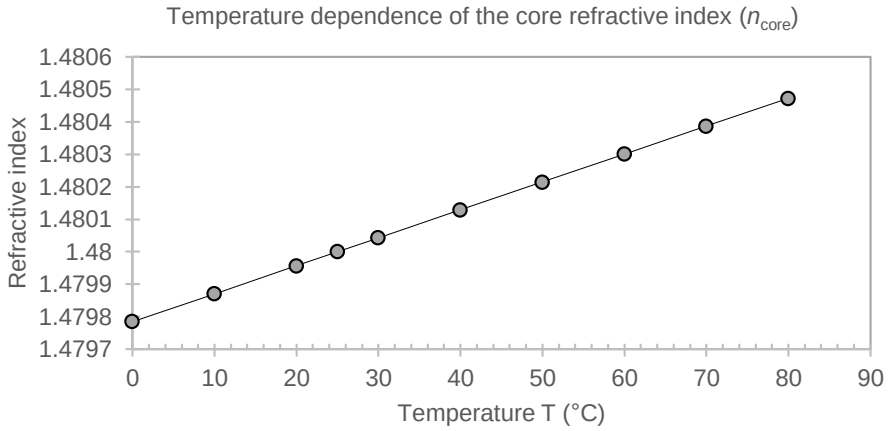

Figure 6.1: The calculated refractive index of the Ge-doped silica fibre for a GI62.5 fibre determined with a reference to the thermo-optic coefficient $\frac{dn}{dT}$ with a value of 8.6 x10^{-6}/°C as a function of various operating temperatures.

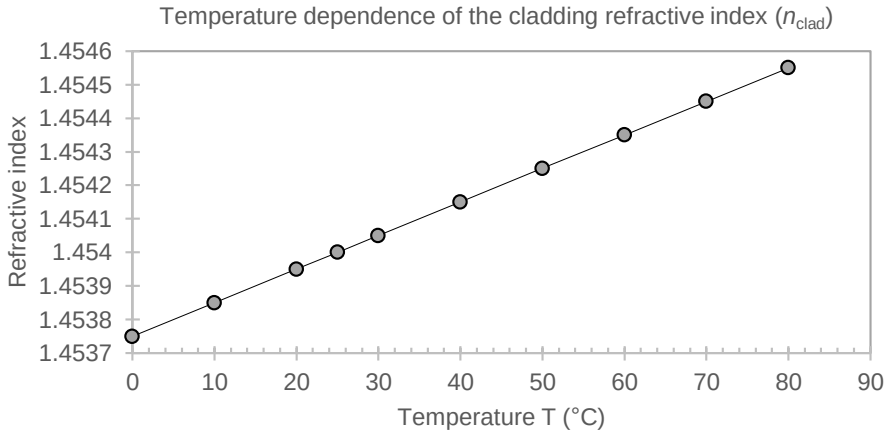

Figure 6.2: The calculated refractive index of the fused silica cladding for a GI62.5 fibre determined with a reference to the thermo-optic coefficient $\frac{dn}{dT}$ with a value of 11 x10^{-6}/°C as a function of various operating temperatures.

Since the refractive index of the fibre is substantially dependent on the temperature around the transmission medium, it can be interpreted from the figure that the refractive index of a GI62.5 fibre core and cladding are found to increase linearly with temperature at a given incident wavelength of light. The result may come as a surprise since the change in index of refraction is inversely proportional to temperature. With a rise in temperature, the refractive index is

generally expected to decrease (and thus reduce the intensity of scattered light within the material) over the entire range of temperature [143, 144, 145, and 146]. On the other hand, the results we have calculated are exactly in agreement with a theoretical interpretation presented by Yong *et al.* [147] and other investigations on temperature-dependence of refractive index of fused silica fibre [148, 149, 150, and 151].

More specifically, the analysis can be made by considering the importance of the thermo-optic coefficient because this value arises from contributions due to interactions of the material's electrons with photons [152]. A decrease in refractive index with increases of the temperature can be found in glasses that have a negative value $\left(\frac{dn}{dT} < 0\right)$ of thermo-optic coefficient. Conversely, a change in index of refraction was found to be directly proportional to temperature for optical glasses that exhibit a positive sign $\left(\frac{dn}{dT} > 0\right)$ of thermo-optic coefficient. Based on the data reported by Ramachandran [153], the behaviour of optical glasses for different thermo-optic values is essentially dependent upon the chemical composition of the materials at specific ambient temperatures. It is important to note that as the temperature increases, the optical path length is expanded with an increase of the index of refraction for a positive $\alpha_{thermal}$ coefficient.

The response of the refractive index changes of the GI62.5 fibre with environmental conditions can be understood from its relatively low thermal expansion coefficient $\alpha_{thermal}$ with a positive $\frac{dn}{dT}$ thermo-optic coefficient. Thus one can see the central role of the thermal properties of a material in the determination of temperature dependence of the change in refractive index of optical fibres.

6.4 Results and discussion

6.4.1 Temperature effect on optical path length

As illustrated above, we have explored the fact that the local refractive index of the fibre core is affected by temperature fluctuations, and its behaviour is significantly dependent on both of the dopants' thermal coefficients. The desired performance of the optical fibre can be simply described based on the thermal properties of the dopant material. It is, therefore, important to determine changes in optical path length of the fibre to investigate how this may effect periodic imaging positions in the graded index fibre. The Ge-doped fused silica glass from which the GI62.5 is fabricated has a relatively small thermal expansion coefficient, $\alpha_{thermal}$, of 0.55×10^{-6}/°C [140] and a positive refractive index thermo-optic coefficient, $\frac{dn}{dT}$ of 8.6 $\times10^{-6}$/°C.

Table 6.1

The final propagation length, L_f, corresponding to the induced refractive index and length changes at various surrounding temperatures T from 0°C to 80°C for a fibre initially 10 mm in length at 25 °C.

T (°C)	Change in optical path length of a fibre (ΔL)	Fibre length at T, L_f (μm)
0	-2.2875	9997.7125
10	-1.3725	9998.6275
20	-0.4575	9999.5425
25	0	10000
30	0.4575	10000.4575
40	1.3725	10001.3725
50	2.2875	10002.2875
60	3.2025	10003.2025
70	4.1175	10004.1175
80	5.0325	10005.0325

Results of the simulation for the determination of the change in the optical transmission length of the GI62.5 fibre are shown in Table 6.1 as a function of temperature using a 10 mm length of fibre at 25°C as the zero reference condition. The results indicate that the fibre length is slightly changed with temperature (where this is assumed to be constant across the whole cross section of the fibre i.e. the conditions are steady state and the fibre is in thermal equilibrium). A decrease in temperature, below the level of that of room temperature ($T_0 = 25$°C), results in a contraction of the actual fibre length, whilst the optical path length is slightly expanded with a gradual increase in the temperature level.

6.4.2 Temperature effect on propagation characteristics

In the previous section we have seen that the thermal properties of dopant materials, described in terms of the linear thermal expansion coefficient and the thermo-optic coefficient, are the major contributing factors in the determination of the optical path length in the fibre. This allows us to investigate the effect of these environmental changes on the important phenomenon of periodic imaging in graded index fibres which is based on the interference of multiple guided modes along the propagation direction.

The self-imaging of the original input beam profile in a graded index multimode fibre is produced in a natural way to periodically reconstruct at self-imaging planes (i.e. at $z = 2L$ where L is the focal distance in the fibre) along the transmission length of the fibre. Possible changes induced by temperature effects have been examined in this study for temperatures in a range of 0°C to 80°C.

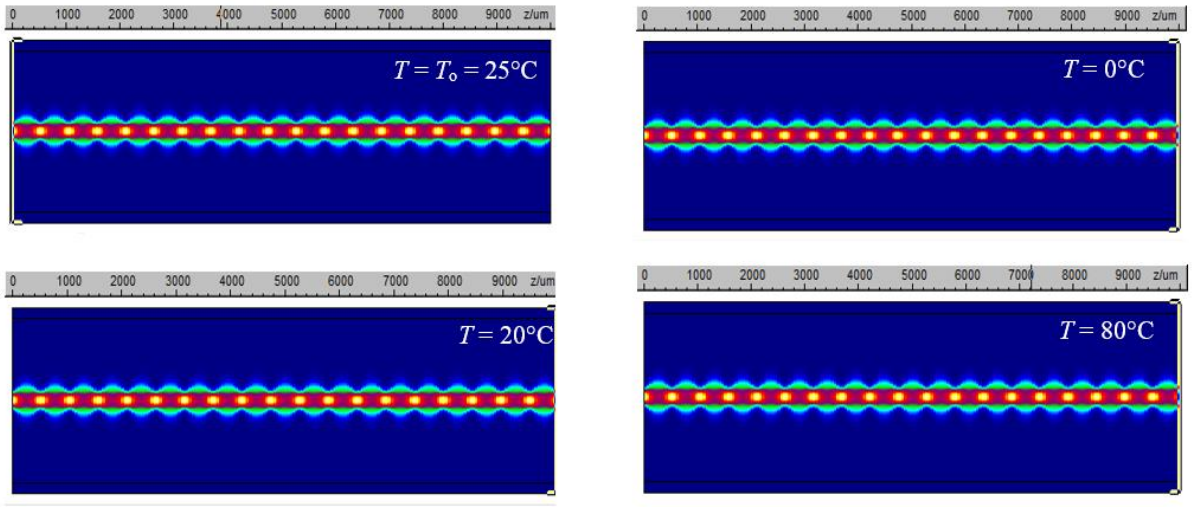

Figure 6.3: Simulated multimode interference pattern within GI62.5 fibre with a 10 μm Gaussian input beam diameter at a wavelength of 1.55 μm for the indicated temperatures.

The location of the self-imaging planes occurring in the GI62.5 fibre at different temperatures of the fibre were determined by simulation. The results are depicted in Figure 6.3 for the indicated operating temperatures. An important conclusion that may be drawn from these results is that the propagation characteristics of the fibre experience a similar trend even though their total transmission lengths are varying, either expanded or compressed, albeit only a few micrometres from the original 10 mm length of the fibre. More interestingly, we found that the first self-imaging length interval of perturbed GI62.5 fibres can be found at almost a distance of 528 μm (i.e. where $z = 2L$ after propagation of a 10 μm diameter input Gaussian beam through the length of the fibre at the room temperature), as can be seen in Figure 6.4.

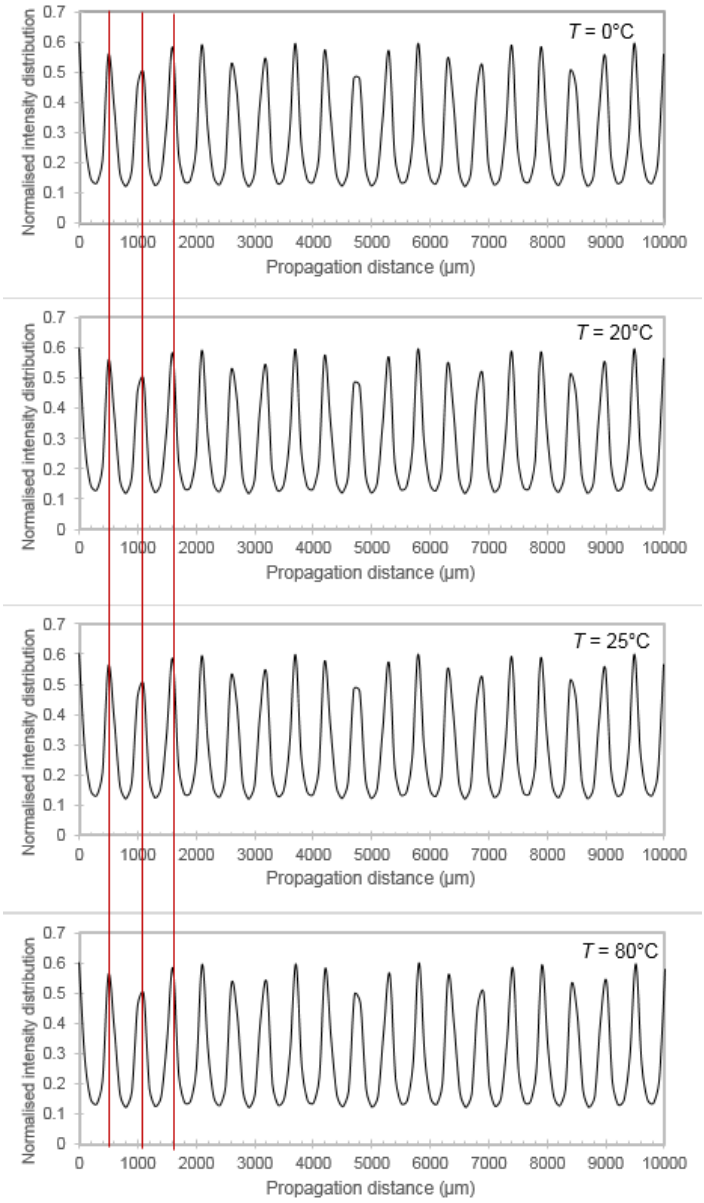

Figure 6.4: The comparison of normalised intensity distributions as a function of propagation distance resulting from a 10 μm diameter Gaussian input beam with a wavelength of 1.55 μm propagating through the length of a GI62.5 fibre for the selected temperatures of 0°C, 20°C , 25°C and 80°C. The red lines shown in the figure indicate the first three peak intensity positions at $z = 2L$, $4L$, and $6L$, respectively.

Table 6.2

The first four self-imaging length intervals of the corresponding fibres, operated at different surrounding temperatures, T_o, for a fibre initially 1 m in length at 25 °C.

T_o (°C)	$z = 2L$ (μm)	(%) difference between z at T=25°C and z at T_o°C	$z = 4L$ (μm)	(%) difference between z at T=25°C and z at T_o°C	$z = 6L$ (μm)	(%) difference between z at T=25°C and z at T_o°C
0	527.463	**0.0014**	1055.159	**0.0013**	1582.560	**0.0014**
20	527.468	**0.0005**	1055.170	**0.0003**	1582.576	**0.0004**
25	527.470	**0.0000**	1055.173	**0.0000**	1582.582	**0.0000**
30	527.472	**0.0004**	1055.177	**0.0004**	1582.587	**0.0003**
80	527.486	**0.0030**	1055.204	**0.0029**	1582.627	**0.0028**

Note that: To confirm the consistency and the percentage changes of self-imaging positions, we have investigated the propagation of along a 1 meter length of the fibre, and the results of simulations from a distance of $z = 2L$ to $z = 60L$ are given in Appendix 2.

Furthermore, after propagating along a length slightly expanded from the original 1 m length of fibre, an initial Gaussian beam comes to reimage periodically at almost the same optimum self-imaging plane to that in fibres experiencing dissimilar temperature conditions. The first three locations of the reconstructed initial beam are given in Table 6.2 for the fibre operated in different harsh environmental conditions and the percentage changes in self-imaging distance under each condition is given in comparison with that of room temperature. It is apparent that the characteristics of the multimode interference pattern seem to be little affected by the temperature perturbation applied to a GI62.5 fibre. In other words, changes in refractive index and the modified optical path length due to a change in temperature are extremely small, even with exposure to extremely high or low temperatures, so it is perhaps not surprising that there are no significant changes in self-imaging positions when operating under different temperature conditions.

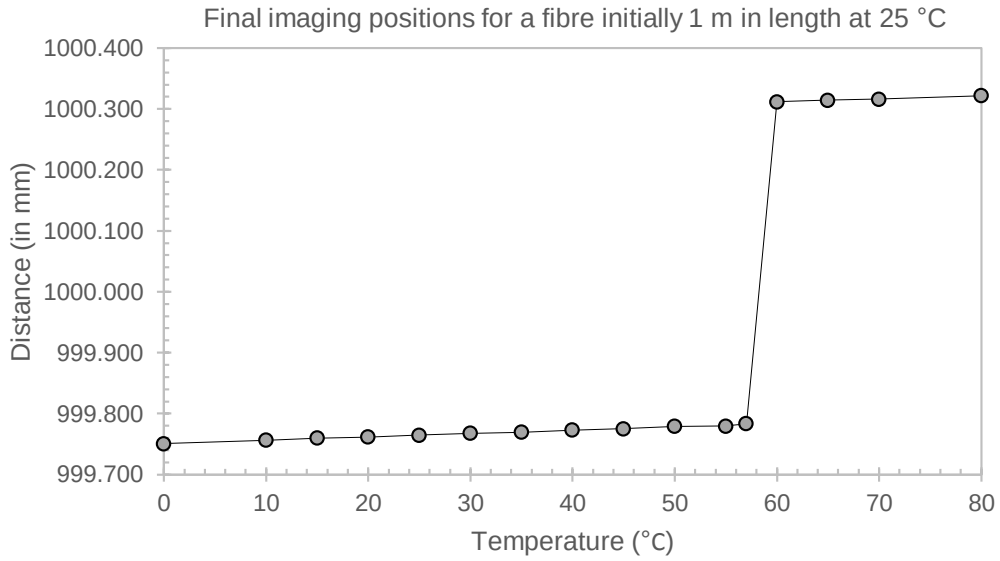

Figure 6.5: The final imaging length, corresponding with the induced refractive index and length changes at various surrounding temperatures T from 0°C to 80°C, for a fibre initially 1 m in length at 25 °C.

The graph in Figure 6.5 compares the change in the final imaging positions of different fibres at various temperature conditions T_o from 0°C to 80°C for a fibre initially 1 m in length at 25°C. One can see various positions (in mm) of the last image before propagating through the end of the fibre for different lengths of the fibre, depending on the temperature conditions. We observe that the final positions of the image are gradually increased with a rise in temperature by a few millimetres. After raising the temperature to a high extreme condition, where T is greater than 60°C, the last imaging positions suffered a dramatic change in their final imaging positions from that of a fibre operated at 25 °C, but still only relatively slightly shifted in position and this trend the tends to rise linearly again as the temperature increases further. The reason for this can be explained from the last three imaging positions, listed in Column A-C in Table 6.3, respectively. From this, it can be seen that the shift in distance between the previous and next imaging plane is approximately at twice the focal length interval, i.e. $z = 2L$. Accordingly, one can determine the next expected self-imaging position of the beam. The estimated final imaging

positions of the beam in Column D can be compared with the optical path length of the fibre, after expansion or shortening, in Column E.

Table 6.3

The first four self-imaging length intervals of the fibre, operated at different surrounding temperatures, T, for a fibre initially 1 m in length at 25 °C.

T (°C)	A Last three final imaging positions (1st in mm)	B Last three final imaging positions (2nd in mm)	C Last three final imaging positions (3rd in mm)	D Expected the last position of the image to emerge (mm)	E Actual length after being expanded or compressed for a fibre initially a 1 m length at 25°C (mm)
0	998.695	999.224	999.751	*1000.279*	*999.771*
10	998.700	999.228	999.756	*1000.284*	*999.863*
15	998.704	999.232	999.760	*1000.288*	*999.909*
20	998.706	999.233	999.761	*1000.289*	*999.954*
25	**998.710**	**999.237**	**999.765**	***1000.293***	***1000.000***
30	998.713	999.240	999.768	*1000.296*	*1000.046*
35	998.714	999.242	999.769	*1000.297*	*1000.092*
40	998.717	999.246	999.773	*1000.301*	*1000.137*
45	998.719	999.247	999.775	*1000.303*	*1000.183*
50	998.723	999.250	999.779	*1000.307*	*1000.229*
55	998.725	999.252	999.780	*1000.308*	*1000.275*
57	998.727	999.255	999.783	*1000.311*	*1000.293*
60	998.728	999.255	999.783	1000.312	***1000.320***
65	998.730	999.258	999.786	1000.314	***1000.366***
70	998.732	999.261	999.788	1000.316	***1000.412***
80	998.738	999.265	999.794	1000.322	***1000.503***

It can be seen from Table 6.3 in Column D that the expected position of the next imaging plane is beyond that of the actual transmission length of the fibre for temperatures from 0°C to 57°C whereas for the temperatures from 60°C is still within the optical path length. Consequently, the last image for these particular fibres can be observed at further distances because of the expanded initial length of the fibre and that is why we see a sudden rise in final positions at high temperatures. However, the re-imaging position where the beam comes to focus and complete one full period over the axial distance, i.e. down the same Columns, can be observed at only very slightly larger distances as the temperatures increase.

Thus it can be seen that the input beam can be detected at various self-imaging planes with extended or reduced optical path lengths and very slight changes, within a few micrometres, in the self-imaging locations of the original transmitted beam profile with changes of temperature. It is, therefore, reasonable to draw the conclusion that the self-imaging effect of the graded index multimode fibre induced by temperature variations has no significant modification on the field intensity profile of the duplicated input beam due to an extremely small change in refractive index and insignificantly modified transmission distance of the perturbed fibre.

6.5 Conclusion

The dopant concentration of the materials employed in a fibre is the key element in the determination of fibre's lifetime and reliability because their thermal properties are related to refractive index and optical transmission path length in the material. A variation of the refractive index that is induced by the thermo-optic effect was taken into account in the investigation of temperature dependence on the propagation in an optical fibre. Also, a relatively low attenuation with a large decrease in optical losses of optical signal that can occur in the perturbed fibre must be ensured for high reliability of the transmission. It is of considerable importance for a fibre to be able to withstand environmental conditions and mechanical constraints in order to improve its transmission efficiency and reduce the amount of light scattered out of the direction of propagation and so minimise optical losses.

For the GI62.5 fibre examined, an insignificant modification of the refractive index profile and optical transmission path length of the fibre that results from the thermo-optic properties of the materials employed was found in the temperature dependence of the propagation in the fibre. Finally, we confirm, based on our simulation results, that the self-imaging phenomenon in GI62.5 fibre, having a fused silica Ge-doped core and fused silica cladding, is nearly completely insensitive to temperature fluctuations and therefore this does not introduce any critical issue for the reimaging of the original input beam profile along the perturbed transmission length interval even under harsh environmental temperature conditions.

Chapter 7

Conclusion and future work

7.1 Conclusion

As we are living in a well-developed technological world, the exponentially increasing demand of global social information in modern communication is expected to continuously increase with new services supported by modern communication systems. For that reason, we are rapidly moving towards a higher network capacity than today's standard systems can handle. Current solutions such as higher symbol rate with multi-level modulation format, existing multiplexed technologies, or by simply adding additional numbers of fibres, come on top of numerous issues and tend to be too costly. Therefore, several research studies are finding multiple ways to handle a continuously increased capacity for the near future.

To begin with, a substantial bandwidth capacity is required in order to support the large amount of information carrying capacity for different types of enhanced communications. To date, the needs for high capacity per fibre scales up progressively each year in relation to the advance in innovations, specifically for storing and switching information between data centre servers. In view of that, high transmission capacity is required for use within short haul optical interconnections. Thus our research studies predominantly were concerned with an improvement of bandwidth capacity deployed for a communication network over only a few meters.

A new frontier of multiplexing, spatial division multiplexing (SDM) is well known as a means to deal with the fibre capacity limit of standard single mode fibre. A newly enhanced multiplexed technology is thus an alternative method and well adapted for an interconnection within data centres or short distance communication networks because there is no need to be concerned about

amplification issues and the problems of equalisation for modal dispersion during the transmission can be improved using a parabolic index profile of a fibre. Thus this short-haul communication can be accomplished by multiplexing a number of optical channels in a multimode fibre with either multi-core or a single core capable of high capacity per fibre.

In our proposed fibre system, we were interested in extending capacity of the SDM fibre through a multimode fibre, supporting a large multiplicity of transmission channels. To meet an enormous carrying capacity required for future optical communications, it would be useful to increase the density of the packed channels and simultaneously propagate them within the same fibre core in which each of the channels carries its own information through various parallel transmission paths. Nonetheless, it is still challenging to handle substantially increased network demands by adding more spatial channels in a single fibre core. The reasons for this are the channel impairments, a limitation of fibre cross sectional area and the fibre perturbations (i.e. bending and environmental conditions) during the propagation.

Nowadays, the use of a quadratic medium has become increasingly popular in several areas of applications. Our research studies have investigated the behaviour of electromagnetic field propagation inside a quadratic GRIN medium in which the distribution of light rays inside the guiding medium can be simplified by examining the interactions between the guided modes inside the proposed fibre configuration. In addition to the capacity enhancement, we have shown in this study how a variety of initial conditions (i.e. a single input Gaussian beam and multi-channel transmissions) propagate and rearrange towards the self-imaging planes in GI-MMFs with various specifications of fibre through the interference effect of the modes shown by our numerical simulation models. The occurrences of arbitrary beam profiles were compared analytically with the fractional Fourier transform approach as the beam propagated inside a quadratic graded index fibre.

By suitably choosing the fibre parameters in the design, the results obtained indicated that the models were working and the re-imaging positions of the beam (i.e. where the strongest focus of the intensity distributions were found) were in a good agreement with the analytical predictions. Thus multimode fibres with a quadratic graded index profile can be used to periodically reimage the original beam profile at every double length repetition of the Fourier length interval (i.e. at $z = 2L$ where L is the Fourier length). Indeed, the transmitted input field profile (i.e. a real image) is reconstructed at every self-imaging length interval after propagating for a distance of $z = 4L$. Due to this reproduction of the beam, it is reimaged in a natural way periodically when propagating through the parabolic graded index profile of the fibre structure. Importantly, it was demonstrated that the self-imaging positions and the evolution of the beam profile are subjected to change according to the fibre specifications (i.e. the fibre core dimensions, numerical aperture) at certain distances.

To cope with inadequate bandwidth capacity and to exploit the advantages from the SDM approach, several points should be taken into consideration when designing an ultra-high capacity fibre with a plurality of optical sources. This is because of the presence of optical channel crosstalk between neighbouring channels inherent in a multiplexing scheme. It is, therefore, essential to decrease the sensitivity to inter-channel crosstalk of the optical channels. In this work, the key requirement for high bandwidth capacity is the design of the optical channel geometrical arrangement so as to suppress any undesired channel crosstalk between the spatially multiplexed channels in a large fibre cross-sectional area. To address the challenges of SDM, there exists multiple ways to meet high capacity demands, including a proper channel geometrical arrangement with a reasonable channel-to-channel pitch and appropriate azimuth alignment between channels resulting in acceptable levels of channel cross-talk.

According to our research studies, we found that the optimum channel-to-channel separation should be approximately 60 μm from the axis of the simulated graded index fibre with a 200 μm core diameter and a relative refractive index difference (Δ) of 0.41%. Moreover, it was demonstrated that arranging the optical channels in a ring-like structure is an effective physical channel arrangement to minimise the crosstalk from nearby channels (rather than a hexagonal structure). It is for this reason, i.e. the similarity of the number of nearby channels in the proposed channel arrangement, that each channel experiences almost an equivalent amount of crosstalk. We were able to achieve a worst case crosstalk, on average, of less than -30 dB after propagating eight spatially multiplexed channels for a 10 mm length of the fibre at a wavelength of a 1.55 μm. This was achieved by arranging the channels to be as close as 45° between two adjacent channels in a ring-like design arrangement. This group of beams come to arrange themselves periodically at the same re-imaging positions as would be the case for a single channel transmission.

Bending and temperature effects are of particular importance to most optical links when operating over greater transmission distances in order to substantially increase the carrying capabilities of long range systems. Thus we were interested to investigate the behaviour of light propagation in the newly designed fibre, when experiencing different disruption conditions in both the cases of a single and multi-channel transmission. From our simulation results, we can draw the conclusion that the bends do not only affect the self-reproduction length intervals but also produce aberrated images in the bent fibre under certain bending conditions. On the other hand, operating the fibre under harsh environmental temperature conditions, a good quality beam profile can be detected at the different self-imaging planes. We have found that the re-imaging positions of the beam profiles is slightly shifted before or after the original imaging planes from where it would be expected to recover the best foci in a non-perturbed fibre with alterations of temperature over quite an extreme range. Thus, overall, it must be concluded that the transmission efficiency and

capability of the fibre to periodically reproduce high quality self-imaging is restricted by the fibre perturbation since the fibre is compromised in much of its effectiveness in its unique property to fully recover the incident fields. Thus the technique might only be suitable over short-haul distances where, particularly, the bending of the fibre can be largely constrained, with any required significant deviations in direction accommodated by exiting the fibre locally to redirect the beam, and the temperature kept relatively constant within a few degrees.

7.2 Future work

Further activities would focus on embedding a greated number of spatial channels per given cross sectional area of the fibre core for space saving, offering the potential of increased information carrying capacity, and satisfying the growth of traffic volume inside data centres. The greatest concern would be focused on the degradations of optical signals and optical crosstalk impairments between the number of independent channels in a new multiplexing technology to allow enhancing transmission capacity along a reduction in costs of future communication systems per channel. Therefore, a highly efficient channel packing is crucial in the design of the SDM network in order to preserve the quality of transmitted information whilst providing large resilience to linear impairment along a realistic transmission link in relation to short reach applications. To ensure a reduction of bending losses and additional transmission link losses, it would be of great value to design a fibre that could withstand tighter bend conditions, to allow bending of the fibre beyond its critical bend radius, so as to improve the transmission efficiency. By doing so, the occurrences of the phenomenon of self-reproduction of the information source which can be reconstructed in a graded index transmission medium could be exploited in a general communication system.

MMF is of particular importance in optical systems, specifically with a GRIN profile because of its remarkable features. This makes a GRIN fibre suitable for deployments in a variety of related areas of studies not only for the optical imaging perspective, but also for near future telecommunications networks with an increased communications carrying capacity. Furthermore, a detailed consideration of the properties of self-reproduction in large-core GI-MMF is beneficial for the future design of robust and flexible fibre devices, working under harsh environmental conditions, e.g. fibre lasers and amplifiers and also for high-resolution medical imaging applications. The aim would be to achieve acceptable image quality of the re-imaged beam with robust thermal properties and flexibility of the fibre.

For the design of a GI-MMF imaging device, it is found that the accuracy of the length of the fibre is a key requirement in order to obtain a periodic duplication of the input field at certain self-imaging length intervals. Moreover, our research studies prove that the re-imaging distance can be practically controlled by selectively choosing the fibre's geometrical parameters, e.g. core diameter, numerical aperture and refractive index of the core and cladding. We can conclude that the self-imaging length interval can be extended to greater distances as the core diameters increase to accommodate a greater number of the excited modes, particularly with lower index dynamic range and difference between the fibre core and cladding.

7.3 Future investigation and design on a silicon-based photonics waveguide.

With the rapid rise in data rates and the vast amount information that is being exchanged between data centres, researchers believe that the use of silicon waveguides could be employed in various fields of studies where optical fibres are presently deployed [158]. A new development technology based on silicon integrated photonics waveguides is capable of transmitting with a faster information transfer rate within/or between microchips, enabling high-speed optical links to/from the microprocessor.

An optoelectronic waveguide uses silicon as an optical medium to propagate the light, has been progressively investigated and developed for several application areas. Due to the flexibility to allow integration with electronics circuits and the benefits that allow integration with numerous electronic microcircuits on a single chip, silicon waveguide technology is also being extensively researched by famous electronics manufacturers, such as Intel, IBM, and through work by academics [159]. Silicon-based photonics waveguides are playing an important role due to them offering great advantages over the existing electrical or optical links. For example, utilising silicon photonics as the optical signal routing and light guiding for short-reach interconnect applications [160].

The rib silicon-based photonic configuration was chosen for a brief investigation, since it exhibits low propagation losses and a reduced amount of scattering at the sidewall of the waveguide [158, 161]. In Figure 7.1 the cross-section of the rib silicon photonic waveguide structure is detailed. The device has a high refractive index contrast between a silicon core and cladding which is made of silicon dioxide. The propagating light is tightly confined within the silicon core where the guided light travels in the plane of the silicon material. This is because of a large index contrast which does not allow light to propagate into the lower and upper cladding layers [162].

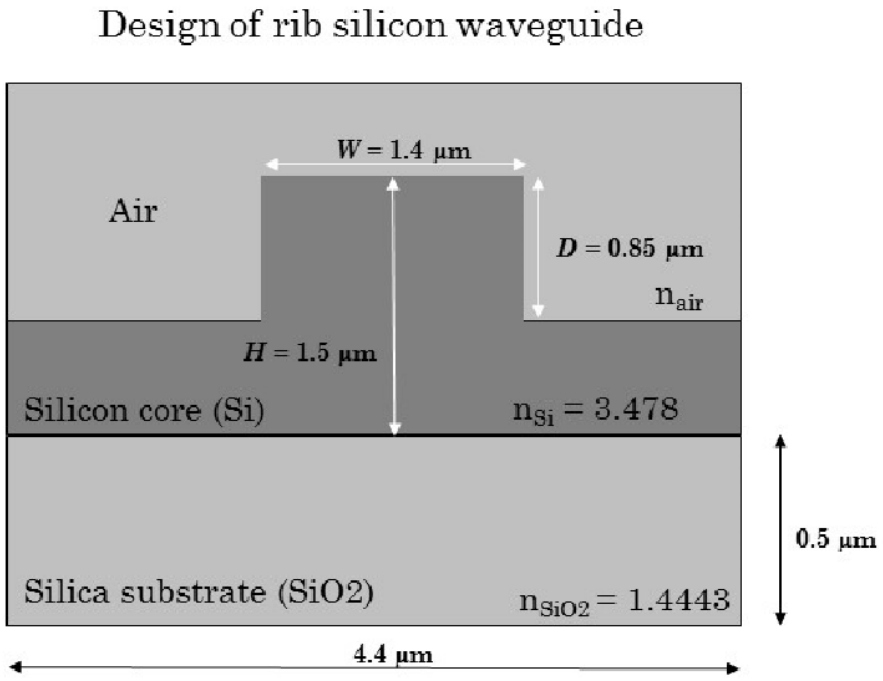

Figure 7.1: A schematic diagram showing the design of a rib silicon-based photonics waveguide with a silicon oxide layer at the bottom. The height *H* of the waveguide is 1.5 µm with an etching depth *D* of 0.85 µm, and a waveguide width *W* of 1.4 µm. The core and undercladding are made of silicon and silicon dioxide materials, respectively.

The silicon-based photonics waveguide was modelled using silicon dioxide, functioning as a bottom oxide cladding layer, with a refractive index of 1.4443, at a fixed operating wavelength of 1.55 µm. Figure 7.1 depicts the schematic diagram of the rib silicon waveguide. The core material is made of silicon (with air on top of the silicon layer that acts as the upper cladding), having a refractive index of 3.478 at an operating wavelength of 1.55 µm in the telecommunication wavelength band and a thickness *H* of 1.5 µm. Moreover, a slight etching depth is required in order to solve the problem of sidewall roughness, resulting in a reduction of propagation losses. The etch depth *D* of this waveguide can be realised by removing part of the silicon core layer to about 0.85 µm. To get the best performance, the most important aspect to consider in the design is the ultra-compactness of the waveguide. The silicon core is made flat along the

substrate and the width *W* of the rib is typically made small, typically with a value of about 1.4 μm.

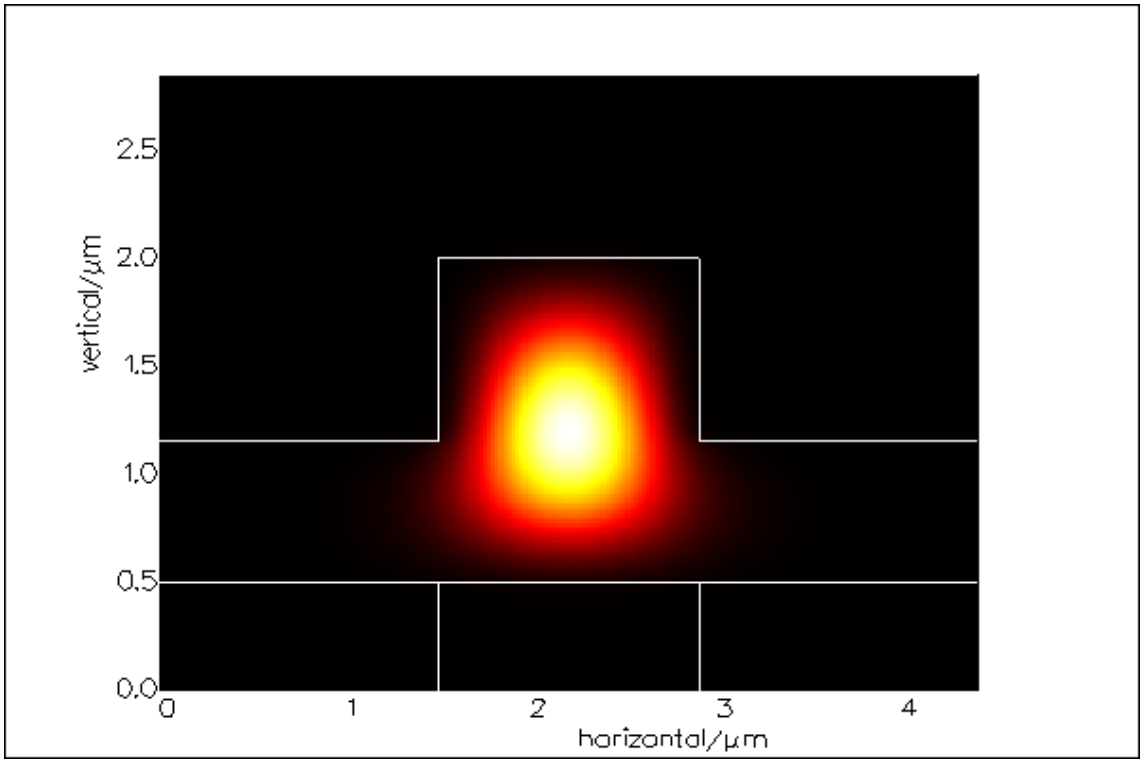

Figure 7.2: The intensity distributions of the fundamental TE-like mode obtained from the silicon photonics waveguide with a 1.4μm width, simulated with the FIMMPROP software.

The transverse field distributions of the fundamental TE-like mode in a silicon-based photonic waveguide can be seen in Figure 7.2 with the refractive index of the mode with the value of 3.41. The simulated field intensity distribution is shown in Figure 7.3 (a), as simulated with FIMMPROP. The variation of intensity of the field distribution can be seen in Figure 7.3 (b) for a propagation distance of a 10 mm length, transmitting an input Gaussian beam with a 10 μm in beam diameter.

It can be seen from the figure that the optical beam is tightly confined within the silicon core because of a relatively large index contrast and thus the majority of the light rays are not allowed to propagate into the cladding layers. Also, a rib silicon waveguide configuration exhibits less scattering light onto the sidewalls.

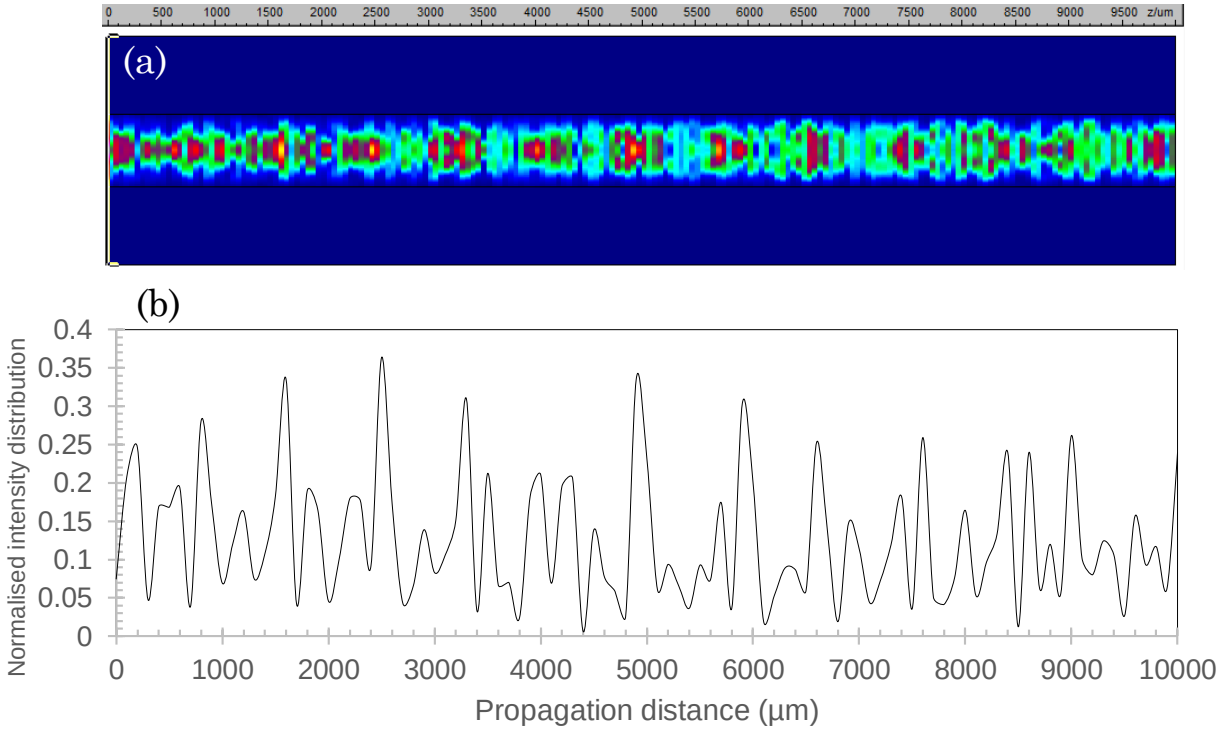

Figure 7.3: The evolution of the propagation through a silicon photonic waveguide from $z = 0$ to $z = 10$ mm: (a) beam intensity in the fibre; and (b) the normalised intensity of the propagated beam profile showing the locations where the intensity distribution peaks. However, the effect of self-imaging is not evident due to the numerous number of modes that are excited.

We can see that only a small portion of light is coupled to the silicon oxide and the air layers. The propagating fields seem to be bouncing between the interfaces of the silica core. Approximately 34.2% of the total power is coupled along a 10 mm transmission length. This is because the waveguide supports only the fundamental TE-like mode and thus the majority of the transmitted power, 13.84% of the total power, is coupled to the first fundamental TE-like mode, and the remaining power is excited to other guided and non-guided modes in the silicon photonics waveguide.

To conclude the consideration of the self-imaging phenomenon, we have found a large variation of the intensity pattern in a silicon photonic waveguide as compared to when the light propagates within a graded index fibre with a multiple number of guided modes, although the propagating mode in the silicon-based waveguide tends to concentrate near the optical axis. Moreover, the periodic reproductions of the initial excitation field at which the excited beam is repeated has not been found along the core of the silicon-based waveguide. The characteristic interference pattern occurring in a silica core exhibits structure like that of a multimode step-index fibre. We believe that the reason for this is because this particular waveguide satisfies a single mode condition in a few micron meters width, whereas a waveguide needs to support more than one guided mode in order to regenerate an excited beam.

In conclusion, a silicon-based photonic waveguide as an emerging technology for high speed digital signalling for optical communications cannot reproduce an initial beam because of its compact design which is the most important key aspect consideration for a future development of low propagation losses.

7.4 Consideration of the self-imaging effect through a silicon-based graded index core waveguide

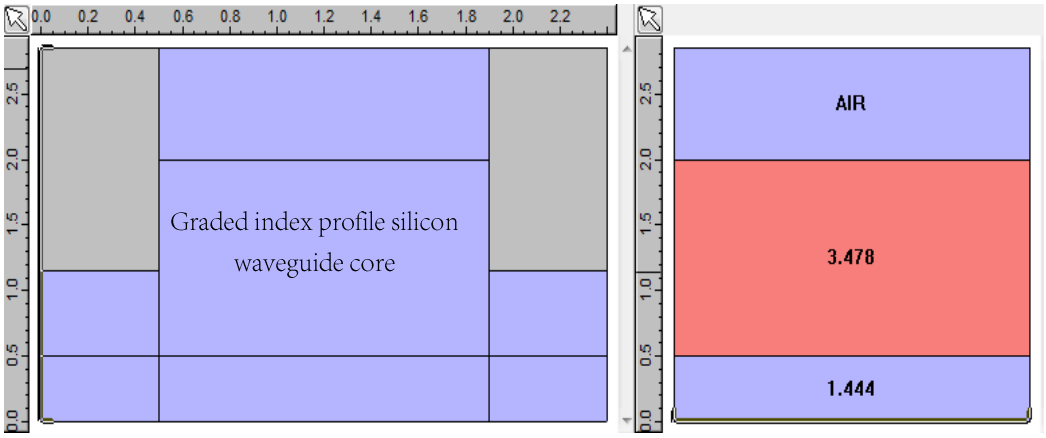

Figure 7.4: The cross-section of the silicon photonics waveguide, modelled with a graded index silicon core layer.

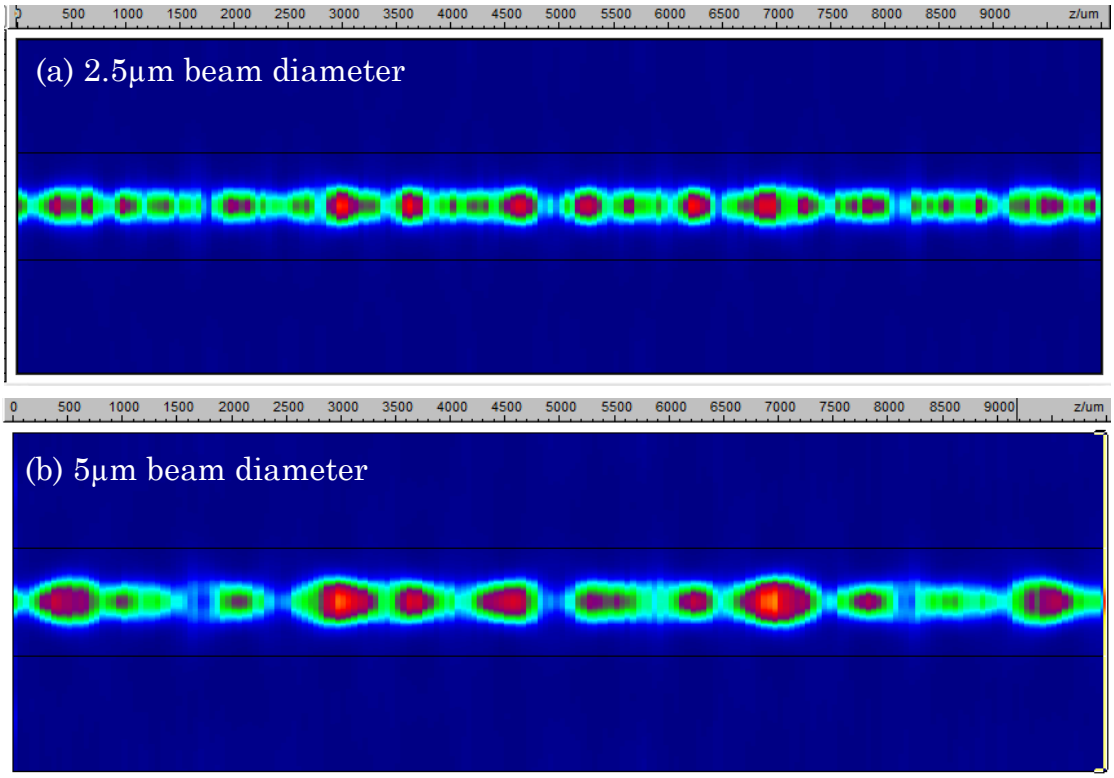

Figure 7.5: The evolution of a single beam propagation through a silicon graded core photonic waveguide from $z = 0$ to $z = 10$ mm with beam diameter of (a) 2.5 µm and (b) 5 µm entering the waveguide at the operating wavelength of 1.55 µm.

The silicon-based photonics waveguide, as depicted in Figure 7.4, has a graded index profile core with the refractive index of 3.478. The design configuration is the same as that shown in Figure 7.1, but with a graded index core in the middle. It was placed on top of the silicon dioxide cladding layer. The simulated intensity distributions are shown in Figure 7.5(a) – 7.5(b) for single channel transmission with an initial Gaussian beam entering the waveguide, having beam diameters of 2.5 µm and 5 µm, respectively. As the beam diameter is made smaller to a value of 2.5 µm, the propagating light is more tightly confined and guided through the silicon core layer. Despite the fact the waveguide core has an index profile with a parabolic shape, it can be seen that the self-imaging effect is hardly retrieved for both cases along a 10 mm propagation length.

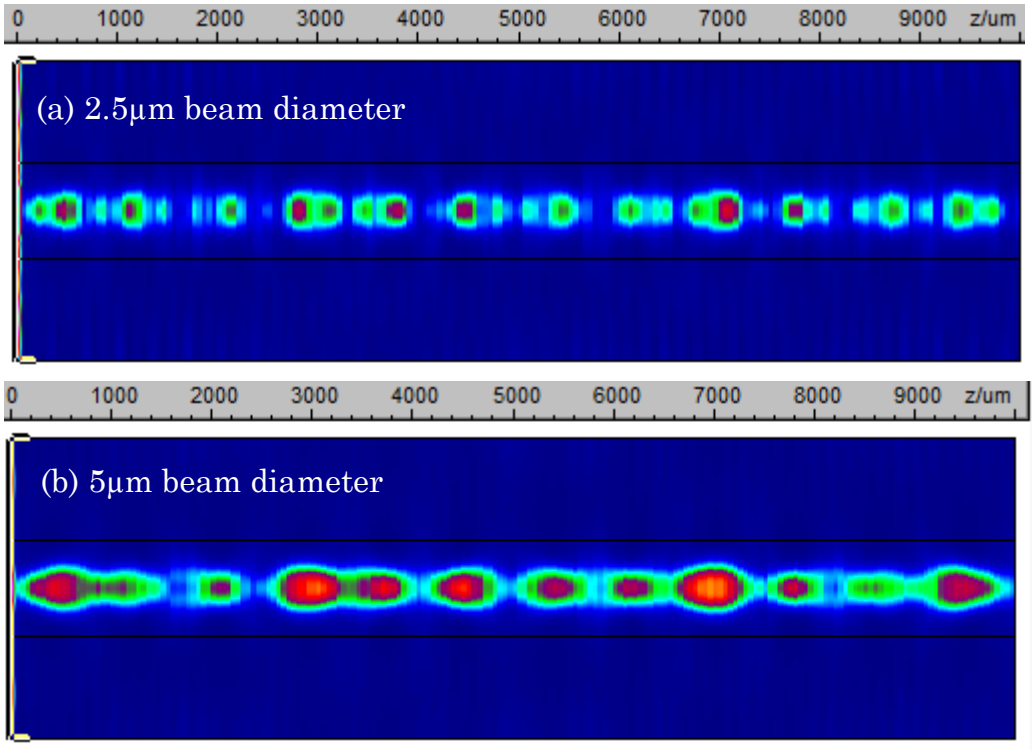

Figure 7.6: The evolution of two beam Gaussian propagation through a silicon graded core photonic waveguide from $z = 0$ to $z = 10$ mm with beam diameters of: (a) 2.5 µm and (b) 5 µm, located at the (-2,0) and (2,0) coordinates, entering the waveguide with an operating wavelength of 1.55 µm.

For multi-channel transmission, the model that is examined comprises of the two initial Gaussian beams with an equivalent beam diameter of 2.5 μm and 5 μm, as shown in Figure 7.6(a) and 7.6(b), respectively. The transmitted independent beams are coupled through the simulation model at a wavelength λ of 1.55 μm along a 10 mm length of the fibre. These Gaussian beams are arranged over the cross-section of the waveguide at the (2,0) and (-2,0) coordinate positions.

When multiple beams are simultaneously propagated in a silicon waveguide, the majority of the light is still tightly confined into the centre of the waveguide. There is not much of the propagating light that escapes into the lower refractive index region. In addition, it is evidently seen from Figure 3 that the reproduction of the multiple input beams was not found as the beams propagate through a silicon waveguide since the self-imaging effect occurs due to the interference between a large number of the modes that are generated within the structure. Likewise, a group of transmitted beams do not come to focus and arrange themselves at the self-imaging position along the length of the silicon waveguide in a multi-channel transmission. The reason for this may be because the physical structure does not support enough numbers of guided modes in the waveguide. The silicon photonic waveguide is designed with an ultra-small width of the silicon core which is a key aspect to low propagation losses and allows it be integrated with other electronic circuits.

References

[1] J.E. Midwinter, *Optical Fibres for transmission*, New York: John Wiley and Sons, 1979.

[2] D. Khoe and H.V.D. Boom, "Trends in Electro-Optical Communication Systems," in *Perspectives on Radio Astronomy-Technologies for Large Antenna Arrays,* pp. 285-294, 1999.

[3] P. J. Winzer, "Challenges and evolution of optical transport networks," in: *36th European Conference on Optical Communication* (ECOC 2010), Torino, Italy, September 19–23, paper We.8.D.1

[4] A. D. Ellis, J. Zhao, and D. Cotter, "Approaching the non-linear Shannon limit," *Journal of Lightwave Technology,* Vol. 28 (4), pp. 423–433, 2010.

[5] T. Morioka, M. Jinno, H. Takara, and H. Kubota, "Innovation Future Optical Transport Network Technologies," *NTT Technique Review*, Vol.9 (8), pp. 1-8, 2011.

[6] R. J. Essiambre, G. Kramer, P. J. Winzer, G. J. Foschini, and B. Goebel, "Capacity limits of optical fiber networks," *Journal of Lightwave Technology*, Vol. 28 (4), pp. 662-701, 2010.

[7] R. W. Tkach, "Scaling Optical Communications for the Next Decade and Beyond," *Bell Labs Technology Journal*, Vol. 14 (4), pp. 3-9, 2010.

[8] W.B. Jones, *Introduction to Optical Fiber Communication Systems*, Oxford University Press, 1995.

[9] O. Bryngadahl and W.H. Lee, "On light distribution in optical waveguides," *Journal of Opt.Soc.Am.,* Vol.68 (3), pp. 310-315 (1978).

[10] S. V. Kartalopoulos, *Introduction to DWDM Technology: data in a rainbow*, Wiley-IEEE Press, 1999.

[11] D.J. Richardson, "New optical fibres for high-capacity optical communications," *Phil. Trans. R. Soc. A* 374: 20140441, 2015.

[12] P.M. Krummrich, "Spatial multiplexing for high capacity transport," *Optical Fiber Technology,* Vol. 17 (5), pp. 480-489, 2011.

[13] P.J. Winzer, "Energy-efficient optical transport capacity scaling through spatial multiplexing," *IEEE Photonics Technology Letters*, Vol. 23 (13), pp. 851-853, 2011.

[14] A.E. Willner, Y. Ren, G. Xie, Y. Yan, L. Li, Z. Zhao, J.Wang, M. Tur, A.F. Molisch, and S. Ashrafi, "Recent advances in high-capacity free-space optical and radio-frequency communications using orbital angular momentum multiplexing," *Philosophical Transactions of the Royal Society a Mathematical Physical and Engineering Sciences*, Vol. 375 (2087), to be published in Feb 2017.

[15] G. Li, N. Bai, N. Zhao, and C. Xia, "Space-division multiplexing: the next frontier in optical communication," *Advances in Optics and Photonics*, Vol. 6 (4), pp.413-487, 2014.

[16] R. Ryf, S. Randel, A. H. Gnauck, C. Bolle, R.-J. Essiambre, P. J. Winzer, D. W. Peckham, A. McCurdy, and R. Lingle, "Space-division multiplexing over 10 km of three-mode fiber using coherent 6×6 MIMO processing," in *Optical Fiber Communication Conference and Exposition and the National Fiber Optical Engineers Conference* (OFC/NFOEC), OSA Technical Digest (Optical Society of America), 2011, paper PDPB10.

[17] G.S.D. Gordon, M.J. Crisp, R.V. Penty, T.D. Wilkinson, and I.H. White, "Feasibility demonstration of a mode-division multiplexed MIMO-enabled radio-over-fibre distributed antenna system," *Journal of Lightwave Technology*, Vol.32 (20), pp.3521-3528, 2014.

[18] T. Ishigure, E. Nihei, and Y. Koike, "Graded-index polymer optical fiber for high-speed data communication," *Applied Optics*, Vol.33 (19), pp.4261-4266, 1994.

[19] Y. Koike, T. Ishigure, and E. Nihei, "High-Bandwidth Graded-Index Polymer Optical Fiber," *Journal of Lightwave Technology*, Vol.13 (7), pp.1475-1489, 1995.

[20] Y. Shao, R. Cao, Y.-K. Huang, P.N. Ji, and S. Zhang, "112-Gb/s Transmission over 100m of Graded-Index Plastic Optical Fiber for Optical Data Center Applications," in *Optical Fiber Communication Conference and Exposition and the National Fiber Optic Engineers Conference* (OFE/NFOEC), 4-8 March 2012.

---------- [**Chapter 2: General background**] ----------

[21] D. Mendlovic and H.M. Ozaktas, "Fractional Fourier transform and their optical implementation: I," *J.Opt.Soc.Am.A*, Vol.10 (9), pp. 1875-1881, 1993.

[22] D. Mendlovic and H.M. Ozaktas, "Fractional Fourier transform and their optical implementation: II," *J.Opt.Soc.Am.A,* Vol.10 (12), pp. 2522-2531, 1993.

[23] D. Mendlovic, H.M. Ozaktas, and A.W. Lohmann, "Graded-index fibers, Wigner distribution functions, and the fractional Fourier transform," *Applied Optics*, Vol.33 (26), pp. 6188-6193, 1994.

[24] Z. Zalevsky and D. Mendlovic, "Light Propagation Analysis in Graded Index Fiber-Review and Applications," *Fiber and Integrated Optics*, Vol. 16, pp. 55-61, 1997.

[25] H.M. Ozaktas and D. Mendlovic, "Fourier transforms of fractional order and their optical interpretation," *Optic Communications*, Vol. 101, pp. 163-169, 1993.

[26] H. M. Ozaktas, M. A. Kutay, and Z. Zalevsky, *The fractional Fourier Transform with applications in Optics and Signal Processing*. New York: John Wiley and Sons Ltd, 2001.

[27] D. Mendlovic, H. M. Ozaktas, and A. W. Lohmann, "Graded-index fibers. Wigner-distribution functions, and the fractional Fourier transform," *Applied Optics*, Vol.33 (26), pp. 6188-6193, 1994.

[28] V. Namias, "The fractional order Fourier transform and its application to quantum mechanics," *J. Inst. Maths. Applics*, Vol. 25 (3), pp. 241-265, 1980.

[29] Y. Bitran, D. Mendlovic, R.G. Dorsch, A.W. Lohmann, and H. M. Ozaktas, "Fractional Fourier transform: simulations and experimental results," *Applied Optics*, Vol. 34 (8), 19995, pp. 1329-1332.

[30] B. M. Hennelly and J. T. Sheridan, "Image encryption and the fractional Fourier transform," *Optik - International Journal for Light and Electron Optics*, Vol.114 (6), pp. 251-265, 2003.

[31] D. Mendlovic, Z. Zalevsky, R. G. Dorch, Y. Bitran, A.W. Lohmann, and H. Ozaktas, "New Signal representation based on the fractional Fourier transform: definitions," *J. Opt.Soc.Am.A*, Vol.12 (11), pp. 2424-2431, 1995.

[32] D. Mendlovic and Z. Zalevsky, "The Fractional Fourier Transform in Information Optics," in *6th International Conference on Education and Training in Optics and Photonics*, SPIE Vol. 3831, pp. 381-385, 2000.

[33] AA.W. Lohmann, "Image rotation, Winger rotation, and the fractional Fourier transform," *J. Opt. Soc. Am. A*, Vol. 10 (10), pp.2181-2186, 1993.

[34] L.M. Bernardo and O.D.D. Soares, "Fractional Fourier transforms and optical systems," *Optical Communications,* Vol. 110, pp. 517-522, 1994.

[35] L.M. Bernardo and O.D.D. Soares, "Fractional Fourier transforms and imaging," *J. Opt. Soc. Am. A,* Vol. 11 (10), pp. 2622-2626, 1994.

[36] S. Kumar and M.J. Deen, *Fiber Optic Communications: fundamentals and applications,* New York: John Wiley and Sons Ltd, 2014.

[37] S. Geckeler, "Physical Principles of Optical Waveguides," *Optical Communications, A Telecommunication Review,* Munich: Siemens AG, John Wiley and Sons, Vol. 6, pp. 9-14, 1983.

[38] J.M. Senior. *Optical fiber communications: principles and practice*. New York: Prentice Hall, 3rd Edition, 1979.

[39] D. Gloge and E. A. J. Marcatili, "Multimode Theory of Graded-core Fibers," *The Bell System Technical Journal*, Vol. 52 (9), pp.1563-1578, 1973.

[40] E. Alon, V. Stojanovic, J.M. Kahn, S. Boyd, and M. Horowitz, "Equalization of modal dispersion in multimode fiber using spatial light modulator," in *Globe Telecommunications Conference*, IEEE Communications Society, pp. 1023-1029, 2004.

[41] B. Franz and H. Bulow, "Mode Group Division Multipleing in Graded-Index Multimode Fibers," *Bell Labs Technical Journal*, Vol. 18 (3), pp. 153-172, 2013.

[42] T. Morioka, "Recent Progress in Space-Division Multiplexed Transmission Technologies," in *Optical Fiber Communication Conference and Exposition and the National Fiber Optical Engineers Conference (OFC/NFOEC),* OSA Technical Digest (Optical Society of America), 2013, paper OW4F.2.

[43] T. Morioka, Y. Awaji, R. Ryf, and D. J. Richardson, "Enhancing Optical Communications with Brand New Fibers," *IEEE Communications Magazine*, Vol.50 (2), 2012, pp. 31-42.

[44] R. J. Essiambre, R. Ryf, N. K. Fontaine, and S. Randel, "Breakthroughs in Photonics 2012: Space-Division Multiplexing in Multimode and Multicore Fibers for High-Capacity Optical Communication," *IEEE Photonics Journal*, Vol. 5 (2), 2013.

[45] W. Shieh, A. Li, A.A. Amin, and X. Chen, "Space-Division Multiplexing for Optical Communications," *IEEE Photonics Society,* (online) Research Highlights-Optical Communications, October 2012.

[46] M. A. Swillam, A. Yehia, A. H. Morshed and D. Khalil, "Self-Imaging in graded index multimode interference devices," in *Proc. Mediterranean Microwave Symposium (MMS'2003)*, Cairo, Egypt, May 6-8, pp. 61-64 (2003).

[47] L. B. Soldano and E. C. M. Pennings, "Optical Multi-Mode Interference Devices Based on Self-Imaging: Principles and Applications", *Journal of Lightwave Tech*., Vol. 13, pp. 615-627, 1995.

[48] C. Yeh, "Guided-Wave Modes in Cylindrical Optical Fibers," *IEEE Transactions on Education*, Vol. E-30, No. 1, pp. 43-51, 1987.

[49] D. Gloge, "Weakly guided fibers," *Apply optics*, Vol.10 (10), pp. 2252-2258, 1971.

[50] D. Marcuse, *Light Transmission Optics*, New York: Van Nostrand Reinhold Co., 1972.

[51] A. Ghatak and G. Thyagarajan, *Introduction to Fiber Optics*, Cambridge University Press, 1st edition, 1998.

[52] A.H. Morshed, "Self-imaging in Single mode-Multimode-Single mode Optical Fiber Sensors," *Electronics, Communications and Photonics Conferences (SIECPC), Saudi International*, April 24-26, pp. 1-5, 2011.

[53] A. Fertman and D. Yelin, Image transmission through an optical fiber using real-time modal phase restoration, *J.Opt.Soc.Am.B*, Vol.30 (1), pp.149-157, 2013.

[54] S.W. Allison and G.T. Gillies, "Observations of and applications for self-imaging in optical fibers," *Applied Optics*, Vol.33 (10), pp. 1802-1805, 1994.

[55] S. Zeng, Y. Zhang and B. Li, "Self-imaging in periodic dielectric waveguides", *Optics Express*, Vol. 17 (1), pp. 365-378, 2009.

[56] H. Li, M. Brio, L. Li, A. Schiilzgen, N. Peyghambarian, and J. V. Moloney, "Multimode interference in circular step-index fibers studied with the mode expansion approach", *J. Opt. Soc. Am. B*, Vol. 24 (10), pp. 2707- 2720, 2007.

[57] W. S. Mohamed, A. Mehta and E. G. Johnson, "Wavelength Tunable Fiber Lens Based on Multimode Interference", *J. Lightwave Tech*., Vol. 22 (2), pp. 469-477, 2004.

[58] A. Kumar, R. K. Varshney, S. Antony and P. Sharma, "Transmission characteristics of SMS fiber optic sensor structures", *Optics Communications*, vol. 219, 215-219, 2003.

[59] V. I. Ruiz-Perez, M. A. Basurto-Pensado, G. Urquiza-Beltran, D. A. May-Arrioja, E. Gasca-Herrera, J. 1. Sanchez Mondrag6n, and P. L. LiKamWa, "Optical Fiber Sensor for Pressure Based on Multimode Interference as Sensitive Element," in *Latin America Optics and Photonics Conference, OSA Technical Digest, Recife, Brazil,* (September 27,2010), paper MB23.

[60] Y. Liu and L. Wei, "Low-cost high-sensitivity strain and temperature sensing using graded-index multimode fibers", *Appl. Optics*, Vol. 46 (13), pp. 2516-2519, 2007.

[61] S. M. Tripathi, A. Kumar, R. K. Varshney, Y. B. P. Kumar, E. Marin and J-P. Meunier, "Strain and Temperature Sensing Characteristics of Single-Mode-Multimode-Single-Mode Structures", *J. Lightwave Tech*., Vol. 27 (13), pp. 2348-2356, 2009.

[62] N. Bhatia and J. John, "Multimode interference devices with single-mode-multimode-multimode fiber structure", *Applied Optics*, Vol.53 (23), pp. 5179-5186, 2014.

[63] K.G. Larkin, "A Beginner's Guide to the Fractional Fourier Transform Part 2: A Brief History of Time Frequency Distributions," *Australian Optical Society NEWS*, pp. 13-17, 2006.

[64] E. Hecht, *Optics*, London: Addison-Wesley, 4th edition, 2001.

[65] J. Goodman, Introduction to Fourier Optics, Roberts&Company Publishers, 3rd edition, 2004.

[66] R. Selvas, I. Torres-Gomez, A. Martinez-Rios, and J. A. Alvarez-Chavez, "Wavelength tuning of fiber lasers using multimode interference effects," *Optics Express*, Vol.13 (23), pp. 9439-9455 (2005).

[67] http://www.rodenburg.org/guide/t100.html, Accessed on 12th Nov 2016.

[68] D. J. Richardson, J. M. Fini, and L. E. Nelson, "Space Division Multiplexing in Optical Fibres," *Nature Photonics*, Vol. 7 (5), pp.354-362, 2013.

[69] S. Berdague and P. Facq, "Mode division multiplexing in optical fibers," *Applied Optics*, Vol. 21 (11), pp.1950–1955, 1982.

[70] L. Gruner-Nielsen, Y. Sun, J. W. Nicholson, D. Jakobsen, R. Lingle, and B. Palsdottir,"Few Mode Transmission Fiber with low DGD, low Mode Coupling and low Loss," in *Optical Fiber Communication Conference*, OSA Technical Digest (Optical Society of America), 2012, paper PDP5A.1.

[71] S. Randel, R. Ryf, A. Sierra, P. J. Winzer, A. H. Gnauck, C. A. Bolle, R.-J. Essiambre, D. W. Peckham, A. McCurdy, and Jr.R. Lingle, "6×56-Gb/s mode-division multiplexed transmission over 33-km few-mode fiber enabled by 6×6 MIMO equalization," *Optics Express*, Vol.19 (17), pp. 16697-16707, 2011.

[72] S. Randel, P. J. Winzer, M. Montoliu, and R. Ryf, "Complexity analysis of adaptive frequency-domain equalization for MIMO-SDM transmission," in *39th European Conference and Exhibition on Optical Communication* (ECON), 2013, pp. 801-803.

[73] N. Bai, E. Ip, Y.-K. Huang, E. Mateo, F. Yaman, M.-J. Li, S. Bickham, S. Ten, J. Liñares, C Montero, V. Moreno, X. Prieto, V. Tse, K. M. Chung, A. P. T. Lau, H.-Y. Tam, C. Lu, Y. Luo, G.-D. Peng, G. Li, and T. Wang, "Mode-division multiplexed transmission with inline few-mode fiber amplifier," *Optics Express*, Vol. 20 (3), pp. 2668-2680, 2012.

[74] N. Bai, E. Ip, M. J. Li, T. Wang, and G. Li, "Experimental demonstration of adaptive frequency-domain equalization for mode-division multiplexed transmission," in *Optical Fiber Communication Conference*, OSA Technical Digest (Optical Society of America), 2013, paper OM2C.5.

[75] H. Kubota, H. Takara, T. Nakagawa, M. Matsu, T. Morioka, "Intermodal group velocity dispersion of few-mode fiber," IEICE Electronics Express, Vol.7 (20), pp.1552-1556, 2010.

[76] J.M. Kahn, K. P. Ho, and M. B. Shemirani, "Mode coupling effects in multi-mode fibers," in *Optical Fiber Communication Conference*, OSA Technical Digest (Optical Society of America), 2012, paper OW3D.3.

[77] F. Ferreira, D. Fonseca, and H. Silva, "Design of few-mode fibers with arbitrary and flattened differential mode delay," *IEEE Photonics Technology Letters*, Vol. 25 (5), pp. 438-441, 2013.

[78] K. S. Abedin, T. F. Taunay, M. Fishteyn, D. J. DiGiovanni, V.R. Supradeepa, J. M. Fini, M. F. Yan, B. Zhu, E. M. Monberg, and F.V. Dimarcello, "Cladding-pumped erbium-doped multicore fiber amplifier," *Optics Express*, Vol. 20 (18), pp. 20191-20200, 2012.

[79] E. Ip, "Gain equalization for few-mode fiber amplifiers beyond two propagating mode groups," *IEEE Photonics Technology Letters*, Vol. 24 (21), pp. 1933-1936, 2012.

[80] S. Randel, R. Ryf, A. H. Gnauck, M. A. Mestre, C. Schmidt, R.-J. Essiambre, P. J. Winzer, R. Delbue, P. Pupalaikis, A. Sureka, Y. Sun, X. Jiang, Jr. R. Lingle, "Mode-multiplexed 6x20-GBd QPSK transmission over 1200-km DGD-compensated few-mode fiber," in *Proc. OFC-NFOEC,* 2012, Paper PDP5C.5.

[81] R. Ryf, N. K. Fontaine, M.l A. Mestre, S. Randel, X. Palou, C. Bolle, A. H. Gnauck, S. Chandrasekhar, X.Liu, B. Guan, R.-J. Essiambre, P.J. Winzer, S.L.-Saval, J.B. -Hawthorn, R. Delbue, P. Pupalaikis, A. Sureka, Y. Sun, L. Grüner-Nielsen, R. V. Jensen, and R. Lingle, "12 x 12 MIMO Transmission over 130-km Few-Mode Fiber," in *Proc. Frontiers in Optics,* 2012, Paper FW6C.4.

[82] H. Takara, A. Sano, T. Kobayashi, H. Kubota, H. Kawakami, A. Matsuura, Y. Miyamoto, Y. Abe, H. Ono, K. Shikama, Y. Goto, K. Tsujikawa, Y. Sasaki, I. Ishida, K. Takenaga, S. Matsuo, K. Saitoh, M. Koshiba, and T. Morioka, "1.01-Pb/s (12 SDM/222 WDM/456 Gb/s) crosstalk-managed transmission with 91.4- b/s/Hz aggregate spectral efficiency," in *Proc. European Conference and Exhibition on Optical Communication* (ECOC), 2012, paper Th.3. C.1.

[83] K. Igarashi, T. Tsuritani, I. Morita, Y. Tsuchida, K. Maeda, M. Tadakuma, T. Saito, K. Watanabe, K. Imamura, R. Sugizaki, and M. Suzuki, "Super- Nyquist-WDM transmission over 7,326-km seven-core fiber with capacity- distance product of 1.03 Exabit/s · km," Optic Express, Vol. 22 (2), 2014.

[84] D. Qian, E. Ip, M.-F. Huang, M.-j. Li, A. Dogariu, S. Zhang, Y. Shao, Y.-K. Huang, Y. Zhang, X. Cheng, Y. Tian, P. Ji, A. Collier, Y. Geng, J. Linares, C. Montero, V. Moreno, X. Prieto, and Ting Wang. "1.05Pb/s Transmission with 109b/s/Hz Spectral Efficiency using Hybrid Single-and Few-Mode Cores," Frontiers in Optics 2012," in paper FW6C.3 (2012).

[85] S. Murshid, B. Grossman, and P. Narakorn, "Spatial domain multiplexing: A new dimension in fiber optic multiplexing," *Optics and Laser Technology*, Vol. 40 (8), pp.1030-1036, 2008.

[86] H. Kubota and T. Morioka, "Few-mode optical fiber for mode-division multiplexing," *Optics and Laser Technology*, Vol. 17 (5), pp.490-494, 2011.

---------- [**Chapter 4: Multiple channels transmission**] ----------

[87] D. Gloge and D. Weiner, "The Capacity of Multiple Beam Waveguides and Optical Delay Lines," *The Bell System Technical Journal*, Vol. 47 (10), pp. 2095 – 2109, December 1968.

[88] K. Appaiah, S. Vishwanath, and S. R. Bank, "Impact of fiber core diameter on dispersion and multiplexing in multimode-fiber links," *Optics Express,* Vol. 22 (14), pp.17158 – 17171, 2014.

[89] D. *Marcuse*, *Light Transmission Optics,* 2nd edition, Van Nostrand Reinhold, Princeton, New Jersey, 1982.

[90] I.J. Goddard and D.P.M. Chown, "A multi-Optical-Frequency Network," presented at EFOC/LAN 87, the Fifth European Fibre Optic Communications & Local Area Networks Exposition, Bessel, Switzerland, 3-5 June 1967.

[91] Y. Miyamoto and H. Takenouchi, "Dense Space-division-multiplexing Optical Communications Technology for Petabit-per-second Class Transmission," *NTT Technical Review*, Vol. 12 (12), pp. 1-7, 2014.

[92] P.J. Winzer, A. H. Gnauck, A. Konczykowska, F. Jorge, and J.Y. Dupuy, "Penalties from in-band crosstalk for advanced optical modulation format," presented in *Proc. ECOC* 2001*,* paper Tu. 5. B.7.

[93] B. Clesca, C. Coeurjolly, S. Gauchard, L. Berthelon, O. Gautheron, and E. Brandon, "Power Limitation in 4x2.5 Gbit/S WDM Transmission Systems,"

presented in *EFOC&N 95, the thirteenth Annual Conference on European Optical Communications and Networks*, Brighton, England, June 27-30, 1995.

[94] T. Watanabe and Y. Kokubun, "Ultra-large number of transmission channels in space division multiplexing using few-mode multi-core fiber with optimized air-hole-assisted double-cladding structure," *Optic Express*, Vol. 22 (7), pp. 8309-8319, 2014.

[95] D. Gloge, "Crosstalk in Multiple-Beam Waveguides," *The Bell System Technical Journal*, Vol. 49 (1), pp. 55-71, 1970.

[96] A. Sano, H. Takara, T. Kobayashi, H. Kishikawa, T. Nakagawa, Y. Miyamoto, Y. Abe, H. Ono, K. Shikama, M. Nagatani, T. Mori, Y. Sasaki, I. Ishida, K. Takenaga, S. Matsuo, K. Saitoh, M. Koshiba, M. Yamada, H. Masuda, and T. Morioka, "409-Tb/s+409-Tb/s crosstalk suppressed bidirectional MCF transmission over 450 km using propagation-direction interleaving," *Optic Express*, Vol. 21 (14), pp. 16777-16783, 2013.

[97] S. Matsuo, Y. Sasaki, T. Akamatsu, I. Ishida, K. Takenaga, K. Okuyama, K. Saitoh, and M. Kosihba, "12-core fiber with one ring structure for extremely large capacity transmission," *Optic Express*, Vol. 20 (27), pp. 28398-28408, 2012.

[98] N. Sangeetha, J. Santhiya, and M. Sofia, "Bend loss in large core multimode optical fiber beam delivery system," *International Journal of Advanced Research in Computer and Communication Engineering*, Vol. 4 (5), pp. 488-491, May 2015.

[99] D. Donlagic, "A low bending loss multimode fiber transmission system," *Optics Express*, Vol. 17 (24), pp. 22081 – 22095, 2009.

[100] N. Lagakos and J. H. Cole, "Fiber Optic microbend acoustic sensor," *Applied Optics*, Vol.19, pp. 3265-3267, 1980.

[101] H. F. Traylor, "Bending effects in Optical Fibers," *Journal of Lightwave Technology*, Vol. LT-2 (5), pp. 617 – 628, 1984.

[102] M. Semenkoff, "Bending Effect on Light Propagation in an Optical Fiber: Application to a Temperature Sensor," *Optics and Lasers in Engineering*, Vol. 17, pp. 179-186, 1992.

[103] J. A. Jay, "An Overview of Macrobending and Microbending of Optical Fibres," *White paper: Corning*, Vol. WP1212, pp. 1-12, 2010.

[104] D. Gloge, "Bending Loss in Multimode Fibres with Graded and Ungraded Core Index," *Applied Optics*, Vol. 11 (11), pp. 2506 – 2513, 1972.

[105] FIMMWAVE MANUAL

[106] D. Donlagic and B. Culshaw, "Propagation of the Fundamental Mode in Curved Graded Index Multimode Fiber and Its Application in Sensor Systems," *Journalof Lightwave Technology*, Vol. 18 (3), pp. 334 – 342, 2000.

[107] W.A. Gambling, "Propagation Characteristics of Curved Optical Fibers," *The transactions of the IECE of Japan*, Vol. E 61 (3), pp. 196 – 201, 1978.

[108] W.A. Gambling, H. Matsumura, C.M. Ragdale, and R.A. Sammut "Measurement of radiation loss in curved single-mode fibres," *Microwaves, Optics and Acoustics*, Vol.2 (4), pp. 134 – 140, 1978.

[109] D. Marcuse, "Curvature loss formula for optical fibers," *J. Opt. Soc. Am*. Vol.66 (3), pp.216-220, 1976.

[110] X. Sun, J. Li, and A. Hokansson, "Study of optical fibre damage under tight bend with high optical power at 2140 nm," in *Proc. SPIE 6433, Optical Fibers and Sensors for Medical Diagnostics and Treatment Applications VII, 643309,* Vol. 8 (10), 2007.

[111] B.E. Knudsen, R.D. Glickman, K.J. Stallman, S. Maswadi, B.H. Chew, D.T. Beiko, J.D. Denstedt, and J.M. Teichman, "Performance and safety of holmium: YAG laser optical fibers," *Journal of Endourol*, Vol.19 (9), pp. 1092-1097, 2005.

[112] O. Wright and D. Largeau, "Fiber-optic differential pressure sensor," *J. Phys. E: Sci. Instrum*, Vol. 20 (1), pp. 46-51, 1987.

[113] D. Donlagic and B. Culshaw, "Microbend sensor structure for use in distributed and quasi-distributed sensor system based on selective launching and filtering of the modes in graded index multimode fiber," *J. Lightwave Technol*, Vol. 17 (10), pp. 1856-1868, 1999.

[114] S. Cattelan, M. Ruzzier, and M. Travagnin, "Macrobending Loss in Bend Insensitive Fibers: A Statistical Parameter," in *Proceedings of the 58th IWCS/IICIT International Wire & Cable Symposium*, Vol. 58, pp. 258-263, 2009.

[115] P.R. Watekar, S. Ju, and W.T. Han, "Design and development of a trenched optical fiber with ultro-low bending loss," *Optics Express*, Vol. 17 (12), pp. 10350 – 10363, 2009.

[116] P.R. Watekar, S. Ju, and W.T. Han, "Single-mode optical fiber design with wide-band ultra low bending-loss for FTTH application," *Optics Express*, Vol. 16 (2), pp. 1180 – 1185, 2008.

[117] A. Natsume, K. Suzuki, and Y. Kozawa, "Fiber Identifier for Bend-insensitive Optical Fibers," *NTT Technical Review Letters*, Vol. 6 (5), pp.1-4, May 2008.

[118] J. Yamauchi, M. Ikegaya, and H. Nakano, "Analysis of bent asymmetric slab waveguides by the beam propagation method," *Optics Communications*, Vol. 79 (5), pp. 291-294, 1990.

[119] R.T. Schermer and J.H. Cole, "Improved Bend Loss Formula Verified for Optical Fiber by Simulation and Experiment," *IEEE Journal of Quantum Electronics*, Vol. 43 (10), pp. 899-909, 2007.

[120] X. Jin, A. Gomez, Kai Shi, Benn C. Thomsen, Feng Feng, George S. D. Gordon, Timothy D. Wilkinson, Yongmin Jung, Qiongyue Kang, Pranabesh Barua, Jayanta Sahu, Shaif-ul Alam, David J. Richardson, Dominic C. O'Brien, and Frank P. Payne. "Mode Coupling Effects in Ring-Core Fibers for Space-Division Multiplexing Systems," *Journal of Lightwave Technology*, Vol. 34 (14), pp. 3365 –3372, 2016.

[121] R.S. Quimby, "*Photonics and Lasers: An Introduction*," 1st Edition, Publisher: John Wiley & Sons, 2006.

[122] https://www.thorlabs.com/thorproduct.cfm?partnumber=GIF625, accessed on 25th November 2016. (Thorlabs Data Sheet)

[123] A.A.P. Boechat, D. Su, D.R. Hall, and J.D.C. Jones, "Bend loss in large core multimode optical fiber beam delivery systems," *Applied Optics*, Vol. 30 (3), pp. 321-327, 1991.

[124] K. Makino, T. Ishigure, and Y. Koike, "Waveguide Parameter Design of Graded-Index Plastic Optical Fibers for Bending-Loss Reduction," *Journal of lightwave technology*, Vol.24 (5), pp. 2108 – 2114, 2006.

[125] http://www.its.bldrdoc.gov/fs-1037/dir-016/_2397.htm, accessed on 28th November 2016.

[126] C. Lee Giles and Walter J. Wild, "Fresnel reflection and transmission at a planar boundary from media of equal refractive indices," *Applied Physics Letters*, Vol.40 (3), pp. 210-212, 1982.

[127] L.M. Bernardo, "Talbot self-imaging in fractional Fourier planes of real and complex orders," *Optics Communications*, Vol. 140, pp. 195-198, 1997.

[128] S. Silva, E.G.P. Pachon, M.A.R. Franco, J.G. Hayashi, F.X. Malcat, O. Frazao, P. Jorge, and C.M.B. Cordeiro, "Ultrahigh-sensitivity temperature fiber sensor based on multimode interference," *Applied Optics*, Vol.51 (16), pp. 3236-3242, 2012.

---------- [**Chapter 6: Temperature effect**] ----------

[129] I.M. Davis, G.S. Glaesemann, S. Ten, and M.J. Winningham, "Optical Fibers Resilient to Failure in Bending under High Power," in *Proceeding of 31st European Conference on Optical Communication ECOC 2005,* paper We 3.4.5, Vol. 3, pp. 471-472, 2005.

[130] R.M. Percival, E.S.R. Sikora and R. Wyatt, "Catastrophic damage and accelerated ageing in bent fibers caused by high optical powers," *Electronics Letters*, Vol. 36 (5), pp. 414-416, 2000.

[131] R. Kashyap and K.J. Blow, "Observation of Catastrophic Self-Propelled Self-focusing in Optical Fibers," *Electronics Letters*, Vol.24 (1), pp.47-48, 1988.

[132] S.L. Logunov and M.E. DeRosa, "Effect of coating heating by high power in optical fibres at small bend diameters," *Electronics Letters*, Vol. 39 (12), pp. 897-898, 2003.

[133] M. Bigot-Astruc, P. Sillard, S. Gauchard, P. Le Roux, and E. Brandon, "Analysis of Coating Temperature Increase in Fibers under High Power and Tight Bending," in *Proceedings of OFC2006*, paper OFK4, 2006.

[134] P.S. Andre, A.M. Rocha, F. Domingues, and A. Martins, "Improved thermal model for optical fibre coating owing to small bending diameter and high power signals," *Electronics Letters*, Vol. 46 (10), 2010.

[135] E.A. Soares and M.T. Dantas, "Bare fibre temperature sensor," *J. SPDE*, Vol. 1367, pp. 261-264, 1990.

[136] S. Poeggel, D. Tosi, D.Duraibabu, G. Leen, D McGrath, and E. Lewis, "Optical Fibre Pressure Sensors in Medical Applications," *Journal of Sensors*, Vol.15, pp. 17115-17148, 2005.

[137] A.M. Scheggi, M. Brenci, G. Conforti, and R. Falciai, "Optical-fiber thermometer for medical use," *IEEE Proceedings*, Vol. 131, Pt. H. No. 4, pp.270-272, 1984.

[138] L. Prod'nomme, "A new approach to the thermal change in the refractive index of glasses," *Physics and Chemistry of Glasses*, Vol. 1 (4), pp. 119-122, 1960.

[139] https://accuratus.com/fused.html, accessed on 13th December 2016.

[140] https://www.thorlabs.de, accessed on 13th December 2016.

[141] J. Canning, "Properties of Specialist Fibres and Bragg Gratings for Optical Fiber Sensors," *Journal of Sensors*, Vol. 1, pp.1-18, 2009.

[142] Y. Son, Y. Won, C. Bae, and S. Han, "Thermal Characteristics of Fiber Bragg Grating temperature sensor in Ge doped and Ge & Boron co-doped fiber," *The 23rd International Technical Conference on Circults/Systems, Computers and Communications* (ITC-CsCC), pp.1805-1808, 2008.

[143] M. Kovacevic and A. Djordjevich, "Temperature Dependence Analysis of Mode Dispersion in Step-Index Polymer Optical Fibers," in *Proceeding in the International School and Conference on Photonics*, PHOTONICA09, Vol. 116 (4), pp. 649-651, 2009.

[144] Y.J. Kim, U.C. Paek, and B.H. Lee, "Measurement of refractive-index variation with temperature by use of long-period fiber gratings," *Optics Letters*, Vol. 27 (15), pp.1297-1299, 2002.

[145] M. Bigot-Astruc, L.A.de. Montmorillon, and P. Sillard, "High-Power Resistance of Bend-Optimized Single-Mode Fibers," *Proceeding of OFC/NFOEX 2008,* paper JWA2, 2008.

[146] A.M. Rocha, A. Martins, M. Facao, and P.S. Andre, "Effect of Bending in SMF Fibers under High Power," *Proceeding of ICTON 2009*, paper Th. B2.1, 2009.

[147] W. Z. Yong, Q. Qi, and S. Shuang-Jin, "Temperature dependence of the refractive index of optical fibres," *Chin. Phys. B*, Vol.23 (3), pp. 034201-1: 5, 2014.

[148] D. B. Leviton and B. J. Frey, "Temperature-dependent absolute refractive index measurements of synthetic fused silica," *Proceedings of SPIE 2006*, Vol. 6273, paper 62732K.

[149] C.Z. Tan and J. Arndt, "Temperature dependence of refractive index of glassy SiO2 in the infrared wavelength range," *Journal of Physics and Chemistry of Solids*, Vol. 6, pp. 1315-1320, 2000.

[150] R.M. Waxler and G. W. Cleek, "The Effect of Temperature and Pressure on the Refractive Index of Some Oxide Glasses," *Journal of Research of the National Bureau of Standards-A. Physics and Chemistry*, Vol. 77A (6), pp. 755-763, 1973.

[151] J. Matsuoka, N. Kitamura, S. Fujinaga, T. Kitaoka, and H. Yamashita, "Temperature dependence of refractive index of SiO_2 Glass," *Journal of Non-Crystal Solution*, Vol. 135, pp. 86-89, 1991.

[152] A. Rostami and S. Makouei, "Temperature Dependence Analysis of the Chromatic Dispersion in WII-Type Zero-Dispersion Shifted Fiber (ZDSF)," *Progress in Electromagnetics Research B*, Vol. 7, pp. 209-222, 2008.

[153] N.G. Ramachandran, *Progress in Crystal Physics*, Vol. 1, edited by S. R. Krishnan (Interscience Publishers, New York, London, 1958), pp. 139 -167.

[154] A. Koike and N. Sugimoto, "Temperature Dependences of Optical Path Length in Organic Glasses," *Reports Res. Lab. Asahi Glass Co., Ltd.*, Vol. 56 (UDC: 535.327 : 666.225), 2006.

---------- [**Updated DSDM approach**] ----------

[155] T. Mizuno, H. Takara, A. Sano, and Y. Miyamoto, "Dense Space-DivisionMultiplexed Transmission Systems Using Multi-core and Multi-Mode Fiber," *J. of Lightwave Technology*, Vol. 34 (2), 2016.

[156] K. Shibahara, T. Mizuno, H. Takara, A. Sano, H. Kawakami, D. Lee, Y. Miyamoto, H. Ono, M. Oguma, Y. Abe, T. Kobayashi, T. Matsui, R. Fukumoto, Y. Amma, T. Hosokawa, S. Matsuo, K. Saito, H. Nasu, and T. Morioka, "Dense SDM (12-core × 3-mode) transmission over 527 km with 33.2-ns mode-dispersion employing low-complexity parallel MIMO frequency-domain equalization," presented at the Optical Fiber Communication Conf.,

[157] T. Mizuno, T.Kobayashi, H. Takara, A. Sano, H. Kawakami, T.Nakagawa, Y. Miyamoto,Y.Abe, T.Goh, M. Oguma, T. Sakamoto,Y. Sasaki, I. Ishida, K. Takenaga, S. Matsuo, K. Saitoh, and T. Morioka, "12-core × 3-mode dense space division multiplexed transmission over 40 km employing multi-carrier signals with parallel MIMO equalization," presented at the Optical Fiber Communication Conf., San Francisco, CA, USA, 2014, Paper Th5B.2.

---------- [**Silicon photonics**] ----------

[158] D. J. Lockwood and L. Pavesi (Eds.), *Silicon Photonics II Components and Integration*, Berlin, Heidelber: Springer, 2011.

[159] B. T. Smith, D. Feng, H. Lei, D. Zheng, J. Fong, and M. Asghari, Fundamentals of Silicon Photonics Devices, *J. Electronic Technical EngineerIT*, pp. 76-78, July 2011.

[160] V. J. Dubois, M. Antelius, H. Sohlstrom, and K. B. Gylfason, A single-lithography SOI rib waveguide sensing circuit with apodized low back-reflection surface grating fiber couping, *in* Proceedings of SPIE –The International Society for Optical Engineering, May 2012.

[161] K. Yamada, Silicon Photonics Wire Waveguides: Fundamental and Applications, *Electronics and Communications in Japan* (Part II: Electronics), Vol. 89 (3), pp.42-55, 2006.

[162] B. Jalali, M. Paniccia, and G. Reed, Silicon photonics , *IEEE Microwave Magazine*, Vol. 7, pp. 58-68, 2006.

Appendix A: Software explanation

A comprehensive study of wave propagation inside the proposed GI-MMF was performed using the commercially available FIMMWAVE™ software by the company PhotonDesign. FIMMWAVE can be used to model a variety of 2-D and 3-D waveguide structures with a variety of different mode solvers. Each of the mode solving methods has its own advantages, enabling the user to choose the most efficient and suitable solver for the design.

In this study, a numerical mode solver is implemented using a full-vectorial finite difference method (FDM) is a suitable choice for modelling an optical fibre with a continuously varying index profile. We used the FDM solver which is included within FIMMWAVE™ to analyse the excitation of various modes in the structure. After modelling the waveguide in FIMMWAVE™, the propagation characteristic of the electromagnetic fields (i.e. in terms of a sum of local Eigenmodes of the fibre) inside the fibre can be modelled using FIMMPROP™, an integrated propagation module as part of the mode solver in FIMMWAVE. The FIMMPROP™ is a versatile tool for visualising what is occurring inside the fibre structure. Its implementation is based on the fundamental theory of the Eigenmode expansion (EME) method. This method is well known as a solution of Maxwell's equations.

There are several advantages of the EME technique over other photonics algorithms such as Finite Difference Time Domain (FDTD), Finite Element Method (FEM), and Beam Propagation Method (BPM) [105]. The EME is a powerful method to study the wave propagation inside any design of photonic device with a level of accuracy, for which the BPM would be inaccurate. The EME is useful for fast design optimisation since its computational speed is much faster than FDTD and FEM in which the field profile needs to be stored at each time step. Therefore, the EME approach is well suited to fully analyse the the wave

propagation that help in understanding the physical mechanism occurring inside the optical fibre.

When calculating the modes of a waveguide in FIMMWAVE™, the two main categories of modes i.e. guided modes and radiation modes, can be found in waveguide sections. The optical field at a given *z*-position is calculated as a linear combination of the decomposition of the field in the corresponding *x*-*y* cross-section. Any field present in the waveguide forms a complete basis set of Eigenmodes. We can express any mode in terms of a solution of Maxwell's Equations as:

$$\Psi(x,y,z) = \sum_{i=1}^{N} C_i \Psi_i(x,y) \exp(i\beta_i z)$$

where the mode profile or the Eigenmode, Ψ_i, with its corresponding propagation constant, β_i, can be automatically determined using the FDM mode solver in FIMMWAVE™. Once the Eigenmodes are known the complex amplitude coefficient of the mode, C_i, can be calculated, corresponding to the power and the phase of each particular mode.

The mode coefficients C_i can be expressed as:

$$C = amplitude \cdot \exp(i \cdot phase)$$
$$C = real + j \cdot imaginary$$

in which the power of the mode can be determined by:

$$P = |amplitude|^2$$

We can inspect the mode amplitude at any z position along the structure and calculate the sum of the modes in order to see the total power that is coupled into the structure (i.e. where $z = 0$) or in any position where the power is lost in the transmission. The accuracy of the device can be improved by including a sufficiently large number of Eigenmodes as well as the spatial resolution. However, there is a trade-off between the computational time and the number of modes. It is therefore required to include all necessary modes (which propagate without loss) to accurately represent the optical field along the structure.

Appendix B: Results for the self-imaging length intervals

The percentage changes of self-imaging positions we have investigated for the propagation along a 1 meter length of fibre, derived from the simulations for distances of $z = 2L$ to $z = 60L$.

T (°C)	$z = 2L$ (μm)	(%) difference	z = 4L (μm)	(%) difference	z = 6L (μm)	(%) difference	$z = 8L$ (μm)	(%) difference	z = 10L (μm)	(%) difference	z = 12L (μm)	(%) difference
0	527.463	0.0014	1055.159	0.0013	1582.560	0.0014	2110.147	0.0015	2637.740	0.0014	3165.140	0.0014
20	527.469	0.0004	1055.170	0.0003	1582.576	0.0004	2110.170	0.0004	2637.767	0.0003	3165.173	0.0003
25	527.470	0.0000	1055.173	0.0000	1582.582	0.0000	2110.178	0.0000	2637.776	0.0000	3165.184	0.0000
30	527.472	0.0004	1055.177	0.0004	1582.587	0.0003	2110.185	0.0003	2637.785	0.0003	3165.195	0.0003
80	527.486	0.0030	1055.204	0.0029	1582.627	0.0028	2110.242	0.0030	2637.852	0.0029	3165.276	0.0029

T (°C)	$z = 14L$ (μm)	(%) difference	z = 16L (μm)	(%) difference	z = 18L (μm)	(%) difference	$z = 20L$ (μm)	(%) difference	z = 22L (μm)	(%) difference	z = 24L (μm)	(%) difference
0	3692.835	0.0014	4220.302	0.0014	4747.760	0.0014	5275.460	0.0014	5802.862	0.0014	6330.444	0.0015
20	3692.873	0.0004	4220.344	0.0004	4747.809	0.0004	5275.514	0.0004	5802.921	0.0003	6330.513	0.0004
25	3692.887	0.0000	4220.359	0.0000	4747.826	0.0000	5275.533	0.0000	5802.941	0.0000	6330.536	0.0000
30	3692.900	0.0004	4220.373	0.0003	4747.843	0.0004	5275.551	0.0003	5802.961	0.0003	6330.559	0.0004
80	3692.996	0.0030	4220.479	0.0028	4747.967	0.0030	5275.686	0.0029	5803.107	0.0029	6330.730	0.0031

T (°C)	*z* = 26*L* (μm)	(%) difference	z = 28L (μm)	(%) difference	z = 30L (μm)	(%) difference	*z* = 32*L* (μm)	(%) difference	z = 34L (μm)	(%) difference	z = 36L (μm)	(%) difference
0	6858.044	0.0014	7385.441	0.0014	7913.137	0.0014	8440.606	0.0014	8968.059	0.0014	9495.766	0.0014
20	6858.113	0.0003	7385.516	0.0004	7913.220	0.0004	8440.691	0.0004	8968.152	0.0004	9495.863	0.0004
25	6858.137	0.0000	7385.542	0.0000	7913.248	0.0000	8440.721	0.0000	8968.184	0.0000	9495.897	0.0000
30	6858.161	0.0003	7385.568	0.0004	7913.277	0.0004	8440.750	0.0003	8968.216	0.0004	9495.930	0.0003
80	6858.334	0.0029	7385.757	0.0029	7913.483	0.0030	8440.962	0.0029	8968.451	0.0030	9496.173	0.0029

T (°C)	*z* = 38*L* (μm)	(%) difference	z = 40L (μm)	(%) difference	z = 42L (μm)	(%) difference	*z* = 44*L* (μm)	(%) difference	z = 46L (μm)	(%) difference	z = 48L (μm)	(%) difference
0	10023.170	0.0013	10550.750	0.0014	11078.350	0.0014	11605.750	0.0014	12133.450	0.0014	12660.920	0.0013
20	10023.270	0.0003	10550.860	0.0004	11078.460	0.0004	11605.860	0.0004	12133.570	0.0004	12661.050	0.0003
25	10023.300	0.0000	10550.900	0.0000	11078.500	0.0000	11605.910	0.0000	12133.620	0.0000	12661.090	0.0000
30	10023.340	0.0004	10550.940	0.0004	11078.540	0.0004	11605.950	0.0003	12133.660	0.0003	12661.130	0.0003
80	10023.590	0.0029	10551.220	0.0030	11078.820	0.0029	11606.240	0.0028	12133.980	0.0030	12661.450	0.0028

T (°C)	*z* = 50*L* (μm)	(%) difference	z = 52L (μm)	(%) difference	z = 54L (μm)	(%) difference	*z* = 56*L* (μm)	(%) difference	58L (μm)	(%) difference	z = 60L (μm)	(%) difference
0	13188.360	0.0014	13716.080	0.0014	14243.480	0.0013	14771.060	0.0015	15298.670	0.0014	15826.060	0.0014
20	13188.500	0.0004	13716.220	0.0004	14243.620	0.0004	14771.220	0.0004	15298.830	0.0003	15826.220	0.0004
25	13188.550	0.0000	13716.270	0.0000	14243.670	0.0000	14771.280	0.0000	15298.880	0.0000	15826.280	0.0000
30	13188.600	0.0004	13716.320	0.0004	14243.720	0.0004	14771.330	0.0003	15298.930	0.0003	15826.330	0.0003
80	13188.940	0.0030	13716.670	0.0029	14244.080	0.0029	14771.730	0.0030	15299.320	0.0029	15826.740	0.0029

Appendix C: List of Publications

S. Jakborvornphan, R. Young, P. Birch, and C. Chatwin, "**Bending effects in large core graded index fibre with multi-channel transmission,**" *Asian Journal of Physics*, Vol. 26 (3), 2017.

S. Jakborvornphan, R. Young, P. Birch, and C. Chatwin, "**High density multi-channel transmission in graded index fibre,**" *Journal of Optical Fibre Technology*, Under review, 12th July 2017.